THE PHYSICAL BASIS OF ELECTROMAGNETIC INTERACTIONS WITH BIOLOGICAL SYSTEMS

PROCEEDINGS OF A WORKSHOP HELD AT THE
UNIVERSITY OF MARYLAND, COLLEGE PARK, MARYLAND
JUNE 15-17, 1977

EDITORS

Leonard S. Taylor and Augustine Y. Cheung

Electrical Engineering Department and the Institute for Physical Science and Technology, Division of Mathematical and Physical Sciences and Engineering and the Department of Radiology, School of Medicine, University of Maryland.



SPONSORED BY THE OFFICE OF NAVAL RESEARCH, THE NAVAL MEDICAL RESEARCH AND DEVELOPMENT COMMAND, AND THE BUREAU OF RADIOLOGICAL HEALTH, FOOD AND DRUG ADMINISTRATION

THE PHYSICAL BASIS OF ELECTROMAGNETIC INTERACTIONS WITH BIOLOGICAL SYSTEMS

PROCEEDINGS OF A WORKSHOP HELD AT THE UNIVERSITY OF MARYLAND, COLLEGE PARK, MARYLAND. JUNE 15-17, 1977

EDITORS

Leonard S. Taylor and Augustine Y. Cheung

Electrical Engineering Department and the Institute for Physical Science and Technology, Division of Mathematical and Physical Sciences and Engineering and the Department of Radiology, School of Medicine, University of Maryland.

SPONSORED BY THE OFFICE OF NAVAL RESEARCH, THE NAVAL MEDICAL RESEARCH AND DEVELOPMENT COMMAND, AND THE BUREAU OF RADIOLOGICAL HEALTH, FOOD AND DRUG ADMINISTRATION.

FOREWORD

This volume contains the proceedings of a Workshop on the Physical Basis of Electromagnetic Interactions with Biological Systems held at the University of Maryland on June 15-17, 1977. The workshop was sponsored by the Office of Naval Research, the Naval Medical Research and Development Command and the Bureau of Radiological Health, Food and Drug Administration.

The wide application of industrial, commercial and military devices and systems which radiate frequencies in the radiofrequency and microwave portion of the electromagnetic spectrum plus numerous only partially understood indications of microwave effects upon living organisms have raised important questions of the physical basis of the interactions of electromagnetic fields with biological systems. These questions must be answered if the development of regulatory standards and of methods and techniques for controlling radiofrequency and microwave exposure is to be achieved. The same questions must be answered in connection with present and proposed therapeutic applications of these waves. The rapid increase in the use of these frequencies makes these questions matters of imperative concern, particularly in view of the possibilities of cumulative or delayed effects of exposure.

The study of electromagnetic interactions with biological systems brings together diverse specialties in the fields of physics, engineering, biology and chemistry in a highly interdependent way. Progress towards practical solutions of the problems involved will depend upon the development of experimental techniques and instruments and of a sufficient general theoretical base to inform and react with the experimental investigations. The purpose of the Workshop on the Physical Basis of Electromagnetic Interactions with Biological Systems was to bring together the leading investigators in the field to present the results of recent research, to determine the present status of the field and the priority of significant problem areas, and to critically evaluate conflicting theoretical interpretations and experimental techniques. These proceedings contain the formal papers prepared by the invited speakers plus a number of contributed papers given by other participants in the Workshop. Transcriptions were made of the discussion periods following each paper and edited versions of these are included; the editors bear the responsibility for any misquotation.

Leonard S. Taylor

Augustine Y. Cheung

TABLE OF CONTENTS

		Page
1.	Survey of Microwave and Radiofrequency Biological Effects and Mechanisms. S. Cleary.	1
2.	Molecular Absorption of Non-Ionizing Radiation in Biological Systems. K. D. Straub.	35
3.	Millimeter Wave and Far-Infrared Absorption in Biological Systems. K. Illinger.	43
4	Cooperative Quantum Mechanical Mechanisms for Resonance Absorption of Non-Ionizing Radiation. I. Grodsky.	67
5.	Basics of ELF Fields and Biosphere Effects. O. Schmitt.	71
6.	Possible Mechanisms of Weak Electromagnetic Field Coupling in Brain Tissue. S. M. Bawin, A. Sheppard and W. R. Adey.	75
7.	Classical Theory of Microwave Interactions with Biological Systems. H. Schwan.	90
8.	Determination of Bound Water in Biological Materials from Dielectric Measurements. E. Grant.	113
9.	Interfacial and Intracellular Water: Expected Anomalies in Dielectric Properties. J. S. Clegg and W. Drost-Hansen.	121
10.	Microwave Frequencies and the Structure of the Double Helix. E. Prohofsky.	133
11.	Techniques of Raman Spectroscopy Applied to Study the Effects of Microwaves upon Synthetic and Naturally Occurring Lipid Membranes. J. P. Sheridan, R. Priest, P. Schoen, and J. M. Schnur.	145
12.	Evanescent Waves and Waves in Absorbing Media. L. Felsen.	149
13.	Microwave and RF Dosimetry. C. K. Chou and A. W. Guy.	165
14.	Electric Field Measurements Within Biological Media. A. Cheung.	217
15.	Some Recent Results on Deposition of Electromagnetic Energy in Animals and Models of Man. O. P. Gandhi and M. J. Hagmann.	243
16.	Thermometry in Strong Electromagnetic Fields. T. C. Cetas.	261
17.	Non-Perturbing Microprobes for Measurements in Electromagnetic Fields. A. Deficis and A. Priou.	283
18.	The Viscometric Thermometer. C. A. Cain, M. M. Chen, K. L. Lam and J. Mullin.	295

Page

19. Microwave Thermography: Physical Principles and Diagnostic Applications. P. C. Myers and A. H. Barrett. 309

20. Design and Standardization of Exposure Systems for RF and Microwave Experimentation. M. L. Swicord and H. S. Ho. 327

21. Calibration Techniques for Microwave and RF Exposure Measurement Devices. H. I. Bassen. 359

22. Workshop Summary: S. Cleary. 383

23. Panel Discussion - Principal Speakers and Participants. 391

24. Workshop Attendees. 397

SURVEY OF MICROWAVE AND RADIOFREQUENCY BIOLOGICAL EFFECTS AND MECHANISMS

S. F. Cleary

Department of Biophysics, Virginia Commonwealth University
Richmond, Virginia 23298

ABSTRACT

Representative works from the recent literature are reviewed to define the nature of the biological effects of microwave and radiofrequency exposure and the proposed basic physical interaction mechanisms. The results of studies of neuroendocrine alterations, hematopoietic effects, and effects on neural systems are considered. It is suggested that biomembranes may be the primary site for microwave and radiofrequency alterations, and that the most likely interaction mechanism appears to involve macromolecular ensembles stabilized by long-range systems of weak time-varying cooperative interactions.

INTRODUCTION

A number of recent developments have resulted in renewed interest in and concern among scientists and the general public about the biological effects of microwave and radiofrequency radiation exposure. Scientific interest has been kindled by reports that have appeared during the past few years which consistently suggest that biological systems, both *in vivo* and *in vitro*, are affected by exposure to field intensities that were formerly thought to be incapable of producing detectable alterations. Not only has increasing evidence appeared implicating low intensity (10 mW/cm^2) fields in alterations in specific biological endpoints, but the types of endpoints have increased and now include a wide variety of effects ranging from subtle behavioral changes to hematopoietic changes. Detailed information on recent scientific findings is provided in symposia proceedings[1,2], review articles[3] and reference works[4]. The reader will note that although a large number of references originate from East European nations and the Soviet Union, Western scientists have recently contributed significantly to the literature on the effects of low intensity microwave exposure. It is obviously not a coincidence that reports of this nature appear at a time when the concern of the general public regarding the possibly harmful effects of exposure to this type of electromagnetic radiation is at an all-time high.

Public concern has been aroused by the news media[5] in which attention has been drawn to a number of international incidents involving intentional exposure of humans to microwave fields. Although there does not appear to be any well-founded evidence that such incidents have, in fact, resulted in deleterious effects, available scientific information regarding microwave effects is not adequate to refute such claims. The public is also justifiably concerned since microwave and radiofrequency devices are proliferating at an increasing rate and the concept of one more form of pollution, an *electromagnetic smog*, is disconcerting, especially to those who have little or no understanding of the potential physical or biological consequences of such exposure.

In order to allay public concern, the scientific community must provide information on the basic physical and biological mechanisms involved in the interaction of electromagnetic fields in this frequency region with living systems. This information must then be applied to the establishment of exposure standards for humans that are both safe and realistic from the point of view of risk versus benefits, a concept that has not yet appeared to be widely applied to problems of microwave biological effects.

The adequacy of current scientific information in this area is the subject of this paper. Selected representative works from recent literature will be reviewed with the purpose of defining the nature of the biological effects of microwave exposure, with special emphasis directed toward effects reported at intensities of 10 mW/cm^2 or less. Such information will provide the background for a review of proposed basic physical interaction mechanisms with an attempt, where possible, to relate cause or mechanism to effect.

BIOLOGICAL EFFECTS

The following areas of microwave biological effects, although not all-inclusive, will be presented to provide a general indication of the results of recently reported studies: neuroendocrine alterations; hematopoietic effects; and effects on neural systems. Microwave-induced lethality, or other high-intensity, apparently thermal phenomena which will not be discussed herein, have been reviewed elsewhere[4]. It should be noted in passing that although causal relationships for such high intensity effects are significantly better established than for low intensity alterations, the basic biophysical molecular interaction mechanisms responsible for microwave induced thermal death are not completely known. The existing data suggests that death due to hyperpyrexia, regardless of the cause, involves the irreversible denaturation of biomolecules, most probably proteins. It is, however, not known which macromolecular species exhibit the greatest sensitivity to the denaturing effects of high intensity microwave fields. Available data at the macroscopic level suggests that the sequence of events leading to thermal death originates in alterations in the central nervous system (CNS), which is interesting in view of the fact that the mammalian CNS also appears to figure prominently in

low-intensity microwave effects, although possibly for completely different reasons. A more detailed understanding of the *in vivo* macromolecular alterations of high intensity thermalizing microwave fields would be of value in furthering our understanding of low intensity reversible microwave effects.

NEURAL EFFECTS OF EXPOSURE TO LOW-INTENSITY FIELDS

Alterations in bioelectrical activity of the CNS of mammals, changes in conditioned and unconditioned behavior of man and experimental animals, as well as functional alterations in excitable cell systems, have been reported to occur as a result of exposure to microwave intensities of 10 mW/cm^2 or less. The results of such studies have been carefully scrutinized to determine if such effects may be attributed to direct microwave-specific alterations or if they are indirect effects of subtle thermal phenomena resulting from microwave energy absorption in neural elements. Theoretical[6] and experimental[7] studies have revealed that at microwave frequencies, geometrical resonances occur in the mammalian brain that are manifested in non-uniform distributions of absorbed energy which, for example, may result in maximum absorption at the anterior hypothalamus, the thermoregulatory center of the brain. Evidence derived from neurophysiological studies suggests that a temperature rise of $0.01^{\circ}C$ could result in a 3% alteration in the firing rate of thermosensitive neurons of the preoptic nucleus of the hypothalamus[8]. Consequently, low-level microwave heating of such neural elements could conceivably induce thermocompensatory responses which would be detected as an alteration in the physiological status of the experimental subject. Such effects would be dependent upon microwave-specific thermal changes. The validity of this concept is dependent upon the creation of non-uniform temperature distributions within the brain due to non-uniform energy absorption. Since the brain is a vascularized organ, conductive cooling by blood circulation would act to reduce non-uniform temperature distributions. The extent to which this occurs is not presently known since this would require *in situ in vivo* temperature measurements during microwave exposure, a difficult task at present. Thus, although non-uniform microwave energy absorption offers an attractive hypothesis for low intensity microwave effects on

the mammalian CNS, additional data is needed before this hypothesis can be accepted.

An alternative mechanism for the induction of CNS alterations by low-intensity microwave exposure is the direct interaction of the microwave field (electric or magnetic components) with neuronal elements. Based on a theoretical analysis of the neurophysiological characteristics of neurons, Schwan[9] has indicated that the field strengths induced in neuronal membranes by low-intensity microwave or radiofrequency fields are probably not of sufficient magnitude to produce functional alterations. At frequencies of greater than 1 MHz, field-induced membrane potentials were calculated to be 10^5 to 10^6 times smaller than the normal resting potential of neurons exposed to microwave intensities on the order of 10 mW/cm^2. The model used for this calculation does not take into account the effect of nerve cell morphology on induced transmembrane potentials. Bernhardt and Pauly[10] have shown, for example, that the membrane potentials generated by alternating electrical fields depend upon the shape and orientation of the cell with respect to the field as well as the frequency and field strength. The membrane relaxation frequency is also dependent upon cell shape, size, and orientation, the membrane properties, and the intra- and extracellular conductivities[9]. On the basis of their analysis, Bernhardt and Pauly[10] indicate that in the case of long prolate spheroids with their semi-axes parallel to the external field, significantly larger potential differences are induced for a given external field strength than for shorter cells of the same type. Such findings suggest that induced transmembrane potentials in neurons may differ markedly from other cell types due, among other things, to morphological factors, especially at frequencies of 100 MHz or less[10]. Similar size and shape dependent induced potential phenomena have been reported for dc fields by Klee and Plonsey[11], who note that the sensitivity of individual cells to the direction of stimulation suggests that a given stimulating configuration may selectively excite only a subpopulation of the exposed cells. Cellular directional sensitivity to stimulation implies that the effects of the electrical activity of neighboring interactive cells must also be taken into account in evaluating the effects of externally applied electrical fields. Directional sensitivity of cells to electrical

fields thus provides a potential mechanism whereby extracellular electrical activity occurring at distributed locations can be summed into a small area of the cell surface which may function as synaptic convergence zones or action potential trigger zones[12]. Somal polarization of up to 4 mV and dendrite and axon terminal polarizations of 6-8 mV are predicted[13] on the basis of this model for applied fields of 0.1 V/cm. Experimental evidence for the directional sensitivity of neurons has been reported by Terzuolo and Bullock[14] who studied the effects of small polarizing currents on the nonadapting stretch receptor of the crayfish and cardiac ganglia of the lobster. It was determined that the pronounced alterations in neuronal firing rates of active cells could be induced by directionally dependent dc voltage gradients of approximately 10 mV/cm, this representing an upper limit for the critical voltage drop across the sensitive area of the neuron which may be more than 50% lower than this value. The gradients for the alteration of the firing rates of active neurons may be several orders of magnitude smaller than the changes in membrane potential for threshold electrical stimulation of nonactive neurons. Terzuolo and Bullock[14] demonstrated that voltage gradients of 200 mV/cm were required to fire silent cells under the same experimental conditions.

Application of the results of such studies to the effects of microwave and radiofrequency fields on neuronal elements must involve consideration of the frequency dependence of the applied fields which results, as pointed out by Schwan[9], in a decrease in the induced transmembrane potential which is directly proportional to frequency. If it is assumed, furthermore, that functional alterations of neurons by impressed fields are dependent upon induced dc potentials, membrane rectification of alternating fields must occur. Field rectification has been demonstrated in artificial bilayer membranes and is theoretically possible in biomembranes[15], but direct experimental evidence for this effect has not been reported. It may be concluded that the specification of a realistic interaction mechanism for functional alterations in neuronal elements by microwave or radiofrequency fields must include factors that have not currently been adequately accounted for such as cell size, shape and functional status (*i.e.*, active or resting), intercellular

interactions, and field rectification by biomembranes. On the basis of current neurophysiological concepts it may be suggested that the results of investigations of isolated nerve preparations must be evaluated with an awareness of possible deviations from *in vivo* exposure effects due to differences in the interacting elements.

Experimental studies have been conducted at various frequencies ranging from extra low frequencies (ELF) to microwave electromagnetic field effects. Tinney, *et al*[16] exposed isolated poikilothermic turtle hearts to 960 MHz continuous wave (CW) fields. In opposition to the anticipated tachycardia which results from generalized heating, microwave exposure in the range of absorbed powers of 2-10 mW/g resulted in significant bradycardia. The authors hypothesize that microwave radiation causes neurotransmitter release by excitation of the nerve remnants in the heart[16]. Atropine, a blocker of the parasympathetic system, and propranol hydrochloride, a sympathetic system blocking agent, resulted in a suppression of the microwave effect when added to the isolated hearts. By administering the drugs separately, evidence was obtained that microwave radiation affects neurotransmitter release; the mechanism for the effect is, however, unknown[16].

In vivo studies of the effects of low intensity microwaves on neurotransmitter release have also been reported. Syngajevskaja, *et al*[17] found that 0.5 mW/cm^2 decimeter wave exposure produced a significant decrease in acetylcholinesterase (Ache) activity in rabbit brains. An increase in acetylcholine and a decrease in Ache in the blood of irradiated animals has also been reported[18]. Repeated exposure of rats to 3 GHz microwaves at intensities of from 10 to 40 mW/cm^2 led to an initial increase followed by a decrease in Ache blood activity[19]. Similar results were reported by Baranski[20] following irradiations of rabbits for two and one half to five months, whereas an eight month exposure at an intensity of 1 mW/cm^2 was without effect. Three hour exposures of guinea pigs to 3 GHz CW radiation at intensities of 3.5 and 25 mW/cm^2 had no effect on Ache brain activity, wnereas pulsed wave (PW) exposures caused a significant decrease in activity. Repeated exposures resulted in increases in Ache activity, the effect being more pronounced following pulsed field exposures[20]. Ache activity in

rabbits repeatedly exposed to CW and PW microwaves for four months was found to decrease in the case of CW exposure and increase as a result of PW irradiation. The midbrain regions were found to be most affected[20]. Microwave-induced alterations in lipid and nucleo-protein metabolism in the brains of experimental animals have also been reported, the alterations again being more pronounced following pulsed field exposure[20].

Merritt *et al*[21] compared the effects of 1.6 GHz microwave and nonradiation heating on neurotransmitter concentrations in the rat brain. Rats exposed for ten minutes to 80 mW/cm^2 experienced a $4^{\circ}C$ rise in rectal temperature as did thermal controls exposed to elevated environmental temperatures. Hypothalamic norepinephrine decreased in irradiated and hyperthermal control animals compared to normothermal controls. Serotonin concentrations were decreased in the hippocampal regions of irradiated rats but not in hyperthermal controls. Similar results were obtained for the dopamine concentrations in the corpus striatum and hypothalamus. Thermographic analyses of the absorbed microwave power distributions indicated that the neurotransmitter alterations were the result of microwave-induced hyperthermia.

Histological effects of low-intensity microwave exposure have been reported by Albert and DeSantis[22]. Chinese hamsters were irradiated with 1.7 GHz CW microwaves at power densities of 10 and 25 mW/cm^2. Exposure for thirty minutes to two hours induced cytopathology in hypothalamic and subthalamic neurons whereas the glial cells appeared normal, as did cells in other regions of the brain. There was no evidence of hemorrhage or edema. No recovery or repair of microwave-induced changes was found in the brains of animals sacrificed two weeks after exposure. These results are in agreement with those reported by Tolgskaya[20] who found that exposure to microwave intensities between 7-9.5 mW/cm^2 for thirty minutes induced cytological changes in the thalamus and hypothalamus of experimental animals. It has also been found that short term (*i.e.*, less than one day) exposures caused lesser degrees of change in neural tissue than chronic low-intensity exposure[23,24].

Modulated low intensity electromagnetic fields have been reported to alter calcium binding in cerebral tissue. Bawin and Adey[25] exposed isolated

chick and cat cerebral tissues for twenty minutes to 0.05, 0.1, 0.56 and 1.0 V/cm fields at frequencies of 1, 6, 16, 32, or 75 Hz. A biphasic response of Ca^{2+} in brain tissue was detected with a maximum suppression of Ca^{2+} efflux occurring at 6 and 16 Hz and for field strengths of 0.10 and 0.56 V/cm. As in the case of alteration in heart rate reported by Tinney, *et al*[16], these results suggest the existence of a biphasic field strength dependence since increasing the field strength to magnitudes greater than 0.56 V/cm reduced the treatment effect. Direct cortical stimulation of the intact cat brain with 200 Hz, 10 msec pulses at intensities of 20-50 mV/cm, on the other hand, resulted in a 20% increase in Ca^{2+} efflux[26]. Radiofrequency fields with a carrier wave frequency of 147 MHz, amplitude modulated at 6, 9, 11, and 16 Hz produced a statistically significant increase[27] in Ca^{2+} efflux from isolated chick forebrain at intensities of 1 to 2 mW/cm^2. A possible mechanism for the effect of low intensity radiofrequency radiation on Ca^{2+} efflux is suggested by the authors. They state[27] that the electrochemical equilibrium that exists in cerebral tissues between ions, polyanionic macromolecules, and glycoproteins of the cell surface may be disrupted by small variations of either the surrounding ionic concentrations or local electrical gradients. Modulations of the radiofrequency field, reflected as slow modulations of the extracellular electric field could thus affect the Ca^{2+} binding to the neuronal membrane. The fact that no effect on Ca^{2+} fluxes was produced by unmodulated fields and that a pulse repetition rate dependent maximum rate of efflux was detected at rates of 11 and 16 Hz indicates that Ca^{2+} movement was critically related to specific slow components of the radiation field. They draw attention to the fact that this frequency effect is consistent with results of other studies using various electrophysiological endpoints and that it supports the finding that specific modulation effects are involved in the reported induction of EEG changes in the cat[28].

Bawin and Adey[29] in discussing the inverse relationship of Ca^{2+} binding effects in neural tissue in response to modulated VHF and ELF fields indicate that the results suggest field interaction with a common substrate which is dependent on the interaction energy provided by the field. The basis for

the amplitude selectivity or biphasic amplitude response of Ca^{2+} binding is suggested as being related to the mode of Ca^{2+} binding to neuronal biomolecules which may consist of strong or weak bonding depending upon site-specific molecular binding sites[29]. The authors state that no completely satisfactory explanation can be given for the biphasic frequency response; they note that subjective time estimates in monkeys are speeded up in the presence of a 7 Hz, 0.10 V/cm sinusoidal field but in order to induce this effect at 45 to 75 Hz larger field strengths are required. Bawin and Adey also state[29] that EEG patterns in the cat are reinforced by VHF fields amplitude modulated at the dominant EEG frequencies but not by CW fields or fields modulated at other frequencies[28]. It is suggested that the frequency specificity of the responses is an indication of a direct field effect on the CNS, rather than a more generalized peripheral transduction.

The results of a large series of investigations by Soviet authors on the effects of microwave radiation on the EEG of rabbits are summarized by Baranski and Czerski[4] who also note, however, that the presence of implanted electrodes during irradiation makes it difficult to evaluate the significance of the findings.

Wachtel, *et al*[30] investigated the electrical activity of individual neurons in *Aplysia* ganglia before, during, and after irradiation with 1.5 and 2.45 GHz, CW and PW microwaves. Alterations were induced in the firing patterns at absorbed powers that were below the level human brain cells would be exposed to from a free field intensity of 10 mW/cm^2. The effects were in part attributed to slight ganglionic warming but in some cases effects induced by microwaves could not be reproduced by nonradiation heating[30]. It is indicated that the current density induced by a 10 mW/cm^2 microwave field is 1000 times greater than the polarizing current densities required to produce an alteration in the firing patterns of ganglia. Field rectification would be necessary, however, for such effects to occur and the positive findings of this study thus provide evidence for such an effect.

Taylor and Ashlemen[31] found that functional alterations could be induced in the spinal cords of cats by 2.45 GHz microwave exposure but the changes could also be produced by nonradiation heating. The fact that the time

interval over which the detected effects occurred was different following microwave exposure was attributed to differences in the time interval of the induced temperature changes. Taylor and Ashlemen[31] conclude that these findings, as well as previous results of studies of evoked thalamic potentials and isolated peripheral nerves, may be explained on the basis of thermal mechanisms.

Servantie, *et al*[32] studied the synchronization of cortical neurons in the rat by pulsed 3 GHz radiation at an average intensity of 5 mW/cm^2 and a pulse repetition rate of 500-600 Hz. Experimental animals were exposed in free space conditions for ten days after which occipital EEG's were recorded. The exposure resulted in the induction of an electrocortical frequency synchronous with the microwave pulse modulation frequency. The induced electrocortical frequency, which is significantly higher than those generally recorded, persisted for a period of hours following the termination of exposure[32].

In addition to biochemical, histological and bioelectrical alterations, microwave exposure reportedly affects behavioral alterations in experimental animals under certain conditions. Galloway[33], for example, tested the effects of high intensity 2.45 GHz, CW microwaves on discrimination and repeated acquisition tasks in rhesus monkeys. The heads of the experimental subjects were exposed to 5, 10, 15, 20, and 25 W for two minutes prior to testing. Convulsions were induced at 15 and 25 W. Animals were irradiated throughout the durations of five consecutive one hour daily testing sessions for a total irradiation time of 40 min/day. No behavioral deficits were detected at integral dose rates of less that 15 W. Exposure to 15 W or more produced either skin burns or severe convulsions without reliably altering task performance. The author suggests that complex tasks, such as repeated acquisition, may be more sensitive to microwave radiation exposure than simple schedule control tasks, but in general the results of this study rule out the existence of low intensity microwave effects on repeated acquisition or discrimination in the rhesus monkey[33].

Roberti and coworkers[34] investigated the effect of 3 and 10.7 GHz microwaves on spontaneous motor activity of rats at field exposure times of up to

408 hours. No differences were found in spontaneous motor activity as a result of exposure. These results contradict the findings of Korbel[35] who reported that rats exposed to 0.3 - 0.9 GHz microwaves for twenty one days at power densities between 0.15 to 0.76 mW/cm^2 exhibited a decrease in motor activity. Another behavioral endpoint was considered by Thomas, *et al*[36] who studied changes in rats conditioned to respond to multiple schedules of reinforcement as a function of low-level microwave exposure. Exposures were for thirty minutes to 2.86 or 9.6 GHz PW microwaves at a pulse repetition rate of 500 Hz. Exposures to either S or X-band frequencies at intensities of 5 mW/cm^2 or greater induced significant alterations in the ongoing behavior of animals trained to respond on multiple reinforcement schedules. The results indicate that not only does low intensity microwave exposure produce CNS alterations, but also that such changes are influenced by the interaction of the organism with the environment[36].

Male rhesus monkeys, trained to respond on an auditory vigilance task were exposed[37] to 2.45 GHz microwaves at intensities of 4, 16, 32, 42, 52, 62, and 72 mW/cm^2 for 30, 60, or 120 minutes. Vigilance performance was not affected except by microwave exposure at the highest intensity. DeLorge[37], comparing the results of his study to other behavioral studies raises the question of the effect of heating and cooling on behavioral responses. The possibility that microwave induced behavioral changes may not be a direct effect of exposure but may instead be due to the heating-cooling cycle of the experimental animal is suggested. The results of such experiments would thus depend upon whether behavioral testing was done during microwave exposure or following exposure when the effect of body cooling would come into play.

Gillard and coworkers[38] exposed rats for two weeks to PW fields with an incident peak power of 2.3 W/cm^2 and an average power density of 0.7 mW/cm^2 at a frequency of 9.4 GHz, after which spontaneous behavior was measured. In sham-irradiated controls, locomotor activity, emotivity and vigilance decreased during the test, while exploratory activity increased. Pulsed field irradiated animals showed an increase in exploratory activity which was slower than the controls; vigilance first increased then decreased, and locomotor activity remained uniform[39]. The authors conclude that exposure to fields

which do not produce detectable temperature elevations alters CNS function in the rat.

Studies of the behavioral effects of low intensity microwave and radiofrequency radiation have produced what appear to be rather contradictory or inconsistent results. This may in part be attributed to the fact that these investigations have involved endpoints that consisted of a number of different functional responses, dependent upon a variety of mental functions. A functional response that appears to be affected consistently by microwave, radiofrequency and other frequencies and types of electromagnetic fields is the subjective judgement of the passage of time. Thomas, *et al*[36] as previously noted, found that exposure of rats to low intensity (*i.e.*, 5 mW/cm^2) pulse modulated microwaves altered the animal's ability to judge the passage of time, a result previously reported by Justesen[39] in the same species. Thomas and coworkers[40] have recently reported that PW 2.45 GHz microwaves at 5, 10, or 15 mW/cm^2 caused a dose-dependent increase in the frequency of premature switching in a fixed consecutive-number schedule in rats following thirty minute exposures, suggesting an alteration in time perception. Using a markedly lower radiation frequency, Gavalas-Medici and Day[41] found exposure of rhesus monkeys to 7 or 75 Hz fields at field strengths as low as 0.10 V/cm caused a reduction in interresponse times in agreement with the results of an earlier study employing a 0.07 V/cm, 7 Hz field[42]. At a field strength of 0.56 V/cm interresponse times were significantly shorter for both 7 and 75 Hz fields and the differences were almost three times greater than at a field strength of 0.10 V/cm. Another indication of an alteration in the "biological clock" was reported by Bliss and Heppner[43] who used a different temporally dependent endpoint, a different species, and a different type of exposure. They investigated the effects of exposure to a zero magnetic field on the entrainment of the circadian activity rhythm of the House Sparrow, *Passer domesticus*. Periodogram analysis showed that the activity period lengths of control birds were longer than the experimental birds. Midpoints of activity time were significantly later for controls than for experimentals[43].

Studies of the interaction of microwave radiation and various drugs that affect the mammalian CNS have also yielded evidence of the sensitivity of

neural elements to low field intensities. Goldstein and Sisko[44] and Cleary and Wangemann[45] detected alterations in the response of rabbits to anesthesia as a result of low intensity CW microwaves at 9.3 and 2.45 GHz respectively. Baranski and Edelwejn[46] investigated microwave-drug interactions in rabbits given CNS stimulants or depressants. Chloropromazine induced rapid synchronization of previously desynchronized EEG patterns which led the authors to conclude that there was an antagonistic interaction of microwaves with this drug which most likely occurred in the activating part of the reticular formation and the cerebral cortex[46]. Servantie, *et al*[47] also found that the susceptibility of mice to the effects of certain drugs was significantly altered by exposure to pulse modulated 3 GHz microwaves at an average intensity of 5 mW/cm^2.

Altered drug tolerance in humans occupationally exposed to microwaves has also been reported by Edelwejn and Baranski[45]. Intravenous injection of cardiazole (Metrazol), a drug which acts on the human CNS, did not induce any effects in normal adult males at a dosage level of 7 mg/kg body weight. However, the drug produced alterations in EEG patterns (theta waves, theta discharges and spike discharges) in microwave workers with over three years of exposure; convulsions occurred forcing the abandonment of the study as being hazardous to the patients. A marked decrease in cardiazole tolerance has also been demonstrated in microwave exposed rabbits[49].

Evidence has also been reported that occupational microwave exposure leads to alterations in human CNS function. The effects, many of which are of a subjective nature such as headaches and fatigue, reportedly occur during the first three months of employment and then recur after another three to four months. After one year of occupational exposure, the symptoms appear to remit for various lengths of time, suggested as being due to an adaptive response, but objective symptoms of various neurovegetative disturbances recur after approximately five years of exposure[50]. The chronic overexposure syndrome in humans is characterized by the occurrence of headaches, irritability, sleep disturbances, weakness, decrease in libido, chest pains, and generalized psycho-physiological depression[50]. Objective symptoms of chronic exposure

include acrocyanosis, hyperhydrosis, dermographism, hypotonia and arm and finger tremors. In general, these finding are attributed to a phasic adaptation response to occupational microwave exposure rather than a well defined clinical response[4]. Similar findings have been reported by Baranski and Czerski[4].

It may be concluded that exposure to microwave and modulated ELF and VHF fields results in a variety of alterations in biological systems, the mechanisms of which are presently obscure. The fact that thresholds for certain types of CNS alterations, such as behavioral changes in experimental animals, appear to be on the order of 10 mW/cm^2, and the fact that such fields are known to produce nonuniform energy absorption in the head, suggests the possibility that thermal gradients and/or nonuniform heating rates may be involved in such effects. The neurophysiological consequences of nonuniform, albeit, low-level brain heating are not well understood at present, preventing more definitive conclusions. Histological evidence of cytopathological alterations in hypothalamic and subthalamic neurons following acute microwave exposure suggests specific sensitivities of brain regions as well as specific cellular sensitivities. Site- and cell-specific microwave-induced alterations in the mammalian central nervous system are also consistent with the finding that specific types of behavioral changes appear to be induced by microwave exposure, such as altered time discrimination. Selective microwave sensitivities within the CNS are also suggested by the results of studies of microwave-drug interactions. Alterations in Ca^{2+} binding in cerebral tissue and in EEG patterns following exposure to pulse-modulated VHF fields and amplitude-modulated ELF fields at field strengths as small as 0.1 V/cm provide evidence of the extreme sensitivity of the mammalian CNS to low frequency and low amplitude electrical fields. A quantitative theory has not been developed to explain this phenomenon, but it has been suggested to involve electric field induced alteration in long range cooperative molecular interactions[29]. It has not yet been established that such effects are induced by microwaves modulated at ELF frequencies.

EFFECTS OF LOW INTENSITY FIELDS ON THE NEUROENDOCRINE SYSTEM

Considering the apparent sensitivity of the mammalian CNS to low intensity microwave irradiation, it would be expected that due to the intimate functional relationship of the CNS to the endocrine system, the latter system would also be affected by microwave-induced stress. The neuroendocrine system is the primary regulator of metabolism and growth and it also functions in the body's defense against both acute and long-term exogenous and endogenous stress. A primary effector of the neuroendocrine system, the hypothalamus, is the thermal control center. Alteration of the body's temperature set-point, either by microwave energy absorption or other factors, would activate a hypothalamic response leading to the release of pituitary hormones thus initiating a sequence of events involving the interactions of various other endocrine glands with concomitant physiological changes including altered hormone levels. The nature of the neuroendocrine stress response, which is in general an adaptive response, varies depending upon the type, magnitude and rate of stress. This must be taken into consideration in interpreting the results of studies of microwave effects on the neuroendocrine response since qualitatively and quantitatively different responses could result from variations in field intensity, duration of exposure, or mode of dose fractionation. Indeed, the reported neuroendocrine effects of microwave exposure include inconsistencies which may be attributed to such factors.

Table II summarizes the results of selected investigations of neuroendocrine effects of exposure to microwave fields of various frequencies and intensities. The specific, intensity dependent nature of such effects are typified by the results of Mikolajczyk[53]. Gonadotropic hormone levels in rats initially increased and then decreased eighteen hours post-exposure to 10 cm radiation at intensities of 10 mW/cm^2 or greater following single or repeated one hour exposures. Alterations in hypothalamic function were indicated by effects upon follicle stimulating hormone (FSH) levels and lutenizing hormone (LH). The growth hormone (GH) levels in rats exposed to 10 mW/cm^2 were not detectably affected. Under some irradiation conditions, GH release was stimulated; in other cases it was suppressed.

Conflicting results have been reported in the case of alterations of thyroid function in experimental animals following microwave exposure. Parker[62], for example, detected a 23% decrease in protein-bound iodine and a 55% decrease in serum thyroxine in rats following sixty hours of exposure to 2.45 GHz CW microwaves at 15 mW/cm^2. Howland and Michaelson[58] reported increased radioiodine uptake in dogs four to twenty-five days post-exposure to irradiation with 1.24 GHz pulse-modulated microwaves for 6 hrs/day for six days at an average power of 50 mW/cm^2. They also found that radioiodine uptake was increased three to four years after exposures at 100 mW/cm^2, suggesting irreversible thyroid dysfunction[58]. Baranski, *et al*[59] also reported increased radioiodine uptake in rabbits repeatedly exposed to 10 cm CW fields at intensities of 5 mW/cm^2. Histological and electronmicroscopic techniques revealed signs of thyroid hyperfunction[59]. No structural or functional changes, other than those attributable to thermal stress, were found by Milroy and Michaelson[61] who exposed rats continuously to 2.45 GHz CW microwaves at 1 mW/cm^2 for eight weeks or for 8 hrs/day at 10 mW/cm^2 for eight weeks.

The adaptive response of rats to microwave exposure following irradiation with 2.86 - 2.88 GHz CW microwaves at intensities between 10 to 120 mW/cm^2 was illustrated by the experiments of Mikolajczyk[63]. The survival time of hypophysectomized rats exposed to 120 mW/cm^2 fields was increased relative to unoperated animals. Alterations in corticosterone levels following 10 mW/cm^2 exposures were suppressed by allowing the animals to habituate to the experimental situation for two weeks prior to exposure. No alterations in FSH or LH levels were detected in another series of exposures at 10 mW/cm^2 that lasted for more than a month. Alterations in carbohydrate metabolism, a possible indirect neuroendocrine effect of microwave exposure, were induced by exposure of rabbits[56] to 3 GHz CW fields at 5 mW/cm^2.

The results of the reported studies of microwave effects on the mammalian neuroendocrine system do not provide a well-defined or specific response pattern. The effects, many of which were elicited by exposures at intensities in excess of 10 mW/cm^2, are consistent with a phasic adaptive stress response. The inconsistencies in the response patterns may be attributed to the specific nature of the heating rates and thermal gradients induced by

microwave as compared to nonradiation heating. Low intensity microwave exposures, which would involve low level gradual heating, would be expected to result in a generalized suppression of neuroendocrine response as reflected in metabolic suppression. Although data on the human response to low-level microwave exposure is very limited, the reported decrease in thyroid function in chronically exposed workers is consistent with this hypothesis.

HEMATOPOIETIC EFFECTS

Studies of the effects of microwave radiation on the mammalian hematopoietic system suggest a more consistent response pattern than neuroendocrine effects, although inconsistencies are again encountered. The results of a selected group of investigations of microwave effects on the hematopoietic system of experimental animals are summarized in Table III. In spite of the variety of microwave exposure conditions involved, certain general conclusions may be drawn from these results and from reported effects of occupational exposure of humans.

The data suggests that chronic low intensity microwave exposure differentially affects blood cells. Pulse-modulated fields generally induce more pronounced changes and microwave exposure results in qualitative and quantitative differences in the hematopoietic system as compared to the effects of nonradiation thermal stress. A rather consistent finding has been that microwave exposure causes transient lymphocytosis and leukocytosis. Erythrocytes appear to exhibit a somewhat lower sensitivity to exposure effects, with some suggestion of an exposure dependent decrease in erythrocyte production[64-66]. Alterations in nuclear structure and in the mitotic activity of erythroblasts, bone marrow cells, and lymphatic cells in both lymph nodes and spleen in guinea pigs and rats following prolonged exposures to 3 GHz microwaves at an intensity of 3.5 mW/cm^2 have been reported by Baranski[65]. Low intensity (3 mW/cm^2) exposures at 2.95 GHz for periods of one to three months altered the circadian rhythms in hematopoietic cell mitosis in rabbits[67]. Repeated daily exposures of mice and rabbits to 0.5 and 5 mW/cm^2 intensities respectively, to 2.95 GHz microwaves for periods of up to six

months, resulted in an increase in lymphoblasts in lymph nodes and in lymphoblastoid transformations during the first two months of exposure and for one month post-exposure, an effect which Czerski[68] indicates to be uniquely related to microwave exposure.

Evidence that low intensity microwave exposure may affect the immunological status of experimental animals is derived from studies of the hematopoietic response. The mobilization of bone marrow granulocyte reserve pools in response to six weeks of exposure at 3 mW/cm^2, as well as a reduction in lysozyme activity in the blood, has been reported by Szmigielski[69]. Microwave exposure has also been reported to increase the number of colony forming units (CFU) in the bone marrow and spleen of mice following a five minute exposure to 2.45 GHz CW microwaves at an intensity of 100 mW/cm^2, evidence of an induced transition of hematopoietic stem cells from a resting to an active state[66].

Hematopoietic alterations in occupationally exposed microwave workers have also been reported. The responses of two groups of microwave workers and an unexposed control group were reported by Sadcikova[70]. The microwave exposed groups showed specific clinical symptoms of microwave exposure but only minor changes in the peripheral blood were detected. Thrombocytopenia and a small decrease in red cell number as well as leukopenia were encountered in the exposed sample[70]. During the early periods of microwave employment, leukocytosis was encountered. Erythrocytes of members of one of the exposed groups reportedly showed signs of deterioration, with a tendency to spherocytosis and increased acid fragility, symptoms usually associated with cell aging. Indications of stimulation of erythropoiesis in bone marrow smears and decreased numbers of mature cells of the neutrophilic series were also detected. Biochemical studies of the serum of occupationally exposed microwave workers have also indicated microwave-induced alterations[71]. The levels of pyruvic acid, lactic acid, and creatinine in the urine were within normal limits, but twice as many potentially exposed individuals showed decreased levels as compared to controls. Increases in the fasting blood sugar levels were also encountered more frequently in microwave workers than in the controls. Serum protein was increased in 75% of the occupationally exposed individuals and elevated beta-

lipoprotein levels were twice as frequent in exposed individuals. Serum cholesterol elevations were found in 41% of the microwave workers compared to 9.5% for the controls[71].

On the basis of the results of investigations of the effects of human exposure and animal experimentation, some of which are summarized in Table III. it may be tentatively concluded that exposure to low intensity microwave and radiofrequency radiation induces transient hematopoietic alterations that appear to be dependent upon the exposure duration and modulation of the radiation field. Although the nature of the alterations are not inconsistent with a physiological response to nonspecific stress, the alterations are not equivalent to those attributable to nonradiation thermal stress. Differences in the response to radiation and nonradiation thermal stress may be due to differences in energy absorption or heating rates but such a conclusion is premature due to the inadequacy of the data. Regardless of the mechanisms, investigations of the effects of chronic low intensity microwave exposure on the mammalian hematopoietic system suggest alterations in immunocompetence, the consequences of which could be of particular significance with respect to the interaction of multiple stresses such as would be involved in microwave exposure of pathogen or drug-stressed animals or humans[3].

PHYSICAL INTERACTION MECHANISMS

The obvious problem encountered in the establishment of causal relationships for low intensity microwave-induced alterations in biological systems is the lack of physical interaction mechanisms to explain such phenomena. In spite of the fact that a number of hypothetical mechanisms, such as field-induced alterations in macromolecular hydrogen bonding, proton tunneling and disruption of bound water, have been suggested, no theoretical or experimental basis has been established for the occurrence of such mechanisms in either *in vivo* or *in vitro* biological systems. It may be concluded that since the energy of a microwave photon is far smaller than the activation energies estimated for such effects, quantized frequency-specific microwave absorption would not appear to be a feasible mode of interaction[72]. This conclusion, however, must

be qualified due to the fact that the activation energies are by and large based on estimates derived from *in vitro* molecular studies rather than *in vivo* systems in which high potential energy states are known to exist that could markedly alter activation energies for the above mentioned phenomena.

Relatively weak interactions or secondary forces are responsible for the molecular conformation as well as for the stabilization of macromolecular complexes such as biomembranes. In view of the fact that many biomolecular functions are dependent upon precise steric interactions, the integrity of the noncovalent secondary bonding is essential for biological function. Such secondary forces, including hydrophobic interactions, hydrogen bonds, and London-van der Waals interactions, correspond generally to significantly lower energies than covalent bonding. Although the actual energies associated with secondary bonding in *in vivo* systems are not known, the potentially low magnitude of such forces in cooperatively bonded *in vivo* macromolecular assemblages suggest that such systems could be subject to perturbation by low intensity microwave or radiofrequency fields. The involvement of cooperative weak secondary bonding and hydrophobic interactions in the stabilization of biomembrane structure and the transient nature of membrane molecular bonding as embodied in the fluid mosaic model of membrane structure draws attention to the biomembrane as a level of organization potentially sensitive to microwave or radiofrequency alterations. The induction of changes in the permeability of neuronal membranes by exposure to extremely weak electromagnetic fields reported by Bawin, *et al*[25,27] and Kaczmarek and Adey[26] provides experimental evidence that biomembranes are, in fact, sensitive to electromagnetic field perturbations. In reviewing the nature of the effects of low intensity microwave or radiofrequency fields on the mammalian central nervous system, the neuroendocrine system, the hematopoietic system, and other organ systems, it may be concluded that membrane alterations are not inconsistent with the reported effects. Obviously the present data is not adequate to support the conclusion that the physical interaction mechanism leading to altered biological function is dependent upon alterations in biomembranes by electromagnetic fields. The need for additional research to determine the effects of such fields on biomembranes is evident.

The most well-characterized interaction mechanism of alternating electromagnetic fields with biomolecules is field-induced rotation. Polar molecules, such as proteins or water, exhibit dielectric relaxation with frequency dispersions that are dependent upon molecular parameters such as size, shape, molecular weight, and dipole moment. Characteristic frequencies, the molecule-specific frequencies of maximum energy exchange with impressed fields, are in the region of 1 to 10 MHz for proteins in aqueous solution, and in the 20 GHz region for free water. A particular dispersion, referred to as the δ dispersion, which has been detected in the 0.1 to 1 GHz regions, is attributed to either field-induced rotation of protein polar sidechains or the rotation of bound water. Although dielectric relaxation of proteins and other biomolecules has been extensively investigated, whether or not this type of interaction results in functional alterations in living systems has not been determined. On the basis of data derived from *in vitro* dielectric dispersion studies of proteins, it appears that microwave or radiofrequency intensities of 10 mW/cm^2 or greater would be required for dielectric relaxation in living systems, although there is much uncertainty in this estimate[72]. It is thus difficult, in view of the paucity of the available information, to determine the role of dielectric relaxation in low intensity microwave or radiofrequency effects on biological systems.

SUMMARY AND CONCLUSIONS

The weight of the scientific evidence that has accumulated during the past few years, some of which is summarized in Tables I, II, and III, lends credence to the hypothesis that low intensity microwave and radiofrequency fields can, in some cases, result in physiological and psychological alterations. These alterations have generally been reported to be reversible and the effects are in many cases induced at intensities that may be associated with low level thermal stress. In experiments in which the effects of radiation heating and non-radiation heating on specific biological endpoints have been compared, more pronounced effects are usually induced by exposure to electromagnetic fields and in some instances decided qualitative differences have been detected. The

extent to which such differences may be attributed to variations in the heating patterns and/or heating rates is not evident at this time due to insufficient data. The rather consistent finding that pulse or amplitude-modulated microwave and radiofrequency fields produce more profound alterations in living systems, and the rather limited data on the frequency dependence of such effects, suggests that physical interactions other than those resulting in generalized heating may be involved in low intensity field effects in biological systems.

Physical interaction mechanisms other than field-induced rotation or dielectric relaxation of polar biomolecules are presently hypothetical. The possible significance of dielectric relaxation in *in vivo* systems exposed to microwave or radiofrequency fields has not been established. On the basis of the known characteristics of biological systems and of the types of effects induced by low intensity fields, the most likely interaction mechanism would appear to involve macromolecular assemblages stabilized by long-range systems of weak time-varying cooperative interactions. Taken with the experimental data on low intensity field effects, it may be suggested that biomembranes may be the primary site for microwave or radiofrequency alterations. There is an obvious need for additional research on the physical interactions of microwave and radiofrequency radiation with biological systems. The gaps in our knowledge that exist at present are so wide that it is not even possible to unequivocally specify the primary site of interaction.

TABLE I NEURAL EFFECTS OF EXPOSURE TO LOW-INTENSITY FIELDS

Independent Variables	Dependent Variables	Experimental Subject	Results and Comments	Reference
960 MHz, CW; 2-10 mW/g (closed system irradiation)	heart rate	isolated turtle heart *(in vitro)*	-bradycardia due to alteration in neurotransmitter release; -biphasic intensity response.	Tinney, *et al*[16]
2.45 GHz, CW; 0.3-1500 mW/g, PW; 0.3-2.2 × 10^5 mW/g temperature controlled exposure (closed system irradiation)	synaptic transmission; neural function	rabbit vagus nerves, superior cervical ganglia; rat diaphragm muscle *(in vitro)*	-no changes other than thermally-induced.	Chou and Guy[51]
10.5 cm, CW; 0.5-10 mW/cm^2; temperature controlled exposure (free space irradiation)	passive and dynamically electrical parameters	skeletal muscle, South American frog *(in vitro)*	-differential effect of microwave exposure on dependent variable time constants; -muscle cells from summer frogs more sensitive than winter frogs.	Portela, *et al*[52]
decimeter waves; 0.5 mW/cm^2 (free space irradiation)	neurotransmitter release in rabbit brain	rabbit *(in vivo)*	-decreased Ache activity	Syngajevskaja, *et al*[17]
10 cm; 1-25 mW/cm^2 (free space irradiation)	neurotransmitter release in brain	rabbits and guinea pigs *(in vivo)*	no alteration due to 8 month exposure at 1 mW/cm^2; -3 hr exposure at 3.5 mW/cm^2; no CW effect, PW decreased Ache activity (guinea pigs); -4 month exposure led to decrease for CW, increase for PW; -midbrain most affected; lipid and nucleoprotein metabolism altered (rabbit).	Baranski[20]
1.6 GHz; 80 mW/cm^2; environmental temperature (free space irradiation)	neurotransmitter release in brain	rats *(in vivo)*	-10 min exposure led to 4°C rectal temperature rise in irradiated and heated controls; -hypothalamic norepinephrine decreased in both groups; -serotonin decreased in hippocampus of irradiated animals only.	Merrit, *et al*[21]
1.7 GHz, CW; 10 and 25 mW/cm^2 (free space irradiation)	histological alterations in brain	Chinese hamster *(in vivo)*	-30 to 120 min exposure led to cytopathology in hypothalamic and subthalamic neurons; -no effect on other brain regions or on glial cells; -no repair evident 14 days post exposure.	Albert and DeSantis[22]
ELF fields, 1-75 Hz; 0.5-1 V/cm (closed system irradiation)	cerebral Ca^{+2} flux	isolated chick and cat cerebral tissue *(in vitro)*	-suppression in Ca^{+2} release from neurons; -biphasic intensity and frequency dependence; -maximum effect at 6 and 16 Hz; 0.1 and 0.56 V/cm.	Bawin and Adey[25]

TABLE I NEURAL EFFECTS OF EXPOSURE TO LOW-INTENSITY FIELDS

Independent Variables	Dependent Variables	Experimental Subject	Results and Comments	Reference
200 Hz; 10 msec pulsed field; 20-50 mV/cm	cerebral Ca^{+2} flux	cat -direct cortical stimulation *(in vivo)*	-20% increase in Ca^{+2} efflux from neurons	Kaczmarek and Adey[26]
147 MHz, AM modulated at 6, 9, 11, 16 Hz; 1-2 mW/cm^2 (closed irradiation system)	cerebral Ca^{+2} flux	chick forebrain *(in vitro)*	-increase in Ca^{+2} from neurons; -no change from unmodulated fields; -maximum rate of efflux at 11 and 16 Hz modulations.	Bawin, *et al*[27]
1.5 and 2.45 GHz, CW and PW (closed irradiation system)	electrical activity of individual neurons	Aplysia ganglia *(in vitro)*	-alterations in neuron firing patterns at intensity equivalent to 10 mW/cm^2 free field exposure; -effects attributed to ganglionic warming, but effects not produced by nonradiation heating.	Wachtel, *et al*[30]
2.45 GHz, CW.	functional alterations in neuronal elements	spinal cord of cats *(in vitro)*	-alteration in evoked potentials, also produced by nonradiation heating but with altered time course.	Taylor and Ashlemen[31]
3 GHz, PW; 5 mW/cm^2; pulse repetition rate 500-600 Hz (free field exposure)	electrical activity of cortical neurons	rat *(in vivo)*	-10 day exposure resulted in synchronization of electrocortical frequency; -synchronization persisted for hours after exposure	Servantie, *et al*[32]
2.45 GHz, CW; 5 to 25 W; 2 min exposure (applicator exposure of head).	behavioral modification (discrimination and repeated acquisition)	rhesus monkey *(in vivo)*	-convulsions induced at 15 and 25 W; -5 day, 40 min/day irradiation produced no behavioral deficits at less that 15 W; -no low-intensity effects.	Galloway[33]
3 and 10.7 GHz, CW; 0.5-26 mW/cm^2; 408 hr exposure (free field exposure).	behavioral modification (spontaneous motor activity)	rats *(in vivo)*	-no effects on spontaneous motor activity.	Roberti, *et al*[34]
0.3-9 GHz, CW; 0.15-0.76 mW/cm^2 (closed system exposure).	behavioral modification (spontaneous motor activity)	rats *(in vivo)*	-decrease in motor activity.	Korbel[35]
2.86 and 9.6 GHz PW; 5 mW/cm^2 or greater; pulse repetition rate 500 Hz (free field exposure).	behavioral modification (multiple schedules of reinforcement)	rat *(in vivo)*	-alteration in ongoing behavior; -changes influenced by interaction of organism with environment; -alteration in the ability to judge passage of time.	Thomas *et al*[36]
2.45 GHz, CW; 4-72 mW/cm^2; 30, 60, 120 min exposures (free field exposures).	behavioral modification (auditory vigilance task)	rhesus monkey *(in vivo)*	-vigilance performance not affected by exposure	deLorge[37]

TABLE I NEURAL EFFECTS OF EXPOSURE TO LOW-INTENSITY FIELDS

Independent Variables	Dependent Variables	Experimental Subject	Results and Comments	Reference
9.4 GHz, PW; 2.3 mW/cm^2 peak, 0.7 mW/cm^2 average; 2 week exposure (free field exposure).	behavioral modification (free field spontaneous behavior)	rat *(in vivo)*	-control results: decrease in locomotor activity, emotivity, and vigilance; increase in exploratory activity; -exposed results: increased exploratory activity (slower than controls); -increase then decrease in vigilance, uniform locomotor	Gillard, *et al*[38]
2.45 GHz, PW; 5, 10, 15 mW/cm^2 30 min exposures (free field exposure).	behavioral modification (fixed consecutive number switching frequency)	rat *(in vivo)*	-dose dependent increase in the frequency of premature switching (alteration in time perception).	Thomas, *et al*[40]
7 or 75 Hz sinusoidally modulated fields; 0.1V/cm.	behavioral modification (interresponse interval response time)	rhesus monkey *(in vivo)*	-reduction in interresponse times at 0.56 V/cm, interresponse 3x times shorter for 7 and 75 Hz than at 0.10 V/cm.	Gavalas-Medici and Day[41]
magnetic field strength (zero field *vs* natural field) (free field exposure).	behavioral modification (entrainment of circadian activity rhythm)	House sparrow *(in vivo)*	-activity period lengths of controls longer than experimentals; midpoints of activity time later for controls.	Bliss and Heppner[43]
9.3 GHz, CW; 0.7-2.8 mW/cm^2; 5 min exposure (free field exposure).	amplitude of cortical brain waves in anesthesized animals (pentobarbital)	rabbit *(in vivo)*	-atypical arousal phenomena 3 to 12 min postexposure followed in 3 to 5 min by longer period of arousal; -atypical behavior.	Goldstein and Sisko[44]
2.45 and 1.7 GHz, CW and PW; 5 to 50 mW/cm^2 (free field exposure).	duration of pentobarbital-induced sleeping time	rabbit *(in vivo)*	-dose dependent analeptic effect.	Cleary and Wangemann[45]
3 GHz, PW; 5 mW/cm^2 average; daily exposure (free field exposure).	effects of drugs on CNS	mice *(in vivo)* rats *(in vitro)*	-exposure delayed onset of pentetrazol-induced convulsion during first 15 days of exposure, reduced latency after 15 days; -decreased susceptibility to curare-like drugs in *in vivo* and *in vitro* systems.	Servantie, *et al*[47]
occupational microwave and RF exposure.	CNS drug tolerance (cardiazole)	humans *(in vivo)*	-altered EEG patterns and convulsions in workers with over 3y microwave exposure (similar results reported in rabbits).	Baranski[48],[49]
occupational microwave and RF exposure.	CNS functional disorders	humans *(in vivo)*	-transient subjective complaints during 1st year of exposure; -phasic adaptation after 1 year; -objective symptoms of neuro-vegetative disturbances after 5 years of exposure (acrocyanosis, hyperhydrosis, dermographism, hypotonia tremors).	Petrov[50]

TABLE II NEUROENDOCRINE EFFECTS OF EXPOSURE TO LOW-INTENSITY FIELDS

Independent Variables	Dependent Variables	Experimental Subject	Results and Comments	References
10 cm, CW; 0.01, 1, 3, 10, 20, and 150 mW/cm^2; 1h/day, single or repeated exposures	endocrine gland hormone levels	rats (*in vivo*)	-increase in gonadotropic hormones followed by decrease 18h postexposure for 10 mW/cm^2 or greater intensities; -alteration in hypothalamic function governing FSH and LH release from pituitary; -no changes in corticosteroid content of adrenals or blood at 10 mW/cm^2 for 15, 30, or 60 min.	Mikolajczyk[53]
10 cm, CW; 50-60 mW/cm^2, 4h/day	adrenal function	rabbits (*in vivo*)	-decrease 7-OCHS in urine, 1st 20 exposures; -return to normal at day 10 due to adaptation; -no changes in 17-CS in urine.	Leńko, *et al*[54]
10 cm, CW; 100 mW/cm^2 10 min exposure/day for 14 days	adrenal alterations	rats (*in vivo*)	-initial decrease in Sudan III positive lipids, birefringent substances, and ascorbic acid; -increase in all variables during course of exposure; -return to normal 2 weeks postexposure.	Leites and Skurichina[55]
10 cm, CW; 5 mW/cm^2 (free field exposure)	carbohydrate metabolism, skeletal muscle metabolism	rabbits (*in vivo*)	-changes in serum pyruvic and lactic acid; -decrease in skeletal muscle glycogen; -altered EMG indicative of changes in muscle metabolism; -altered carbohydrate metabolism.	Baranski, *et al*[56]
decimeter waves, 40 mW/cm^2; 1 hr daily exposure, prolonged duration	adrenal cortex alterations, serum electrolytes	rats (*in vivo*)	-no effect on serum Na^+ or K^+; -increase in Ca^{+2} and Cl^- in serum and urine.	Nikogasjan[57]
1.24 GHz, PW; 360 HZ pulse repetition rate; 2 msec pulse, 50 mW/cm^2; avg. power; 6 hr/day fir 6 days.	thyroid alterations	dogs (*in vivo*)	-increased radioiodine uptake 4 to 25 days postexposure; -radioiodine uptake increased 3-4 yrs postexposure to single 100 mW/cm^2 exposure to 1.28 GHz, PW.	Howland and Michaelson[58]
10 cm, CW; 5 mW/cm^2, repeated exposure	thyroid function	rabbits (*in vivo*)	-increased radioiodine uptake -histologic and electron-microscopic signs of thyroid hyperfunction.	Baranski, *et al*[59]
meter, decimeter waves; 70 mW/cm^2; 30 min.	endocrine function	dogs rabbits, (*in vivo*)	-increased adrenal ascorbic acid concentration following 70 mW/cm^2; -decrease following 5 mW/cm^2; -thermal intensities suppress pituitary and adrenal functions; -low-intensity exposure stimulates.	Syngayevskaya[60]
2.45 GHz, CW; 1 mW/cm^2; continuous exposure, 8 wks; 10 mW/cm^2, 8 hr/day for 8 weeks.	thyroid function	rats (*in vivo*)	-no structural or functional changes other than attributable to thermal stress.	Milroy and Michaelson[61]
2.45 GHz, CW; 15 mW/cm^2; 60 hr exposure.	thyroid function	rats (*in vivo*)	-23% decrease in protein-bound iodine and 55% decrease in serum thyroxine	Parker[62]
2.86-2.88 GHz, CW; 10-120 mW/cm^2	survival time, endocrine function	rats (*in vivo*)	-survival time of hypophysectomized rats increased at 120 mW/cm^2; -2 week habituation before exposure at 10 mW/cm^2 suppressed alterations in corticosterone levels; -daily exposures at 10 mW/cm^2 for > 1 mon. did not alter gonadotropins (LH and FSH); -single exposures induced detectable alterations	Mikolajezyk[63]

TABLE III HEMATOPOIETIC EFFECTS IN EXPERIMENTAL ANIMALS

Investigator (Ref)	Radiation Frequency (GHz)	Intensity (mW/cm^2)	Exposure Duration	Species	Results ↑ denotes increase ↓ denotes decrease
Deichman[14]	24	20,10	varied	rat	-leukocyte↑ -lymphocyte↑ -neutrophil↑ -all cell counts returned to normal in 7 days
Kitsovskaya		10 to 100	varied	rat	-leukocyte↓
Michaelson	1.28,2.8	100-165	7 hr.	dog	-maximum increase in ^{59}Fe incorporation at 45 days post-exposure
Baranski[17]	3.0	3.5	4 hr/day	rats	-leukocyte↑ -altered nuclear structure -altered mitotic activity in erythroblasts, bone marrow cells and lymphatic cells in lymph nodes and spleen
Rotkovska and Vacek[18] Vacek[18]	2.45	100	5 min.	mice	-leukocyte↑ (two maxima) -total cell volume in the bone marrow and spleen↓ -^{59}Fe incorporation into spleen↑ -nucleated cells in spleen↓ immediately postexposure -nucleated cells in spleen↑ 4-7 days postexposure -total cell number in femur↑ 5-7 days postexposure -colony forming unit numbers of stems cell↑, return to normal by 12 hrs. postexposure
Czerski[21]	2.95	3	2 hr/day for 37 days pulsed and CW. 2 hr/day for 79 days CW	rabbits	-erythrocyte production↓ -alterations in circadian rythms in hematopoietic cell mitosis
Czerski[22]	2.95	0.5	2 hr/day for	mice	-lymphoblasts in lymph nodes↑ -lymphoblastoid transformations↑ during first 2 months and 1 month postesposure
Szmigielski[24]	3	1;5	15,30, 60 min	granulocyte cells in culture	-liberation of hydrolases (1 mW/cm^2) -cell death (5 mW/cm^2; 60 min) -lysosomal enzyme release (5 mW/cm^2; 60 min)
Wangemann and Cleary[27]	2.45	5,10,25	2 hr.	rabbit	-serum Glucose↓ -blood urea nitrogen↑ -uric acid↓ -all values return to normal 7 days postesposure

REFERENCES

1. *Biological Effects of Non-ionizing Radiation*, E. Tyler, ed., Ann. New York Acad. Sci. 247 (1975).

2. *Biological Effects of Electromagnetic Waves*, Selected Papers of the USNC/URSI Annual Meeting, Boulder, Col., October 1975. C. C. Johnson and M. L. Shore, ed., HEW Publication (FDA) 77-8010, December 1976.

3. S. F. Cleary, in *Biological Effects of Microwave and Radiofrequency Radiation*, CRC Critical Reviews in Environmental Control, CRC Press, Cleveland, Ohio 1977.

4. S. Baranski and P. Czerski, in *Biological Effects of Microwaves*. Dowden, Hutchinson and Ross, Inc., Stroudsburg, Pa. 1976.

5. P. Brodeur, New Yorker Magazine, December 13, 1976.

6. A. R. Shapiro, R. F. Lutomirski and H. T. Yura, IEEE Trans. MTT-19, 187 (1971).

7. C. C. Johnson and A. W. Guy, Proc. IEEE 60, 692 (1972).

8. T. Nakayama, *et al*, Am. J. Physiol. 204, 1122 (1963).

9. H. P. Schwan, in *Biological Effects and Health Implications of Microwave Radiation*, S. F. Cleary, ed. BRH/DBE 70-2 (PB 193 858) Rockville, Maryland (1970).

10. J. Bernhardt and H. Pauly, Biophysik 10, 89 (1973).

11. M. Klee and R. Plonsey, IEEE Trans. BME-23, 347 (1976).

12. M. G. F. Fuortes, K. Frank and R. Becker, J. Gen. Physiol. 40, 735 (1957).

13. L. Hause, in *Electroanesthesia: Biomedical and Biophysical Studies*. A. Sances and S. J. Larsen, ed. Academic Press, New York, p. 176 (1975).

14. C. A. Terzuolo and T. H. Bullock, Proc. Nat. Acad. Sci. 42, 687 (1956).

15. H. G. L. Coster, Biophys. J. 5, 669 (1965).

16. C. E. Tinney, J. L. Lords and C. H. Durney, IEEE Trans. MTT-24, 18 (1976).

17. V. A. Syngajevskaja, O. S, Ignatiera and T. P. Pliskina. (Cited in (4), p. 112). (1962).

18. V. A. Syngajevskaja. (Cited in (4), p. 112). (1968).

19. S. V. Nikogosjan. (Cited in (4), p. 112) (1960).

20. S. Baranski. (Cited in (4), pps. 108-112). (1967).

21. J. H. Merritt, R. H. Hartzell and J. W, Frazer. in *Biological effects of Electromagnetic Waves*, Proc. 1975 USNC/URSI Annual Meeting, HEW Publication (FDA) 77-8010 (1976).

22. E. N. Albert and M. DeSantis, in *Biological Effects of Electromagnetic Waves*, Proc. 1975 USNC/URSI Annual Meeting, HEW Publication (FDA) 77-8010 (1976).

23. M. S. Tolgkaya: in *Soviet Research on the Neural Effects of Microwaves*, p. 7, trans. C. Dodge, *et al.* ATD Abstracts, Washington, D. C. (1966).

24. S. Baranski, Amer. J. Phys. Med. 51, 182 (1972).

25. S. M. Bawin and W. R. Adey, Proc. Natl. Acad. Sci. 73, 1999 (1976).

26. L. K. Kaczmarek and W. R. Adey, Brain Res. 66, 537 (1974).

27. S. M. Bawin, L. K. Kaczmarek and W. R. Adey, Ann. New York Acad. Sci. 247, 74 (1975).

28. S. M. Bawin, R. J. Gavalas-Medici and W. R. Adey, Brain Res. 58, 365 (1973).

29. S. M. Bawin and W. R. Adey, in *Biological Effects of Electromagnetic Waves*, Proc. 1975 USNC/URSI Annual Meeting, HEW Publication (FDA) 77-8010 (1976).

30. H. Wachtel, R. Seaman and W. Joines, in *Biological Effects of Non-ionizing Radiation*, P. Tyler, ed. Ann. New York Acad. Sci. 247, 46 (1975).

31. E. M. Taylor and B. T. Ashlemen, in *Biological Effects of Non-ionizing Radiation*, P. Tyler, ed. Ann. New York Acad. Sci. 247, 63 (1975).

32. B. Servantie, A. M. Servantie and J. Etienne, in *Biological Effects of Non-ionizing Radiation*, P. Tyler, ed. Ann. New York Acad. Sci. 247, 82 (1975).

33. W. D. Galloway, in *Biological Effects of Non-ionizing Radiation*, P. Tyler, ed. Ann. New York Acad. Sci. 247, 410 (1975).

34. B. Roberti, *et al*, in *Biological Effects of Non-ionizing Radiation*, P. Tyler, ed., Ann. New York Acad. Sci. 247, 417 (1975).

35. S. F. Korbel, in *Biological Effects and Health Implications of Microwave Radiation*, S. Cleary, ed., BRH/DBE 70-2 (PB 193 858) Rockville, Md. (1970).

36. J. R. Thomas, E. D. Finch, D. W. Fulk and L. S. Burch, in *Biological Effects of Non-ionizing Radiation*, P. Tyler, ed., Ann. New York Acad. Sci. 247, 410 (1975).

37. J. O. deLorge, in *Biological Effects of Electromagnetic Waves*, C. C. Johnson and M. L. Shore, ed., Proc. 1975 USNC/URSI Annual Meeting, HEW Publication (FDA) 77-8010 (1976).

38. J. Gillard, *et al*, in *Biological Effects of Electromagnetic Waves*, C. C. Johnson and M. L. Shore, ed., Proc. 1975 USNC/URSI Annual Meeting, HEW Publication (FDA) 77-8010 (1976).

39. D. R. Justesen in *Digest of Papers*, Joint U. S. Army/Georgia Institute of Technology Microwave Dosimetry Workshop, M. Grove, ed., Walter Reed Army Institute of Research, Washington, D. C., 78 (1971).

40. J. R. Thomas, S. S. Yeandle and L. S. Burch, in *Biological Effects of Electromagnetic Waves*, C. C. Johnson and M. L. Shore, ed., Proc. 1975 USNC/URSI Annual Meeting, HEW Publication (FDA) 77-8010, 201 (1976).

41. R. Gavalas-Medici and S. R. Day, in *Biological Effects of Electromagnetic Waves*, C. C. Johnson and M. L. Shore, ed., Proc. 1975 USNC/URSI Annual Meeting, HEW Publication (FDA) 77-8010, 215 (1976).

42. R. J. Gavalas, D. O. Walter, J. Hamer and W. R. Adey, Brain Res. 18, 491 (1970).

43. V. L. Bliss and F. H. Heppner, in *Biological Effects of Electromagnetic Waves*, C. C. Johnson and M. L. Shore, ed., Proc. 1975 USNC/URSI Annual Meeting, HEW Publication (FDA) 77-8010, 225 (1976).

44. L. Goldstein and F. Sisko, in *Biological Effects and Health Hazards of Microwave Radiation*, Polish Medical Publishers, Warsaw, Poland (1974).

45. S. F. Cleary and R. W. Wangemann, in *Biological Effects of Electromagnetic Waves*, C. C. Johnson and M. L. Shore, ed., Proc. 1975 USNC/URSI Annual Meeting, HEW Publication (FDA) 77-8010, (1976).

46. S. Baranski and Z. Edelwejn, in *Biological Effects and Health Hazards of Microwave Radiation*, Polish Medical Publishers, Warsaw, Poland (1974).

47. B. Servantie, *et al*, in *Biological Effects and Health Hazards of Microwave Radiation*, Polish Medical Publishers, Warsaw, Poland (1974).

48. Z. Edelwejn and S. Baranski, Lek. Wojsk. 42, 781 (1966).

49. S. Baranski and Z. Edelwejn, Acta. Physiol. Polon. 19, 37 (1968).

50. I. R. Petrov (ed.). *Influence of Microwave Radiation in the organism o of Man and Animals*, NASA TT-F-708, Feb. 1972.

51. C-K. Chou and A. W. Guy: *The Effects of Electromagnetic Fields on the Nervous System*, Scientific Report No. 6, Bioelectromagnetic Research Laboratory, Department of Rehabilitation Med., Univ. of Washington, School of Medicine, Seattle, Wash. (1975).

52. A. Portela, *et al*, *Transient Effects of Low Level Microwave Irradiation on Muscle Cell Bioelectric Properties, Water Permeability and Water Distribution*, (Contract No. N00014-68-C-01313) (1975).

53. H. Mikolajczyk, Med. Lotnicza 39, 95 (1972).

54. J. Leńko, A. Dolatowski, L. Gruszecki, S. Klajman, and L. Januszkiewicz: Przeglad LeKarsbi 22 (Series II), 296 (1966).

55. F. Leites, and L. A. Skurichina, Bjul. Eksper. Biol. Med. 52, 47 (1961).

56. S. Baranski, Z. Edelwejn and Z. Kaleta, Med. Lotnicza 24, 103 (1967).

57. S. V. Nikogosjan, in *Voprosy Biologitcheskogo Dieistvija Sverchvysokotchastotnogo (SVTch) Electromagnitnogo Polja*, Tez. Nautch. Konf. Leningrad p. 33 (1962).

58. J. W. Howland and S. Michaelson, in *Proceedings Third Annual Tri-Service Conference on Biological Hazards of Microwave Radiating Equipment*. C. Susskind, ed., Univ. of California, Berkeley, Calif. 25 (1959).

59. S. Baranski, K. Ostrowski and W. Stodolnik-Barańska, Acta Physiol. Polon. 23, 608 (1973).

60. V. A. Syngayevskaya, G. F. Pleskena-Sinenka and O. S. Ignatyeva, in *Questions of the Biological Effects of SHF-VHF Electromagnetic Fields*, Kirov Order of Lenin Military Medical Academy, Leningrad, USSR, p. 50 (1962).

61. W. C. Milroy and S. M. Michaelson, Aerospace Med., 43, 1126 (1972).

62. L. N. Parker, Amer. J. Physiol. 224, 1388 (1973).

63. H. J. Mikolajczyk, in *Biological Effects and Health Hazards of Microwave Radiation*, Polish Medical Publication, Warsaw, Poland, 46 (1974).

64. W. J. Deichman, J. Miale and K. Landeen, Toxicol. Appl. Pharmacol. 6, 71 (1964).

65. S. Baranski, Aerospace Med., 42, 1196 (1971).

66. D. Rotkovska and A. Vacek, Ann. New York Acad. Sci. 247, 243 (1975).

67. S. Baranski, P. Czerski and S. Szmigielski, Postepy. Fiz. Med. 6, 93 (1971).

68. P. Czerski, Ann. New York Acad. Sci. 247, 232 (1975).

69. S. Szmigielski, J. Jeljas and M. Wiranowska, Ann. New York Acad. Sci. 247, 305 (1975).

70. M. N. Sadcikova, in *Biological Effects and Health Hazards of Microwave Radiation*, Polish Medical Publishers, Warsaw, Poland, 268 (1974).

71. E. KlimKova-Deutschova, in *Biological Effects and Health Hazards of Microwave Radiation*, Polish Medical Publishers, Warsaw, Poland, 268 (1974)

72. S. F. Cleary, Health Phys. 25, 387 (1973).

MOLECULAR ABSORPTION OF NON-IONIZING RADIATION IN BIOLOGICAL SYSTEMS

Karl David Straub

Veterans Administration Hospital and Departments of Medicine and Biochemistry
University of Arkansas for Medical Sciences, Little Rock, Arkansas 72206

ABSTRACT

Absorption of non-ionizing electromagnetic (EM) radiation by biologically important molecules can occur by many different mechanisms over the frequency range from several Hertz through the millimeter microwave region. The absorption of EM radiation is determined by the bulk dielectric properties of living tissues, cells and biomolecules in solution. However, the existence of diverse and complex molecular structures characteristic of biological systems makes it necessary to consider the details of absorption and dissipation of EM energy. In addition, the biological function of the molecular species absorbing energy needs to be studied to understand the significance of the EM absorption. Among many possible examples the following five are given: (1) The network of membranous lipid-containing structures within and at the outside limit of cells poses a series of barriers to thermalization of the absorbed radiation. Thus, adiabatic conditions may be maintained in small membrane-bound volumes for much longer periods of time than in simple solution. Large thermal gradients and temperature elevations can result. (2) Subsequent temperature elevation may cause membrane structures or complex protein assemblies to pass through phase transitions, altering their properties. (3) Spatial anisotrophy in the arrangement of large molecular assemblies such as found in mitochondria and ribosomes results in specialized functions which can be completely changed if some of the molecules are rotated or translated by EM radiation. (4) Quantum effects such as proton tunneling with resulting isomerization of DNA base pairs may also be influenced by EM radiation. (5) Otherwise random motion of "gates" in excitable channels of nerve membranes may be brought into forced oscillation by EM radiation, with resultant membrane depolarization. Detailed knowledge of structure and function of the biological system thus reveals many perturbations which might be induced by EM absorption, and, conversely, EM radiation can be used to probe biological structure and function.

The bulk dielectric properties of biological material have been under investigation for over 50 years. The dielectric constants of the molecular constituents of living cells and the complicated assembly of cells and organs have been measured at frequencies from below 100 Hz to over 10 GHz. The dispersions of dielectric constant with frequency seen in various tissue and cellular suspensions can be understood in terms of certain specific relaxation mechanisms. Schwan and Kay[1] observed in muscle tissue three regions of dispersion of the dielectric constant which they called the α region at about 100 Hz, the β region which occurs between 100 KHz and 1 MHz and the γ region at 10-20 GHz. Subsequent studies have identified dielectric dispersion of water not only in the 10-20 GHz range observed for "free" water, but also dispersions of ice at 1-10 KHz and a dispersion between 50 and 200 MHz due to "bound" water held in the sphere of hydration of macromolecules such as proteins[2-4]. Thus, the dispersion in tissue is composed in part of relaxation of water in various states of association with cellular structures which limit rotation to a greater or lesser extent.

Rotation of water is characteristic of dielectric dispersion of small polar molecules and even the polar side chain of larger molecules such as proteins. Thus, Pennock and Schwan[3] determined that dispersion in hemoglobin solution between 50 and 100 MHz was due to rotation of polar side chains. The dispersion in the regions between 1 MHz and 100 MHz is further complicated by the finding[5] that there exists an additional dispersion due to the induced dipole moment of the protein backbone which has a dielectric constant greater than 20. Other large macromolecular constituents of the cell may also be expected to have such induced dipole moments. Finally, the helix-coil transition in proteins also has a relaxation in this region sometimes called the "chemical" relation[6]. Such dispersions due to conformational transitions may contribute little to the overall dielectric constant even at their maximum dispersion; however, conformational transition induced by electromagnetic radiation may have functional effects, although the displacement from the already rapid transitions due to thermal agitation is quite small.

At lower frequencies, larger cellular structures become responsible for dispersion. In the β region, Schwan[7] has attributed the dispersion to the

change in polarization which occurs at the boundary of phases of different dielectric constant, the so-called Maxwell-Wagner effect. In the cell, the most likely boundary is the cell membrane where a lipid-water transition occurs. Such an interpretation was further verified using the dielectric dispersion of yeast at 100 KHz. Upon treatment with cetyl trimethyl ammonium bromide, a detergent which disrupts the cell membrane, the 100 KHz dispersion disappeared[8].

Most tissues and cells exhibit a strong dispersion in the α region at 100 Hz and below, with the apparent dielectric constants increasing to very large values, with even DNA having a dielectric constant of 240-340 at 100 Hz[9]. At least part of the dispersion at these low frequencies can be ascribed to movement of ionic countercharges in the fixed charge latticework of large assemblies of macromolecules such as bacterial cell walls; the same dispersion can be seen in ionic exchange resins[10].

While the bulk dielectric constants of living matter can be fairly well understood by the foregoing discussion, other more highly specific absorptions of electromagnetic radiation may be important but not be observable against the background of strong absorption by the more non-specific mechanisms.

It was pointed out by Löwdin[11] several years ago that the DNA double helix formed by complementary hydrogen-bonded base pairs could have the position of the proton shifted from one nucleic acid to its complementary neighbor by a tunneling process. Subsequent replication of the sequence would then yield a complete alteration of the base pair from A-T to G-C or vice versa. In the same paper[11], the author suggested that such a tunneling process might be induced by electromagnetic radiation of the proper frequency. No experimental evidence of such assisted tunneling in DNA has yet been reported. However, it is interesting to note that recent experiments[12] indicate that at low temperatures ($< 25^{\circ}K$) carbon monoxide can tunnel to form a ligand in heme proteins. The possibility of tunneling of large atomic masses such as CO and assistance by electromagnetic radiation at lower frequencies bears further investigation.

The highly oriented assemblies of macromolecules which make up functioning units of the cell such as ribosomes or mitochondria depend on correct

positioning of neighboring molecules for sequential reactions[13]. The induction of rotation of one or more molecules within such an assembly might disrupt function transiently or permanently if the rotation is to a new stable position. No experimental evidence is available concerning such rotation, but measurements of the functioning of the assembly would probably be much more sensitive to such an effect than measurements of dielectric constant.

Another possible interaction of electromagnetic fields in living cells might occur by bringing into forced oscillations "gating" molecules which are postulated to control ionic conductivity in excitable membranes. Armstrong and Bezanilla[14] have attributed the frequency dependent capacitance of squid axons to these gating molecules[15]. Polarization currents dependent on membrane potential in muscle membrane are also thought to be due to gating molecules with large permanent dipole moments[16]. While single peak-to-peak amplitude of external a-c fields would need to be large to cause the gate molecules to undergo a transition, much smaller amplitudes could cause transitions over a period of time if the gating molecules were brought into gradually increasing forced oscillations.

Whatever the mechanisms of absorption of electromagnetic radiation, the energy absorbed must be dissipated and thermalized. The rate and pathways of thermalization of absorbed energy in the living system have been little explored. Recent studies[17] using laser enhanced chemical reactions in the gas phase, have indicated that equipartition of electronic energy into vibrational modes is not immediate but may take as long as 10^{-5} sec. Such slow distribution of energy allows time for enhanced reactivity of one particular vibrational mode[18]. If such unexpected delays in reaching thermal equilibrium occur in rotational and translational excitations, enhanced reaction rates might be observed in living systems excited by electromagnetic radiation of comparatively low frequencies.

Barriers to thermalization might well be cellular structures with low thermal conductivity such as the cell membrane. As a consequence of electromagnetic radiation absorption within a relatively thermally isolated volume, energy dissipation would be slowed enough so that temperature rise would occur in that volume. At least in one model membrane system, detergent

vesicles, temperature rise was seen to occur and persist after visible light excitation of a dye within the vesicles[19]. Highly localized temperature elevations due to thermal barriers might then cause susceptible proteins to denature even if the temperature elevation is not more than 8-10°C. Some denaturations of proteins can occur over very narrow temperature ranges[20].

In addition, temperature dependent phase transitions in lipid membranes can be induced over the entire physiological range. In several membrane-bound enzyme systems the transition of the lipid phase is accompanied by functional changes in certain membrane-bound enzyme activity[21,22].

Because of the thickness of the cell membranes (~100 Å), even a small absolute difference in temperature between two sides of the membrane results in a large thermal gradient across the cell membrane. Such thermal gradients can be coupled to flow of solutes and solvents known as the Ludwig-Soret effect. The phenomenological equation can be written in terms of non-equilibrium thermodynamics[23]. In cell membranes, the thermal diffusion coefficient is undetermined but with large thermal gradients both ionic and osmotic gradients could be established.

Further analysis should include consideration of behavior of membranes as thin films, the existence of electrically ordered domains within the cell or at the membrane, and the restrictions on relaxation mechanisms due to finite small size of the molecular structures of the cell. Experimental techniques are presently capable of exploring most of the proposed interactions of non-ionizing electromagnetic radiation with biological materials. In addition, detailed molecular mechanisms of energy absorption and dissipation are being formulated in simpler systems which may have important implications for biological assemblies.

REFERENCES

1. H. P. Schwan and C. F. Kay, Ann. N. Y. Acad. Sci. 65, 1007 (1957).
2. H. P. Schwan, Ann. N. Y. Acad. Sci. 125, 344 (1965).
3. B. E. Pennock and H. P. Schwan, J. Phys. Chem. 73, 2600 (1969).
4. E. H. Grant, G. P. South, S. Takashiwa and H. Ichimura, Biochem. J. 122, 691 (1971).
5. R. H. Tregold and P. N. Hole, Biochen. Biophys. Acta 443, 137 (1976).
6. G. Schwartz and J. Seelig, J. Biopolymers 6, 1263 (1968).
7. H. P. Schwan, Adv. Biol. Med. Phys. 5, 147 (1957).
8. Y. Sugiura and S. Kaga, Biophysical J. 5, 439 (1965).
9. D. N. Goswani and N. N. Das Gupta, Biopolymers 13, 1549 (1974).
10. C. W. Einolf and E. L. Carstensen, J. Phys. Chem. 75, 1091 (1971).
11. P. Löwdin, Biopolymers, Symp. 1, 161 (1964).
12. N. Alberding, R. H. Austin, F. W. Beeson, S. S. Chan, L. Eisenstein, H. Frauenfelder and T. M. Nordlund, Science 192, 1002 (1976).
13. V. P. Skulachev, in *Energy Transducing Mechanisms*, E. Racker (ed.), University Park Press, Baltimore, p. 31 (1975).
14. C. Armstrong and F. Bezanilla, Ann. N. Y. Acad. Sci. 264, 265 (1975).
15. S. Takashima and H. P. Schwan, J. Memb. Biol. 17, 51 (1974).
16. W. Almers, R. H. Adrian and S. R. Levinson, Ann. N. Y. Acad. Sci. 264, 278 (1975).
17. A. Yogev and Y. Haas, Chem. Phys. Letts. 21, 544 (1973).
18. A. Kaldor, W. Braun and M. Kurylo, J. Chem. Phys. 61, 2496 (1974).
19. E. Balint, J. Hevesi and E. Lehoczki. Presented at First European Biophys. Congr., Vienna (1971).
20. P. J. Flory, J. Cellular Comp. Physiol. 49, Suppl. 1, 175 (1957).
21. N. Gruener and Y. Avi-Dor, Biochem. J. 100, 762 (1966).
22. J. S. Charnock, D. A. Cook and R. Casey, Arch. Biochem. Biophys. 147, 323 (1971).
23. A. Katchalsky and P. F. Curran, *Nonequilibrium Thermodynamics in Biophysics*, Harvard University Press, Cambridge, Mass., p. 181 (1967).

* *

DISCUSSION

I would like to emphasize that, of course, the double well hydrogen bond is asymmetric. As far as I know, the most complete treatment of the DNA problem was a calculation by von Meissen in 1967-68, who schematically investigated the movement of hydrogen from one set of base pairs to the other in a concerted sense. That is to say, movement in which one hydrogen will move in one direction and the other will move the opposite way. Because, if only a single hydrogen moves ionization results and that is a very unlikely process. Owing to the fact that their computational facility was not sophisticated enough to have a large enough basis for the electronic wave functions for the electrons involved here, a double minimum for this concerted motion was not seen. However, when that calculation was repeated for the simplest case, formic acid, there were fewer electrons involved and it was possible to use a large basis for their calculation, a double minimum for this concerted motion was seen. Thus, it is an open question. To turn to another point, the matter of vibrational relaxation is very important. It has been known experimentally with respect to vibrational relaxation in colliding gas molecules, for quite a while, that vibrational relaxation is much less efficient than rotational. If one asks the question how rapidly does an induced rotation relax, whether it be induced by electromagnetic f field or by molecular collision, it is clearly much more efficient in rotation than a vibrational excitation. Therefore, the interesting effects which you alluded to as having to do with vibrational relaxation are going to occur at much higher than megahertz or gigahertz frequencies. There aertainly certainly must be an effect in the infrared region where vibrational effects localized to a specific portion of the molecule are important. As to the matter of moving dipoles inside a membrane, there have been other experiments involving pulsed kilovolt fields which were said to induce transitions. Would that happen in an ordinary experiment? [Illinger].

Straub: I do not think it would.

What sort of time constants do you think would be involved; what frequencies would be needed to produce the forced oscillation? [Illinger].

Straub: In the kilohertz range.

I would like to address Dr. Illinger's remarks. I think we should be very careful in trying to extrapolate data that we get from optical frequencies down to lower frequencies. In addition to the differences in mechanisms, the quantum energy levels are also different. You mentioned the thermal shock effect which occurs when you radiate cellular structures with a laser radiation. I think that probably is also involved as well as the simple thermalization of energy. [Lin].

Straub: The shock wave does not occur at frequencies at which the molecule does not absorb the energy. We do not see denaturation when we are off the absorption peak. The shock wave you are talking about is, in reality, a consequence of electronic relaxation.

At least in one case, you said that when dye was injected the increase was observed.

Straub: That is another problem. You mean in the isolated vesicle system. There needs to be some more experimentation there, just to see what the thermal conductivity of the membrane is, if nothing else. We do not know that yet.

MILLIMETER WAVE AND FAR INFRARED ABSORPTION IN BIOLOGICAL SYSTEMS

K. H. Illinger

Department of Chemistry, Tufts University
Medford, Mass. 02155

ABSTRACT

The hierarchy of interactions of millimeter wave and far infrared radiation with biological systems is surveyed. The significance of existing experimental data and theory is summarized and problems and applications discussed.

INTRODUCTION

The biophysical problem of the interaction between electromagnetic radiation and biological systems can be formulated at a series of levels of organization: (a) interaction with the separate (unperturbed) molecular components; (b) interaction with the relevant molecular systems *in situ* in a biological environment, perturbed by local (intrinsic) electromagnetic fields and by intermolecular forces (*e.g.* biopolymer configurational dynamics in the presence of the local fields due to membranes and ionic and dipolar components); and (c) interaction with the totality of the biological system, including levels of organization higher than those encompassed in (b), as illustrated in Fig. 1. Considerable information has been amassed, albeit in restricted frequency ranges, concerning the spectroscopic and dielectric properties of principal molecular components: H_2O, biopolymers, and other molecular components of biological systems[1-7]. Experimental data in the frequency region above 30 GHz and, in particular, in the region between millimeter wave and far infrared frequencies (30 - 10000 GHz, is, however, sparse, incomplete even for H_2O[8-15], and the subject of considerable controversy in the case of biological systems[16-22]. The theory of the collisional perturbation of the spectra of ordinary fluids in this frequency range, which spans the threshold between the diabatic and adiabatic limits toward which the interaction tends at low and high frequencies, respectively, is only partially developed[3,23]. Detailed spectroscopic theory is virtually undeveloped for non-equilibrium, steady-state, open thermodynamic systems, which characterize the behavior of biological entities (in contrast to the equilibrium thermodynamics characteristic of simple fluids).

Recent formal theoretical work[24-29], tentatively supported by experimental findings, suggests that a crucial aspect of the electromagnetic field interaction of biological systems in the millimeter wave and far infrared region may lie in the existence of long range collective molecular interactions, within membranes, associated with coherent electromagnetic oscillations

in this frequency regime, and resulting in coupled biochemical reactions (*e.g.* enzyme-substrate interactions) with (extremely low frequency, ~ 10-100 Hz) oscillatory kinetics[30]. This is in accord with the hypothesis[31-34] that there exists a subtle interplay between internal fields and the conformation and collective interactions of biomolecules that play a pivotal role in controlling membrane transport and in other primary biological functions occurring within the greater membrane[35]. These and related studies further imply that: (a) the refinement of theoretical biophysical models beyond the heuristic state now extant, and (b) their test and refinement via millimeter wave and far infrared spectroscopy of biological materials may serve to elucidate fundamental aspects of biophysics, including enzyme selectivity and catalysis[25], coding of cellular differentiation[36], and aspects of neurological function[37].

The existing tentative experimental evidence and state-of-the-art theoretical constructs cited in the above indicate that molecular systems comprised of biopolymers, structured H_2O and ions, *in situ* of membrane intrinsic fields, exhibiting long-range molecular interactions and coherent electromagnetic oscillations in the millimeter wave and far infrared region, may be a pervasive entity in fundamental biological systems. In consequence, the experimental mapping of the millimeter wave and far infrared spectrum of such systems would provide detailed phenomenological information, even within the context of the current elementary state of pertinent biophysical theory. The experimental determination of the inherent oscillation frequencies of different molecular systems (*e.g.* different enzyme-substrate combinations) and different membrane environments (*e.g.* different cell types), would serve as a definitive biophysical characterization of such systems, and would complement biochemical information on fundamental biophysical function. As a corollary to such investigations, one may inquire concerning the conditions under which there may exist intervention in biological function by the presence of external (environmental and technological) electromagnetic fields in the millimeter wave and far infrared regions. In order to proceed toward these goals, several interrelated lines of attack must be entered upon; they are briefly outlined below.

TOTAL ATTENUATION FUNCTION FOR A BIOLOGICAL SYSTEM

From basic dielectric theory[38], the relationship between the attenuation function, $\alpha(\omega)$, and the complex permittivity, $\chi^*(\omega)$, for all but ferromagnetic materials, is given by:

$$\alpha(\omega) = (\omega/2^{1/2}c)\left[\left\{[\chi'(\omega)]^2 + [\chi''(\omega)]^2\right\}^{1/2} - \chi'(\omega)\right]^{1/2}$$

$$= (\omega/2^{1/2}c)\left[\chi'(\omega)\left\{\left(1 + \tan^2\delta(\omega)\right)^{1/2} - 1\right\}\right]^{1/2} \qquad (1)$$

Here $\omega = 2\pi\nu$ is the angular frequency. The loss tangent, $\tan\delta(\omega)$, is defined by: $\tan\delta(\omega) = [\chi''(\omega) / \chi'(\omega)]$, $\chi^*(\omega) = \chi'(\omega) - j\chi''(\omega)$, and c is the velocity of light *in vacuo*. In the limit $\tan^2\delta(\omega) << 1$, Eq. (1) reduces to the special case:

$$\lim \alpha(\omega) = (\omega/2c)\,\chi''(\omega)\,[\chi'(\omega)]^{-1/2}$$

$$\tan^2\delta(\omega) << 1 \; . \qquad (2)$$

A closely related quantity is the dielectric conductivity, $\delta(\omega)$, given by:

$$\delta(\omega) = \varepsilon_o\omega\chi''(\omega) = 2c\varepsilon_o\,[\chi'(\omega)]^{1/2}\left\{\lim \alpha(\omega)\right\}$$

$$\tan^2\delta(\omega) << 1 \qquad (3)$$

where ε_o is the permittivity of free space.

Quantitative experimental measurements provide the real and imaginary parts of the complex permittivity, $\chi^*(\omega)$, the optical constants, or $\alpha(\omega)$ directly. In comparing results with experimental values of the spectroscopic absorption coefficient defined by Beer's law,

$$[I(\omega)/I_o(\omega)] = [E^2(\omega)/E_o^2(\omega)] = \exp\left\{-[2\alpha(\omega)]Nz\right\}, \qquad (4)$$

we require $[2\alpha(\omega)]$, in neper cm^{-1}, since the (spectroscopic) intensity $I(\omega)$ after travel of a distance z, in cm, in the dielectric goes as $E^2(\omega)$, while the attenuation function, Eq. (1), is defined by:

$$[E(\omega)/E_o(\omega)] = \exp\left\{-\alpha(\omega)\,Nz\right\} \; . \qquad (5)$$

where $E(\omega)$ is the electric-field strength, and N the number of molecules per cm^3.

The analysis of the experimental attenuation function, $\alpha(\omega)$, in biological systems requires generalization of the theory of collisional perturbation of molecular spectra to systems which includes a (thermally decoupled) contribution from coherent oscillations, absent in the case of simple fluids. The conventional formulations of the theory of pressure broadening[39-45] assume, *inter alia*, thermal equilibrium of the Planck distribution type between the absorber-emitter system and its surrounding thermal bath which produces, via intermolecular forces, the collisional perturbation of the absorber-emitter spectrum. With this assumption, it is possible to establish a rigorous, and elegant, criterion[5,46] for the adiabatic and diabatic limits of the collisional perturbation and to partition the absorption spectrum of the system (at least to first approximation) into a relaxation spectrum (the low-frequency, diabatic regime) and a resonant spectrum (the high-frequency, adiabatic regime), whose detailed boundaries depend on the characteristic absorption frequencies ω_{mn}, and relaxation times, $\langle\tau_k(o)\rangle$, of the system, and on the average thermal energy, kT. The existence of metastable states, associated with coherent electromagnetic oscillations, decoupled to a considerable degree from the thermal bath, introduces a third regime, not represented in the conventional model. Heuristically, this quasi-resonant regime could be parameterized, in terms of existing theory, as being (phenomenologically) intermediate between the two conventional regimes. Fig. (2) depicts schematically the contributions to the various regimes, as a function of $(h\omega/kT)$. A more incisive approach consists of the specialization of the formal theory of cooperative phenomena[47] to the general problem of calculating the attenuation function of biological fluids.

In principle, the attenuation function, $\alpha(\omega)$, contains complete information concerning the coupling between a system and external electromagnetic fields, the only limitation being the exclusion of magnetic permeability effects within the framework of Eq. (1). This restriction could readily be relaxed by including the latter; no compelling reasons appear, however, to exist for such an extension. It must be recognized that $\alpha^o(\omega)$ and $\alpha(\omega)$, Fig. (1), may differ in a non-trivial fashion owing to the existence of intrinsic fields,

$E_{intr}(\omega,t)$, and intermolecular perturbations (including chemically reactive interactions), $V(\omega,t)$, in biological systems. As a result, the attenuation function $\alpha^{o}(\omega)$ for the molecular components, unperturbed by $E_{intr}(\omega,t)$ and $V(\omega,t)$ as they exist in a biological system, may not be an invariably reliable guide to the assessment of coupling to biological systems. In fact, the interaction terms $[E_{intr}(\omega,t) + V(\omega,t)]$ may alter χ_o sufficiently substantially that some dielectric properties, not exhibited by the unperturbed system, may emerge. As Fröhlich[24] suggests, the *raison d'être*, in an evolutionary sense, for the extraordinarily high intrinsic electric fields in biological membranes ($\sim 10^5$ V/cm) may be the establishment of the resultant unusual dielectric properties of *in situ* biomolecular systems which, via collective behavior, permit biological systems to perform tasks (such as information acquisition and discrimination in the ubiquitous presence of inherent thermal noise) and whose sophistication may border on the limits set by quantum-mechanical principles. In this connection, the extent to which quasi-resonant interactions between coherent electromagnetic fields and biological systems may be operative in the millimeter wave and far infrared region is of crucial importance to the question of the existence of bioeffects.

ATTENUATION FUNCTION FOR FREE H_2O

A salient contribution to the total attenuation function, $\alpha(\omega)$, of biological systems, in fact the dominant contribution at millimeter wave and far infrared frequencies in representative systems, is the absorption due to free H_2O. This contribution forms the virtually ubiquitous background to spectroscopic properties of biological systems, although the contributions due to free H_2O and to structural H_2O differ for different biological systems. A recent analysis[9] of the existing experimental data on free H_2O[14] establishes the complex permittivity of the fluid with good precision to $\sim$ 35 GHz. In the range between 100-10000 GHz, however, there is a paucity of experimental data, and its uncertainty increases with increasing frequency. Furthermore, in the high frequency portion of this spectroscopic region, the inaccuracy of the Debye theory limit[39-44] for the attenuation function, $\alpha(\omega)$, as a function of the complex permittivity, $\chi^*(\omega)$, severely affects the accuracy of the analysis of the experimental data. While the projection of the Debye

type limit is reasonably accurate in the region ~ 100 GHz, existing treatments of the high frequency limit of the relaxation spectrum of polar fluids require extension and refinement. In this frequency region, the Debye relaxation parameter must become frequency dependent and tend toward infinity for fundamental physical reasons. An existing heuristic treatment[23], which represents this modification, may be employed to refine the representation of $\alpha(\omega)$ and its relation to $\chi^*(\omega)$. In particular, it is expected that the detailed analysis of the real and imaginary part of the (frequency-dependent) complex permittivity in terms of the Argand diagram and via the closely related Cole-Cole distribution of the relaxation times[1] may require modification within the context of a frequency dependent relaxation parameter in the high frequency limit of the relaxation spectrum. Qualitatively, while the prediction, on the basis of the Debye model, of a constant (asymptotic) attenuation distance for H_2O in the millimeter wave region and the low frequency portion of the far infrared region is correct, it is expected that there may exist a window (relatively large attenuation distance) between the broad rotational relaxation spectrum in the millimeter wave and far infrared region and the discrete, resonant (intramolecular-vibrational) transitions in the infrared region. An additional complication arises from the existence of translational and librational quasi-lattice modes in liquid H_2O in the far infrared region[10]. Inasmuch as the relaxation absorption spectrum of free H_2O serves as an efficient attenuator of millimeter wave and low-frequency far infrared radiation (the attenuation distance, $[\alpha(\omega)]^{-1}$), is of the order of 10^{-2} cm in the 10^{-1} cm wavelength range, and since, in contrast, this constant attenuation due to the relaxation regime cannot persist in the high-frequency limit, an accurate characterization of this contribution to $\alpha(\omega)$ over the entire range in which (quasi-resonant) coherent oscillations may be expected to occur, is of considerable interest. Fig. (3) represents $\alpha(\omega)$ for the relaxation spectrum of free H_2O as computed from the collisional-perturbation model[23].

THE ROLE OF STRUCTURAL H_2O

Structural H_2O is a salient entity in the stabilization of conformational structures of biopolymers in general[13,48], and appears to be a crucial

component in the formation of metastable states associated, in particular, with coherent electromagnetic oscillations. As a component in the free-H_2O--structural-H_2O mixture, the latter contributes a broad relaxation regime absorption, with a maximum value for $\chi''(\omega)$ at a frequency intermediate to the corresponding critical frequencies for free liquid H_2O and ice. Selective absorption of electromagnetic radiation into the (continuum) energy levels of a particular component of a molecular system which is totally collision-broadened (*i.e.* operating wholly in the relaxation regime) is improbable. Thus although free H_2O and structural H_2O exhibit different (temperature-dependent) frequency profiles for their individual contributions to the attenuation function, $\alpha(\omega)$, the relatively efficient and non-selective (with respectto frequency) interconversion of electromagnetic field energy into rotational and translational diffusion of *both* systems tends to vitiate any selective processes in the relaxation regime. In the extreme of highly efficient interconversion, the strongly selective intervention of external electromagnetic radiation, in the region below ~ 10 GHz, into the properties of structural H_2O, would be unlikely. However, the actual efficiency of this intercoversion, as a function of T, and, in particular, any resulting biologically important selectivity, is as yet an unresolved question. Indeed, Grant[49] has directed attention to the potential role of structural H_2O as principal absorber (via its relaxation spectrum) in the low-frequency portion of the relaxation spectrum of free H_2O below ~ 10 GHz. In addition, in view of the role that structural H_2O plays in the establishment and stabilization of the metastable state, selective interactions involving structural H_2O in the millimeter wave and far infrared region would appear to be possible.

Considerable controversy exists as yet concerning the equilibria and dynamics of H_2O molecules in general cellular systems, particularly, with respect to the proportion of free H_2O and structural H_2O. In part, this arises from the ambiguities inherent in the analyses of relaxation dynamics of rotationally- and irrotationally-bound and (rotationally and translationally) free H_2O from proton magnetic resonance spectroscopy[13,15,50-52]. The attenuation function for structural H_2O has been characterized[4,42] to ~ 30 GHz, but no experimental data is available in the millimeter wave and far infrared region. As indicated, structural H_2O is considered to be an indispensible

building block in the system associated with the long-range collective interactions and the coherent electromagnetic oscillations. As such, its attenuation function *in situ* of membrane fields, in the millimeter wave and far infrared region, is requisite to the analysis of the collisional perturbation it imposes on the remainder of the system, while, acting, in the main, together with the ionic and dipolar components, to stabilize the biopolymeric conformations which maintain the metastable state, and serving further to decouple it partially from the thermal bath provided primarily by free H_2O. The extent of such decoupling is reflected in the narrowness (relative to the rotational-relaxation absorption) of the linewidth of the coherent oscillations. Tentative, and as yet controversial, experimental data on the frequency-width of external-field interactions[19-21] appear to implicate the inverse of the rotational relaxation time[4,49] of structural H_2O, ~ 0.3 GHz. This implies a linewidth to frequency ratio, or effective spectral resolution, $\approx$ (0.3 GHz/40 GHz) $\approx 10^{-2}$, for this quasi-resonant interaction. If this assessment is correct, considerably higher resolution would be obtained for coherent oscillations with frequencies ~ 300 GHz, with $R \approx 10^{-3}$, thus allowing for the possibility of observing any existing fine structure in the coherent oscillations of the metastable state(s), as well as the resolution of a mixture of systems with different characteristic frequencies.

In this connection, it should be stated that the inherent spectroscopic resolution of frequency-phase-locked millimeter wave spectrometers, employing injection phase-locked backward-wave oscillator sources[53] or solid state Gunn diode or IMPATT oscillator sources[54], is of the order of 10^{-6} (30 kHz at 50 GHz) or better, exceeding by several orders of magnitude the effective resolution expected for the quasi-resonant absorptions discussed above. The frequency widths reported in the literature[19-21] may, however, be upper limits, since no frequency stabilization appears to have been employed in the experiments, and since the detection method may artificially broaden the frequency width. Direct spectroscopic experiments would achieve a lower limit to the resolution in the linewidth and optimize resolvability of any fine structure in the spectroscopic features.

Experimental determination and theoretical analysis of the millimeter wave and far infrared spectra of structural H_2O is thus of interest, to permit

characterization of the high frequency limit of its rotational-relaxation to the total attenuation function, together with any modification of the quasi-lattice vibrations (librational and translational) structural H_2O from those encountered in the far infrared spectrum of free H_2O. Because of the difference in the size and nature of the hydrogen-bonded clusters of structural H_2O, differences in its quasi-lattice vibrations, as compared to free H_2O, are expected.

TEMPERATURE DEPENDENCE OF THE TOTAL ATTENUATION FUNCTION

The temperature of the thermal bath (consisting primarily of free H_2O) will affect the electromagnetic-field interaction of a biological system containing metastable states in a complicated fashion. Whereas the temperature dependence of the attenuation function of ordinary polar fluids is well understood[1-3,39-44], within the framework of the conventional theory of pressure broadening, the complexity of the present system introduces several new features. The thermal energy of the heat bath will, in itself, affect the population of the metastable state(s) associated with the coherent oscillations. In fact, a certain threshold of thermal energy input (including energy arising from non-reactive, collisional interaction, and, in a crucial fashion, the energy associated with specific chemical transformations) per unit time is requisite to produce excitation of the coherent modes[24,29]. This would imply a rough threshold temperature, T_0, for the maintenance of the cooperative system. In addition to this temperature-threshold criterion, the temperature of the thermal bath for $T > T_0$ will affect the degree of collisional perturbation of the system producing the coherent modes, as well as varying the detailed attenuation functions for free and structural H_2O, repectively, affecting the stability of the conformation of the biopolymer-structural H_2O-ions system. At a sufficiently high temperature, T_1, a second threshold, the onset of the destabilization of the latter system, delimits the effective temperature regime, $T_0 < T < T_1$, in which the associated biological functions are operational. In view of the complexity of the temperature dependence of the total attenuation function, in particular the contribution due to the coherent regime, a heuristic model seems desirable as an

initial goal. Combined (possibly synergistic) effects of the temperature change of the thermal bath and of external millimeter wave and far infrared electromagnetic fields (which are, of course, interrelated since the latter will, in general, influence the former) are relevant to biomedical applications.

Existing experimental work[16-22] on the millimeter wave spectra of biological systems is limited to the frequency region ~ 35 - 175 GHz, and is made controversial, in part, owing to the difficulty with which experimental artifacts, in particular the existence of internal reflections of (coherent) millimeter wave radiation, are eliminated in such experiments. In addition, absolute power measurements become increasingly difficult with increasing frequency in millimeter wave spectroscopy and for this reason, power densities reported in connection with biological effects may be in serious error. The intensity of absorption of electromagnetic radiation by the system containing the metastable states will depend on the concentration of such states in a given biological system. Since such concentrations typically may be small, the large quasi-resonant attenuations claimed in some of the existing experimental work may be artifacts. Other experimental work[19-22] rests on the response spectrum of cellular activity as a function of the frequency (and power density) of the external electromagnetic field. In these investigations, the narrow-band (quasi-resonant) response is taken to be evidence for the intervention of the external electromagnetic field in the population of the metastable state, which reflects itself in a perturbation of the chemical reaction(s) in which it is involved and, ultimately, in a perturbation of cellular activity. Threshold and saturation phenomena, with respect to power density of the external electromagnetic field, have been claimed experimentally[19-21], and are accomodated in an extension of the Fröhlich model[26].

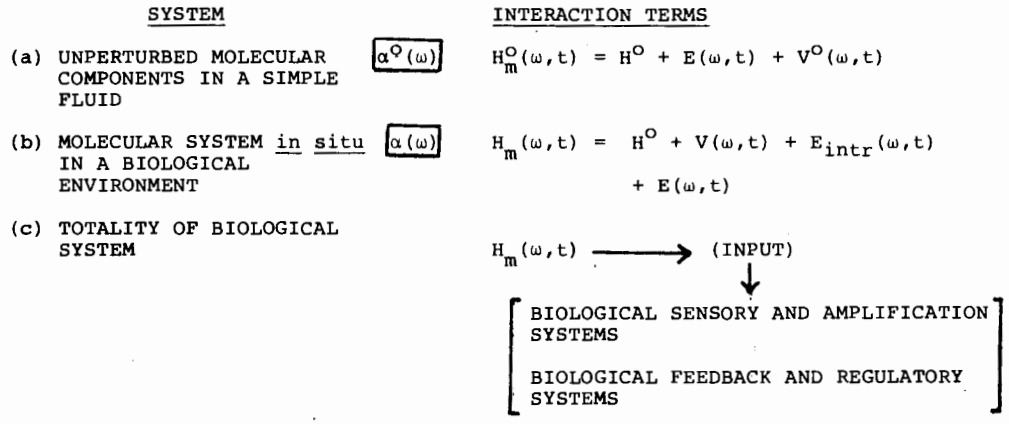
Although the establishment of interactions may be most readily made via an examination of external-field intervention in the cellular activity of the system involving the metastable state(s), and while such studies bear a direct relevance to possible biomedical applications, it would be of considerable interest to obtain *direct* spectroscopic information (transition frequencies and intensities) on the photon-induced coherent regime transitions. As indicated

previously, extension of the conventional spectroscopic theory is required to provide a meaningful analysis of transition probabilities and linewidths for such transitions. From the experimental point of view, reliable determination of these quasi-resonant transitions, arising from a relatively low concentration of absorbers, compared with the predominant absorption due to free H_2O and structural H_2O, requires refinement and development of spectroscopic techniques.

THE GENERAL RADIATIVE TRANSFER PROBLEM FOR A BIOLOGICAL SYSTEM

One may inquire concerning the general problem of the interaction of a molecular or biological fluid with electromagnetic radiation, and the subsequent interconversion of electromagnetic energy and the energy associated with internal degrees of freedom of the system, with the eventual establishment of a steady state. The most general case is that of a biological entity in which the intervention of internal temperature regulatory systems, in response to external thermal stress, play a decisive role in addition to interactions at lower levels of organization; case (b) in Fig. (1). Limiting the present considerations to the latter, as throughout this discussion, one may proceed to distinguish between three different types of electromagnetic field sources: (a) blackbody radiation at a given temperature T (with an associated Planck distribution in radiation flux density over frequency, as a function of T), (b) monochromatic radiation, and (c) coherent monochromatic radiation. Such a differentiation is appropriate since (unperturbed) environmental fields, except for frequencies below $\sim$ 1 kHz, are exclusively in category (a), while scientific and technological electromagnetic field sources are frequently monochromatic and coherent, in the case of microwave, millimeter wave and laser sources. Although engineering aspects of this radiative transfer problem have been worked out, the more general problem for a biological fluid does not appear to have been examined in detail. In particular, the general system delineated previously, including the coherent-oscillation regime, as well as the diabatic and adiabatic regimes, has not been treated. Fig. (4) contrasts schematically the cases delineated above.

The following rough generalizations may be made within the framework of the conventional model (exclusive of coherent excitations) for monochromatic


SYSTEM
INTERACTION TERMS
(a) UNPERTURBED MOLECULAR COMPONENTS IN A SIMPLE FLUID
$\alpha^{O}(\omega)$
$H_m^{O}(\omega,t) = H^{O} + E(\omega,t) + V^{O}(\omega,t)$
(b) MOLECULAR SYSTEM in situ IN A BIOLOGICAL ENVIRONMENT
$\alpha(\omega)$
$H_m(\omega,t) = H^{O} + V(\omega,t) + E_{intr}(\omega,t) + E(\omega,t)$
(c) TOTALITY OF BIOLOGICAL SYSTEM
$H_m(\omega,t)$ (INPUT)
BIOLOGICAL SENSORY AND AMPLIFICATION SYSTEMS
BIOLOGICAL FEEDBACK AND REGULATORY SYSTEMS

H^{O}: UNPERTURBED MOLECULAR SYSTEM

$E(\omega,t) = E_0(e^{i\omega t} + e^{-i\omega t}) \rho(\omega)$; EXTERNAL EM FIELD

$V^{O}(\omega,t)$: INTERMOLECULAR POTENTIAL ENERGY IN A SIMPLE FLUID

$V(\omega,t)$: INTERMOLECULAR POTENTIAL ENERGY [NON-REACTIVE AND REACTIVE COLLISIONS] IN A BIOLOGICAL ENVIRONMENT

$E_{intr}(\omega,t) = E_1(0) + E_2(\omega,t)$; INTRINSIC EM FIELDS

$E_1(0)$: static-field components

$E_2(\omega,t)$: oscillatory field components

Figure 1.
Hierarchy of Interactions of Electromagnetic Fields with Biological Systems.

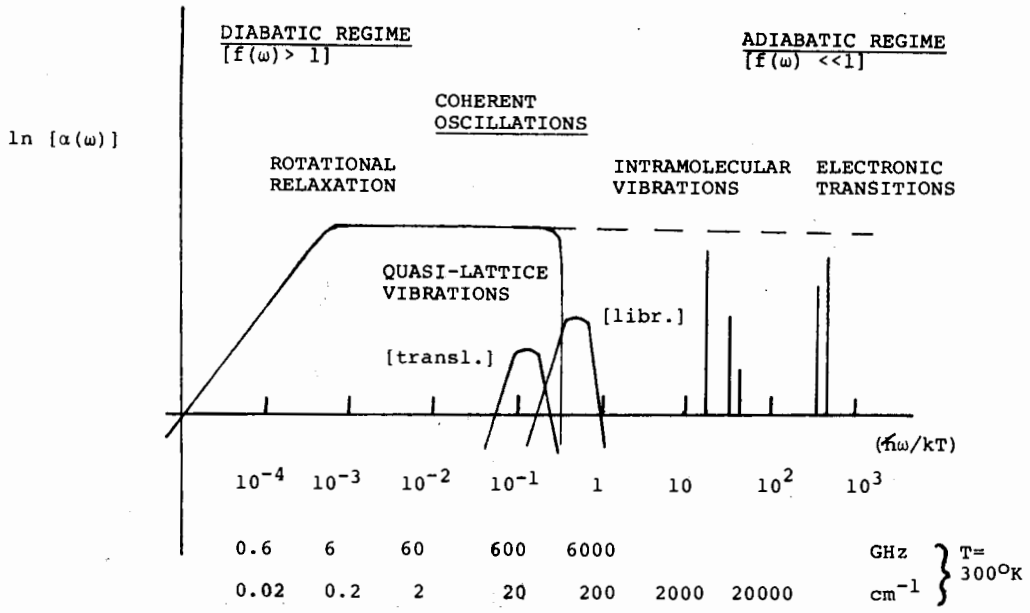


Figure 2.
Contributions to the Total Attenuation Function $\alpha(\omega)$ of a Biological System.

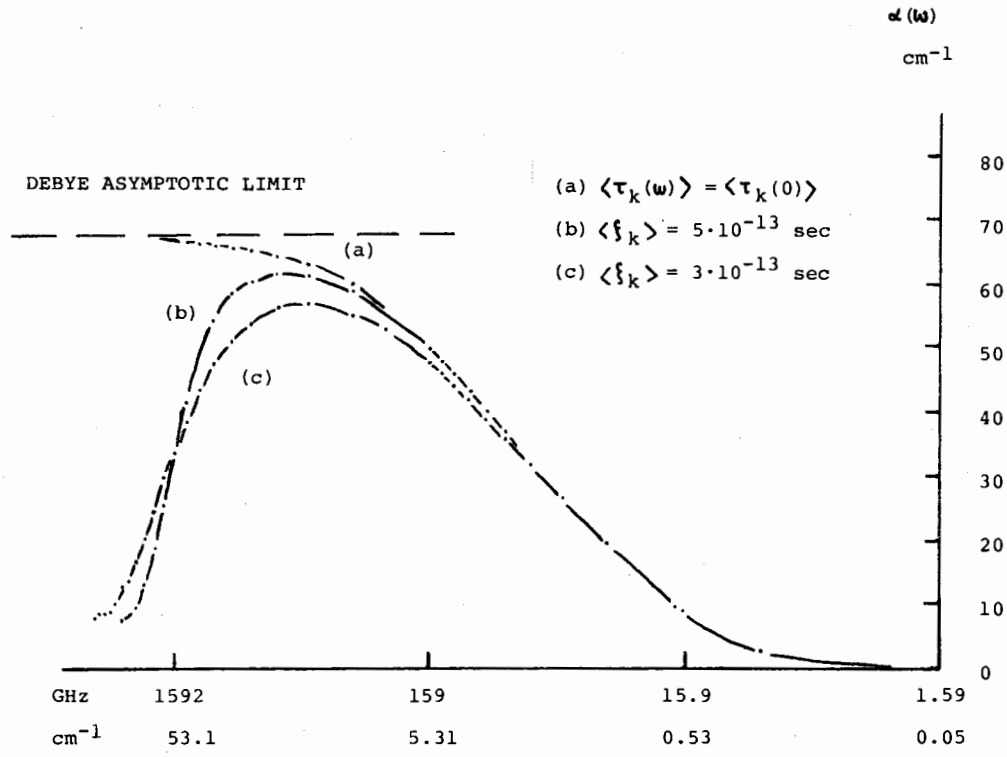


Figure 3.
Attenuation Function, $\alpha(\omega)$, for H_2O, calculated via Reference 16.

radiation. In the diabatic (relaxation) regime, the thermalization of electromagnetic energy is highly efficient and thus the selective excitation of specific degrees of freedom is unlikely, whereas in the adiabatic (resonant) regime the probability of initial selective excitation of specific degrees of freedom increases, albeit depending in detail on the extent of relaxational deactivation from the state(s) resonantly excited by the photon. In the case of intramolecular vibrational excitations in the infrared region, internal conversion of specific vibrational excitation in polyatomic molecules into other degrees of freedom in the same molecule can be quite efficient; electronic excitation, at visible and ultraviolet frequencies, may initiate specific photochemical processes. Even low-frequency [$\hbar\omega_{mn} << kT$] transitions can be pumped by resonant interactions in a simple fluid, *if* relaxation to equilibrium with the thermal bath is sufficiently inefficient and if there exists a small (finite) number of excited states. An example, albeit without demonstrated biological endpoint, is the case of transitions between nuclear spin energy levels, split in the presence of an external magnetic field. In the case of the coherent oscillations attributed to biological systems, the efficiency of the thermalization of the electromagnetic radiation will depend, *inter alia*, on the extent of thermal decoupling of the metastable state(s) from the heat bath. A radiative transfer model including a coherent oscillation regime is necessary to analyze this problem. Whether or not coherent electromagnetic radiation in the millimeter wave and far infrared region can effectively pump molecules in and/or out of the metastable state(s) linked to collective biochemical reactions (and, as a possible biological endpoint, to cell activity) is a question of critical importance to the existence or non-existence of associated bioeffects.

APPLICATIONS

Although previous sections of this discussion are directed toward basic research in the spectroscopic and dielectric properties of biological systems, with a view toward the elucidation of fundamental biophysical questions, there also exist several potential pragmatic applications of some importance in this category of inquiry. They are briefly sketched below.

A direct corollary of the (even completely phenomenological) analysis of

the coherent regime spectra of biological systems is the correlation of such spectra with cell type and type of substrate-interactant system. How fine-grained such an analysis can be made to be remains to be determined; *viz.*, the extent to which spectroscopic differentiability obtains for different systems will depend on (a) differences in the characteristic frequencies among systems and (b) the linewidths of coherent regime spectroscopic lines, as well as the experimentally attainable resolvability. Under favorable conditions, differentiation of cell type and reaction type might be achieved, permitting use of the spectroscopic technique for diagnosis of cell type and function. Differentiation between normal and tumor cells has been claimed in the literature[17,55-57], but experimental artifacts may be operative in some of the experimental work. If such claims can be substantiated, the phenomenology of coherent regime spectra might not only be of utility in the diagnosis of malignant tissue, but may shed some light on the detailed nature of the perturbation of normal cell function by malignancy. It is further possible that intervention in the collective-mode chemical reactions involving metastable states (with coherent modes) via millimeter wave electromagnetic radiation may have therapeutic, as well as diagnostic, implications.

Conversely, if such controlled (beneficial) biomedical applications were possible, it is requisite to inquire into possible bioeffects and health implications of technological electromagnetic radiation in the coherent regime frequency region. In point of fact, several technological applications must be considered in this context: (a) multichannel millimeter wave communications systems [waveguide and open transmission systems], (b) millimeter wave high-resolution radar, and (c) microwave power transmission, along terrestrial and proposed satellite-based transmission routes through the earth's atmosphere[58,59]. In connection with these existing and proposed man-made electromagnetic radiation fields, one may ask the general question concerning the coupling of electromagnetic radiation with the entire biophysical model envisaged by Fröhlich[24,29], encompassing the coherent regime oscillations associated with the metastable state and the coupled ELF oscillations arising from the oscillatory biochemical reactions. Fig. (5) provides a schematic view of components of these systems. On the basis of current evidence, and the (as yet incomplete) understanding of underlying biophysical

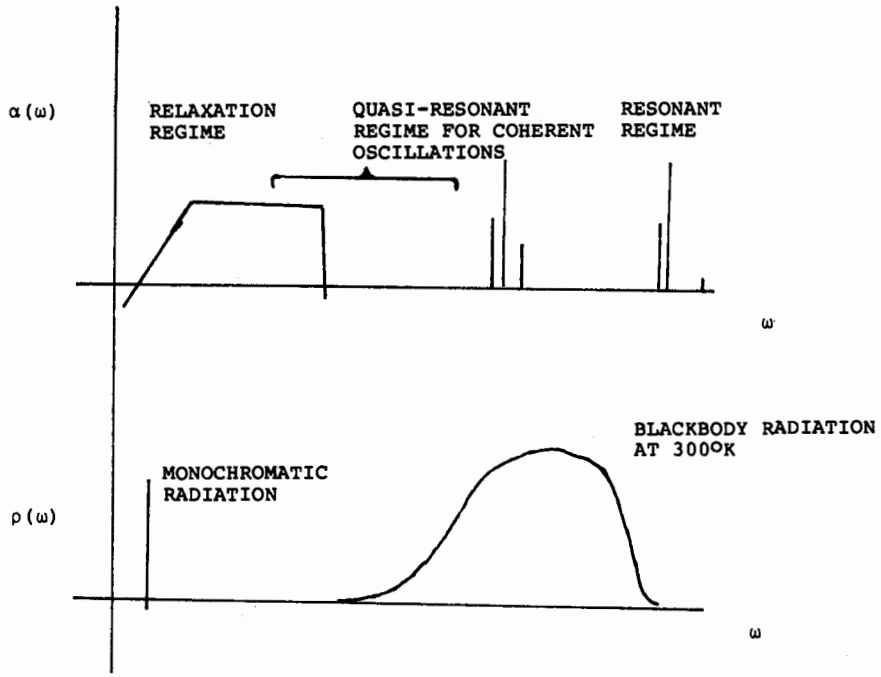


Figure 4. Schematic Representation of the General Radiative Transfer Problem in a Biological System.

mechanisms, one may speculate along the following lines concerning external electromagnetic field interactions with this system. Three possible leverage points for perturbation may be identified: (a) the membrane intrinsic electric field, which is responsible for setting up the metastable state(s), (b) the coherent regime frequency branch in the ~ $10\text{-}10^{+3}$ GHz region, which is associated with the long range molecular interactions, leading to the coupled biochemical reactions, and (c) the resulting ELF frequency branch in the ~ 10-100 Hz region[30]. Thermal fluctuations cause time-variant electromagnetic fields, with a vanishing time average, and may superimpose on the average membrane intrinsic field, and cause occasional sporadic nerve impulses[29]. In a system close to the triggering threshold, at a given instant in time, an external field may, in principle, add to the fields caused by thermal fluctuations and lead to sporadic impulses[60]. However, strong intervention in the average membrane field, and hence significant perturbations of its *time average* properties by external fields is not predicted except for very high (static) field strengths, close to the dielectric breakdown of bulk tissue. Intervention in the ELF branch ($\approx$ 10-100 Hz) of the cooperative system by external fields is probably weak, while coupling with coherent electromagnetic radiation in the coherent regime branch ($\approx$ 10-1000 GHz) may occur. This (highly tentative) analysis appears to be in harmony with the type of (unperturbed) environmental terrestrial electromagnetic fields[5] that exist, if one may assume that evolutionary development would emerge in a fashion (for a pervasive biophysical system) so as to minimize coupling with the unperturbed environment and optimize the operation of the biophysical system and associated biological function. While atmospheric electric fields in the ELF region are prevalent and may reach substantial field strengths, the millimeter wave region of the terrestrial background electromagnetic field is a quiet zone, contributed to only by the (extremely low field strength) low frequency tail of terrestrial blackbody radiation, which peaks in the infrared region, and the (extremely low field strength) contribution of the cosmic millimeter wave blackbody radiation arising from the (drastically red-shifted) electromagnetic pulse attendant to the initial phase of the formation of the universe. Furthermore, none of the environmental contributions consist of coherent radiation, in contrast to the technological applications cited above. Considerable

additional work, beyond the present state-of-the-art, will be required to delineate significant coupling mechanisms and associated bioeffects with the interlacing systems toward whose behavior Fig. (5) attempts to chart avenues of *inquiry*, rather than purporting to provide definitive conclusions.

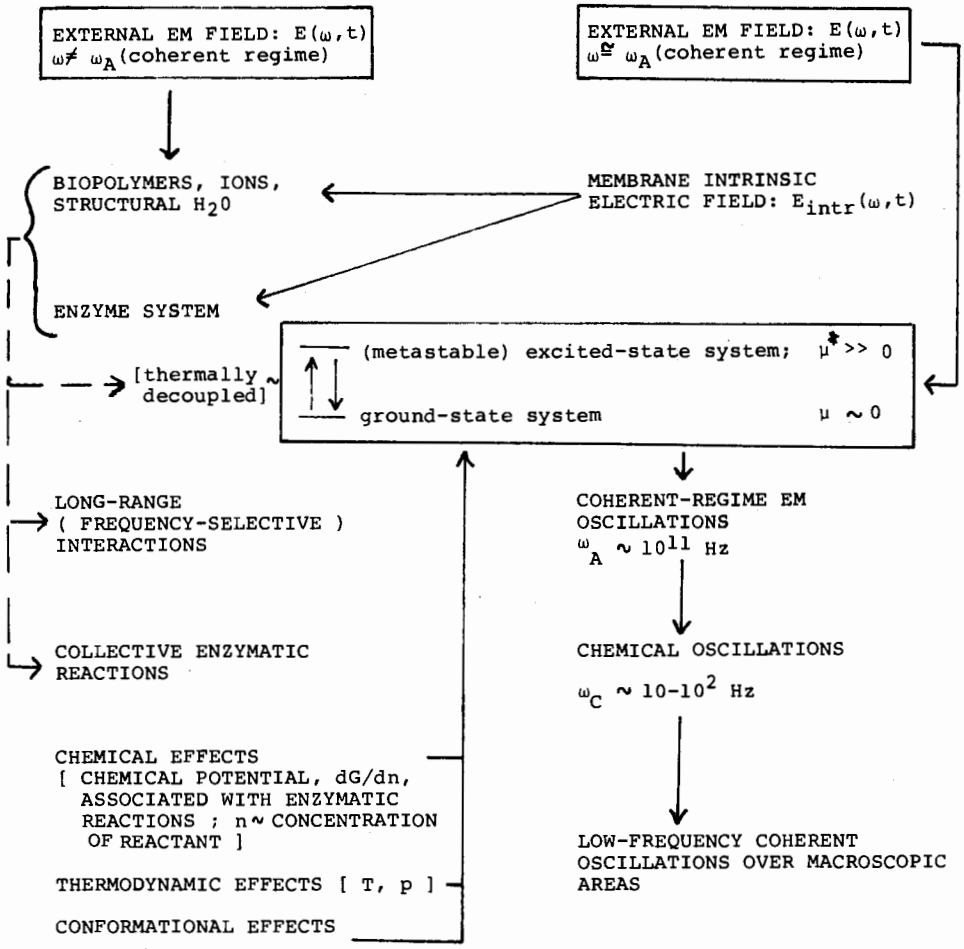

EXTERNAL EM FIELD: E(ω,t)
ω≠ ω_A (coherent regime)
EXTERNAL EM FIELD: E(ω,t)
ω≅ ω_A (coherent regime)
BIOPOLYMERS, IONS, STRUCTURAL H2O
MEMBRANE INTRINSIC ELECTRIC FIELD: E_intr(ω,t)
ENZYME SYSTEM
[thermally decoupled]
(metastable) excited-state system; μ* >> 0
ground-state system μ ~ 0
LONG-RANGE (FREQUENCY-SELECTIVE) INTERACTIONS
COLLECTIVE ENZYMATIC REACTIONS
COHERENT-REGIME EM OSCILLATIONS ω_A ~ 10^11 Hz
CHEMICAL OSCILLATIONS ω_C ~ 10-10^2 Hz
CHEMICAL EFFECTS [CHEMICAL POTENTIAL, dG/dn, ASSOCIATED WITH ENZYMATIC REACTIONS ; n ~ CONCENTRATION OF REACTANT]
THERMODYNAMIC EFFECTS [T, p]
CONFORMATIONAL EFFECTS
LOW-FREQUENCY COHERENT OSCILLATIONS OVER MACROSCOPIC AREAS

Figure 5.
Schematic Representation of Biological System and Possible Modes of Interaction with Electromagnetic Fields.

REFERENCES

1. R. H. Cole, Prog. in Dielectrics 3, 47 (1961).
2. K. H. Illinger, Progr. in Dielectrics 4, 37 (1962).
3. N. E. Hill, W. E. Vaughan, A. H. Price and M. Davies, *Dielectric Properties and Molecular Behavior* (Van Nostrand-Reinhold, London, 1969).
4. H. P. Schwan, in *Biological Effects and Health Hazards of Microwave Radiation* [Proceedings of an International Symposium, Warsaw, October 15-18, 1973], P. Czerski et al., Eds., (Polish Medical Publishers, Warsaw, p. 152 (1974)).
5. K. H. Illinger, Progr. in Dielectrics 4, 160 (1962).
6. H. P. Schwan, Neurosciences Res. Progr. Bull. (Mass. Inst. of Tech.) 15, 88 (1977).
7. K. H. Illinger, Neurosciences Res. Progr. Bull. (Mass. Inst. of Tech.) 15, 64 (1977).
8. F. Franks, Ed., *Water, A Comprehensive Treatise* (Plenum Press, New York 1972-5). Vol. I, Chap. 5.
9. Ibid,, Vol. I, Chap. 7.
10. Ibid,, Vol. I, Chap. 5.
11. Ibid, Vol. II, Chap. 7.
12. Ibid, Vol. III, Chap. 8.
13. Ibid, Vol. V, Chap. 6.
14. H. P. Schwan, R. J. Sheppard and E. H. Grant, J. Chem. Phys. 64, 2257 (1976).
15. H. P. Schwan and K. R. Foster, Biophys. J. 17, 193 (1977).
16. S. J. Webb and A. D. Booth, Science 174, 72 (1971). See also: S. J. Webb and M. E. Stoneham, Phys. Letters 60A, 267 (1977).
17. M. E. Stamm, W. D. Winters, D. L. Morton and S. L. Warren, Oncology 29, 294 (1974).
18. C. F. Blackman, S. G. Benane, C. M. Weil and J. S. Ali, Ann. N. Y. Acad. Sci. 247, 352 (1974).

19. N. D. Devyatkov, Sov. Phys. - Uspekhi (Translation) 16, 568 (1974).
20. L. A. Sevast'yanova and R. L. Vilenskaya, ibid 16, 570 (1974).
21. A. Z. Smolyanskaya and V. L. V ilenskaya, ibid 16, 571 (1974).
22. A. J. Bertaud, M. Dardalhon, N. Rebeyotte and D. Averbeck, Compt. rend. Acad. Sci. (D) (Paris) 281, 843 (1975).
23. K. H. Illinger, in *Biologic Effects of Electromagnetic Waves* [Compilation of selected papers of the 1975 Annual Meeting, U. S. National Committee, International Union of Radio Science (Nat. Acad. Sci. - Nat. Res. Council)], in press.
24. H. Fröhlich, Proc. Nat. Acad. Sci. 72, 4211 (1975).
25. D. E. Green, Ann. N. Y. Acad. Sci. 227, 6 (1974).
26. D. Bhaumik, K. Bhaumik and B. Dutta-Roy, Phys. Lett. 56A, 145 (1976).
27. H. Fröhlich, Nature 228, 1093 (1970).
28. A. Milanovich, A. Yeh, A. Barkin and A. Harney, Biochem. Biophys. Acta 119, 243 (1976).
29. H. Fröhlich, Neurosciences Res. Progr. Bull. (Mass. Inst. of Tech.) 15, 67 (1977).
30. F. Kaiser (to be published).
31. G. Ehrenstein and H. Lecar, Ann. Rev. Biophys. Bioeng. 1, 347 (1972).
32. R. E. Taylor, Ann. Rev. Phys. Chem. 25, 387 (1974).
33. C. M. Armstrong, Quart. Rev. 7, 179 (1974).
34. S. McLaughlin and M. Eisenberg, Ann. Rev. Biophys. Bioeng. 4, 335 (1975) G. Ehrenstein, Phys. Today 29, 33 (1976).
35. F. O. Schmitt and F. E. Samson, Neurosciences Res. Progr. Bull. (Mass. Inst. of Tech.) 7, 277 (1969).
36. B. A. Horwitz and L. P. Horwitz, J. Theor. Biol. 42, 168 (1973).
37. F. O. Schmitt, P. Dev and B. H. Smith, Science 193, 114 (1976).
38. See, for example, E. U. Condon and H. Odishaw, eds., *Handbook of Physics* (McGraw-Hill, New York 1967), 2nd ed., p.4 - 107 ff.
39. J. H. Van Vleck and V. F. Weisskopf, Rev. Mod. Phys. 17, 227 (1945).
40. J. H. Van Vleck and H. Margenau, Phys. Rev. 76, 1211 (1949).
41. H. Fröhlich, Nature 157, 478 (1946).

42. H. Fröhlich, *Theory of Dielectrics* (Oxford University Press, London 1949), p. 173.
43. R. Karplus and J. Schwinger, Phys. Rev. 73, 1020 (1948).
44. P. Debye, *Polar Molecules* (Chemical Catalog Co., New York, 1929), Chap. 5.
45. G. Birnbaum, Adv. Chem. Phys. 12, 548 (1967).
46. H. Margenau and M. Lewis, Rev. Mod. Phys. 31, 569 (1959).
47. H. Haken, Rev. Mod. Phys. 47, 67 (1975).
48. R. Cooke and I. D. Kuntz, Ann. Rev. Biophys. Bioeng. 3, 95 (1974).
49. E. H. Grant, R. J. Sheppard and G. P. South, Proc. 5th European Microwave Conf., p. 366 (1975).
50. P. T. Beall, C. F. Hazlewood and P. N. Rao, Science 192, 904 (1976).
51. K. R. Brownstein and C. E. Tarr, Science 194, 213 (1976).
52. K. R. Foster, H. A. Resing and A. N. Garroway, Science 194, 324 (1976)
53. M. E. Hines, R. J. Collinet and J. G. Ondria, IEEE Trans. MTT-16, 738 (1968).
D. B. Bechtold, Dissertation, Tufts University, October 1975.
54. J. Daprowski, C. Smith and F. J. Bernues, Microwave J., October 1976, p. 41.
R. S. Henry, Rev. Sci. Instrum. 47, 1020 (1976).
55. F. Dietzel, Strahlentherapie 148, 531 (1974).
56. F. Dietzel, D. Ringleb, U. Schneider and H. Wricke, Strahlentherapie 149, 438 (1975).
57. F. Dietzel, Naturwissenschaften 62, 44 (1975).
58. M. D. Gross and G. Colombo, Abstracts, USNC/URSI (Nat. Acad. Sciences - Nat. Res. Council) Meeting, 11-15 October 1976, Sect. 5.
59. P. E. Glaser, Phys. Today 30 (2), 30 (1977).
60. For a general discussion, *vid.*: W. R. Adey and S. M. Bawin, eds. Neurosciences Res. Progr. Bull., 15, No. 1 (1977).

* *

DISCUSSION

I am somewhat concerned about your suggestion that it might be possible to couple electromagnetic energy into protein molecules by way of bound water. I have been performing studies in muscle tissue on and off for the past few years and have found that the Vienna NMR data seem to indicate that the bound water in muscle tissue seems to completely exchange within free water within microseconds. Secondly, the dielectric dispersion studies conducted by Dr. Schwan and others seem to indicate that at best the contribution of bound water to the tissue type of activity is no more than a few percent. Don't these two factors seem to indicate that it would be extremely unlikely to couple any energy into proteins? It seems that the bound water is coupled to the free water and that essentially all the energy goes into the free water in tissue. [Foster].

Illinger: It is certainly true that the free water absorption is dominant at some frequencies. Professor Grant suggests that whereas bound water absorbs at lower frequencies, there is a crossover. Moreover, the extent of interaction between the structural water and the free water is not completely established.

There is no evidence that it is not free.

Illinger: I disagree. For example, in DNA there are some water molecules which are hydrogen-bonded to the biopolymer itself; the water molecule is in the framework of the biopolymer. That is certainly different from water molecules which are hydrogen-bonded to the cells. The efficiency of the interconversion of rotational relaxation of the two types of water must be far different.

Dr. Foster has made the point that if you have coupled free water then it is practically impossible to couple energy through to a resonant structure.

Illinger: I would not say it is impossible. It is strongly attenuated. One has to ask at the same time about the sensitivity of coherent systems to electromagnetic radiation.

It seems to me that it is scarcely meaningful to perform experiments looking at muscles as a whole. There are many classes of proteins, and so forth. There are also many differences in membrane characteristics between say muscle membrane tissue, for example, and the surface proteins in brain. These proteins are only 0.1 percent of the w/v totality of brain tissue. And I am quite sure that experiments on the brain would not see anything that is meaningful relating to this class of protein, which however, by specific

experiment can be shown to have quite singular susceptibility, not shared by muscle, to certain types of electromagnetic fields in their calcium binding characteristics. Therefore, I think that Dr. Illinger's point is very well taken: there are differences in the resonances. Moreover, if I understood the comment correctly, it was to the effect that there appears only to be a very small percentage of the picture that could relate to some aspect of bound water. That small percentage may indeed be at the crux of the question.

Illinger: That is certainly true.

I thought it might be appropriate to mention some experiments that were carried out in Germany by Professor Keilmann and his colleagues. Professor Keilmann could not attend but asked to have the following abstract made known to the attendees. I understand that the paper will appear shortly in Physics Letters: [Taylor].

RESONANT GROWTH RATE RESPONSE OF YEAST CELLS IRRADIATED BY WEAK MICROWAVES: (W. Grundler, F. Keilmann and H. Fröhlich) The growth behaviour of yeast cultures in aqueous suspension was monitored by visible light extinction and showed an exponential growth rate reproducible within ± 3% limits. When the cultures were irradiated by c.w. microwave fields of a few mW/cm^2 the growth rate either stayed constant or was considerably enhanced or reduced depending on the frequency around 42 GHz. A spectral fine structure with a width of the order of 10 MHz was observed. Careful temperature monitoring excludes a trivial thermal origin of this effect.

Illinger: If the defined frequency structure is 100 megahertz, this is indeed, a resonant transition. One further comment -- while a biological end point such as a cell growth may appear at 42 gigahertz with high frequency specificity, the contribution to the total attenuation function due to that oscillation (which may have very low transition probability) may be virtually invisible. But that does not mean that the electromagnetic field has not interacted with the system.

Would you define what you mean by coherent regime? And also I would like to know the source and frequencies of the intrinsic oscillation.

Illinger: We are referring to an assembly of biopolymers within the membrane intrinsic field which produce oscillations which are coherent electromagnetically. The sources of the intrinsic oscillations are vibrations. The whole theory has a formal resemblance to the Einstein condensation of a gas. Fröhlich suggests that the frequencies may be as low as 10 gigahertz and may go up into the hundred or thousand gigahertz region.

COOPERATIVE QUANTUM MECHANICAL MECHANISMS FOR RESONANCE ABSORPTION OF NONIONIZING RADIATION

Irvin T. Grodsky
Cleveland State University, Cleveland, Ohio

ABSTRACT

Recently there has been a steadily increasing amount of evidence that certain types of nonionizing radiation are resonantly absorbed by vertebrate brain tissue: windowed both in frequency (VHF modulated and VLF) and amplitude (power). Concurrently, evidence is mounting that the morphological structures in microtissue samples indicate strong similarities to inorganic quantum amplification devices, such as tunnel diodes, liquid crystals (smectic laminar), and population inversion systems (lasers, masers...). In this talk we hope to emphasize these analogies mathematically as homomorphisms, and indicate potential experiments capable of differentiating between which functions utilize which quantum-cooperative dynamics.

* *

DISCUSSION

In your model vibrations of a sheet of ions on a substrate gives rise to a low frequency branch on the order of 10 to 100 Hertz. Isn't an interaction at 10 to 100 Hertz so strongly damped by collisions that it could never be maintained? How could it maintain itself at the level documented by EEG? [Illinger].

Grodsky: Resonance absorption occurs and oscillations are maintained.

What is the width of the EEG frequencies? [Illinger].

Most of the energy is between one and seven to ten Hertz, depending on the brain tissue. Eighty percent of the energy is below ten Hertz, and the effective spectrum is certainly below 100 Hertz. [Adey].

These are the effective bosons then?

Grodsky: They are the quasi-particles of the system.

Are you suggesting that as you heat, this model actually becomes spontaneously ordered? That is what one of your slides seems to suggest. [Davis].

Grodsky: It is disordered.

You showed ordering with increase in temperature. Secondly, are the predictions of the model the same, independent of activation energy for the spinning of these dipoles? They are not completely free to move are they? [Davis].

Grodsky: No. As I say, the only computations done on the computer so far are calculations allowing the dipoles to be in only two states, up or down. That is the first approximation; the second approximation would be three states, four states, and so on.

Do you include an activation energy? [Illinger].

Grodsky: Yes, we must. There is a definite difference between the down and up states in interaction energy.

Is there a difference dpending on the magnitude chosen for that activating energy? [Illinger].

Grodsky: Yes. It moves the bands up.

I asked that question because there is another model due to Kaiser which suggests that associated with the excitation of the system to the excited states and due to oscillations of the population of the metastable state, the frequency of this oscillation comes out to be of the same order of magnitude as the EEG frequencies. In this model there is no problem of relaxation damping. These "chemical oscillations" are an alternative model for the EEG. [Illinger].

Grodsky: There has been a great deal of concern about noise, but we are doing this at a .027 electron volts and I think one must understand the difference between local noise and noise which is localized, and the propagation of a signal down the scale. The point is that when one looks at the transmission of the slow waves and/or the action potential which I call a catastrophic event, one can see very easily that because the EEG is say 80 percent below 10 Hertz, its band width is very low and the thermal noise is very low in its band.

SOME BASICS OF ELF FIELDS AND THEIR BIOSPHERE EFFECTS

Otto H. Schmitt

University of Minnesota
Minneapolis, Minnesota

ABSTRACT

We briefly discuss the significance of possible biological effects of ELF fields and describe experiments that we have carried out to determine whether low frequency magnetic fields can be perceived by humans. The problem of sublimal "hints" in such experiments is emphasized.

For over a half a century we have been living in an environment of man-made electric and magnetic fields and field gradients which, in the ELF power line frequency ranges, are much stronger than those that occur naturally. Except, of course, for direct shock hazard, these fields have had no apparent effects, good or bad. With a few special exceptions, the strengths of environmental fields to which we, our domestic animals and crops, wildlife and the biosphere at large are being exposed is not rising dramatically as it is in other spectral regions of non-ionizing radiation, except perhaps for somewhat more shortrange exposure as we use more hand-held electric tools and applicances and view TV and computer terminal screens. Surgical implantation and intimate attachment of electrical monitoring, control and prosthetic systems has, however, made some of us about two decimal orders of magnitude more susceptible to these fields.

We, therefore, find ourselves for the first time required to develop sound metrics for evaluating ELF biomedical effects and developing wise optimization rules on which to base regulatory limitation of strong ELF fields in populated regions. We must also be guided by these rules in requiring susceptible systems to be made as insensitive as practical to the fields and must restrict susceptible individuals and systems from entering dangerously strong field areas.

Besides this very practical matter of evaluating and providing regulatory controls for these tangible and reasonably well understood effects, there is arising a large folklore, backed by some reputable research, that alerts us to the fact that there probably are some subtle biological effects of ELF fields. Fortunately, none of these to date appears to offer major hazard or even great inconvenience to individual members of the biological community, or to this community at large statistically, as do ioning radiations. We can, therefore, investigate them thoroughly, but with less frantic emergency than would be the case were there substantial evidence of potentially catastrophic effects.

In order to have good measuring tools for evaluating ELF effects, it is almost necessary to rewrite several of the familiar electrical engineering and physics formulations into easily usable field forms, especially with respect to Maxwell's "displacement current." The induction processes also need special treatment and we need a family of specially designed measuring instruments conforming more directly to biomedical effect algorithms.

It is unexpectedly difficult to design workable, reasonably economical and ethically acceptable experimental procedures to determine whether some of the suspected subtle ELF effects are real, experimental artifacts, or merely statistical accidents. Very large statistical sample populations, protected under unusually severe control against aliasing or accidental correlation with forcing function, are required. Even the usual double-blind experimental designs are often susceptible to unplanned coherencies.

We have carried out one experimental project to determine whether humans can consciously perceive, at a statistically significant level, whether they are, or are not, in a moderate-strength, lower-frequency magnetic field. We also examined these subjects' ability to learn by biofeedback training to perceive such fields.

In general they do not appear to be able to perceive, or to learn to perceive, such fields. A few individuals proved to be almost incredibly skillful in extracting relevant hints from diverse environmental signals, so that without intentional cheating, they appeared, even with careful experimentation, to be true "perceivers." In fact they were putting together, in a very clever, self-taught synthesis, subtle sublimal leakages of informational clues.

It is impossible to review in a brief presentation the hundreds of experimental studies that have been undertaken during the last decade, largely as a result of increased interest in possible effects of power and telecommunication systems on man and his biophysical environment, but also as a result of certain proven high sensitivities to weak fields as in the electrosensitive fishes where special electrosensitive transducer organs are found.

Birds, insects, microorganisms, plants, as well as man, have been reported to have ELF sensitivities, but unfortunately many of the experiments are marred by experimental design flaws, have intrinsic limitations, or have not been replicated reliably. One is left with the overall impression that moderate level ELF fields have little direct adverse effect on biological systems but may possibly play a role by intruding competitively into a multivariate filled-channel communication and control system that is more and more frequently found to operate, especially in highly organized biological organisms and systems.

POSSIBLE MECHANISMS OF WEAK ELECTROMAGNETIC FIELD COUPLING IN BRAIN TISSUE[+]

S. M. Bawin, A. Sheppard and W. R. Adey[*]

Department of Anatomy and Brain Research Institute
School of Medicine, University of California
Los Angeles, California 90024

ABSTRACT

In a search for long range order in anionic binding sites on cell surface macromolecules, we have used ELF fields in the range 1 to 100 Hz, VHF fields at 147 MHz amplitude modulated at frequencies from 1 to 30 Hz, and 450 MHz UHF fields also amplitude modulated at frequencies from 1 to 30 Hz. We have found a series of amplitude and frequency "windows" that strongly suggest resonant interactions based on long range order. ELF fields between 6 and 20 Hz *reduced* $^{45}Ca^{2+}$ efflux from chick and cat forebrain tissue by about 15%, with a maximum effect for fields in air at 10 and 56 V/m. Effects were insignificant at 5 and 100 V/m. Isolated chick cerebral tissue was also exposed to a 147 MHz field, 0.8 mW/cm^2 and amplitude modulated at frequencies from 0.5 to 35 Hz. There was a frequency "window" for *increased* efflux (15%) at modulating frequencies from 9 to 20 Hz. We have varied the intensity of a 450 MHz field, amplitude modulated at 16 Hz, from 0.05 to 5 mW/cm^2. There is a "window" in incident field strength for increased $^{45}Ca^{2+}$ efflux only between 0.1 and 1.0 mW/cm^2. We hypothesize that membrane surface charge sites behave "coherently" over a considerable area, and that a coherent patch may be triggered to change state by a very weak trigger at one point. This triggering event may involve proton tunneling at the boundary of such a patch.

[*]Present address: Research Service, Jerry L. Pettis Memorial Veterans Hospital, Loma Linda, California 92357.

[+] Material in this paper will be published in an expanded version in Bioelectrochemistry and Bioenergetics.

INTRODUCTION

Since 1975, evidence has accumulated that the binding and release of calcium in brain tissue involves processes radically different from simple equilibrium states[1]. Calcium ions are essential in the release of transmitter substances from prosynaptic nerve terminals and in transductive coupling of immunological, endocrine and neurophysiological stimuli at the membrane surface, as well as in ensuing transmembrane coupling. This new evidence suggests that for cerebral tissue, at least, it may be necessary to substantially revise generally accepted views on the structural and functional basis of excitation, particularly in regard to the role of weak electrical gradients in the immediate environment of brain cells.

The response of cerebral tissue to certain low level oscillating environmental electromagnetic fields is anomalous in that a sharply modified release of calcium has been found only in a narrow range of frequencies between 6 and 20 Hz. Responses also occur with radiofrequency fields amplitude modulated in the same narrow range of low frequencies, but are qualitatively different. The second quite unexpected finding is that these sensitivities occur only within a range of field strength or a power window. The appearance of sharp upper and lower field intensity thresholds distinguishes these findings from what is expected of chemical reactions in simple equilibrium systems.

The data strongly suggest that the binding and release of calcium occurs cooperatively as the result of long-range interactions between anionic charge sites on the binding substrate. A striking aspect of these studies has been the consistent occurrence of major shifts in calcium efflux (in excess of 10 per cent) with fields that produce very small gradients in the extracellular space surrounding cell membranes. The extracellular fields are about 10^{-7}V/cm and 10^{-3}V/cm for the low frequency and modulated radio frequency experiments respectively. They are thus far below transmembrane gradients of 10^{3}V/cm associated with a typical synaptic depolarization. Moreover, the gradients induced in the extracellular space along the membrane surface would be about

10^3 times larger than any transmembrane components of the same field, because the low specific resistance of extracellular fluid, about 4 ohm-cm^{-1}, shunts a current around the membrane, which has a transmembrane resistance of about 5,000 ohms/cm^2.

Thus, on biophysical grounds alone, large shifts in calcium efflux induced by the imposed fields would be expected to occur primarily in the extracellular fluid and at cell membrane surfaces. This *a priori* consideration fits well with the huge differences in calcium concentration between the extracellular space and the general cytoplasm of the cell. Typically, calcium concentration in cerebral extracellular space is 2.4 mM; within the cytoplasm, it is around 10^{-8}M. Organelles, such as mitochondria, which have much higher concentrations[2], may not participate in the dynamic exchanges associated with membrane excitation[3].

FREQUENCY AND POWER WINDOWS IN SENSITIVITY OF CEREBRAL TISSUE TO OSCILLATING EM FIELDS

Extremely low frequency (ELF) sinusoidal fields from 1 to 75 Hz have been tested for effects on calcium efflux from freshly isolated neonate chick cerebral hemisphere and cat cerebral cortex[4]. Electric gradients in air ranged from 0.05 to 1.0 V/cm. Tissue gradients could not be measured, but were estimated to be of the order of 0.1 μV/cm. Both frequency and amplitude sensitivities were observed. A decrease in calcium efflux of 12 to 15 per cent occurred at frequencies of 6 and 16 Hz. For chick tissue, the field threshold in air for this response was around 0.1 V/cm, and for cat cortex around 0.6 V/cm. At intensities above or below these levels, trends towards a decreased efflux that were not statistically significant were observed (Fig. 1).

Studies with very high frequency (VHF), 147 MHz, radio fields, amplitude modulated in the same low frequency band (0.5 to 35 Hz), also produced shifts in calcium efflux from chick cerebral tissue[5]. At modulation frequencies from 6 to 20 Hz, there was a significant increase in calcium efflux, reaching a maximum of more than 15 per cent, and following a smooth "tuning curve" over this range. No significant changes occurred at higher or lower modulation

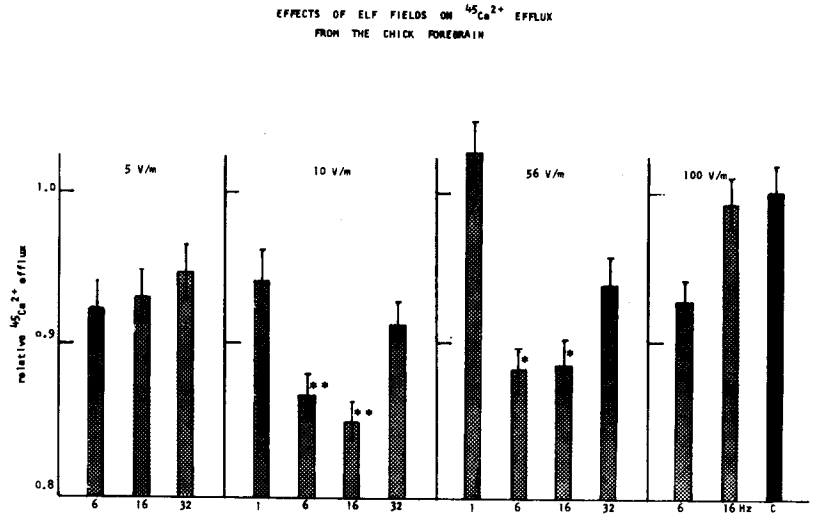


Fig 1.
Effects of low frequency fields on efflux of $^{45}Ca^{2+}$ from freshly isolated chick cerebral hemisphere for 4 different field intensities (5, 10, 56 and 100 V/m). Field frequencies from 1 to 32 Hz are shown on the abscissae. Efflux levels normalized with respect to control efflux levels (C) shown in extreme right bar. Variance indicated as SEMs. ** p less than 0.01; * p less than 0.05. (From Ref 4.)

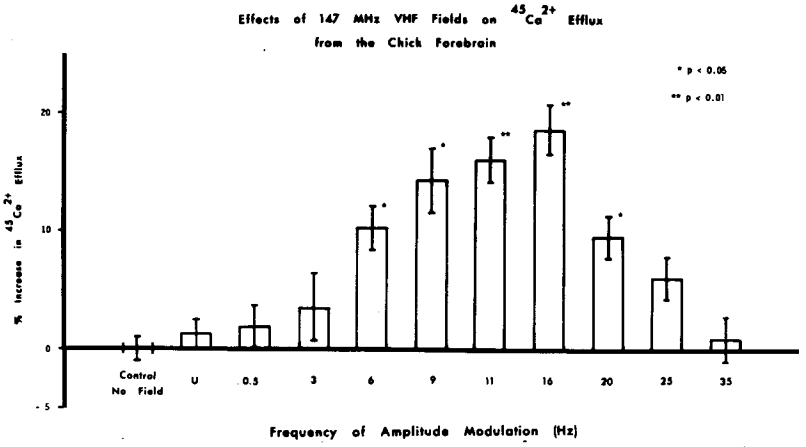


Fig 2.
Effects of changing frequency of amplitude modulation from 0.5 to 35 Hz on $^{45}Ca^{2+}$ efflux from chick cerebral tissue. U, unmodulated 147 MHz carrier produced no significant changes. (From Ref 5.)

frequencies, nor with an unmodulated carrier wave (Fig. 2). It should be noted that the increased efflux observed with these 147 MHz fields mirrors the curve for decreased efflux produced by ELF fields. This point is discussed below, although no adequate biophysical or structural model can be offered at this time. Fields were maintained constant at 0.8 mW/cm^2 in these studies. Tissue gradients were not measured, but would be expected to be about 10 mV/cm, a value consistent with actual measurements at 450 MHz described below.

Studies at 450 MHz have confirmed sensitivity of cerebral calcium efflux to a UHF field amplitude modulated at 16 Hz, and have also disclosed a power window[1]. Using a fixed modulation frequency of 16 Hz, the incident field intensity was varied from 0.05 to 5.0 mW/cm^2. An increased efflux of 10 per cent or more occurred from chick cerebral hemispheres with field intensities between 0.1 and 1.0 mW/cm^2. No increase was noted at 0.05 mW/cm^2, nor at 2.0 and 5.0 mW/cm^2. The power window thus appears to be narrow for this particular field condition, covering about an order of magnitude. At the same time, its boundaries appear sharp, passing from non-significant effects to a full response in excess of 10 per cent of control values within a 2:1 power range (Fig. 3). We have measured tissue field levels in cerebral tissue with an implantable probe designed by H. I. Bassen of the Bureau of Radiological Health[6] and developed by Collins Radio Company. Measured values agree well with calculated levels. A 2.0 mW/cm^2 field produces a gradient of the order of 10 mV/cm.

All essential aspects of similar power and frequency windows at 147 MHz have now been confirmed in independent studies by Blackman, *et al*[7]. They tested a 147 MHz field with an incident energy density of 0.75 mW/cm^2, amplitude modulated at 3, 9, 16 and 30 Hz. Increased efflux of calcium from chick cerebral tissue was observed at modulation frequencies of 9 and 16 Hz, but not at 3 or 30 Hz. In a second series of experiments, they used a fixed modulation frequency of 16 Hz and tested incident power levels of 0.5, 0.75, 1.0, 1.25, 1.5, 1.75 and 2.0 mW/cm^2. The curve for calcium efflux was an inverted-U, with significantly increased levels only in the vicinity of 0.75 mW/cm^2. They conclude that their data support the concept and location of a modulation frequency window as well as a power density window in the patterns of calcium efflux.

Our discussion of these frequency and power constraints in tissue interactions with EM fields requires a brief review of recent research in the molecular biology of cell membranes, and the implications of related biophysical models.

THE STRUCTURE OF CELL MEMBRANES

The cell membrane has long been described in terms of a lipid bilayer. With the progression from light to electron microscopy, the membrane became identified with the plasma membrane in standard electron micrographs. It is now known[8] that the plasma membrane is part of a much broader bounding structure, the "greater membrane". In this model, there are macromolecular lamellae on the outer and inner surfaces of the bilayer. In part, at least, these covering macromolecules are protrusions from intramembranous particles (IMP) that lie within the bilayer. This complex organization and its possible significance in transductive coupling of weak electrical and chemical stimuli has been reviewed elsewhere[1].

COHERENT STATES OF FIXED CHARGES ALONG THE MEMBRANE SURFACE

Singer and Nicolson[9] have extended the greater membrane concept in the "fluid mosaic" model, emphasizing the lateral mobility of certain IMPs within the lipid layers. These protruding terminals of protein molecules are composed of sugar molecules. They are acidic and have numerous negative charge sites. The surface formed by these negatively charged binding sites constitute a polyanionic sheet. From studies of biopolymer sheets, including poly-l-glutamic acid, Schwarz[10,11] concluded that these charges may behave coherently, with adjacent elements having the same energy levels. A coherent domain of anionic fixed surface charge sites at the membrane surface requires energy to raise them above the ground state. In some membrane surface phenomena, energy is supplied by metabolic processes, as in the immunological "patching" reaction at the surface of lymphocytes. There is as yet no precise knowledge about sources of energy that might contribute to coherent surface charge states.

Implicit in the concept of a coherent domain is the expectation that for the duration of the coherent state, this patch of membrane surface would be thermally "quiet", that is, isolated from the randomization of energy levels which is characteristic of the non-coherent condition. Such a system could be restored to the ground state by an extremely weak trigger, at the level of thermal noise or below. The action of a weak trigger at one point in a coherent system resulting in an effect at a remote site elicits a far greater release of energy than the trigger itself[12]. There is an avalanche or domino effect, best expressed in the term "quantum amplification".

COOPERATIVE PROCESSES BETWEEN SURFACE FIXED CHARGES

Cooperative processes occur, or are suspected to occur, in a variety of biological systems. For example, a single photon of visible light with an energy of 0.6 eV produces a perception of light. Its absorption by the disc within a retinal receptor causes the release of about 1400 calcium ions, which migrate outward to the receptor membrane[13]. The triggering energy of the single quantum is several orders of magnitude less than that required to release these calcium ions from their binding sites.

For brain tissue, evidence from our electromagnetic field experiments suggests that binding of calcium ions is highly sensitive to weak imposed fields. A fully successful model must specify the location of the calcium ions susceptible to the electromagnetic fields, and the competitive binding of other cations (including the monovalent ions sodium, potassium and hydrogen) to the same or adjacent sites on a suitable macromolecular, polyanionic substrate. This first step is impeded because the binding energies for these ions remain conjectural. For calcium, at least, binding may occur directly to carboxyl groups, whereas O-sulfate groups offer a looser electrostatic attraction through an atmosphere of water molecules[14]. In dielectric measurements over the spectrum from 10 MHz to 50 GHz water molecules close to macromolecular surfaces exhibit dielectric properties different from those of molecules remotely located. These measurements show that it is no longer possible to regard water as behaving uniformly throughout the extracellular and intracellular compartments.

Electrophysiological evidence also supports the concept of interaction between calcium and cell surface macromolecules in functional modulation of the intercellular space. An apparent reduction in extracellular calcium concentration by as much as 20 per cent occurs during cerebellar stimulation, but measuring techniques would not distinguish between actual removal of calcium from the extracellular space and an alteration in its state of binding to surface polyanions. The latter explanation would appear more probable with respect to the major part of the extracellular calcium. There is a sharp increase in the electrical impedance of cerebral tissue associated with increased extracellular calcium levels[15]. In these measurments, the major part of the impedance measuring current travels in extracellular channels (Fig. 4).

The reciprocal contours of calcium efflux curves from cerebral tissue in ELF and VHF/UHF field exposures suggest that calcium ions may be bound to surface macromolecules in at least two different ways. As discussed elsewhere[4], a plausible but so far untested explanation may lie in the concept of strong attachment to single molecular strands and weaker bonding between strands[16]. These different modes of bonding might be amenable to manipulation by the widely differing energies in weak ELF and much stronger radiofrequency field interactions.

DIELECTRIC CHARACTERISTICS OF THE COUNTER ION LAYER

Micron diameter resin particles with porous surfaces have effective dielectric constants as high as 10^6 at frequencies below 1KHz[17]. The findings may be relevant to interactions of the numerous finer branches of cerebral dendrites with surrounding electric fields. This model considers the case of porous particles with a uniform volume distribution of fixed charges. The boundary region is characterized by a very large, radially-directed static field with a corresponding radial variation in the distribution of mobile ions. The external electric field causes a polarization of the ionic atmosphere, an effect that can be expressed by an additional "apparent" dielectric constant of the particle, exceeding the actual dielectric constant by several orders of magnitude at low frequencies. The magnitude of the low frequency

dielectric constant is proportional to the size of the particle and the square root of the fixed charge concentration in the porous material.

As discussed elsewhere[4], this phenomenon at the surface of small particles or tubes with diameters in the range of most branches of cerebral neuropil suggests that ionic movements in oscillating electric fields close to such a membrane surface may be severely attenuated except at very low frequencies. This attenuation would apply to the transfer of thermoelectric noise. With a specific resistance for brain tissue of 300 ohm-cm and an effective frequency bandwidth from 0 to 100 Hz, the equivalent noise voltage would be of the order of 10^{-8} V/cm. This tentative model is of interest in view of observed sensitivities of 10^{-8} V/cm in marine vertebrates and the behavioral and neurochemical effects seen in birds and man and other primates attributable to oscillating gradients less than an order of magnitude larger.

Preliminary models of membrane excitation based on quantum mechanical aspects of cooperative charge interactions have been formulated by Fröhlich[18-20]. Fröhlich has modeled long range coherence and energy storage based on dipole interactions and the recurrence of certain bonds, such as H-bonds, in macromolecules. High sensitivity of biological systems to weak electromagnetic fields would then relate to a mechanism through which they store energy, and in so doing, overcome thermal noise. Extremely high frequency oscillations at 10^{11} to 10^{12} Hz would occur simultaneously with limit-cycle behavior at very low frequencies. Grodsky[21,22] has considered the membrane lipid bilayer as a sheet of dipoles under an electric strain attributable both to the dipoles' mutual interactions and to the local electric field generated by cations in the polyanionic glycoproteins of the outer membrane. This system will respond to a surrounding electric field with a change in long range order, a phase transition occurring over a narrow range of fixed temperatures below a critical point (The Néel temperature). The system will oscillate with most energy in a narrow low frequency band.

ACKNOWLEDGEMENTS

These studies were supported by the Bureau of Radiological Health Grant USPHS 3-RO1-FD678-01 and by National Science Foundation Grant GB-27740, and US Air Force Contract F44620-70-C-0017 and Office of Naval Research Contract N-00014-A-200-4037.

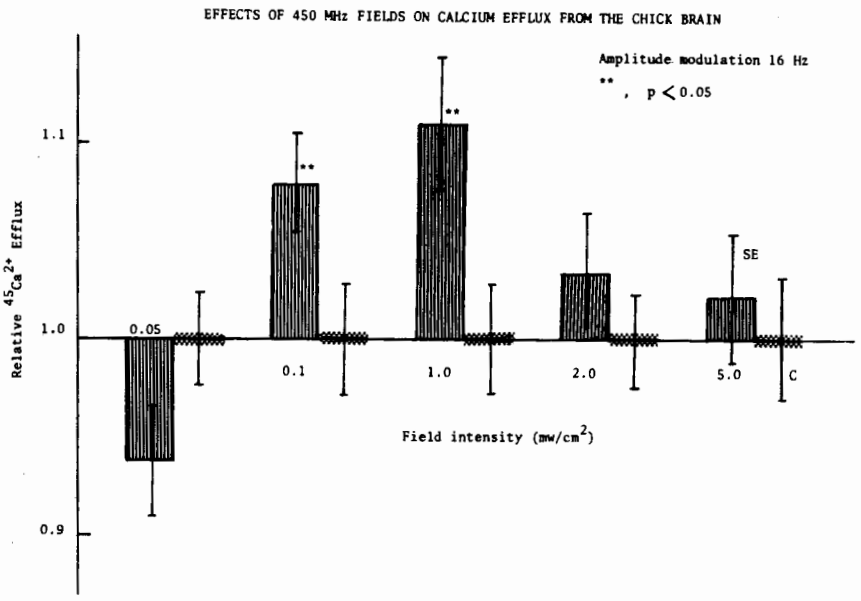


Fig 3.
Effects of changing intensity of 450 MHz field amplitude modulated at 16 Hz on efflux of $^{45}Ca^{2+}$ from chick cerebral hemispheres. Cross hatched bars show levels of efflux from control specimens tested simultaneously in same series of exposures. Variance shown as SEMs.

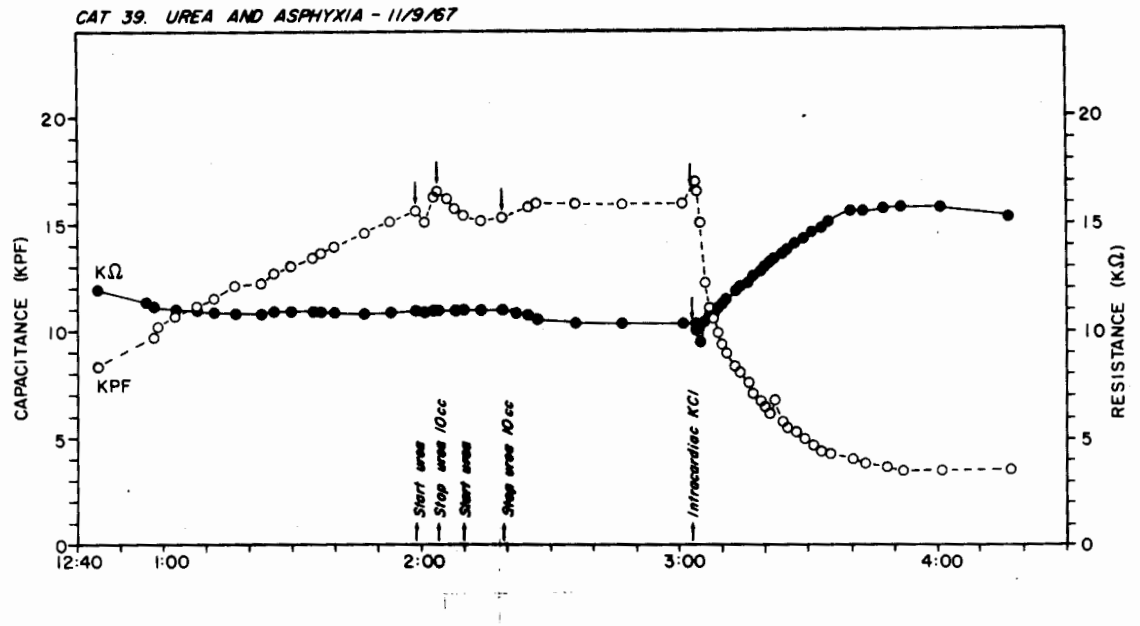

CAT 39. UREA AND ASPHYXIA - 11/9/67
CAPACITANCE (KPF)
RESISTANCE (KΩ)
KΩ
KPF
Start urea
Stop urea 10cc
Start urea
Stop urea 10cc
Intracardiac KCl
12:40
1:00
2:00
3:00
4:00

Fig 4.

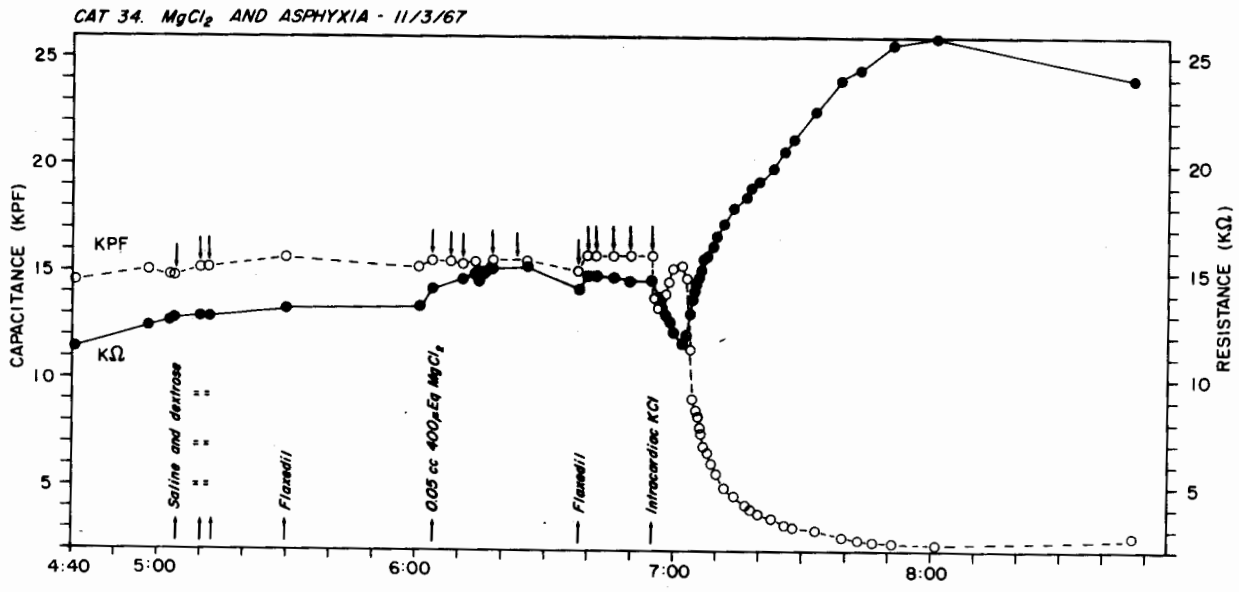

CAT 34. MgCl2 AND ASPHYXIA - 11/3/67
CAPACITANCE (KPF)
RESISTANCE (KΩ)
KPF
KΩ
Saline and dextrose
Flaxedil
0.05 cc 400μEq MgCl2
Flaxedil
Intracardiac KCl
4:40
5:00
6:00
7:00
8:00

Fig 4.

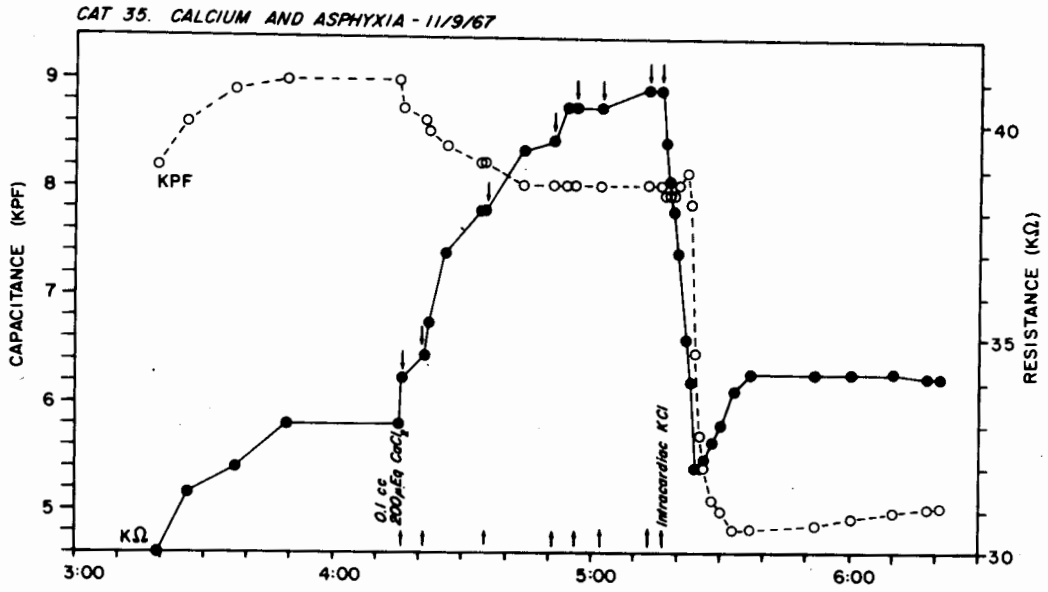


Fig 4.
Cerebral impedance measured with stainless steel coaxial bipolar electrodes in cerebral tissue of cat, showing effects of intravenous urea followed by asphyxiation (bottom). Calcium sharply increases impedance. Solid circles, resistive component of impedance; open circles, reactive component. Units on ordinates: kilohms and nanofarads. (From Ref 19.)

SUMMARY

1. The effects of weak electromagnetic fields have been tested on the efflux of calcium from cerebral tissue of chick and cat. The data strongly suggest that the binding and release of calcium occurs cooperatively as the result of long-range interactions between anionic charge sites on the binding substrate.
2. Extremely low frequency (ELF) fields at frequencies of 6 and 12 Hz and gradients in air of 0.1 to 0.5 V/cm decreased calcium efflux by 12 to 15 per cent. Higher and lower frequencies were without significant effect. For chick tissue, the field threshold in air was 0.1 V/cm and for the cat around 0.6 V/m. At intensities above and below these levels, effects became statistically insignificant.
3. With 147 MHz amplitude modulated fields, calcium afflux from chick cerebral tissue increased for modulation frequencies from 6 to 20 Hz, with a maximum of more than 15 per cent. No significant changes occurred at higher or lower modulation frequencies, nor with an unmodulated carrier wave.
4. With 450 MHz fields amplitude modulated at 16 Hz, increased calcium efflux from chick cerebral tissue occurred at field intensities between 0.1 and 1.0 mW/cm^2. No increase was noted above or below these levels.
5. This series of amplitude and frequency windows is discussed in relation to possible modes of cooperative organization of cell membrane surface glycoproteins in the binding and release of calcium.

REFERENCES

1. W. R. Adey, BioSyst. 8, 163 (1977).
2. A. L. Lehninger, Proc. Nat. Acad. Sci. U.S.A. 60, 1073 (1968).
3. L. J. Mullins, Fed. Proc. Wash. 35, 2583 (1976).
4. S. M. Bawin and W. R. Adey, Proc. Nat. Acad. Sci. U.S.A. 73, 1999 (1976).
5. S. M. Bawin, L. K. Kaczmarek and W. R. Adey, Ann. N. Y. Acad. Sci. 247, 74 (1975).
6. H. Bassen, M. Swicord and J. Abita, Ann. N. Y. Acad. Sci. 247, 481 (1975).
7. C. S. Blackman, *et al*, Proc. URSI Symposium Biological Effects of Electromagnetic Waves, Airlie, Va. (1977).
8. F. O. Schmitt and F. E. Samson, MIT Neurosci. Res. Prog. Bull. 7, 277 (1969).
9. S. J. Singer and G. L. Nicolson, Science 175, 720 (1972).
10. G. Schwarz, Biopoly. 5, 321 (1967).
11. G. Schwarz, Eur. J. Biochem. 12, 442 (1970).
12. A. Katchalsky, MIT Neurosci. Res. Prog. Bull. 12, 11 (1974).
13. R. A. Cone, in *Functional Linkings in Biomolecular Systems*, F. O. Schmitt, D. M. Crothers and D. M. Schneider, eds. Raven Press, New York, 1975.
14. A. S. Perlin, Fed. Proc. Wash. 36, 101 (1977).
15. W. R. Adey, *et al*, Exp. Neurol. 23, 29 (1969).
16. A. Katchalsky, in *Connective Tissue. Intercellular Macromolecules*, Little, Brown, Boston 1964.
17. C. W. Einolf and E. L. Carstensen, J. Phys. Chem. 75, 1091 (1970).
18. H. Fröhlich, Int. J. Quant. Chem. 11, 641 (1968).
19. H. Fröhlich, Phys. Lett. 44A (6) (1973).
20. H. Fröhlich, MIT Neurosci. Res. Prog. Bull. 15, 67 (1976).
21. I. T. Grodsky, Ann. N. Y. Acad. Sci. 247, 117 (1975).
22. I. T. Grodsky, Math. Biosci. 28, 191 (1976).

* *

DISCUSSION

You indicate that these extremely long waves were in some way involved in the transfer of information from the brain. It is well known that the information that can be transmitted on a carrier signal is a function of the frequency of the carrier signal. A carrier signal in the 16 Hertz range can at most transmit only a few bits per second. [Illinger].

Adey: That is if you assume the channel is unidirectional. Here we have a low frequency carrier that is distributed in a complex way through fine nerve cell dendrites so that the field has spatial and temporal configurations. One of the new accomplishments of sensory physiology is the work showing that the retina is an essentially silent organ right down to the point where the ganglion cells fire. Information transfer is by slow wave to slow wave, slow wave to slow wave. Nevertheless, the aggregate information handling capacity of the system is measured in millions of bits per second, by reason of its organization as a parallel process r.

How do you account for the amplitude window in the model? [Illinger].

Adey: The question of that amplitude window led us into considering tunneling. My speculation has been that if there is tunneling it is occurring along the membrane. Others say it could be through the membrane as part of a transmembrane coupling even in the face of enormous electric strain that is present on the lipid bylayer. There is the related question of where demodulation of the RF signal occurs in the tissue; even though it produces chemical changes, it is small enough to be very difficult to pick up with anything as large as a microelectrode.

One other question. There is a rough correlation between the frequency of the effects and the EEG frequency range. I understand that different types of animals have different EEG frequencies. Have there been experiments to correlate the effects that you have seen among species? [Illinger].

Adey: As to your premise, it is fascinating that the cerebral ganglia of all animals, whether of an ant, an octopus, or man display this curious low frequency oscillation with most energy below 30 Hertz, and certainly 99 percent below 100 Hertz. In terms of frequency specificity between species, I do not know of any experiments that have been done in the context of either imposed environmental fields or direct stimulation. Incidentally, it is very curious that the EEG in the invertebrate tends to be mu h less regular in oscillation. It is an irregular and often spike-like low frequency discha . Also, in the invertebrate, one can very often record on the surface of the ganglion the volume conducted discharge of a single cell over distances that would lead to their complete attenuation and disappearance in mammals. This may relate to differences in macromolecular content of extracellular fluid in invertebrates and vertebrates.

Have you looked at the relationship between the amplitude window and the frequency effect to see if there is a shift in the resonant peak frequency with amplitude? [Swicord].

Adey: There is some possibility that some monkey behavioral data can be interpreted that way. The monkeys performing the time-testing task in Dr. Medici's experiments over the last ten years must estimate a five second period. The greatest sensitivity appears to be at seven Hertz, and the field threshold, if there is a threshold for an observable behavioral effect, is somewhere between one and ten volts per meter. At 75 Hertz little is observed below 50 or 60 volts per meter. Curiously, there is not a clear response at 100 volts per meter. Thus, in this context there is an amplitude "window." Similar observations were made in cats by Dr. Bawin at 147 megahertz. There, the effects were clear at 1.0 mW/cm^2, and appeared to be in the noise at around 0.1 mW/cm^2. Studies by Dr. Blackman at EPA cited here have indicated a power window for calcium efflux from cerebral tissue at around 1.0 mW/cm^2 for a 147 MHz, 16 Hz modulated field. This agrees with data presented here for a power window at 450 MHz with incident fields around 1.0 mW/cm^2 and amplitude modulated at 16 Hz.

CLASSICAL THEORY OF MICROWAVE INTERACTIONS WITH BIOLOGICAL SYSTEMS

H. P. Schwan

Department of Bioengineering, University of Pennsylvania
Philadelphia, Pennsylvania 19104

ABSTRACT

The established mechanisms responsible for the interaction of microwaves and other electrical fields with biological systems are surveyed. Foremost is the heat development which results from the absorption of microwaves. The relative contribution to this heat development caused by the various tissue constituents including ions, water, biopolymers, bound water and lipids are discussed. Direct field interactions with various biocomponents are also considered. These include membrane interactions, biopolymer interactions, interactions with biological fluids, and field-generated forces acting on biological particles and cells. These forces are frequently neglected in discussions and yet pertain to a large number of published observations.

INTRODUCTION

This article is restricted to a survey of available biophysical knowledge of microwave interactions with biological systems. No attempt is made, however, to discuss medical findings. Table I indicates the several topics in this paper.

TABLE I:
MECHANISMS OF FIELD INTERACTIONS

Heat Development
Membrane Interactions
Biopolymer Interactions
Biological Fluids
Field Generated Forces

HEAT DEVELOPMENT

The heat development per volume unit caused by the absorption of electrical energy is given by

$$H = E^2 \kappa$$

where E is the electrical field strength and κ is the electrical conductivity of the absorber. Hence, the conductivity κ simply expresses the conversion of electrical energy into heat per unit volume. The conductivity largely controls the heat development. The dielectric constant of various tissues determines, together with the conductivity, the distribution of the field patterns in complex tissue arrangements. The conductivity may be expressed as a sum of various parts as indicated in Table 2. Here the various contributions to the total conductivity, κ, are indicated for ions (subscript I), water (W), biopolymers (B), bound water (BW) and lipids (L). The ionic contribution κ_I is frequency independent and has a value of approximately 10 mMhos/cm for the abundant tissues with high water content and frequencies

above about 0.1 GHz. All other contributions are frequency dependent, and can be represented by either a single or a sum of Debye expressions as stated by the second equation of Table 2. This equation holds perfectly for water, but only approximately for protein bound water. In the equation the dependence on the frequency, f, is a function of two constants: One is the characteristic frequency, f_c, and the other the conductivity limit increase, $\Delta\kappa = \lim \kappa$, for $f >> f_c$. $\Delta\kappa$ in turn depends on the characteristic frequency, f_c, and the dielectric constant increment $\Delta\varepsilon = \varepsilon_0 - \varepsilon_\infty$ as stated in the last equation of the table. Here the dielectric increment, $\Delta\varepsilon$, is defined as the difference in the dielectric constants for frequencies $f << f_c$ and $f >> f_c$. They may be chosen for water at 100 MHz and 100 GHz in order to exclude additional relaxation and resonance phenomena which occur at radio frequencies and in the far optical range which are of no interest in this context.

TABLE 2:

HEAT DEVELOPMENT RELATIONS

$$\kappa = \kappa_1 + \kappa_W + \kappa_B + \kappa_{BW} + \kappa_L$$

$$\kappa = \Delta\kappa \frac{f^2}{f^2 + f_c^2}$$

$$\Delta\kappa = \Delta\varepsilon \cdot \varepsilon_0 \cdot 2\pi f_c$$

$$\Delta\varepsilon = \varepsilon_0 - \varepsilon_\infty$$

(ε_0 dielectric constant of free space)

Further details are provided in Table 3 which summarizes characteristic frequencies, dielectric increments and corresponding κ-values. Little is known for membrane lipids, but the κ-contribution is probably unimportant since the membrane lipids occur typically at a tenfold lower concentration than tissue proteins in high water content tissues. The frequency dependent κ-contributions approach their quoted limit values at high frequencies, $f >> f_c$, and at the

frequency f_c, κ-values are equal to half the limit values. The data for water are very well established. The values quoted for biopolymers and bound water are approximate and may readily vary by a factor of two or more with the type of biopolymer and the amount of bound water as well as the distribution of characteristic frequencies observed for bound water. Bound water properties have been discussed by Schwan[1,2], Grant[3,4], Pennock and Schwan[5], Harvey and Hoekstra[6]. Biopolymer properties have been summarized by Oncley[7] and more recently by Takashima[8].

TABLE 3:

SUMMARY OF KNOWN DATA

	f_c	$\Delta\varepsilon$	κ(mMho/cm) (100% Concentration)
Ions			10
Water	20 G	78	0 → 800
Biopolymers	~1 M	~1000	0 → 0.05
Bound Water	~1 G	~100	0 → 5
Lipids			? (Small)

[κ in Tissues with High H_2O Well Known, κ in Lipids, Bone, etc., Poorly Understood]. All κ-Values are for 100% Concentration.

Figure 1 displays the relationships of Table 3. The volume specific absorption rate as expressed by κ is greatest for electrolytes up to about 0.5 MHz. Water dominates above 4 or 5 MHz. Bound water may be the major absorber between 0.4 and 4 GHz, depending on its detailed properties. The dashed curves present the same data, but take into account the relative abundance of the various constituents in tissues of high water content, such as muscle. It thereby establishes the relative contribution to κ by the various tissue components. A 75% water content is assumed with the other 25% largely being proteins. A tenfold smaller amount of lipids, primarily in the form of membranes of cells and subcellular organelles, is neglected as probably too small. In this presentation, the ionic contributions and water clearly dominate over the total frequency range. Biopolymer and protein bound water contribute only insignificantly to the total absorption of energy.

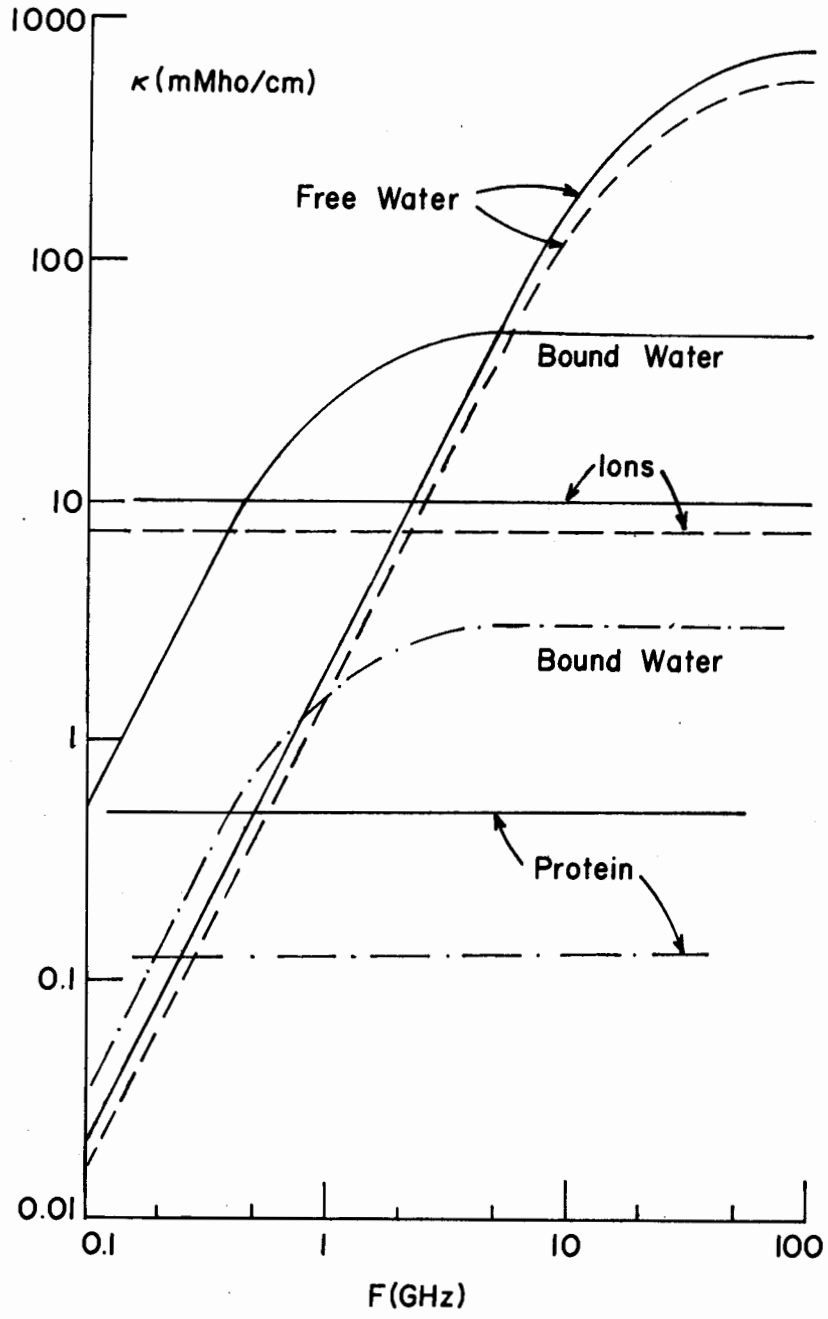


Figure 1.
Conductivities of free water, protein bound water, physiological electrolyte (ions) and proteins are indicated by the solid curves. The dashed curves represent the relative contributions of the various components to the total conductivity of tissues with high water content.

The above statements are primarily based on the analysis of tissue dielectric properties by Schwan[1], incorporating tissue data by Schwan and Li and Herrick, *et al.*, as reviewed by Schwan[1,9], and Johnson and Guy[10]. The bound water and biopolymer contributions were estimated from the bound water work carried out by Grant[3,4] and Schwan[1,2,5] and their associates and by Oncley[7] and Takashima[8]. The analysis is therefore restricted to an upper frequency of about 10 GHz and more dielectric data are needed at higher frequencies. It is possible that additional vibrational and other modes of interaction may occur above 30 or 100 GHz as reviewed by Illinger[11]. But the nonresonant behavior of water has been fairly well established up to nearly 100 GHz (Schwan, *et al.*,[12]) and appears to preclude the possibility of resonant types of interactions at frequencies below 100 GHz. It also must be pointed out that the above analysis applies to the abundant tissues with high water content. Little is known for other tissues including bone and fatty tissues; the bound water contribution in cerebral tissues may be larger.

MEMBRANE INTERACTIONS

Table 4 attempts to summarize information relevant to electrical fields and their effects on biological membranes. Membrane destruction can be achieved with low frequency alternating fields of the order of some hundred millivolts across the membrane, as later described. The propagation of action potentials along nerves is initiated or interfered with by pulses or low frequency potentials of roughly 10 mV across the membrane. Corresponding current densities and field strength values in tissues and the medium external to the affected cell are of the order of 1 mA/cm^2 and 1 V/cm[13,14,15].

TABLE 4:

ELECTRICAL FIELD EFFECTS ON MEMBRANES

	ΔV_M	E, *in situ*
Membrane Destruction	100-300 mV	
Action Potential (Excitation)	10 mV	1V/cm
Subtle Effects	0.1 - 1 mV	
Extraordinary Sensitivities		
A. Related to Membranes	0.1 μV	0.01 μV/cm
B. Possibly not Related to Membranes	< 1 nV	0.1 μV/cm
Microwave Sensitivities (1 GHz)	1 μV	1 V/cm

In recent years some extraordinary sensitivities have been reported. Electrosensitive species such as rays and sharks detect fields of intensities as low as 0.01 μV/cm. In order to achieve these sensitivities they sample the field over considerable distances with the aid of special organs, the Ampullae Lorenzini, and operate over a small frequency range extending from dc to only a few Herz[14,16]. Unconfirmed reports also indicate effects due to ELF fields of the order of V/cm in air on timing responses and calcium efflux[17,18]. Corresponding *in situ* fields would be of the order of 0.1 μV/cm as listed in the table and corresponding fields across membranes below 1 nV. It is, however, not yet obvious if the reported effects are caused by membrane processes and hence the reduction of external fields to *in situ* fields and then membrane potentials is not necessarily sensible. A more detailed discussion of this topic is given by Schwan[15] and Bawin and Adey[17] and the detailed report of the National Academy of Sciences-National Research Council on the Biological Effects of Electric and Magnetic Fields[14].

Microwave sensitivities of the order of 1 V/cm *in situ* have been frequently reported and correspond to external flux values of the order of 1 to 10 mW/cm^2 (see for example the recent text by Baranski and Czerski[19]). Some suspect that these sensitivities correspond to direct interactions with the central nervous system. However, it is straightforward to translate *in situ*

field levels to corresponding membrane potentials and these are at levels of the order of 1 μV or less depending on microwave frequency as discussed by Schwan[15]. The implications of these calculations have been challenged[19,20] by the argument that we do not yet know how the brain processes information. But the writer finds it difficult to see how this rather general and no doubt valid statement pertains to his calculation of microwave-induced membrane potentials. At microwave frequencies field strength levels in membranes and *in situ* field levels are comparable within one order of magnitude. This must be so since *in situ* currents readily pass the membranes and enter the cell interior as well as the interior of subcellular organisms[1]. Moreover, dielectric constants of membranes (about 10) and cellular fluids (about 60 or less, depending on frequency) are similar in magnitude[1]. Hence, the membrane potential is simply the product of *in situ* field strength and membrane thickness of about 10^{-6}cm. This simple argument does not depend on any particular model.

It may be argued that the microwave-induced membrane potential of about 1 μV is comparable and even higher than the perception level across the endepithelium of the Ampullae of Lorenzini. However, it should be realized that the high sensitivity of this endorgan is only achieved over a narrow bandpath range of some Hertz. If microwave sensitivities existed over such narrow bandpath ranges they would be hardly noticeable experimentally.

It also should be noted that the sensitivities of excitable cells to electric fields decrease rapidly as the electric stimulus is applied for time periods decreasingly short in comparison to the refractory period of the order of 1 msec. Hence, quotation of reported low frequency membrane sensitivities as done by Frey[20] carries no implication with regard to sensitivities claimed at microwave frequencies corresponding to time periods of the order of 1 nsec., which is a million times smaller than the refractory period. More recently, it has been postulated[21] that microwave fields may well be perceived, provided that they are modulated with frequencies below 10 or 20 Hz. This would be possible in principle if induced *in situ* fields and currents could be rectified with some degree of efficiency so that microwave fields would generate detectable low frequency currents. No evidence for such a mechanism has been

demonstrated so far at the membrane level.

The writer believes that reported extraordinary sensitivities to microwaves should be confirmed by independent investigators and that the experimental regime must be carried out with the greatest care in order to avoid artifacts and provide hard statistical evidence. In the meantime, the reported evidence can neither be accepted or refuted with certainty. It should also be pointed out that for external flux levels of the order of 1 to 10 mW/cm^2 subtle temperature elevations become apparent in man and animals which may well be perceptible but which are not therefore necessarily dangerous[10]. There is some evidence[22] that the development of "hot spots" is more likely in small animals than in man. If this can be definitely established, higher sensitivities can be expected in small animals than in man and extrapolation from animal experiments to man becomes difficult. Finally, it must be stated that work with pulsed microwave fields may well be able to produce the acoustic effect investigated by Frey[23]. This effect was long suspected to represent a direct interaction of microwaves with the central nervous system. However, more recent work by Foster and Finch[24] and by Chou, *et al.*[25], supports a reasonable classical macroscopic and thermoacoustic explanation. Therefore, reported effects on the behavior of test animals exposed to pulsed fields cannot be quoted as evidence for a direct nonthermal microwave interaction with the central nervous system.

The above excitation threshold of approximately 10 mV across the membrane pertains to signals of a duration comparable to the refractory time constant of about 1 msec. It is, therefore, also typical of alternating fields of a frequency not much in excess of 1 KHz. At low frequencies, the cell membranes are subject to a potential which is comparable to the external field strength sampled over the dimensions of the cell. For example, for spherical cells the membrane potential is equal to 1.5 ER, where E is the field strength in the medium and R is the cell radius, as indicated in Table 5. Hence, it is possible to translate membrane potentials into average *in situ* current densities. Evoked membrane potentials of 10 mV correspond to typical cell sizes and to typical resistivity values in the range of a hundred ohm-cm to tissue current densities around 1 mA/cm^2. This rough low frequency value is similar to the

current density evoked in tissue by a microwave field intensity of 10 mW/cm^2; it has been suggested[26], therefore, that a current density of about 1 mA/cm^2 may serve as a frequency independent guide number for safety standards over the total frequency range.

In Table 5 available evidence on the threshold of biological excitation phenomena is summarized for various fields. In cardiology extended experience exists with pacemakers and threshold values range about 0.1-10 mA/cm^2 depending on electrode size and other parameters[27]. In electrohypnosis, electrosleep and electrical anaesthesia total currents applied are about 10 to 100 mA. Corresponding current densities in the brain may be estimated based on the work by Driscoll[28]. For a total current applied to the head of 1 mA, internal brain current densities[28] are of the order of 10 $\mu A/cm^2$. Hence 10-100 mA total current corresponds to brain tissue current densities of the order of 0.1-1 mA/cm^2. Very extended work[13] has been carried out on electrical hazards caused by low frequency potentials applied to the human body. The values quoted in the table as thresholds for sensation, "let go" current and fibrillation are all consistent[13] with a current density of about 1 mA/cm^2. Thus membrane potentials in the mV range as discussed above are consistent with the experience gained with pacemakers, and the effects on brain tissue and in the electrical hazards field.

TABLE 5:

BIOLOGICAL THRESHOLDS

Cardiology	0.03 - 10 mA/cm^2
Electrosleep and Electrical Anaesthesia	10 - 100 mA
Electro-Hazards:	
Sensation	1 mA
"Let Go"	10 mA
Fibrillation	100 mA
Biophysics and Axonology	1 mA/cm^2
$\Delta V_m = 1.5$ ER	(10 μ, 1 mV)
$\Delta V_m = R \cdot J(mA/cm^2)$	

BIOPOLYMER INTERACTIONS

Considerable work has been done on the interaction of electrical fields with biopolymers. The behavior of proteins has been investigated in detail at radiofrequencies by Oncley[7]. Low frequency work and radiofrequency work of more recent origin on proteins and nucleic acids has been summarized by Takashima and Minakata[8]. All reported interactions are of the nonresonant relaxation type characterized by the Debye equation again quoted in Table 6. These interactions are linear and reversible up to field strength values of many volts per centimeter in the suspending medium. The limit of linearity may be estimated from the Langevin equation and is in the KV/cm range. Hence interactions in the V/cm range are characterized by responses accompanied by changes in potential energy which are very small in comparison with the thermal energy, KT. More simply expressed, the degree of orientation experienced by a polar protein molecule exposed to a field of 1 V/cm is very small. Thermal collisions with other molecules are far more effective than the field in affecting the orientation and virtually prevent any degree of orientation with the field.

Biopolymer interactions are due to either partial rotation of the total molecule or, at microwave frequencies, also include relaxation effects due to partial rotation of polar groups or of protein bound water[2,3]. Resonant responses are possible at frequencies above 100 GHz where the viscous properties of water do not prevent resonances. But none have been identified. A detailed discussion of these speculative responses was given by Illinger[11,29].

Table 6 summarizes established mechanisms in the radiofrequency and microwave range. There have been identified rotational relaxation mechanisms caused by polar molecular properties and counter-ion relaxation effects as investigated theoretically by Schwarz[30] and experimentally by Schwan, *et al.*,[31,32]; f_c are the characteristic frequencies and $\Delta\varepsilon$ the dielectric increments extrapolated to the case of 100% volume occupancy. All values are approximate and amino acids have smaller and nucleic acids frequently have larger dielectric increments than proteins. More details are given in the quoted references[7,8]. Corresponding conductivities have been discussed above in the section on thermal effects.

TABLE 6:

SUMMARY OF ESTABLISHED MECHANISMS IN BIOPOLYMERS

$\varepsilon^* = \varepsilon_\infty + \Delta\varepsilon/[1+jf/f_c]$

	Mechanisms	f_c	$\Delta\varepsilon$
Proteins	Rotational Relaxation	1 - 10 M	1000
Amino Acids	Rotational Relaxation	100-1000	Small
Nucleic Acids	Counter-Ion and Rotational Relaxation	LF , RF	Large
Protein Bound Water	-	100-3000	100

Figure 2 attempts to summarize the work on bound water and partial molecular rotation. The effective dielectric constant of the hydrated hemoglobin molecule is plotted versus frequency. The dielectric constant is rather strongly frequency dependent, probably due to the frequency-dependent properties of the hemoglobin bound water and partial rotation. For a more detailed analysis of this curve see Schwan (pp. 192 to 198 of Reference 1).

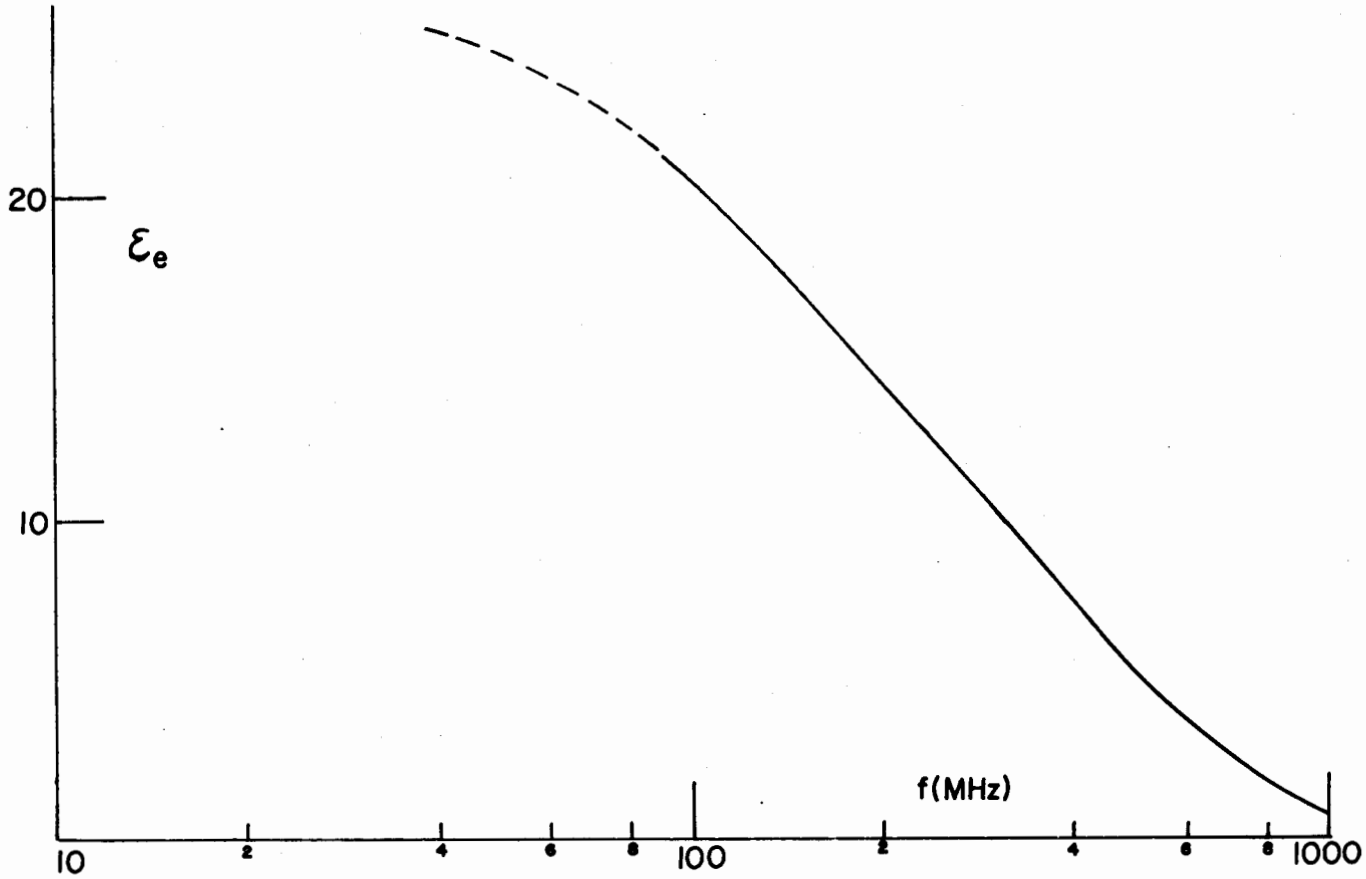


Figure 2.
The effective dielectric constant of the hydrated hemoglobin molecule as a function of frequency. A value of 0.3 g bound water per g protein is assumed. The result is not strongly dependent on the assumed hydration value.

Data published by Schwan and his colleagues on hemoglobin and by Grant and his group on albumin are quite similar and similar conclusions were reached. A more detailed discussion on this topic is given by Grant in this volume.

In summary it can be stated that known interactions of biopolymers with electrical fields at alternating frequencies up to 100 GHz are of the relaxational type. The viscous properties of water appear to preclude resonant type interactions. The relaxation responses result in part from the polar properties of the biological macromolecules and from counter-ion displacement effects. They are well in the linear range at the typical field strength levels of about 1 V/cm and above and, hence, do not suggest any irreversible and biochemically significant changes. It has been suggested[33] that these considerations are outdated and that quantum-mechanical considerations are appropriate. In the writer's opinion, however, this speculation is unsupported. The work of Illinger[11] and of Fröhlich[34] are both only suggestive and pertain to frequencies above 30 to 100 GHz. Grodsky's interesting suggestions[35] are difficult to apply to any particular frequency range.

BIOLOGICAL FLUIDS

The above discussions on biopolymers are based on results obtained with suspensions of biological macromolecules. These data and their interpretation are only applicable to the biological fluids external to cells and subcellular particles and to the cytoplasm if it can be assumed that tissue water is identical with free water. This assumption has been challenged by Ling[36] whose induction hypothesis assigns entirely different properties to tissue water. Ling's induction hypothesis has not met with general acceptance and experimental verification appears difficult. On the other hand, the dielectric properties of tissues are consistent with the assumption that tissue water has very similar, if not the same, properties as free water except for the small fraction of protein bound water discussed before. The mobility of ions in tissue water appears to be comparable to that in electrolytes. The static dielectric constant of tissue water as determined at 100 Mhz compares with that of free water if due allowance is made for the volume

fraction occupied by biological macromolecules. Also the relaxation time of tissue water seems to be close to that of normal water[37]. These considerations were already indicated twenty years ago and more recently in somewhat greater detail[37,38]. However, all these arguments have been advanced only for tissues with high water content and invite further refinement. Virtually little is known for tissues with low water content as far as the interpretation of dielectric data is concerned.

FIELD GENERATED FORCE EFFECTS

Electric fields can directly interact with matter and create forces that can act on molecules as well as on cellular and larger structures. Most of these interactions are reversible and do not necessarily have demonstrable biological effects. An example is the movement of ions in an ac field, which is inconsequential, provided that the field is weak enough to prevent undue heating from molecular collisions (*e.g.*, below about 1 V/cm, corresponding to 1 mA/cm^2 in a physiological medium). Another example is the orientation of polar macromolecules. For field strength values of interest here, only a very partial preferential orientation with the field results. Complete orientation and consequent dielectric saturation requires field strengths of thousands of volts per centimeter. (Changes of this magnitude do occur in membranes on depolarization. Hence, field-induced orientation and changes in orientation of membrane molecules appear possible. Corresponding tissue current densities would be in milliamperes per square centimeter, as discussed above.)

Electric fields can interact just as well with nonpolar cells and organelles in the absence of any net charge. These "ponderomotive" forces are well known and understood. Any system exposed to an electric field will tend to minimize its electric potential energy by appropriate rearrangement. This statement is equally true for dc and ac fields, because the potential energy is a function of the square of the field strength. Inasmuch as the induced dipole moment of a cell or large particle depends on both the square of field strength and the volume, it is not surprising that the threshold field to overcome thermal agitation is proportional to $R^{-1.5}$, where R is the effective radius of the particle. Experimental evidence confirms the principle;

threshold field values for responses of 10 μm cells are about 10 V/cm. But for 10 nm macromolecules, they are about 10 kV/cm and comparable with the fields needed for complete orientation, owing to the existence of a typical dipole moment of about 10 debyes.

Table 7 summarizes observed manifestations of field-generated forces. The field effects may manifest themselves as orientation of particles in the direction of the field or perpendicular to it. Or "pearl chain" formation, *i.e.*, the alignment of particles in the field direction may occur. This has long been considered a mysterious demonstration of microwave induced biological effects. Deformation or destruction of cells can be achieved with fields. The movement of cells in inhomogeneous electrical fields can be affected.

TABLE 7:
FIELD GENERATED FORCES

Orientation
"Pearl Chain" Formation
Deformation
Movement
Destruction

Zimmerman, *et al*[39]., have observed the destruction of red cells and ghost formation. Neumann and Rosenheck[40] studied the effects of fields on chromaffin vesicles. Friend, *et al*[41]., as well as Goodman[42] studied the effects of fields on fairly large cellular organism. Orientation effects have been observed by Teixerira-Pinto, *et al*[43]., by Sher[44] and Novak[45]. Pohl[46] developed "dielectrophoresis" as a tool of separating cells in inhomogeneous fields. And Elul, *et al*[47]., observed cell destruction phenomena and cell shape changes. No attempt is made here to summarize the total literature on this topic and additional discussions have been presented elsewhere[48,49]. Some of these field-generated force effects can be very startling and dramatic especially near the tip of small electrodes. Of a similar nature is the movement of magnetotactic

bacteria recently reported by Blakemore[50] in magnetic fields of fairly low intensity. Apparently, these bacteria are equipped with magnetic properties and are therefore significantly oriented by the magnetic field and motivated to move in the field direction.

Experimental and theoretical evidence indicates that pulsed fields cannot have greater effects than continuous fields of the same average power[51]. Hence, modulation is not expected to have special effects.

Field forces due to the induced dipole moment of the field have been listed as evidence of nonthermal action of electric fields on biologic systems. However, the effects require fairly large field strength frequently above those that give rise to heating or stimulation of excitable tissues. The field forces also depend on the electric properties of the particle considered and its environment.

A more detailed derivation of the dielectrophoretic force in lossy dielectric media has been given by Sher[52] and is based in turn on a derivation of the potential electric energy of a lossy dielectric body given by Schwarz[53]. However, it now appears that an error occurred in Sher's derivation and the writer has calculated that at least for low and radio frequencies the force acting on a particle is proportional to particle volume, the gradient of the external field squared and the external dielectric constant. Hence it would not be surprising if all sorts of biological particles of different effective complex dielectric constants behave similar in an electrolyte medium. Figure 3 illustrates this fact. Neumann and Rosenheck's results on chromaffin vesicles are combined with E.Coli data obtained by Sher and erythrocyte data obtained by Sher and silicon particles (full circles), also by Sher[44]. The total material fits convincingly the solid line of slope -1.5 which is demanded by the theoretical requirement that particle volume must be inversely related to the square of the threshold field strength mentioned above and discussed in greater detail elsewhere (Schwan and Sher[54]).

The dashed curves in Fig. 3 pertain to another model. It is assumed that the threshold of a cellular response or destruction is reached when the induced membrane potential reaches the dielectric breakthrough level. This level may well be in the range of 0.1 to 1 V across the membrane, corresponding

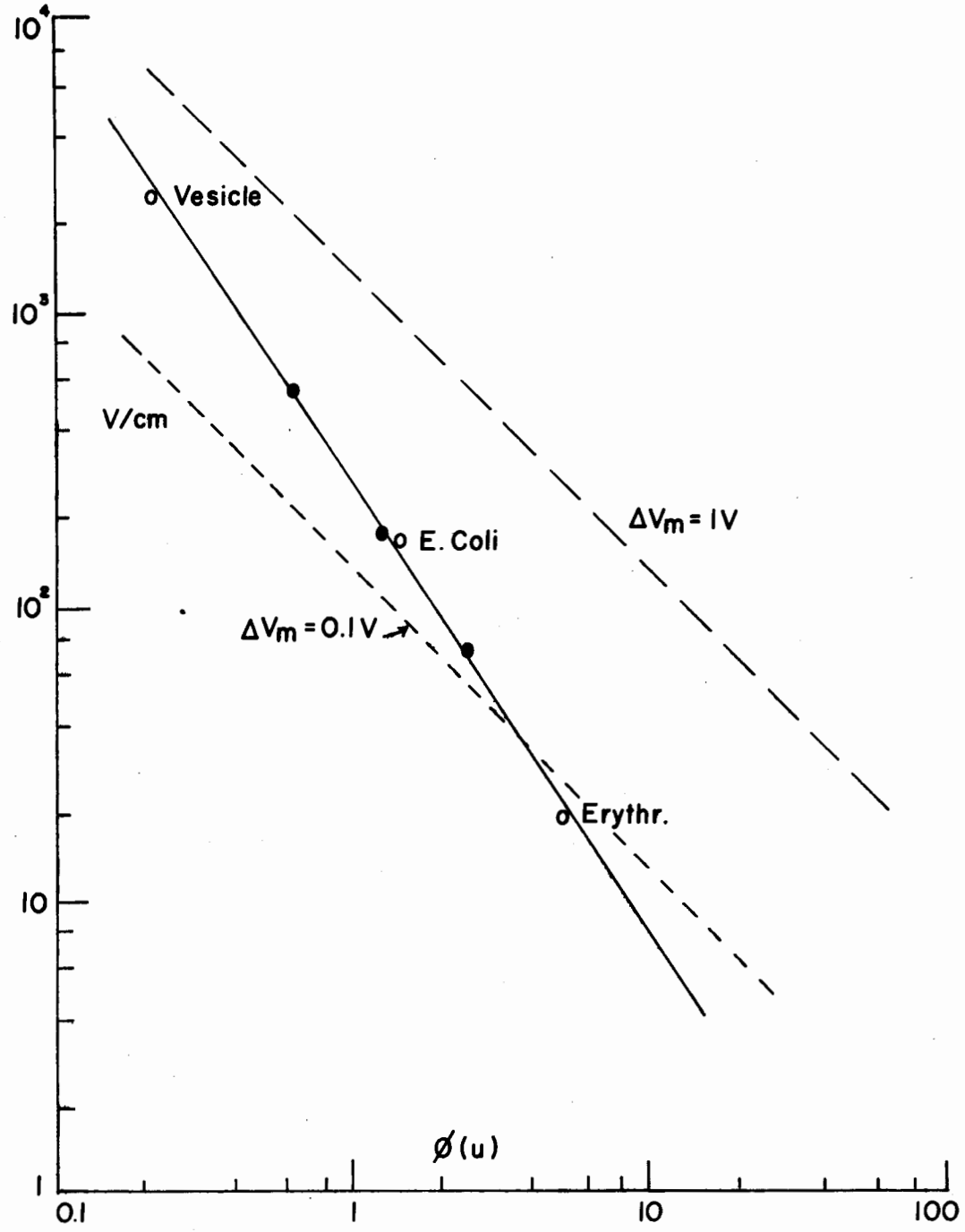


Figure 3.
Threshold field strength values as function of particle size. The solid curve assumes field generated force effects. The dashed curves assume damage resulting from membrane breakdown at the quoted membrane potentials of 0.1 and 1 Volt. The open circles represent results obtained with biological cells and the full circles data with silicone particles. The data fit the theoretical demand indicated by the solid line and appear to be insensitive to the dielectric properties of the particles as predicted by theory.

to membrane field strength levels from 100 KV/cm to one million V/cm. The inverse relationship of the threshold field level in the medium with the particle diameter follows from the equation $\Delta Vm = 1.5\ ER$ already quoted in Table 5. The dashed curves establish threshold particle relationships somewhat similar to those resulting from a consideration of field-generated forces. Hence, in practice it may at times be difficult to separate biological effects due to either field-generated forces from those due to induced membrane potentials which are intolerably high.

In general, available evidence and present understanding indicate that significant effects with field-evoked forces require field strength values above 1 V/cm in the medium, unless cellular dimensions are well above 100 μm.

REFERENCES

1. H. P. Schwan, in *Advances in Biological and Medical Physics*, Vol. V, ed. by J. H. Lawrence and C. A. Tobias, Academic Press, Inc., New York 1957.
2. H. P. Schwan, Ann. N. Y. Acad. of Sci. 125, 344 (1965).
3. E. H. Grant, Ann. N. Y. Acad. of Sci. 125, 418 (1965).
4. E. H. Grant, J. Mol. Biol. 19, 133 (1966).
5. B. Pennock and H. P. Schwan, J. Phys. Chem. 73, 2600 (1969).
6. S. C. Harvey and P. Hoekstra, J. Phys. Chem. 76, 2987 (1972).
7. J. L. Oncley, in *Proteins, Amino Acids and Peptides as Ions and Dipolar Ions*, ed. by E. J. Cohn and J. T. Edsall, Reinhold New York, N. Y. 1943.
8. S. Takashima and A. Minakata, in *Digest of Dielectric Literature*, Nat. Acad. Sci.- Nat. Res. Council, Vol. 37, 1975.
9. H. P. Schwan, in *Therapeutic Heat*, 2nd Ed., Eliz. Licht Pub., New Haven, Conn. 1965.
10. C. C. Johnson and A. W. Guy, Proc. IEEE 60, 692 (1972).
11. R. H. Illinger, in *Biologic Effects and Health Hazards of Microwave Radiation*, ed. by P. Czerski, *et al.*, Polish Medical Publishers, Warsaw 1974.
12. H. P. Schwan, R. J. Sheppard and E. H. Grant, J. Chem. Phys. 64 (5) (1976).
13. H. P. Schwan, NWL Technical Report TR-2713, U. S. Naval Weapons Lab., Dahlgren, Va. 1972.
14. *Biologic Effects of Electric and Magnetic Fields Associated with Proposed Project Seafarer.* National Academy of Sciences - National Research Council, Washington, D. C. 1977
15. H. P. Schwan, IEEE Trans. MTT-19, 146 (1971).
16. A. J. Kalmijn, Nature 212, 1232 (1966).
17. S. M. Bawin and W. R. Adey, in Proc. Nat. Acad. Sci. USA 73, 1999 (1976).
18. R. Gavalas-Medici and S. R. Day-Magdaleno, Nature 261, 256 (1976).
19. S. Baranski and P. Czerski, *Biological Effects of Microwaves*, Dowden Hutchinson & Ross, Inc., Stroudsburg, Pa. 1976.
20. A. H. Frey, IEEE Trans. MTT-19, 153 (1971).
21. S. M. Bawin and W. R. Adey, in Neurosci. Res. Prog. Bull. 15, 1 (1977).
22. H. N. Kritikos and H. P. Schwan, IEEE Trans. BME-22, 457 (1975).

23. A. H. Frey, J. Appl. Physiol. 17, 689 (1962).

24. K. R. Foster and E. D. Finch, Science 185, 256 (1974).

25. C. K. Chou, R. Galambos, A. W. Guy and R. H. Lovely, J. Microwave Power 10, 361 (1975).

26. H. P. Schwan, IEEE Trans. BME-19, 304 (1972).

27. O. Z. Roy, J. R. Scott and G. C. Park, IEEE Trans. BME-23, 45 (1976).

28. D. A. Driscoll. An Investigation of a Theoretical Model of the Human Head with Application to Current Flow Calculations and EEG Interpretation. Ph.D. Thesis, May 1970, University of Vermont.

29. R. H. Illinger, Concurrent Presentation.

30. G. Schwarz, J. of Phys. Chem. 66, 2636 (1962).

31. H. P. Schwan and J. Maczuk, in *Proceedings of the First National Biophysics Conference*, Yale University Press, 1959.

32. H. P. Schwan, G. Schwarz, J. Maczuk, and H. Pauly, J. Phys. Chem. 66, 2626 (1962).

33. P. Czerski. Discussion remark in: *Fundamental and Applied Aspects of Nonionizing Radiation*, ed. by S. M. Michaelson, M. W. Miller, R. Magin, and E. L. Carstensen, p. 19. Plenum Press, New York 1975.

34. H. Fröhlich, in *Brain Interactions with Weak Electric and Magnetic Fields*, ed. by W. R. Adey and S. M. Bawin, Neurosci. Res. Prog. Bull. 15, 67 (1977).

35. I. T. Grodsky, in *Brain Interactions with Weak Electric and Magnetic Fields*, ed. by W. R. Adey and S. M. Bawin, Neurosci. Res. Prog. Bull. 15, 72 (1977).

36. G. N. Ling, C. Miller, and M. M. Ochsenfeld, in *Physicochemical State of Ions and Water in Living Tissues and Model Systems*, ed. by C. F. Hazlewood. Ann. N. Y. Acad. of Sci. 204 (1973).

37. H. P. Schwan, and K. R. Foster, Biophys. J. 17, 193 (1977).

38. H. P. Schwan, in *Brain Interactions with Weak Electric and Magnetic Fields*, ed. by W. R. Adey and S. M. Bawin, Neurosci. Res. Prog. Bull. 15, 88 (1977).

39. U. Zimmermann, G. Pilwat and R. Riemann, Biophys. J. 14, 881 (1974).

40. E. Neumann and K. Rosenheck, J. Memb. Biol. 10, 279 (1972).

41. A. W. Friend, E. D. Finch and H. P. Schwan, Science 187, 357 (1974).

42. E. M. Goodman, B. Greenebaum and M. T. Marron. Effects of Extremely Low Frequency Electromagnetic Fields on Growth and Differentiation of Physarum Polycephalum, Technical Report Phase I (Continuous Wave). University of Wisconsin 1975 and E. M. Goodman, B. Greenebaum and M. T. Marron. Effects of Extremely Low Frequency Electromagnetic Fields on Physarum Polycephalum. Technical Report, Office of Naval Research Contract N-00014-76-C-0180. University of Wisconsin 1976.

43. A. A. Teixeira-Pinto, L. L. Nejelski, J. L. Cutler and J. H. Heller, Exp. Cell Res. 20, 548 (1960).

44. L. D. Sher, Mechanical Effects of AC Fields on Particles Dispersed in a Liquid: Biological Implications. Ph. D. Thesis, University of Pennsylvania, Philadelphia, Penn. 1963.

45. B. Novak and F. W. Bentrup, Biophysik 9, 253 (1973).

46. H. A. Pohl, J. Biol. Phys. 1, 1 (1973).

47. R. Elul, J. Physiol. 189, 351 (1967).

48. H. P. Schwan, Field Interactions with Biological Matter. Ann. New York Acad. Sci. (In Press).

49. S. M. Bawin and W. R. Adey, in *Brain Interactions with Weak Electric and Magnetic Fields*, Neurosci. Res. Prog. Bull. 15, (1977).

50. R. Blakemore, Science 190, 377 (1975).

51. L. D. Sher, E. Kresch and H. P. Schwan, Biophys. J. 10, 970 (1970).

52. L. D. Sher, Nature 220, 695 (1968).

53. G. Schwarz, J. Chem. Phys. 39, 2387 (1963).

54. H. P. Schwan and L. D. Sher, J. Electrochem. Soc. 116, 170 (1969).

DETERMINATION OF BOUND WATER IN BIOLOGICAL MATERIALS FROM DIELECTRIC MEASUREMENTS

E. H. Grant
Physics Department, Queen Elizabeth College, London, W8 7AH, U. K.

ABSTRACT

For aqueous biological materials variations in permittivity occurring between 100-1000 MHz are principally due to the water of hydration and the hydration of such materials can be determined by measurement of the dielectric permittivity. Measurements of the static permittivity and the relaxation time can be used to predict the absorption of microwave energy by a hydrated biological macromolecule, based on a suitable model. Using a spherical shell model for the macromolecule and the experimentally determined permittivities and conductivities, we have calculated the variation of specific energy absorption as a function of frequency and found that in a certain frequency region the absorption is much greater for bound water than for free water.

INTRODUCTION

The dielectric method of investigating hydration depends on the fact that bound water possesses electrical and mechanical properties different from those of free water. The differences in the electrical behaviour are noticed experimentally by the observation that bound water exhibits dielectric dispersion (the δ-dispersion) in the frequency region of hundred of MHz whereas free water disperses at much higher frequencies (1-100 GHz). Since most biological molecules relax at frequencies well below 100 MHz it follows that changes in permittivity occurring between 100-1000 MHz in an aqueous biological material are due to the water of hydration, and therefore that dielectric measurements made in this region may be interpreted in terms of the quantity and nature of the bound water present. This is one method of studying hydration by dielectric methods and is quite sensitive in that the value of the hydration, w, is directly proportional to the total amplitude of the δ-dispersion. A variation of this technique which is easier to carry out experimentally is to determine the permittivity of the biological solution at one single frequency, say 800 MHz, near the high frequency limit of the δ-dispersion. The difference between this measured permittivity and that of pure water at the same frequency is termed the dielectric decrement. It is customary to divide this by the concentration of solute material present to obtain the specific decrement, δ , which at 800 MHz may be written δ_{800}. The value of δ_{800} is a function of the quantity of bound water present, and therefore leads to another means of measuring hydration, w. In this method there may be considerable error in the value obtained for w because only part of δ_{800} is due to bound water (the rest is due to the biological macromolecules); another uncertainty is ignorance of the precise mixture relationship used to calculate w from δ_{800}. This method can be used with profit to measure *differences* in hydration when molecules of similar size and shape are involved in which case systematic errors cancel out.

HYDRATION

Absolute values of w determined from the amplitude of the δ-dispersion are considerably more accurate than when obtained from δ_{800} but the experimental technique is more demanding in that measurements have to be made over a wide frequency range instead of at one frequency only. In both cases the hydration which is measured corresponds to the water molecules which are unable to rotate in an electric field at frequencies around 1 GHz. This may be termed "irrotationally bound" water.

Of a different character is the water carried bound by a biological macromolecule when the macromolecule exhibits dielectric relaxation in a radiofrequency field (frequencies less than about 10 MHz). In this case the hydration corresponds to "highly viscous" water, *i.e.*, the difference with free water appears in the mechanical properties rather than the electrical properties. This hydration is determined by calculating the volume of the hydrated macromolecule from its measured dielectric relaxation time. The volume of the macromolecule as deduced by an independent method (*e.g.* X-ray crystallography) is then deducted from that of the hydrated unit to give the hydration. There is no reason to expect this value of hydration to agree with those obtained from either of the other two methods referred to above.

In many practical situations such as non-ionizing radiation hazards or the use of electromagnetic waves to produce hyperthermia the mechanisms of interaction between the radiation and the biological material is the same as that involved in measuring the irrotationally bound water, w, and it is therefore *this* definition of hydration which is appropriate to the calculation of absorption of microwave energy by biological tissues.

Specific examples of the use of the δ-dispersion to investigate the properties of bound water present in protein solutions occur in some studies carried out on haemoglobin[1], myoglobin[2] and serum albumen[3]. For each of these proteins the associated water of hydration was found to exhibit a relaxation time, τ, of around 1ns at room temperature compared with the corresponding relaxation time of 10ps for free water. These observed large differ-

ences in the relaxation times did not appear in the values of static permittivity, ε_s ; on the contrary, the value of ε_s for bound water which gave the best fit to the experimental data was in the range of 80 - 100 which accords with the well known values of ε_s which have been directly measured for water and ice. Using these values of τ and ε_s for bound water it is possible to predict the absorption of microwave energy by a hydrated biological macromolecule, provided a suitable model is adopted and certain assumptions made.

SHELL MODEL

It is convenient mathematically to consider a hydrated macromolecule as a sphere surrounded by a bound water shell, the whole unit being submerged in a continuum to represent the free water (Fig. 1). In this model the permittivities of the core, hydration shell and free water are designated ε_p, ε_h and ε_w respectively; the corresponding conductivities are σ_p, σ_h and σ_w. To obtain values for the energy absorption in the three media it is necessary to calculate the electric field strength, E, in each of them after which the absorption of energy per unit volume, A, can be found by using the simple relationship

$$A = \frac{1}{2} \sigma E^2 \quad .$$

Relative values of A have been calculated[4] for the three media using the values of ε_h and σ_h measured in the above experimental investigations[1-3] and adopting the well known literature values[5] of ε_w and σ_w. The calculations are relatively insensitive to the values chosen for ε_p and σ_p ; ε_p in practice was taken as 5 and the calculations were carried out for values of σ_p of zero and $10^{-2}\ \Omega^{-1}\ m^{-1}$. The relative field strngths in the three regions were obtained from the appropriate potential functions.

The variation of the specific energy absorption with frequency is shown in Fig. 2 for free and bound water, arbitrary units being adopted for the ordinate. The graph shows that *for this simple model* a frequency region exists where the absorption of energy per unit volume of bound water

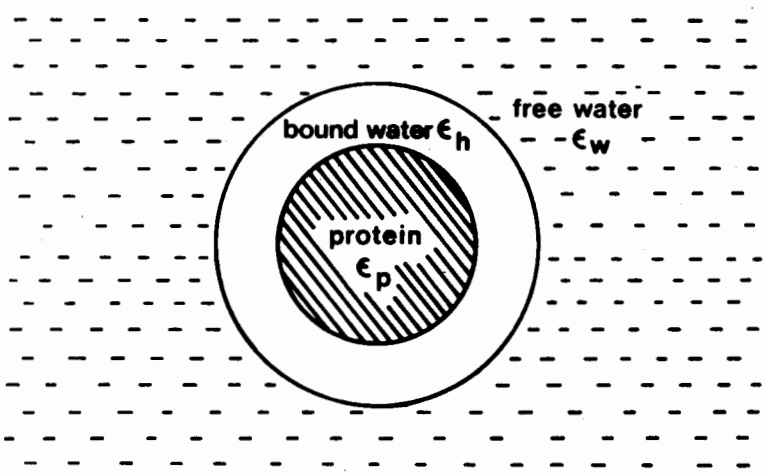


Figure 1.

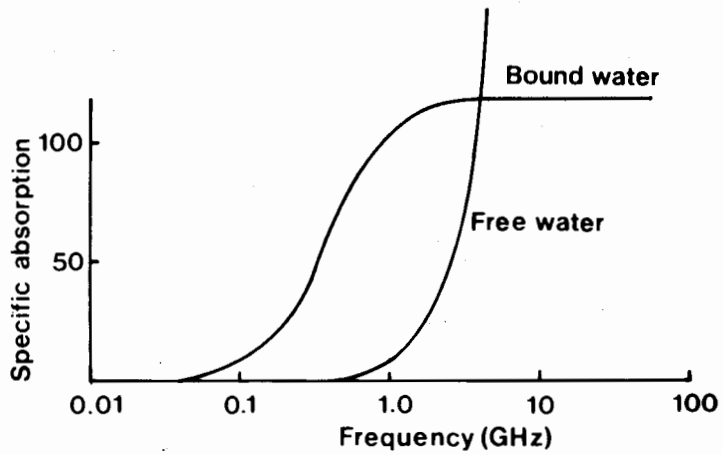


Figure 2.

is considerably greater than that of free water. For biological materials which have a large bound water content (such as lens tissue) this finding could be of important consequence in evaluating microwave radiation hazards, particularly if an attempt is to be made to build a frequency factor into the maximum recommended power levels for personnel exposed to microwaves. The importance of the findings is further enhanced when it is remembered that the bound water is immediately adjacent to the vital biological macromolecules.

REFERENCES

1. E. H. Grant, G. P. South, S. Takashima and H. Ichimura, Biochem. J. 122, 691 (1971).

2. E. H. Grant, B. G. R. Mitton, G. P. South and R. J. Sheppard, Biochem. J. 139, 375 (1974).

3. C. G. Essex, M. S. Symonds, R. J. Sheppard, E. H. Grant, R. Lamote, F. Soetewey, M. Y. Rosseneu and H. Peeters, Phys. Med. Biol. (1977 - In Press).

4. E. H. Grant, R. J. Sheppard and G. P. South, in *Proceedings of the 5th European Microwave Conference*, Hamburg, 1975.

5. H. P. Schwan, R. J. Sheppard and E. H. Grant, J. Chem. Phys. 64, 2257, (1976).

* *

DISCUSSION

I was interested in the excellent data which Dr. Grant obtained at 70 GHz, ε" in particular. Some years ago I argued, as you indicated in your model, that the calculation of the dielectric constant is not straightforward. All that one can say is, what is the effective dielectric constant of the dehydrated molecule; one has to make some assumption with regard to the core or the shell in order to derive the quantity of interest. This relates to the relative contribution of the bound water to the dielectric increment. As I pointed out, we do not have that problem with regard to conductivity. The relative contribution of bound water to the overall conductivity at very high frequencies is very small by comparison with that of free water. With the accurate data you obtained at 70 GHz you should now have an excellent chance to get much more precise data for the conductivity. [Schwan].

Grant: It is just a matter of time now. We have just made the measurements on pure water, which I put up on the board, but we have not yet made any measurements on biological solution. That would be the next thing to do, continuing it over the whole frequency range, down to your own measurements at 1 GHz.

What is the frequency at the crossover between absorption in free water and water of hydration? [Cleary].

Grant: The crossover between the free water and the water of hydration was at about 4 GHz. I must point out that the model is sensitive. It depends upon considering the protein as a sphere surrounded by a uniform shell. I think that if one tried other particle shapes and other shell forms, one would still find that bound water absorbs more than free water, but the crossover frequency may change.

One question which we have not really faced is the extent of the water which is modified by proximity to an interface and which may extend for far larger distances than we have discussed, say two molecular-layers. I am afraid that this is the type of subject that we do not have time for this morning. I hope for an opportunity to discuss it tomorrow. We do have considerable evidence that there are very significant extensive structures in modified water layers both around macromolecules as well as inside cells. [Drost-Hansen].

INTERFACIAL AND INTRACELLULAR WATER: EXPECTED ANOMALIES IN DIELECTRIC PROPERTIES

James S. Clegg and W. Drost-Hansen

Laboratory for Quantitative Biology and
Laboratory for Water Research, Department of Chemistry
University of Miami, Coral Gables, Florida 33124

ABSTRACT

Brief consideration is given to the extensive evidence that water adjacent to surfaces in inanimate systems differs markedly in its properties from ordinary bulk water. Calculations of the amount of intracellular surface area (rat liver cells) strongly suggest that a large fraction of intracellular water should be so perturbed, by proximity to various ultrastructural surfaces. Such "vicinal water" can be expected to play an important role in the interactions of biological systems with electromagnetic radiation, particularly in the microwave region.

INTRODUCTION

The purpose of this note is to call attention to the anomalous structure of water at interfaces in general and in cells in particular. Such water appears to be structurally different from bulk water and, as a consequence, is expected to possess dielectric properties distinctly different from bulk water. Two questions arise:

1) What types of structures predominate in such surface-modified water?
2) Over what distances do such structures extend?

At the moment, the structure of bulk water escapes a reasonably detailed description. In fact, several mutually exclusive theories are currently available for the structure of bulk water. Hence it is hardly surprising that the structure of vicinal water is not known. However, it appears likely that the second of the questions posed above can be answered to a first approximation.

It appears that vicinal water extends over far larger distances than normally assumed; namely, of the order of 30 to 300 molecular diameters of a water molecule (*i.e.*, about 0.01 to 0.1 μm). A large amount of evidence is available to substantiate this claim. For instance, studies by Peschel[1] and by Peschel and Adlfinger[2,3] have clearly shown the long-range effects of quartz surfaces on the structure of vicinal water as revealed by disjoining pressure measurements and measurements of viscosity of water confined between two quartz plates.

Other unusual properties which may be of interest in connection with microwaves (and particularly in the treatment of malignancies by hyperthermia) is the enhanced thermal conductivity reported for vicinal water[4]. Drost-Hansen[5] has speculated on the role that vicinal water might play in hyperthermia treatment of cancers. A number of studies in the literature suggest that the dielectric constant of vicinal water is also unusual[6]. DC conductivity measurements[7] tentatively suggest that the energies of activation for the movement of ions in vicinal water may be notably larger than for ions in solution. Some tentative calculations indicated thicknesses of 0.01 to 0.10

μm for the surface modified water. Finally, we point out the unusual heat capacity of vicinal water reported by Bruun and Drost-Hansen[8]. Some measurements indicated that the apparent heat capacity of water at a variety of interfaces is approximately 25% larger than the heat capacity of bulk water, and Clegg[9] observed a similar circumstance for the water of intact living cells. Such observations may be of some significance in the nature of the interactions of microwaves with biological systems.

COLLECTIVE BEHAVIOR

Although at the moment it is not possible to describe the structure or structures of vicinal water, a number of observations are pertinent in this connection. It has been observed from temperature studies that vicinal water is capable of undergoing phase transitions. Evidence has been presented[5,10,11] for the existence of thermal anomalies at no less than four different temperature ranges between the freezing and boiling points of water: 14-16°; 29-32°; 44-46°; 59-62°C. These anomalies suggest that the transitions are due to cooperative (collective) effects among very large numbers of water molecules comprising the vicinal layers.

A typical example of the type of thermal anomalies frequently observed is given in Figure 1. These data were reported by Wiggins[12] for the distribution of sodium and potassium ions in the narrow pores of a silica gel and her findings have recently been confirmed by Hurtado and Drost-Hansen[13].

The thermal anomalies are sometimes manifested as exceedingly sharp changes in slope, as in the experiments of Wiggins (Fig. 1). At other times the anomalies appear as relatively sharp peaks, as for instance, in data for surface entropies[14]. In other cases they appear as somewhat broader peaks or minima: thus Bruun, Sörensen and Drost-Hansen (unpublished data; see Reference 14) obtained anomalous minima in the excess ultrasonic absorption of vicinal water in 10% aqueous suspensions of small (0.091 μm) polystyrene spheres.

Other evidence for the collective behavior of large numbers of water molecules has been reported. Workman and Reynolds[15] observed the occurrence of large electrical potentials between a freezing ice crystal and the

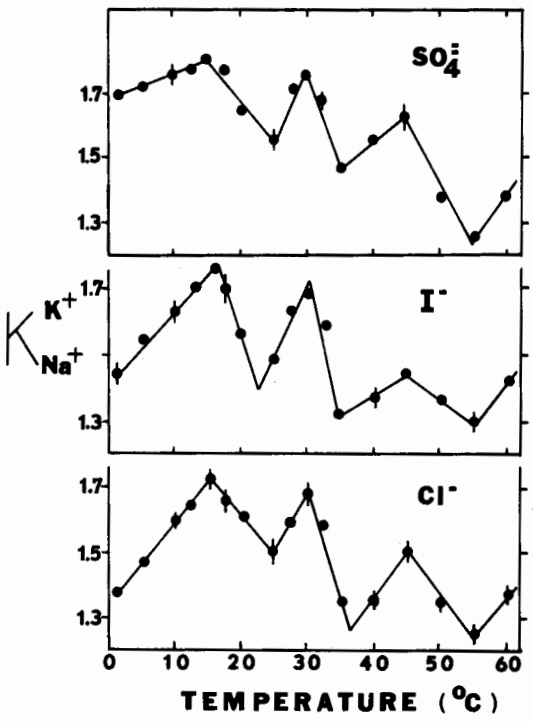


Figure 1.
Variation of the selectivity coefficient, $K^{K^+}_{Na^+}$, with temperature in silica gel (Davidson, code 950). These data are from the work of Wiggins (1975) The vertical lines indicate standard deviations from the means (n = 6 to 8). The selectivity coefficient is given by

$$\lambda_{K^+} \quad \lambda_{Na^+}$$

where λ refers to the apparent partition coefficients, the ratio of the ion concentration in the pore water of the gel to that in the bulk aqueous phase.

supernatant unfrozen solution. These results have been interpreted by Drost-Hansen[16] to be the result of cooperative behavior of aggregates containing of the order of 10,000 to 100,000 water molecules.

In connection with the properties and structure of interfacial water we also call attention to the existence of high-pressure ice polymorphs. No less than eight such high-pressure polymorphs have been reported[17] with static dielectric constants varying from 5 to 80, and densities varying from 0.92 to 1.65 g/cc. Furthermore, it is of importance to note that with a single exception the lattice energies of all these different high pressure polymorphs are less than 250 calories/gram (*i.e.*, about 40% of RT at room temperature).

From observations of the type reported above it is suggested that extensive cooperativity occurs among very large numbers of water molecules that are in proximity to an interface. Although the interactions are weak, they extend over large distances. Clearly, such behavior can best be described as the result of collective, cooperative processes. In this connection recall the analysis of Fröhlich[18] who suggested that macromolecules in solution may represent a system of coherent oscillators, revealing a large degree of collective motion. It may also be suggested that water at interfaces could be structured differently under conditions far away from equilibrium - the "dissipative structures" of the type implied in the theory of Prigogine and Glandsdorff[19,31]

While most of the direct evidence presently available has been obtained from non-biological systems, it seems most likely that such long-range, weakly interacting structures also occur intracellularly and that these vicinal water structures can be expected to possess dielectric properties notably different from those of bulk solutions. As a consequence, it is reasonable to expect that such water, compared with bulk water, may exhibit decidedly different properties in high frequency electromagnetic fields. Indeed, if very large amounts of vicinal water can be demonstrated to be present in cells the consequences would also be far-reaching in terms of cellular structure and function.

ESTIMATE OF VICINAL WATER CONTENT

The foregoing account suggests that one can approximate the proportion of

vicinal water in cells by estimating the amount of intracellular surface area available to perturb water. We have carried out this exercise for rat liver cells, one of the best known eucaryotic cells[9]. These, and some additional calculations, are given in Table 1 for *membrane surfaces* along with supporting evidence and some details of the calculations. It is important to realize that these numbers do *not* include water molecules interior to the membrane surface; also, the membrane surfaces are taken as *molecularly smooth*. Both considerations will *minimize* the estimates of vicinal water. If we recall the evidence, summarized in the preceding sections of this paper, that the vicinal water layer adjacent to surfaces is of the order of 30-300 molecular diameters, and if we take the lower end of this range, then roughly 30% of the total cell water should find itself sufficiently close to a membrane surface to have its properties altered, compared with water in the bulk. Table 2 provides some estimates of additional intracellular surfaces that are non-membraneous, yet resolvable with the electron microscope. For these surfaces, a layer of 30 molecules would require about 11% of the total water in the average liver cell. It should be realized that two additional major ultrastructural surface components of cells are not included in these calculations: the *nuclear matrix* (a meshwork of interlacing protein filaments[20]) and the "microtrabecular cytoplasmic filament network" recently shown to be a feature of several animal cells[21]. These two components represent what must be an enormous, but unknown amount of surface area. Consequently, these structures and the data in Tables 1 and 2 suggest that of the order of one-half of the intracellular water could be vicinal water.

Note that these estimates have not taken into account the water of hydration associated with ions, metabolites, dissolved macromolecules (*i.e.*, tRNA's, proteins, etc.) and formed elements such as glycogen granules. In other words, crude though these calculations may be, they do suggest that at least 50% of the total water in these liver cells must be sufficiently perturbed, due to direct solvation or proximity to a surface, that its properties should differ significantly from neat water. The metabolic consequences of the presence of such large amounts of vicinal water in cells has been considered in some detail elsewhere[9,22].

TABLE 1.

Estimates of the amount of surface area per rat liver cell for various membrane-bounded organelles*

Cell Structure	Total Surface Area (μm^2)	Total Water Molecules (x10 ^{12})	% of the Total Intracellular Water
Cell Membrane	1,300	0.78	0.43
Nuclear Envelope	300	0.18	0.10
Endoplasmic Reticulum:			
Smooth	16,900	10.14	5.63
Rough	25,400	15.24	8.47
Golgi Apparatus	2,100	1.26	0.70
Mitochondria:			
Envelope	8,700	5.22	2.90
Cristae	35,500	21.30	11.83
Lysosomes	240	0.14	0.08
Peroxisomes	1,050	0.63	0.35
Totals:	91,490	54.89	30.49

* Data for the surface areas of these structures are from the detailed study by Loud[26] and the description of Novikoff and Holtzman[27]. The total number of water molecules per liver cell (1.8×10^{14}) was calculated from the measurements of Seglen[28], after correction of dry weight due to glycogen loss. The column *Total Water Molecules* represents the number of water molecules required to fill 30 layers on each of these surfaces, taking the surface coverage of one water molecule to be 5×10^{-8} μm^2.

TABLE 2

Estimates of the amount of surface area per rat liver cell for various non-membranous ultrastructural surfaces*

Cell Structure	Total Surface Area (μm^2)	Total Water Molecules ($x10^{-12}$)	% of the Total Intracellular Water
Ribosomes	4,000	2.40	1.33
Interphase Chromosomes	5,000	3.00	1.67
Actin-Micro-filaments	25,000	15.00	8.33
Totals	34,000	20.40	11.33

*Estimates for an average mammalian interphase chromosome were taken from DuPraw[29]: 0.023 x 760 μm. These were taken as rods for surface area estimates and the number of chromosomes per cell was assumed to be 46. The ribosomal surface areas were calculated on the basis of 3×10^6 ribosomes per cell, taking the ribosome to be a sphere of 200 Å diameter[27]. The total surface area of micro-filaments was approximated by the reasonable assumption that 2% of the total protein was actin that was polymerized into filaments of 80 Å diameter[30]. The total protein per liver cell was calculated from the measurements of Seglen[28]. Other considerations are the same as described in Table 1. The surface area estimates given here are considered to be minimal.

One might suppose from the foregoing that various kinds of physical measurments of the structure of intracellular water would easily reveal the presence of a large fraction of *non-bulk water* in cells. As it turns out, however, the subject is very controversial and cannot be treated here. It can be said[23] that a number of studies of *non-freezable water*, and of *solute exclusion* in intact cells and tissues do indeed indicate that between 25-35% of the total water is appreciably different from bulk water. However, the results of a large number of studies employing nuclear magnetic resonance have been interpreted variously, some investigators concluding that a very large proportion of cellular water, perhaps all of it, is more structured than bulk water (see Chang, *et al*[24], for references) whereas others[25] claim that only a very small percentage of cellular water differs from bulk water. The situation is obviously controversial in terms of current NMR research. It is quite clear, however, that the conclusions of the former group are much more consistent with the notion advanced in the present paper.

Inasmuch as the status and disposition of intracellular water are important to the interpretation and understanding of the interactions of electromagnetic radiation with biological systems, it may be useful to consider the vast internal surface areas of cells and their ability to perturb water that is proximal to them.

ACKNOWLEDGEMENT

Supported in part by a grant from the U. S. National Science Foundation (PCM76-24037).

REFERENCES

1. G. Peschel, Z. Phys. Chem. Neue Folge 59, 27 (1968).
2. G. Peschel and K. H. Adlfinger, J. Coll. Interf. Sci. 34, 505 (1970).
3. G. Peschel and K. H. Adlfinger, Z. Naturforschung 26a, 707 (1971).
4. M. S. Metsik and G. T. Timoshchenko, in *Research in Surface Forces*, (B. V. Deryagen, ed.) vol. 3, p. 34. Consultants Bureau, N. Y. (1971).
5. W. Drost-Hansen, in *Chemistry of the Cell Interface, B.* (H. D. Brown, ed.) Chapt. 6, p. 1. Academic Press, N. Y. (1971).
6. M. S. Metsik, V. D. Perevertaev, V. A. Liopo, G. T. Timoshchenko and A. B. Kiselev, J. Coll. Interf. Sci. 43. 662 (1973).
7. J. A. Schufle, C. T. Huang and W. Drost-Hansen, J. Coll. Interf. Sci. 54, 184 (1976).
8. C. V. Bruun and W. Drost-Hansen, in *Colloid and Interface Science*, (M. Kerker, ed.) vol. 3, p. 531. Academic Press, N. Y. (1976).
9. J. S. Clegg, in *Cell-associated Water*, (W. Drost-Hansen, ed.). Proceedings of a Workshop, 1st Int. Congress on Cell Biology, Boston, 1976; to be published by Academic Press, N. Y., 1978.
10. W. Drost-Hansen, Chem. Phys. Let. 2, 647 (1969).
11. W. Drost-Hansen, Ind. Eng. Chem. 61 (11), 10 (1969).
12. P. M. Wiggins, Clin. Exp. Pharmacol. Physiol. 2, 171 (1975).
13. R. Hurtado and W. Drost-Hansen, in *Cell-associated Water*, (W. Drost-Hansen, ed.). Proceedings of a Workshop, 1st Int. Congress on Cell Biology, Boston, 1976; to be published by Academic Press, N. Y., 1978.
14. W. Drost-Hansen, in *Chemistry and Physics of Interfaces*, (S. Ross, ed.) American Chemical Soc. Publ., Wash., D. C. (1965).
15. E. J. Workman and S. E. Reynolds, Phys. Rev. 78, 254 (1950).
16. W. Drost-Hansen, J. Coll. Interf. Sci. 25, 131 (1967).
17. D. Eisenberg and W. Kauzmann, *The Structure and Properties of Water*, Oxford University Press, London (1969).
18. H. Fröhlich, in *Theoretical Physics and Biology*, (M. Marois, ed.) p. 13. Elsevier Publ. Co., Inc., N. Y. (1969).
19. P. Glansdorff and I. Prigogine, *Thermodynamic Theory of Structure, Stability and Fluctuations*. Wiley-Interscience, N. Y. (1971).
20. J. M. Keller and D. E. Riley, Science 193, 399 (1976).

21. K. R. Porter, in *Cold Spring Harbor Conferences on Cell Proliferation*, (B. Goldman, T. Pollard and J. Rosenbaum, eds.) vol. 3, Book-A, pp. 1-28. Cold Spring Harbor Lab. Publ., Wash. 1976.

22. J. S. Clegg, J. Cell Physiol. 91, 143 (1977).

23. R. Cooke and I. D. Kuntz, Ann. Rev. Biophys. Bioeng. 3, 95 (1974).

24. D. C. Chang, C. F. Hazlewood and D. E. Woessner, Biochim.Biophys. Acta 437, 253 (1976).

25. K. R. Foster, H. Resing and A. N. Garroway, Science 194, 324 (1976).

26. A. V. Loud, J. Cell Biol. 37, 27 (1968).

27. A. B. Novikoff and G. Holtzman, *Cells and Organelles*, 2nd edition, Chapter 2.12. Holt, Rinehart and Winston, N. Y. 1976.

28. P. O. Seglen, Exp. Cell Res. 82, 391 (1973).

29. Du Praw, E. J., *Cell and Molecular Biology*, Table 18-1. p. 522. Academic Press, N. Y. 1968.

30. T. D. Pollard and R. R. Weihing, CRC Crit. Rev. Biochem. 2, 1-65 (1973).

31. W. Drost-Hansen, Physics and Chemistry of Liquids 7, 243 (1977).

MICROWAVE FREQUENCIES AND THE STRUCTURE OF THE DOUBLE HELIX

E. W. Prohofsky

Department of Physics, Purdue University
West Lafayette, Indiana 47907

ABSTRACT

We have calculated the vibrational modes of homopolymer DNA double helices. These calculations have been refined by comparison with i.r. and Raman observation from 1200 cm^{-1} to about 200 cm^{-1}. The agreement is reasonably good. These calculations also indicate the existence of a number of bands within the microwave region of the spectrum. It is possible to use these calculations to predict absorption. Low lying vibrational modes are also of importance in predicting conformation, or shape, changes in macromolecules. We believe that a mode near 0.3 cm^{-1} is involved in the B to A conformation change of DNA. Conformation changes can alter biological function and in this sense the low lying vibrational modes can effect function. Some insight may be gained from these studies into possible mechanisms by which electromagnetic interactions can effect vibrational modes which in turn effect conformation and biological function.

VIBRATIONAL MODES AND RADIANT ABSORPTION

We have for some time been investigating the vibrational modes of nucleic acid double helices[1-6]. These studies have been carried out for both A and B conformation DNA as well as A conformation RNA. The calculated frequencies have been compared to observed infrared and Raman lines and the force constants used in the calculations have been refined by forcing better fits of the theoretical results to the observed spectra[6]. A comparison of the calculated frequencies to observed lines is displayed in Fig. 1. These lines are those associated with the nucleic acid backbone vibrations.

With force constants refined by comparison with infrared and Raman lines one can calculate all the vibrational modes of the double helices. We have carried out such calculations[4,5] for the two duplex homopolymer DNA compounds poly (dG) • poly (dC) and poly (dA) • poly (dT). These compounds are relatively easy for calculations as the same base pair repeats the entire length of the double helix. In this situation one may use methods developed for crystalline solids which are also composed of repeating units. In Table 1 we show the frequencies of the zone center of the twenty five lowest vibrational bands. All these frequencies below 200 cm^{-1} are below the range of any reported observations that we have been able to find. The lower frequencies are well within the range of microwave frequencies.

Any direct absorption of microwave radiation by the double helical DNA would take place by resonant interaction of the microwave field with these vibrational modes. Such interactions are certainly expected to take place. The strength of the interaction can be approximated by estimating the unbalanced charge distribution and by using the calculated vibrational displacements to determine the polar moment associated with a particular vibration. The polar moment interacts directly with the electromagnetic field and the energy transferred to the vibrational mode can then be calculated. This approach has been used in analyzing linear dichroism at higher frequencies[7]. Such an approach can in principle predict the microwave absorption by double helical DNA.

The frequencies of these low lying modes can be altered somewhat by weak long range interactions between various parts of the helix. These weak

forces play a negligible role in determining high frequencies and cannot be refined from higher frequency experimental data. Low frequency absorption or scattering data of which we have found very little can however be used to determine these important long range interactions.

BIOLOGICAL ROLE OF LOW FREQUENCY VIBRATIONS

It has become increasingly clear that the shape or conformation of biological macromolecules is of great importance in determining their function. It is also apparent that changes in conformation occur during function and in addition changes in conformation can also act as switching mechanisms which alter function. A theoretical understanding of how and why conformation changes occur is an important element in understanding biological function. The problems in understanding conformation changes are, however, very difficult.

The problem of conformation change in macromolecules is analogous to the problem of displacive phase change in crystalline solids. A very powerful method for analyzing such change that has proven extremely successful is the method of soft mode analysis. In this method the phase change arises from a particular vibrational mode which becomes unstable and whose displacement becomes large enough to *distort* the structure into the new conformation. The analysis can be made rigorous and works primarily because the vibrational modes are the normal motions of the structure and changes in conformation must follow along the lines of these natural motions. We have applied this method to the B to A conformation change of double helical DNA[4,5].

A gel of natural DNA fully hydrated is in a B conformation double helix. When dried in dry air the double helix changes to A conformation. We have calculated the effects on the vibrational modes which would arise from a decrease in dielectric constant of the material which we associate with the removal of water of hydration. We have applied this perturbation to the duplex homopolymers poly (dG) • poly (dC) and poly (dA) • poly (dT). We find that a low lying mode does become unstable indicating a conformation change for poly (dG) • poly (dC) at about a few percent change in dielectric constant.

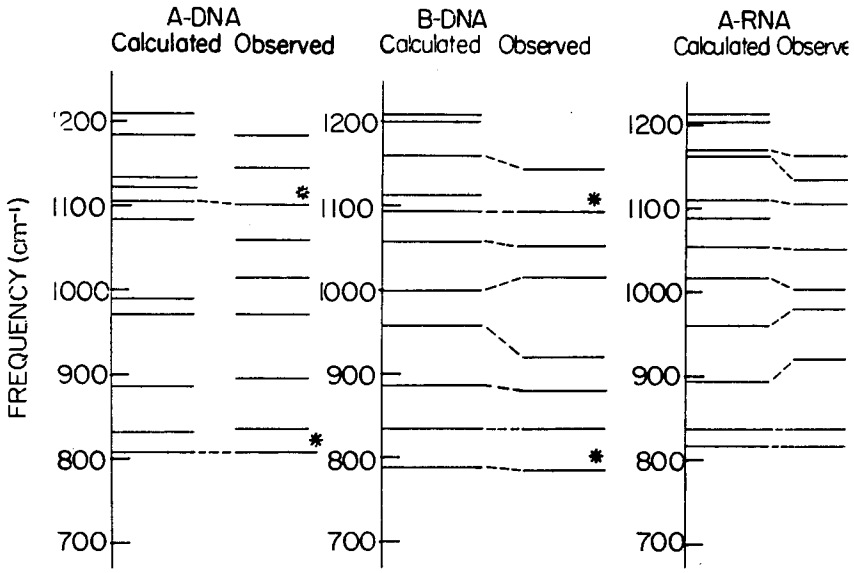


Figure 1.
A comparison of observed Raman and infrared lines with calculated vibrational mode frequencies for A-DNA, and A-RNA. The dashed lines are drawn to connect modes in which the character of the theoretical mode (i.e., the distribution of energy among the various chemical bands) matches that assigned by the experimenter to the observed lines. The character of many observed lines are not specified. The asterisks indicate modes which were used in a refinement procedure described in reference three.

We find that no such mode softening occurs for poly (dA) • poly (dT). Both results are in agreement with observation. The frequency for the unstable mode as a function of change of dielectric constant is shown in Fig. 2. The mode that goes unstable agrees very well in actual atomic displacements with those needed to change the conformation from B to A.

It has been suggested that a conformation change similar to this one occurs locally *in vivo* when DNA switches to actively transcribing RNA[8]. RNA occurs only in A conformations. It may be that a non-polar enzyme is able to induce some conformation change by replacing water in the region of the double helix and this change may aid its function. This case gives some insight into the role that vibrational modes can play in biological function.

MICROWAVE ABSORPTION AND BIOLOGICAL EFFECTS

In the previous section we have discussed the role of vibrational modes on the conformation or shape of biological macromolecules. Changes in conformation can be viewed as arising from instabilities in one or possibly more vibrational modes. Any interaction which enhances the amplitude or enhances mixing of various modes can alter the mode structure and even the conformation of the macromolecules. Microwave absorption is a transfer of energy from a microwave field to the very vibrational modes of the macromolecules we are discussing.

In the case of the B to A conformation change of double helical DNA the mode of interest which drove conformation change is calculated to be at $0.3\ cm^{-1}$. This is roughly 10^{10} Hz. The frequency of modes of structural importance are certainly low enough to be effected by electromagnetic radiation. Several modes which exist at higher frequency may be involved in similar dynamical roles. Pumping on these modes can cause instabilities which can effect function. Microwave absorption may also alter the interaction of modes which can alter instabilities driven by other phenomena.

ACKNOWLEDGEMENT

This work was supported by NSF Grant DMR74-14367.

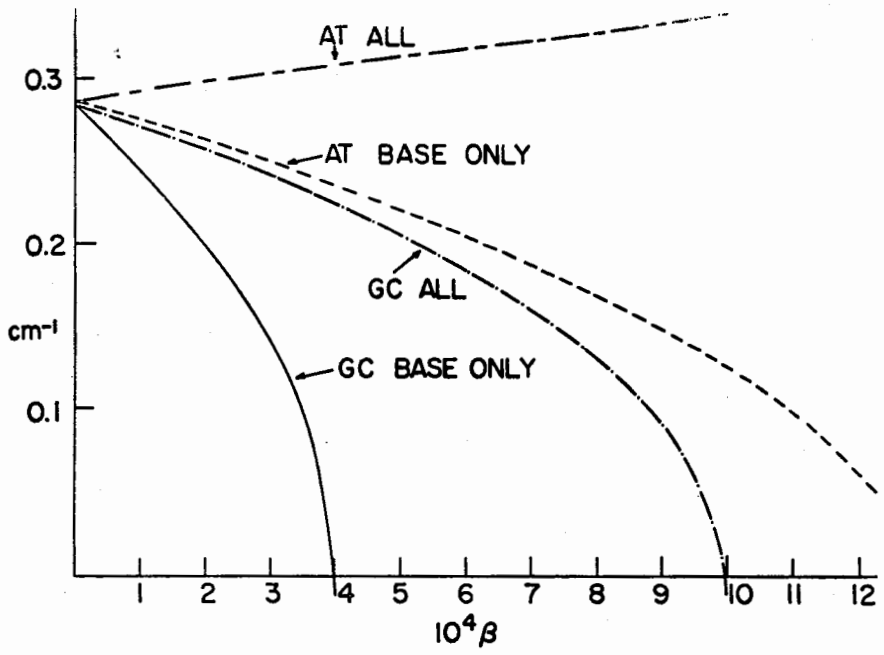


Figure 2.
The frequency of the unstable mode which is linked to the B and A conformation change as a function of change in dielectric constant. The frequency is in cm^{-1}. The equation $\varepsilon^{-1} = \varepsilon_o^{-1} + \beta$ defines β where ε is the instantaneous constant and ε_o is the dielectric constant when the gel is fully hydrated. AT refers to poly (dA) • poly (dT) and GC refers to poly (dG) • poly (dC). Base only refers to a calculation in which the interaction between atoms in the backbone was set to zero. This enhancement of the instability indicates that the source of the instability lies in the interaction of the bases and that the backbone interactions tend to stabilize the structure. For a fuller discussion see reference two.

TABLE 1

List of the Lowest Frequency Twenty Five Vibrational Modes for 10-fold B-poly (dA) • poly (dT) and poly (dG) • poly (dC). (Frequency in cm^{-1})

poly (dA) • poly (dT)		poly (dG) • poly (dC)	
.29	78.69	.28	82.21
2.14	86.66	2.10	95.56
4.35	94.43	4.88	101.38
4.90	101.95	5.02	105.63
7.65	102.87	8.01	121.59
13.38	146.68	13.31	143.29
17.22	157.13	21.00	163.87
26.96	167.26	27.20	167.18
30.12	177.24	31.51	175.50
31.48	178.30	33.03	183.72
35.69	187.07	40.00	189.53
54.26	187.83	63.56	194.42
64.23		67.88	

REFERENCES

1. E. W. Prohofsky, Phys. Lett. 50A, 327 (1975).
2. E. W. Prohofsky and J. M. Eyster, Phys. Lett. 50A, 329 (1975).
3. J. M. Eyster and E. W. Prohofsky, Biopolymers 13, 2505 (1974).
4. J. M. Eyster and E. W. Prohofsky, Phys. Rev. Lett. 38, 371 (1976).
5. J. M. Eyster and E. W. Prohofsky, Biopolymers 16, 965 (1977).
6. K. C. Lu, E. W. Prohofsky and L. L. Van Zandt, Biopolymers. To be published.
7. C. Beetz, G. Ascarelli and S. Arnott, Private communication.
8. S. Arnott, *et al*, Nature (London) 220, 561 (1968).

* *

DISCUSSION

It is not just the charges that are important in the interactions; there are local dipole moments, in fact, local higher moments. Why do you expect to get all of the information just out of the charges?

Also, when calculating going from the A configuration to the B configuration, you only considered nearest neighbor bases for the forces. [Rabinowitz].

Prohofsky: Ten neighbor bases, actually. The dielectric constant is a very crude, rough parameter, assumed to be geometry-independent in that region. This is still just a phenomenological model.

There are just a couple of water molecules in there. [Rabinowitz].

Prohofsky: They are not even in there, they are on the side but they are rotating. It is a one percent effect. If you look at the numbers, it is conceivable that you could achieve roughly that order of magnitude just in the dielectric constant.

Have you tried to use parameters other than just charge parameters? [Rabinowitz].

Prohofsky: The problem with multipoles is that if you look at the base, the displacement of a dipole is comparable to the interbase distance. The monopole approximation is better.

It cannot be a better approximation. The atomic dipoles have to be more effective than just the monopoles. [Rabinowitz].

Prohofsky: They show up more in the Raman spectrum and I agree, it is an approximation. The point is that if you really fit charges, they contain some information about the dipoles in them as well, because they are fitted parameters. Again, one could go to higher approximation where one puts a dipole charge as well on each bond. They are perhaps twice as large on a double bond, half as large on a single bond. If one tries these approximations, tries to fit all of these parameters, it can be done but it becomes very involved. We wanted to see first how well the first approximation works. We have fit six lines very well with the monopole rigid ion approximation. It works to some extent.

If I understand you correctly, you are saying that the vibration that might be involved in the microwave region is a motion which is essentially like the sketch on the blackboard. [Illinger].

Prohofsky: Roughly. Think of it as a ladder in two parts, curved and twisted as well.

My question is, are there any experimental measurements? There is an analogous experiment on the microwave absorption of the alpha helix, for PBLG, polybenzoglutinzte (ph) where all hydrogen bonds are lined up along the axis of the helix so that there is an exchange of dipole moment with vibration that has been observed around 20 GHz or so, by Manso Davies. Here, of course, the hydrogen bonds are essentially perpendicular to the axis so that motion will not modulate the position of the hydrogen bonds very well. [Illinger].

Prohofsky: The vibration is right in the middle of the water absorption band. I do not know of any experimental absorption measurement technique that would work there. We have not calculated that absorption for these modes yet and have only started thinking about microwave absorption really over the last few months. I really do not know what I would predict. You realize that the mode is quite different in proteins because of that hydrogen bond. This is a very low lying mode in part because there are no bonds being stretched by that kind of motion; it is quite different.

That is one reason I make this point because whereas in the alpha helix, an electromagnetic field at these frequencies does, in fact, modulate the hydrogen bond and it is, therefore, conceivable that there might be disruptive and irreversible effects. That does not appear to be the case in DNA. [Illinger].

Prohofsky: I think they are quite different; it is not safe to go from the protein case to the DNA case. They are quite different in those particular motions.

I wanted to make a small point. The soft mode method that you are applying was essentially developed by Randolph and others using methods from hydrogen physics. There has been a recent breakthrough by Fisher of which you are probably aware. We now know that in a system like this, when you go through a first-order based transfer, there has to be a low span with the lowest frequency touching zero. [Brodsky].

Prohofsky: For a first-order transition, it is a little more complicated than the second-order and, in fact, we use that effect to do a better job of predicting the A conformation.

There has to be a condensation effect. [Brodsky].

Prohofsky: Yes, they are equivalent, using different terminology.

In this kind of approximation, what is your guess, if any, about the specific heat involved in this transition? [Brodsky].

Prohofsky: This is a very low lying mode compared to the ones that are involved in all solid state transitions. It is, initially, very low lying. I do not imagine it is very significant but I do not know. Also, it is not a second-order phase transition; it is in fact first-order because you change the length of a given unit cell. First-order means there are some further interactions going on with other modes involved and, in fact, if you look at these other modes you will find you do a better job of predicting the new A conformation because you see that you are involving an uncurling of the double Helix as well, that is a higher order effect.

Therefore, you are saying that in the phase transfer ---? [Brodsky].

Prohofsky: There is a first-order transition; I am not sure what the changes are associated with that.

That would imply that in the phase diagram, the difference between the phases would be rather flat. [Brodsky].

Prohofsky: Just so.

Inasmuch as the counter ion sheath is so important for stability in the DNA duplex; could you comment on its neglect? [Atkinson].

Prohofsky: I said water alters the effects of dielectric constant. I am sure the ion sheath contributes to it too.

It would simply be of paramount importance. [Atkinson].

Prohofsky: It is known that the experimental effect does occur when you take away water. I do not think you are removing any of the ions in the proximity of the double Helix. It is just being dried in air. The other thing is, the force constants have been fitted. It is a little bit like pseudo-potential calculations, that ends up with a number that represents a whole slew of effects, all intermixed, when you use fitted parameters. To some extent, they represent reality, including effects of counter ions, but I admit it is a very crude model. However, at this level it already discriminates between poly (dG) • (dc) and the poly (dA) • (dT) as was pointed out, and in fact some such soft mode does have to occur to describe a conformation change.

I am not saying that this is a completed work by any means, however.

You say that you have a fairly good agreement between calculated and the Raman experimental measurements? [Sheridan].

Prohofsky: To about 200 reciprocal centimeters, where the data exists.

You are not doing any experimental studies yourself? [Sheridan].

Prohofsky: There is a person at Purdue who is beginning to look at lower frequencies, trying to push down to 10 reciprocal centimeters. The problem is that you can fit perfectly at the higher frequencies. You tend to have very good leverage for fitting the large force constants. But there are also very weak force constants much like the ones we have estimated for electrostatic effects. They will be different, for different materials; you do not have any leverage for fitting them by looking at only the high frequency lines. What we need, really, is to improve the low frequency spectrum. You may say why do you have to do it if you are going to measure it anyhow, but in fact, we could predict much of the low frequency spectrum better and better, as we fit the lower frequencies. But we really cannot fit the very weak forces by looking at the high frequencies.

So the wave number estimate --- ? [Sheridan].

Prohofsky: It is a very crude estimate.

But it would be a soft mode, if we could see it? [Sheridan].

Prohofsky: It should; something has to go to zero frequency, that is an essential based on much more precise arguments which appear in group theory. Also, modes should in fact exist at very low frequencies, corresponding to moving a lot of mass coherently up and down. That should be a very low-lying, optical mode. In fact, we know the geometry of the double helix very well, but we know the force constants very poorly. Thus, I have more confidence that this type of mode character exists than I have of what its absolute frequency is.

I also believe it should be the lowest lying of the modes. It is moving the most mass coherently.

TECHNIQUES OF RAMAN SPECTROSCOPY APPLIED TO STUDY THE EFFECTS OF MICROWAVES UPON SYNTHETIC AND NATURALLY OCCURRING PHOSPHOLIPID MEMBRANES

J. P. Sheridan, R. Priest, P. Schoen, and J. M. Schnur
Naval Research Laboratory, Washington, D. C. 20375

ABSTRACT

Advanced non-perturbative optical techniques are being applied by our research group to probe the molecular order of synthetic and naturally occurring phospholipid membranes as a function of applied C.W. and pulsed microwave radiation. Single component, binary mixtures, and naturally occurring bovine material have been systematically characterized as a function of temperature using Raman scattering to provide information about the phase diagram and order of the lipids within the membrane. These characterized materials are then studied under microwave radiation. Our preliminary results using Raman spectroscopy show lipid chain disorder induced by microwave radiation at approximately 10 mW/cm^2 in the 2 GHz frequency regime. These effects were found in naturally occurring bovine sphingomylen materials and were most pronounced in the biologically interesting temperature region 32-37°C. A possible explanation of these results will be proposed.

* *

DISCUSSION

What frequency were you using? [Cleary].

Sheridan: Two and a half or three gigahertz; there is very little difference in that frequency range.

You attributed the effect to differential thermal gradients produced in the layer. I was wondering why you selected that model as opposed say to a field-induced effect? [Cleary].

Sheridan: As a physical chemist with a thermodynamic background, this seems to me to be a plausible model. I have not thought seriously of field-induced effects; that is a good point.

What happens when you turn off the field; where does it end up on your curve? [Rabinowitz].

Sheridan: It is a reversible perturbation and the spectrum relaxes back to the higher order after the field is turned off.

What if you did not cool it as much? [Rabinowitz].

Sheridan: The body does have some thermostatic ability. The argument is always that it has more than enough to handle lowpower radiation, but I add that it is not a flowing system in totality. There are many heterogeneous regions with thermal barriers.

How long is the relaxation time? [Rabinowitz].

Sheridan: I have not measured the times for relaxation accurately.

I take it you attribute some of these effects to the thermal gradient within the membrane. But in the infrared, Raman absorption is strongly temperature dependent because it depends on the population in the two states. To what extent can you unravel this problem of judging how many molecules there are in the Raman excited state, and the dependence of that on the temperature, the intensity of the absorption, and the temperature gradient across the membrane. [Illinger].

Sheridan: I do not think that is going to be anything like the effect of changing the conformation, which has a much more marked effect on the relative intensity of these conformation sensitive bands. I think these are much more dominant factors, but I have not really attempted to do that sort of unravelling.

But the Raman is temperature dependent? [Illinger].

Sheridan: We must look at a system that is going to be reasonably conformationally stable over some long temperature range to make the measurement. From that very point, it is a strongly temperature dependent function. If you go back to the gel phase, that change throws the system into a certain configuration. You cannot determine, with any experimental accuracy, the change in relative intensity until a rotational isomer starts to become a load at the beginning of the phase transition, and must look over a fairly wide temperature range. As far as being a relative measure of the degree of change in order, I think the measurement is reasonably accurate.

I am asking this because, as you know, there have been many studies of Raman spectra as functions of microwave radiation. Frequently, the fact that the Raman intensity is temperature dependent, even for a simple molecule which does not undergo conformation changes, has been overlooked. I wonder to what extent you can separate that general effect from the much more interesting aspect that you pointed out. [Illinger].

Sheridan: I do not know. Do you know if reasonably good estimates have been made for simple molecules?

In the Raman effect you observe a transition between two states, but unfortunately people do not usually measure both the Stokes and the anti-Stokes lines. [Illinger].

Sheridan: That is difficult to do and the contribution of the anti-Stokes wave numbers is almost negligible.

In fact, the intensity of these transitions depends upon the population of the ground state. That is clearly temperature dependent even for a simple molecule, such as H_2. [Illinger].

Sheridan: Over five or ten degrees, but it is negligible compared to the changes that one sees as a result of conformation changes.

I am not criticizing your work but there are many studies in the literature of Raman lines under microwave exposure where the intensities are strong enough to cause purely thermal effects which have been attributed to other effects. That is a caution that has to be made. I would also like to remark that this matter of Raman spectroscopy is very interesting in the context of coherent vibrations. A question that arises here is what is the resolution of Raman lines at low frequencies where the changes are of the order of 100 GHz *or so? It is my impression that this resolution is not obtainable.* [Illinger].

Sheridan: That is correct; no observations have been made of such low frequency modes at all, because of experimental difficulties of obtaining measurements that close to the laser line. I think just the observation of such low frequencies, discussed by the previous speaker, could be of tremendous interest.

My point is that some of the modes that one thinks might occur in the coherent spectrum may not be optically active but may be Raman active, so that Raman spectroscopy may be the only way one can look at them, unfortunately. [Illinger].

EVANESCENT WAVES AND WAVES IN ABSORBING MEDIA*

Leopold Felsen

Department of Electrical Engineering
Polytechnic Institute of New York
Brooklyn, New York

ABSTRACT

Recent developments in the treatment of high frequency evanescent waves are described. The method of evanescent wave tracking is discussed and the application of this technique to rays in lossy dielectrics is suggested.

*Based on a minimally edited version of the transcribed lecture. The material presented is summarized to a large extent in the paper "Evanescent Waves," by L. B. Felsen, J. Opt. Soc. Am. 66, no. 8, 751 (1976).

INTRODUCTION

This paper describes some high frequency methods that can be employed for diagnostics of dielectric materials. Our remarks are restricted, primarily, to some new techniques that have been developed for propagation of fields in lossless materials, but we will indicate appropriate places for modification in the case of loss, since the concepts that are introduced will apply as well to the lossy case.

GENERAL THEORY

When we are discussing the high frequency interaction of fields with materials, whether they are electromagnetic fields, acoustic fields, or any other kind, we mean that the wavelength of the radiation is small compared to the scale of any inhomogeneities that the material may possess. Therefore, the high frequency field provides a high resolution probe in contrast to low frequency fields whose wavelength is large compared to the scale of inhomogeneities. Thus, if one wishes to diagnose in detail the characteristics of a material by some sort of transmission measurement, then it is necessary to employ sufficiently high frequencies in order to obtain resolution. High frequency fields that are employed with materials are typically millimeter wave fields or optical fields since these fields can be focussed to a fine spot and then used for selective probing. Thus, we are led to the problem of characterizing the propagation of electromagnetic or other fields that are confined to a very limited spatial region (*i.e.*, in the form of a beam). If the beam is focussed, this region can be small compared to the inhomogeneity we wish to explore.

Beam fields, since they are confined locally in space, are a special class of what one may call evanescent fields. What we now discuss are some new ideas in the theory of propagation of evanescent fields; the usual non-evanescent fields and electromagnetic beams are special cases of these evanescent fields. It turns out that even though evanescent fields refer

essentially to lossless media, the theory can also be extended to the dissipative case. The principal difference between ordinary propagating fields and evanescent fields or fields in lossy media is that the former have real phase while the latter have complex phase.

High frequency fields satisfy properties of propagation which can be referred to as *local*. These local propagation properties can be effectively schematized by using certain trajectories along which the field propagates. These trajectories are known in the classical literature as the rays of geometrical optics, and a rigorous connection between geometrical optics and wave theory can be demonstrated. The kinds of ideas that we discuss have to do with the generalization of geometric optics to accommodate evanescent fields which do not have real phase but have complex phase.

Where do evanescent fields occur? The conventional types of evanescent fields arise, for example, when radiation is guided inside a dielectric layer, as shown in Fig. 1. The fields are trapped by total reflections, and are therefore evanescent wiggly arrows on the outside of the layer. Totally reflected fields also occur when a beam is incident on an interface at an angle steeper than the critical angle. There are evanescent field types, called leaky waves, which travel along interfaces shedding radiation by virtue of energy leakage into the second medium. Evanescent fields also occur on the dark side of what is called a "caustic" in geometrical optics. A caustic is the envelope of a family of rays along which fields are concentrated; outside the caustic, in the weak field region, evanescent fields are required in order to describe the wave phenomena. In these examples, the material media do not possess dissipation; yet, the local fields have complex phase.

Also included among this class of fields, but usually not recognized as such, are aussian beams. A Gaussian beam is a field that is highly concentrated in the vicinity of a preferred axis and decays very rapidly away from that axis according to a quadratic law of variation with the distance. Confinement of beam modes in dielectric regions, which have a gradient in refrac tive index such that the energy becomes guided, likewise involves a special case of evanescent fields.

Thus evanescent fields have broad ranges of application. One can easily generalize the concepts introduced here to the case of lossy media since the main departure from the ordinary description of local fields is the fact that these fields possess a complex phase, as do the fields in a dissipative medium.

LOCAL FIELDS

We now review briefly the general ideas underlying local fields. In a true plane wave field, Fig. 2, which is non-evanescent, the field has a plane phase front; the perpendicular trajectories to the phase front are referred to as rays. The amplitude of this field is constant and the phase is real. In a local plane wave field, these characteristics are satisfied locally. A simple example is a field that has a spherical wave front. Taking a section of a spherical wave front, drawing a local tangent plane, and considering the propagation of this section in the direction perpendicular to the phase front, we deal with a local plane wave field. It is *local* because as it propagates, its amplitude decreases as the wave front expands. That is, a local plane wave field has an amplitude that can depend on distance. The same ideas can be applied to an arbitrary phase front. Drawing a local sphere and a local tangent plane one again finds that in any particular direction the field amplitude decreases as the wave front expands. Equivalently, as the tube of rays, in which energy is conserved, expands, the amplitude, proportional to the square root of the energy density, varies inversely with the square root of the ray tube cross section.

These are the basic ideas that apply to local plane wave fields under ordinary conditions. The description fails, however, in focal regions, where rays converge because the ray tube cross section then tends to zero, Fig. 3. A similar failure of ray optics occurs in the vicinity of caustics, Fig. 3, whether in free space or in guiding regions,where rays are curved and trapped by medium inhomogeneity. Required modifications of the ray optical theory are well understood and easily carried out.

In the case of evanescent fields, there is a different phenomenology, Fig. 4. Evanescent plane waves also possess plane phase fronts but the amplitude varies exponentially in the phase front. The orthogonal trajectories to

Figure 1. Evanescent Fields

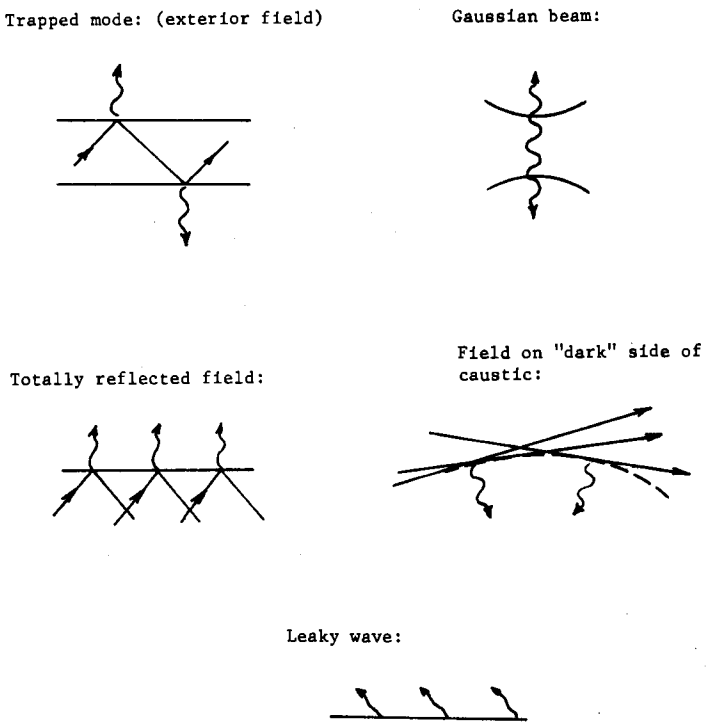


Figure 2. True and Local Non-Evanescent Plane Wave Fields

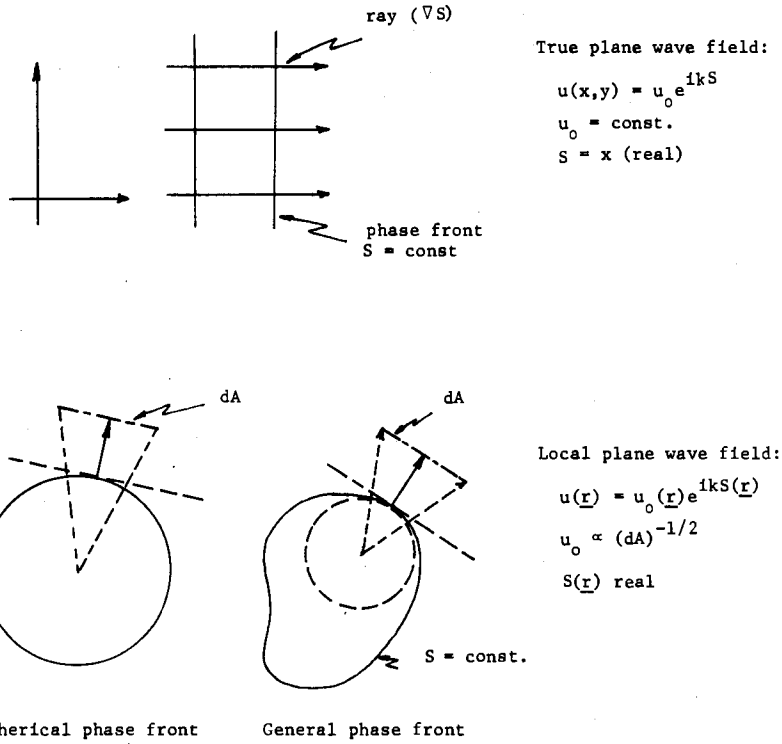


Figure 3. Failure of Plane Wave Field in Focal Regions

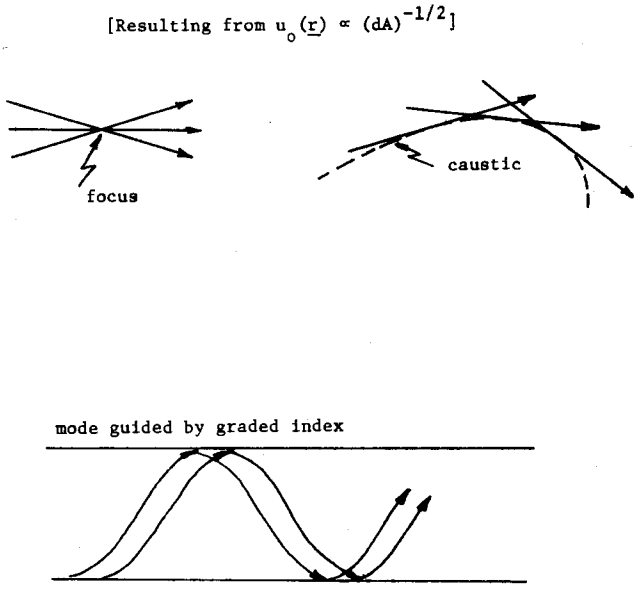
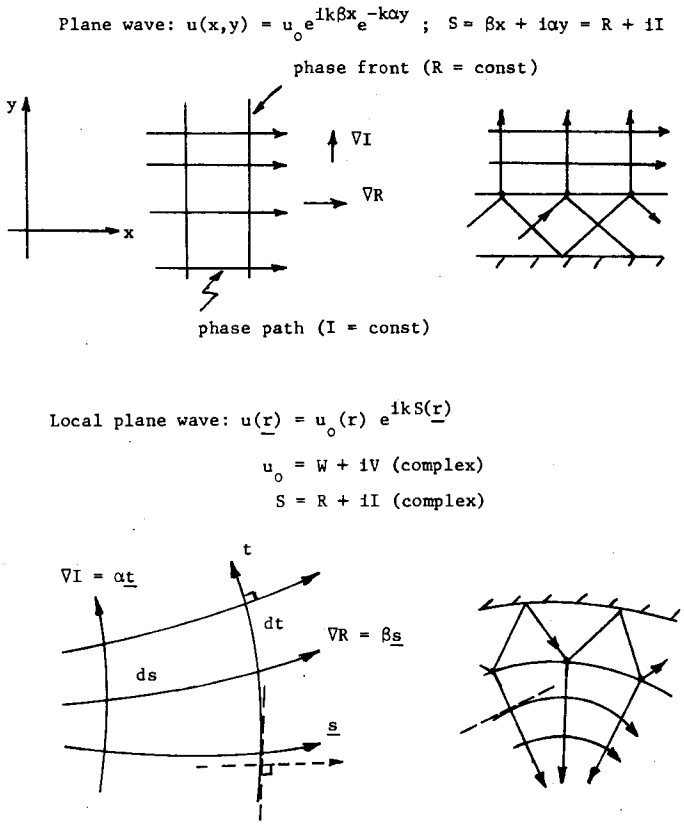


Figure 4. Evanescent Waves


Plane wave: $u(x,y) = u_o e^{ik\beta x} e^{-k\alpha y}$; $S = \beta x + i\alpha y = R + iI$
phase front (R = const)
y
x
∇I
∇R
phase path (I = const)
Local plane wave: $u(\underline{r}) = u_o(r)\, e^{ikS(\underline{r})}$
$u_o = W + iV$ (complex)
$S = R + iI$ (complex)
t
∇I = α$\underline{t}$
dt
∇R = β$\underline{s}$
ds
$\underline{s}$

the phase front are not referred to as rays, but as *phase paths*, since these are the paths along which the equiphase surface advances. One may define a phase gradient β in the direction of propagation of the phase front, and an amplitude gradient α in the direction of amplitude decay, perpendicular to it. Thus, we now speak of fields which have complex phase, S. The real part R varies most rapidly in the propagation direction of the phase front; the imaginary part I varies most rapidly in the perpendicular direction of maximum decay. The composite phase is thus $S = R + iI = \beta x + i\alpha y$.

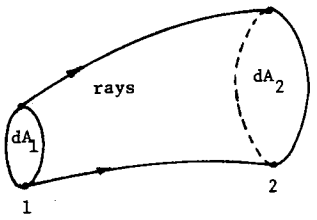
One may apply the concept of local fields by assigning a variable amplitude and a complex phase to plane wave fields. In these circumstances, the orthogonal grid of phase paths in the direction s and field decay in the directions t, as illustrated, will, in general, be curved. Contrary to light rays which characterize local plane wave fields with real phase that travel along straight lines in a homogeneous medium, local plane wave fields with complex phase travel along curved trajectories in a homogeneous medium.

This occurs because these fields may have different propagation speeds on on different parts of a wave front, thereby causing one portion of the wave front to advance more rapidly than another, as a result, the wave front bulges out. Explained thereby is the spreading of a Gaussian beam from its narrowest portion, the waist, where the phase front is a plane, a natural consequence of evanescent wave propagation rather than a phenomena of diffraction, as often noted in the Optics literature.

RAY TRACING

Non-evanescent fields can be tracked through a material medium by looking at the configuration of geometrical rays. The field amplitude along a ray can be calculated by invoking conservation of energy in the ray tube, Fig. 5, and the phase is obtained by integrating along a ray. For evanescent waves, one does precisely the same thing, except that the tracking is now done along the phase paths illustrated in Fig. 5. From the geometry (spreading or contraction) of phase paths, one can construct the complete characteristics of the local field by subsequent integration. Conversely, by monitoring the phase and amplitude of a field as it traverses a material medium, whether it be a

Figure 5. Wave Tracking Procedures



Homogeneous local plane waves:
(geometrical optics)

$$u(\underline{r}) \sim u_o(\underline{r}) e^{ikS(\underline{r})}$$

u_o , S real

$$u_o(\underline{r}_2) = u_o(\underline{r}_1)\ [n(\underline{r}_1)dA_1/n(\underline{r}_2)dA_2]^{1/2}$$

$$S(\underline{r}) = \int_1^2 n\,ds$$

Inhomogeneous local plane waves:
(evanescent wave tracking)

$$u(\underline{r}) \sim u_o(\underline{r}) e^{ikS(\underline{r})}$$

$S = R + iI$

$\ell n\, u_o = W + iV$

$\nabla R = \beta \underline{s}$, $\nabla I = \alpha t$

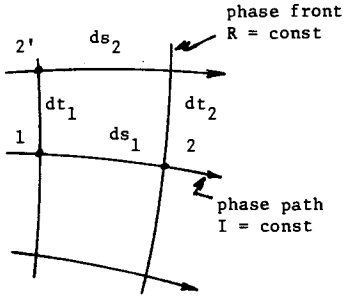
$\beta = dR/ds$, $\alpha = dI/dt$

$\alpha_2 = \alpha_1 dt_1/dt_2$, $\beta_2 = \beta_1 ds_1/ds_2$

$\beta^2 - \alpha^2 = n^2$

$R = \int_1^2 \beta ds$, $I = \int_1^{2'} \alpha dt$

W and V obtained from transport equations



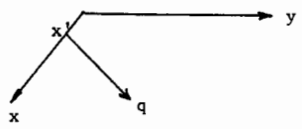
phase path curved if $d\alpha/dt \neq 0$ on a phase front

beam field or an ordinary plane wave field, one may, by an inverse process, attempt to reconstruct the characteristics of the medium through which the field has passed.

I had indicated before that propagation of evanescent fields in general takes place along phase trajectories which are curved even in a homogeneous medium. That goes against the grain of those who think in terms of light rays and geometrical optics because ordinary optical fields travel in straight lines in a homogeneous and lossless environment. It is possible to incorporate the generalized class of fields with complex phase within a theory of rays, but one is now forced to leave real coordinate space and go into a complex space. To appreciate this fact, consider an ordinary real geometric optical ray in a two dimensional (x,y) coordinate space; it has real slope, q, the ratio of wave numbers k_x, k_y of plane waves that propagate along the x and y directions. If q is complex, as it would be for an evanescent plane wave, or in a lossy medium, then one cannot apply the same equations, with all coordinates kept real. This is schematized in Fig. 6 where we have adopted a complex x-coordinate but have retained a real y-coordinate. In this complex coordinate space, the fields are tracked along straight rays. An observable point on a complex ray is where the ray intersects the real x,y plane. Each such intersection point determines a point on a phase path in real space. It can now be appreciated why the phase paths are generally curved. Each complex ray describes a plane wave field with a particular complex wave number; along a different complex ray, the wave number is different. Intersection points with real coordinate space thus identify evanescent plane waves with different wave numbers and hence different propagation directions and propagation speeds. This results in wave front deformation and consequent bending of the phase paths.

An advantage of tracking complex fields rather than real fields is illustrated in Fig. 7. A gaussian beam in free space can be characterized in terms of geometric optical rays that are generated by hyperbolic caustics. As noted previously, we run into difficulty at the caustics, and would have to generalize the theory of geometrical optics to describe the field there. On

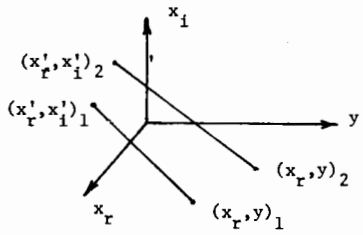
Figure 6. Complex Rays



Real ray:

$x - x' = qy$, q real

$q = k_x/k_y$ for ordinary plane wave



Complex ray: (inhomogeneous plane wave)

$(x_r - x_r') + i(x_i - x_i') = (q_r + iq_i)y$

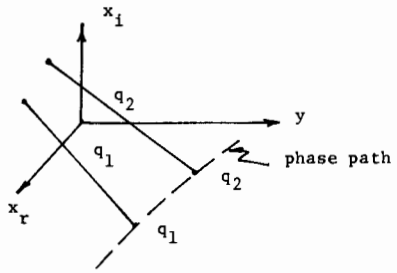
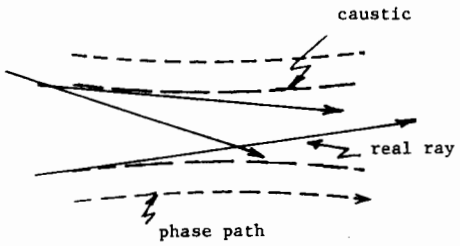


Figure 7. Beam Mode in Free Space

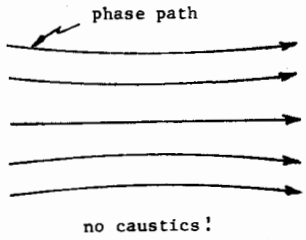
S real:

Inaccurate for low-order modes



S complex

Accurate for all modes



the other hand, if we make the local plane wave phase complex, then the phenomena of caustics and ray crossings disappear. Thus one actually has a simpler description using evanescent fields than one would have by using ordinary geometric optical fields.

DIFFRACTION OF EVANESCENT FIELDS

Under illumination by a non-evanescent field, an object such as a straight edge or rounded obstacle casts a shadow whose boundary separates the illuminated from the shadow region, Fig. 8. The shadow boundary is established by the ray that starts from the source and grazes the edge of the object. Surrounding the shadow boundary is a transition region wherein takes place the rapid decay of the field from the illuminated portion to the shadow portion. The penetration of the fields into the shadow region along a rounded object is by the so-called creeping waves which leak energy off tangentially and continuously as they travel around the object. These waves are much weaker in the shadow region than the waves that are caused by diffraction at a sharp endge.

When the incident field is an evanescent wave or a Gaussian beam, phenomena change drastically. It turns out that the shadow boundary is not established by an extension of the phase path that just hits the edge; in fact, it is displaced. Also, the transition region wherein the fields change very rapidly is much more narrowly confined. The whole question of the shadow boundary becomes a matter of ambiguity, both in the cases of rounded and sharp objects, since the exponentially small incident field may be overpowered by other (*e.g.*, diffracted) constituents.

Something peculiar can happen also in the case of scattering from a smooth object such as illustrated in Fig. 8. Normally, we expect that the reflected field from the front of the object will be considereably larger than the scattered field that goes around the back, sheds energy continuously, and then emerges in the forward direction. But for evanescent fields or beams, the phenomenology is quite different. If the strongest part of the beam does not strike the object, the field reflected from the front of the object can

be very weak because the incident field is outside the main region of the beam. The diffracted field that travels around the back can then be dominant. Thus, when dealing with beam scattering, it may be necessary to worry about field constituents that are insignificant when the incident field is non-evanescent.

CONVERSION OF POINT SOURCE FIELDS INTO BEAM FIELDS

There is a very effective analytical method that has been developed for dealing with beam fields, summarized in Fig. 9. The field of an ordinary oscillating source, in two dimensions, emits a cylindrical wave field, G. Taking the coordinates of that source, which are real, and allowing them to become complex by the substitution $\underline{\rho}'_b = \underline{\rho}' + i\underline{b}$, we find that G now represents a Gaussian beam. The beam has the following properties: It propagates along an axis parallel to b, and its waist (narrowest portion) is located at $\underline{\rho}'$.

The same procedure can be followed in three dimensions for a spherical wave, which is converted into a rotationally symmetric beam by the same type of source point displacement. This simple method extends the whole machinery available for analysis of propagation and scattering of fields excited by ordinary sources to the case where the incident field is a narrowly confined beam. Viewed from the vantage point of medium diagnostics, the complex-source-point method permits the generation of results for a high resolution probing field from those for a field with isotropic pattern characteristics.

DISSIPATIVE MEDIA

In dissipative media, it is the material losses that give rise to fields with complex phase. Although the methods for evanescent fields, as described above, have been applied primarily to lossless media, the basic attributes of complex phase make these techniques relevant also to fields in lossy media. While some applications to lossy media have already been pursued, this subject area needs to be developed further.

Figure 8. Formation of Shadow Boundaries

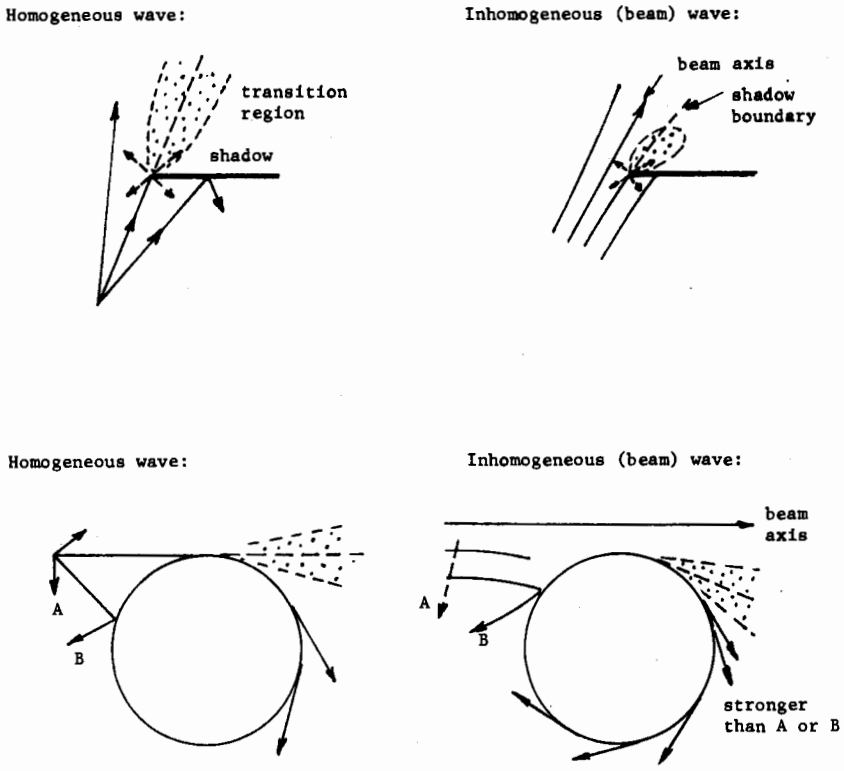
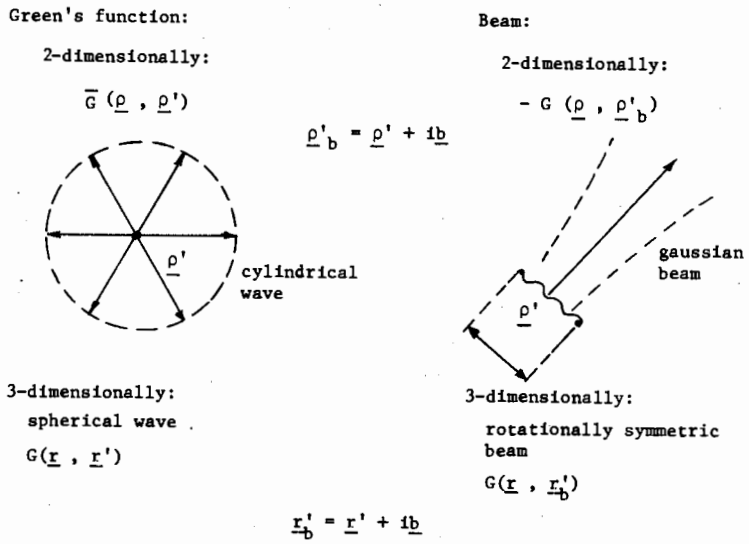


Figure 9. Relation between Green's Function and Beam Solutions



* *

DISCUSSION

You say that evanescent fields can bend in a homogeneous medium. I do not understand where the asymmetry enters if one starts with the Gaussian beam. [Brodsky].

Felsen: The general asymmetry refers to just a portion of the field: *e.g.*, one side of a Gaussian beam. The complete field is symmetrical about the beam axis.

One other question, in complex space are you in what we mathematically call C_2 *instead of* C_1? [Brodsky].

Felsen: One can play this game in many different ways. Talking about Gaussian beams, for example, it turns out that one can characterize a Gaussian beam by going into complex space. For the two-dimensional case, using complex space for one coordinate and staying in real space with the other, the Gaussian beam has some sort of equivalent smeared out source even in this complex space. However, going to a completely complex space where x and y are both complex, turns out to be simpler: a single point in complex space generates the field. In most cases, it is simpler to make everything complex. The real problem arises when one tries to apply this to some sort of diagnostic procedure where one cannot calculate phase paths analytically, and the only effective way for tracking is by computer. In a step-by-step tracking procedure of evanescent fields, difficulties arise because there are two sets of trajectories: the phase paths and the (orthogonal) paths of amplitude decay. Thus, two parameters must be determined at each tracking step: The real phase change and the change in the evanescent character.

If I understand what you are saying, in the ray approximation, it is easier to go to C_N *in complex variables and dimensions than it is to use a* C_1? [Brodsky].

Felsen: Correct, it is easier conceptually and mathematically. The problem, of course, is that the real world is not in C_N; it is in real space.

You are saying the computation is simple? [Brodsky].

Felsen: The analytics are simple. If, however, you try to do the calculation numerically, you would like a method where real data can be tracked. Consider a lossy dielectric material to which a field is applied at the input end. What comes out at the other end? It is necessary to track trajectories step by step through the profile. If the medium is slightly lossy, it is possible to approximate by using geometric optical ray paths as the unperturbed solution and by

including appropriate attenuation factors. This procedure can be worked into a systematic perturbation scheme. For highly lossy media, this does not work; it is bound to yield strong errors. One must then develop a scheme for tracking fields in lossy media. There is no good theory now. Conceptually, we know how it will work. The ray travels in complex space along a straight line. But how do we track in real space? - That is the difficulty. Attempting to do this calculation numerically, one has to keep track of several parameters, whereas in ordinary geometrical optics, one needs to keep track only of the phase front and hence the geometrical optical rays. This means that for fields with complex phase, the tracking (along inclined trajectories) is less local than for fields with real phase. There is also a question of whether the process is entirely unique.

One difficulty you did not mention, which might be important in a biological system that is not homogeneous, is anisotropy in the medium. Rays in such media are no longer perpendicular to the phase front and the energy propagates in directions which are not normal to the phase fronts. [Davis].

Felsen: We have considered that case. The main worry is not the anisotropy but the fact that one deals with fields in media which are strongly absorbing. Theories have been worked out for wave packets or pulses propagating through isotropic absorbing material, and also through anisotropic material, as long as the absorption is not too strong. One may then develop some sort of perturbation technique. But for strong absorption these become very difficult problems. There is not even a clear understanding of group velocity in a dissipative medium. As many as six different definitions have been given. A unique definition, using complex space can be made but the physical interpretation is far from obvious.

If one took the classical solution for the lossy sphere, could one easily observe these effects by running out the numbers in the classical solution? [Taylor].

Felsen: You can observe all of these effects, but of course what you need to do is interpret the effects in a classical solution in a more general way so that it can be applied to non-classical geometries, a deformed sphere, for instance. Now to implement this in a step-by-step numerical method has posed severe difficulties and a lot of open problems still need to be addressed.

Is it correct that this technique can also be applied to cases where you have both evanescent and propagating fields at the same time? [Kent].

Felsen: I am not talking about near fields. As you come very close to the source in terms of wavelength, we must modify the present procedure.

MICROWAVE AND RF DOSIMETRY

Chung-Kwang Chou and Arthur W. Guy

Bioelectromagnetics Research Laboratory
Department of Rehabilitation Medicine
University of Washington School of Medicine
Seattle, Washington 98195

ABSTRACT

Factors which determine the microwave and RF power absorption in tissues are pointed out to emphasize the complexity of the microwave and RF dosimetry. Quantification of power absorption is therefore necessary for any meaningful research results. We have summarized current available instrumentations and techniques for measuring microwave and RF field intensity in air and specific absorption rates in tissues. Also presented is current research at the Bioelectromagnetics Research Laboratory on the applications of the dosimetric techniques in assessing power absorption in animals or human models and in establishing threshold for observed biologic effects.

INTRODUCTION

Although there are several thousand papers in the literature pertaining to the biological effects of microwaves, controversial results prevent any conclusions regarding the safety level of microwave or RF exposure. The major reason is that many investigators lack adequate understanding and techniques on microwave and RF dosimetry. Approaches and concepts used in ionizing radiation have often been incorrectly applied in nonionizing radiation. Although the known biological effects of ionizing radiation are better understood than those of nonionizing radiation, the dosimetry problem of the latter is very different and much more difficult than the former. Unlike ionizing radiation, the same incident power density measured in the air can cause considerably different biological effects in different animals or tissues because of differential absorption of electromagnetic (EM) fields in the exposed objects.

The absorption of electromagnetic fields is determined by many factors which will be elaborated in the next section. Among these factors, the size and shape of objects, the frequency of the applied EM fields and orientation of object with respect to the polarization of EM fields can affect energy coupling by several orders of magnitude. Without quantitative measurements of the actual energy or field inside the exposed object it is difficult to compare research results using different animals and experimental approaches; it is impossible to extrapolate the research results to human to draw any meaningful conclusions about the safety level of microwave or RF exposure.

There have been some questions among investigators concerning the most meaningful parameters to measure. Wacker and Bowman[1] suggested using the square of the magnitude of the electric field or energy density in tissues to quantify hazards. Schwan[2] proposed using current density in tissues as the useful parameter. Many investigators have measured the rate of absorbed energy density in tissue which is defined as specific absorption rate (SAR). It really makes no difference which of the above parameters are chosen since they are directly related. The important concept is to measure the EM

field in the exposed tissues. Therefore, the following two steps are necessary to sufficiently quantify the biological effects of the EM energy and to apply this data for promulgating rational human exposure standards[3]: (1) determine what level of SAR in the tissues of an animal or specimen will produce an effect or damage, and, (2) determine what level of incident power density or field strength will produce the same SAR in the tissues of humans.

In addition to the hazard problem of nonionizing radiation, beneficial medical applications of the EM energy have also become popular research topics recently, expecially in the cancer hyperthermia. Due to the poor understanding of the interactions of EM fields and tissues, very limited success of cancer hyperthermia treatment has been achieved. It has been known for many years that heat alone, or heat combined with other therapies, can be very effective for cancer treatment[4,5,6]. With conductive heating it is impossible to elevate the temperature of deep tissue without causing damage to the skin and fat layer. Diathermy treatments using ultrasound, shortwaves and microwaves have been shown to elevate deep tissue temperature several degrees[7,8]. In order to apply the penetrating microwave or RF energy for tissue heating, measurements of SAR in tissue are required for effective treatment in cancer hyperthermia.

To study both the hazardous and beneficial effects of EM energy, we need to measure both the incident power density in the air and the SAR in the tissues. Only then will a clear understanding be determined of how EM fields interact with tissue, whether on a microscopic or macroscopic scale, or on the entire body structure, or whether an observable effect is thermal or nonthermal in origin or is merely an artifact to the nature of the experimental approach. By taking proper account of body size of the experimental animals, along with accurate *in vivo* dosimetry, the results from an investigation using rats can be related to those from another study on cats, monkeys, dogs, frogs or tissue samples in test tubes.

In this paper we first discuss the factors which determine the microwave or RF power absorption to emphasize the complexity of the microwave and RF dosimetry. Then we summarize the current available intrumentations and techniques for measuring the incident power density and the SAR. Finally, the

applications of techniques in assessing SAR in animals or human models and in establishing thresholds for observed biologic effects are presented.

FACTORS WHICH DETERMINE MICROWAVE AND RF POWER ABSORPTION IN TISSUE AT THE SAME INCIDENT POWER DENSITY

Tissue Dielectric Properties

In general, tissues can be divided into high water content tissues such as muscle, skin, liver, and kidney; and low water content tissues, such as fat and bone. Other tissues containing intermediate amounts of water, such as brain, lung, and bone marrow have dielectric properties between the high and low water content tissues. The dielectric constants and the conductivities of tissue vary over a wide range with the frequency of the applied EM fields and also vary slightly with temperature. Detailed values of dielectric constant and conductivity of both types of tissues can be found in Johnson and Guy[3].

The SAR in the tissue is related to the conductivity and the induced electrical field in the tissue. For tissues with different dielectric properties, it is obvious that the power absorption differs in different tissues.

Tissue Geometry

Reflection and transmission occur at tissue boundaries. The amount of reflection and transmission depends on the difference of the impedances of the two mediums and also on the thickness of the tissues. SAR in humans with two-inch fat measures differently than SAR in humans with one-inch fat. Tissues with curvature, such as arm or leg, produce different SAR than flat areas, such as the human back. Spherical structures like the head can have another type of SAR than that of the cylindrical legs. Multiple scattering in the curved structures usually produces focusing of EM fields and results in hot spots in the exposed object.

Tissue Size

Figure 1 illustrates that at the same frequency (918 MHz) and incident

power density, the theoretical SAR in a sphere is more than two times higher in magnitude for sphere of 3 cm in radius than in 7 cm sphere. The SAR patterns in the two spheres at the frequency (2450 MHz) are also different (See Figure 2 a,b). It is therefore erroneous to conclude that CNS effect on cat or monkey at certain incident power density can produce the same effect on humans.

Frequency of EM Fields

As mentioned above, the dielectric properties vary with frequency. Therefore, the penetration of fields and SAR pattern in the tissue are different at various frequencies. The geometry and the size of tissue also determine SAR patterns at different frequencies. Figures 2b and 2c shows the two types of SAR patterns in human-head size sphere at 918 and 2450 MHz. For a 3 cm radius sphere in the frequency range of 100 MHz - 10 GHZ, the peak SAR varies more than two orders of magnitude (Figure 3). At lower frequencies between 10 KHz - 800 MHz, the average SAR in ellipsoid models also varies in several orders (up to seven orders) depending on the size of the ellipsoid models and the frequency of EM fields[9,10]. When the object is exposed to frequencies near resonance the SAR can be much higher[11,12].

Polarization of EM Fields

It has been shown that when the polarization of the electrical field is parallel to the long axis of the exposed object the SAR is the highest[9,11]. The amount of difference depends on the ratio of the length and the diameter of the object. For a rat-size ellipsoidal model exposed to 10 MHz RF fields the average SAR for electrical field parallel to the long axis of rat model is about 20 times higher than that for a perpendicular polarization case[9]. This example illustrates that the power absorption in a freely moving rat exposed to a constant incident power density RF radiation can vary about 20-fold, depending on the orientation of the rat with respect to the polarization of the electrical field.

Source Geometry and Size

For far-field radiation, this is not a problem, since the field pattern is independent of the source. In ordinary laboratory experiments near-field

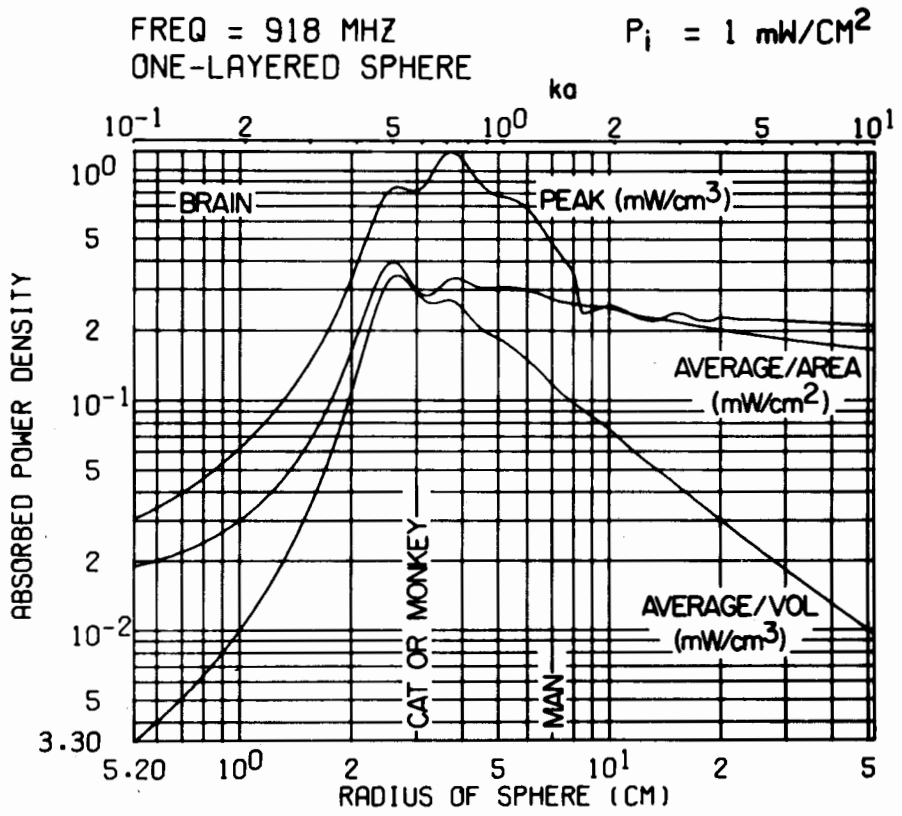


FIGURE 1 Theoretical SAR (absorbed power density) for spherical models of brain tissue exposed to 1 mW/cm^2 plane wave source.

exposures are usually necessary, especially for diathermy treatment or cancer hyperthermia. The field patterns in near-field regions are determined by the geometry and size of the EM source. When a human thigh is exposed to 2450 MHz waves with diathermy C director, the SAR measured in the tissue is different from that with an A or B director. Many investigators are developing applicators for more uniform and localized heating of deep tumors. The SAR pattern of each applicator will depend on the geometry and size of the applicators.

Surroundings of Exposed Object

If the exposed subject is near a ground or a conductor plate, the SAR in the object can be enhanced[12]. The existence of other animals in the same cage can also cause great variation in SAR due to the scattering between animals. Local nose or mouth touching between animals can induce hot spots at point of contact due to the high current density flow between the animals. An example of increased SAR at the contact point between a phantom model and a water bottle will be shown later.

Artifact

Metal implants can cause great intensification and modification of SAR pattern in the tissue[3]. The field enhancement at the tip of a metal electrode depends on the length and the diameter of the electrode[13]. Thermograms showing this artifact will be presented in a later section.

INSTRUMENTATIONS FOR INCIDENT POWER DENSITY MEASUREMENTS

Narda 8100 Series Survey Meter

A thermocouple described by Aslan[14] consists of a pair of thinfilm, vacuum-evaporated electrothermic elements that function as both antenna and detector. The sensor materials are antimony and bismuth deposited on a plastic or mica substrate, all secured to a rigid dielectric material for support. The length of the dipoles is small (compared to a wavelength) allowing the unit to monitor power with minimum perturbation of the RF field. The dc output of the sensor is directly proportional to the RF power heating the element.

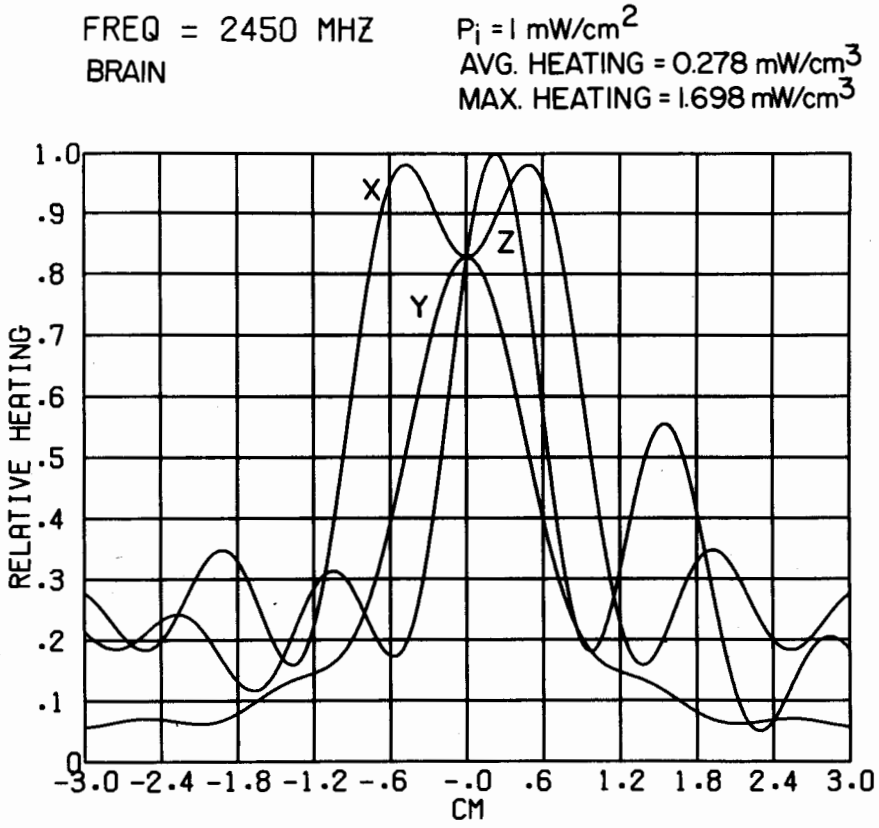


FIGURE 2a Theoretical SAR along the x,y anc z axes models of brain tissue exposed to a plane wave source (Incident power density 1 mW/cm^2 propagation along the z axis, and electrical field polarized along the x axis with origin at center of sphere).

With the thin-film elements oriented at 90° to each other and connected in series, the total dc output is independent of orientation and field polarization about the axis of the probe and is proportional to the square of the electric field vector. Lead wires carrying the dc output of the thermocouples are shielded with ferrite material and maintained perpendicular to the plane of the antennas. They will, therefore, be invisible to the propogating wave when the antenna is placed parallel to the phase front. The dc output is connected to an electric voltmeter calibrated to read field density directly in mW/cm^2. The meter has an appropriate time constant to read average power when the meter is used to measure modulated RF power density. The meter is designed to operate at 918 and 2450 MHz for measuring power denities between 0.2 to 200 mW/cm^2. Since the dipoles lie in one plane, the meter sensing probe must be oriented so probes are parallel to the EM wave front. Sometimes this is impossible for near-zone fields since there may be field components in three orthogonal directions.

Narda 8300 Series Broad Band Survey Meter

Aslan[15] has developed an improved isotropic, wide-band, field sensor. The sensor is composed of three elements arranged in orthogonal configuration. The elements are lossy and are heated by the field. Each element consists of a series of thin-film thermocouples deposited on a plastic substrate. The instrument is used where the wavelength is long compared to the length of the thermocouple strips and since their resistance is very high, field perturbations are negligible and the heating in each strip is proportional to the square of the electric field component along it. Since the elements are relatively long, however, the instrument can only be used where the field variation is small over the region occupied by the three orthogonal sensing elements. The meter is designed to operate over the .4 to 40 GHz frequency range for measuring electric field strengths of 34 to 340 V/m or .3 to 30 mW/cm^2.

NBS (National Bureau of Standard) Meter

Another type of broad band isotropic field sensor has been described by Bowman[16]. This sensor consists of three orthogonal dipoles with diode detectors connected between the arms of the dipoles. The signals from the dipoles

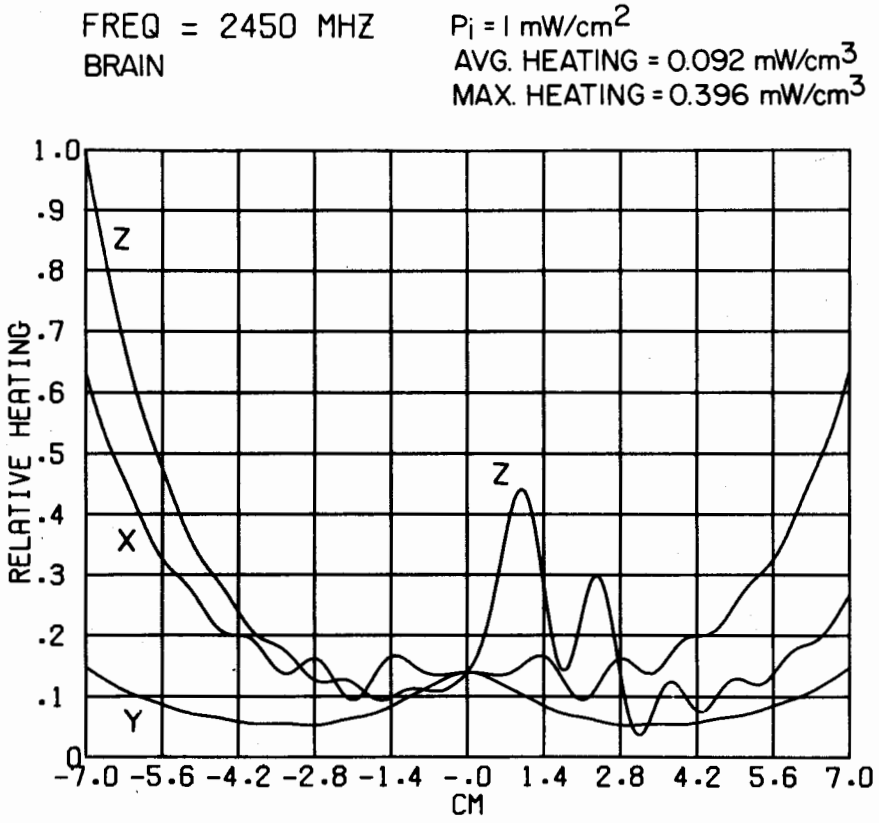


FIGURE 2b Theoretical SAR along the x,y and z axes models of brain tissue exposed to a plane wave source (Incident power density 1 mW/cm^2 propagation along the z axis, and electrical field polarized along the x axis with origin at center of sphere).

are conducted independently through high-resistance leads that are transparent to the microwave fields. For low intensity fields that have wavelengths large compared to dipole lengths, the detected signals from each orthogonal element of the field sensor are proportional to E^2. For fields with high intensities, the nonlinear characteristics of the summing amplifier provide an extended dynamic range. The instrument is calibrated to display $\varepsilon_o E^2/4$, the electric energy density. The meter is useful in the frequency range .03 to 3 GHz for electric field strengths of .9 to 4750 V/m, or 0.0002 to 6000 mW/cm^2.

Golay Cell Probe

Fletcher and Woods[17] have developed a broad-band, isotropic field sensor which is comprised of a pair of thin-walled, air-filled spheres connected by tubes to a sensitive differential pressure transducer. One sphere is coated with a resistive film that is heated by the EM field to produce a pressure differential between the spheres. The non-coated sphere provides compensation for changes in ambient temperature or pressure. This probe can accurately sum the intensities of multifrequency fields between 0.4 to 40 GHz. However, the slow response time (about 20 seconds) limits the usefulness of this probe. Also, the sensitivity is limited to between 0.3 and 30 mW/cm^2. This probe was marketed by the Wayne Kerr Company, Ltd., New Malden, Surrey, England but was removed subsequently[16].

BRH Electric Field Probe

Bassen, *et al*[18] have developed a miniature, broad-band, electric field probe capable of measuring the total electric field between 915 MHz to 10 GHz in free space. This probe can also be used for measuring fields within animal tissue or phantom materials at frequencies below 3 GHz. The microwave detector consists of Schottky diodes which have the broadest square-law dynamic range and frequency range in microminiature monolithic form. The diode is in contact with dipole elements and connected by high impedance leads to an amplifier. The output of the amplifier is then transmitted to a read-out electronic meter via fiber optics to minimize any perturbation of fields. The meter has been completed and is being evaluated in several laboratories.

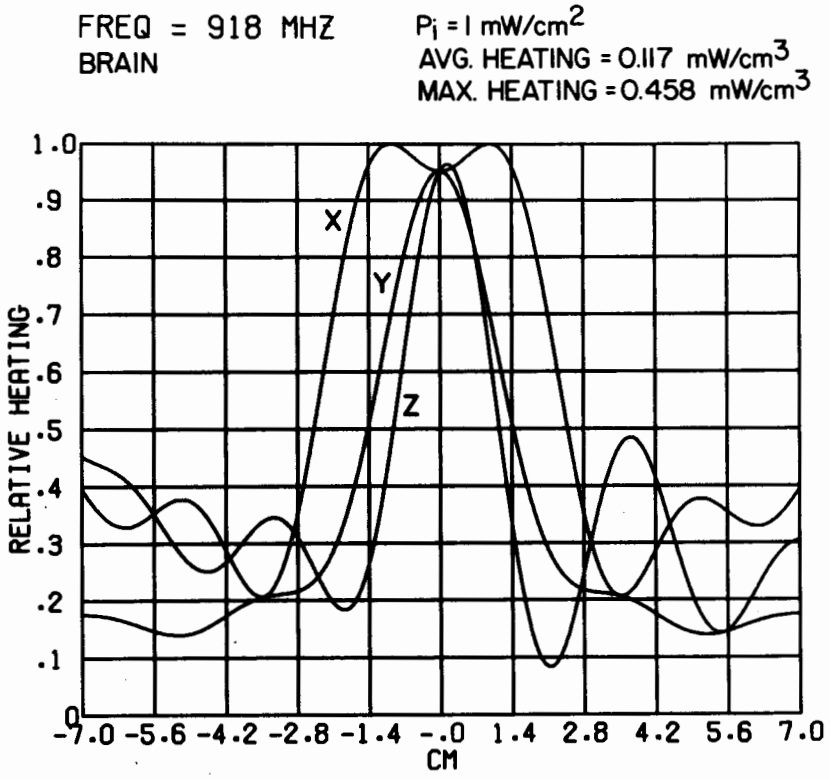


FIGURE 2c Theoretical SAR along the x, y and z axes models of brain tissue exposed to a plane wave source (Incident power density 1 mW/ cm^2 propagation along the z axis, and electrical field polarized along the x axis with origin at center of sphere).

Pyroelectric Probe

This probe utilizes the pyroelectric effect of crystals with spontaneous polarization[19]. The spontaneous polarization of the crystal depends on the temperature of crystal. When thermal energy is transferred to the crystal by EM radiation, the radiation can be detected via the pyroelectric effect. Two conductive electrodes are connected to the two surfaces of a thin-slab, pyroelectric material and are connected to a preamplifier to monitor the pyroelectric current flow which is proportional to the rate of temperature change with time. This probe has been tested for measurement of microwave power density under far-field conditions throughout the 2.0 - 12.0 GHz frequency range. This probe can tolerate very high power radiation. However, the requirement for modulated radiation makes this probe less practical.

Magnetic Field Probe

Up to the present time, power density in the near field has often been measured with the use of directive, resonant antennas or short electric dipoles measuring electric field. Both these methods have limited applicability. The measurements of the power density in the near field needs the use of a probe sensitive to the electric and magnetic field simultaneously, having definite sensitivity for both components, flat frequency response and omnidirectional radiation pattern. For this purpose Babij and Trzaska[20] use sensors with a number of loops, dipoles or unipoles. In most of them, electric dipoles are formed by electrostatic screening of loops. The simplest sensor consists of two loops in each plane; electric field detector is connected between the screens of the loops. The probe with triple quadrant antennae consists of three perpendicular loops, screens of which make three quadrant antennae with common arms. To improve its radiation pattern for the electric field an additional unipole was added. The unipole of the modified triple quadrant antennae makes another three quadrant antennae with the screens of the loops. Another probe consists of three loops, inside them are immersed three orthogonal dipoles. Each dipole is placed in the plane of different loops to minimize mutual couplings. This probe has three modifications. The first uses (as electric dipoles) two equal parts of the screen of each loop, the other uses only half of

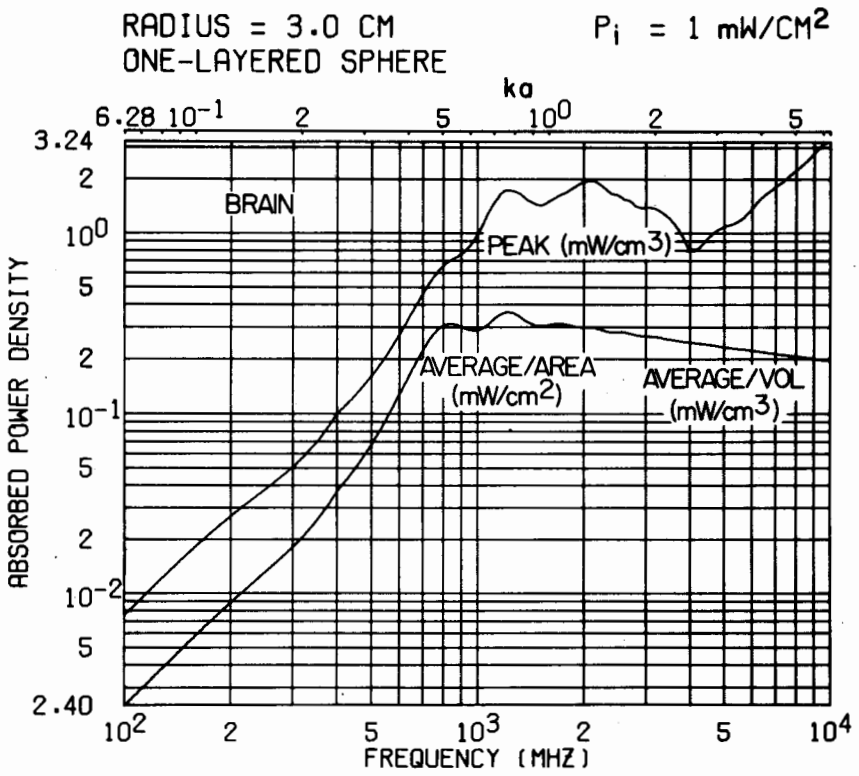


FIGURE 3 Theoretical SAR for 3 cm spherical models of brain tissue exposed to 1 mW/cm^2 plane wave at different frequencies.

the screen and the third uses an unscreened loop for the electric field as well. The main problem here is to get sufficient sensitivity for the magnetic field. All these probes are designed for frequencies below 300 MHz. This probe is not available on the market yet.

TECHNIQUES FOR SPECIFIC ABSORPTION RATE MEASUREMENTS

Many of the following techniques involve the measurement of temperature rise after the microwave or RF exposure. The heating pattern is first determined by the power absorption in tissue, *i.e.*, the SAR in tissue; then the heat diffusion and blood circulation will modify the heating pattern in the tissue. The body tissues are known to be poor heat conductors; the conductivity of unperfused body tissues is comparable to that of cork[21]. Vigorous blood flow increase in muscle during diathermy treatment was observed only after about 8 - 10 minute exposure with a deep tissue temperature near 43° C [8]. However, the skin flow increases tremendously when the skin temperature was elevated. Therefore, the SAR pattern should be measured before it is altered by heat diffusion and blood flow. High-power and short-term radiation are necessary for this measurement. Phantom materials[22] with dielectric properties close to real tissues have been developed. The heat conductivity of the material is also similar to tissues. We have used the phantom tissues extensively for measuring SAR in tissues. Sacrificed animals have also been used. The phantom tissues and sacrificed animals eliminate the blood flow problem. In live animals the blood flow reduces the temperature rise in the exposed tissue. The SAR pattern measured is actually a modified one.

The high power exposure produces a rapid and measurable temperature rise in the tissue and the short exposure period ensures that there is no loss due to cooling or diffusion, so the SAR is related to the exposure time, t, temperature rise, ΔT, and heat specificity of tissue, c, by this simple relation: $SAR = 4.186 \times 10^3 \, c\Delta T/t$, where SAR in W/kg, ΔT in $^{\circ}$C, c in kcal/kg$^{\circ}$C, and t in sec. The measured SAR can then be used to relate the input power of the source to the SAR in the tissue under normal lower power exposure conditions.

Glass Probe and Thermocouple Combination

This technique[3] utilizes a small diameter plastic or glass tube sealed at one end and implanted at the location where a measurement of the absorbed power is desired. The tube, illustrated in Figure 4, is long enough so that the open end, fitted with a plastic guide, protrudes from the tissue. A very small diameter thermocouple is inserted into the tube with the sensor located at the probe tip and an initial temperature is recorded. The thermocouple is quickly withdrawn from the tube and the animal is exposed under the normal conditions of the experimental protocol with the following exceptions. Instead of using the power level normally chosen for a given experiment, a very high power burst of radiation of duration sufficient to produce rapid but safe temperature rise in the tissue is applied to the animal. The thermocouple is then rapidly returned to its original position and the new temperature is recorded for several minutes. The temperature versus time curve is then extrapolated back in time to the period when the power was applied; the SAR can be calculated from the differences between initial and final extrapolated temperatures.

Fiber-Optic Liquid Crystal Probe

Rozzell *et al*[23] and Johnson *et al*[24] have developed a probe for measurement of temperature in tissues under exposure to electromagnetic fields. The probe is essentially transparent to the electromagnetic field since it does not possess metallic parts. It untilizes fiber optics to transmit information to and from a sensor tip that consists of a liquid crystal thin film. The sensor tip, which is inserted into the tissue at the point where temperature or dosimetry information is needed, consists of a bulk liquid crystal encapsulated between two nested mylar cups and fitted over the tip of the fiber optic bundle. One-half of the fiber optic strands are used to transmit red light from the light-emitting diode into the liquid crystal material, and the other half carries scattered red light back to a photodetector. Any temperature change in the liquid crystal shifts the color center resulting in a change in backscattering of the red light. Tests have shown that the probe is capable of measuring the true temperature in tissues exposed to electro-

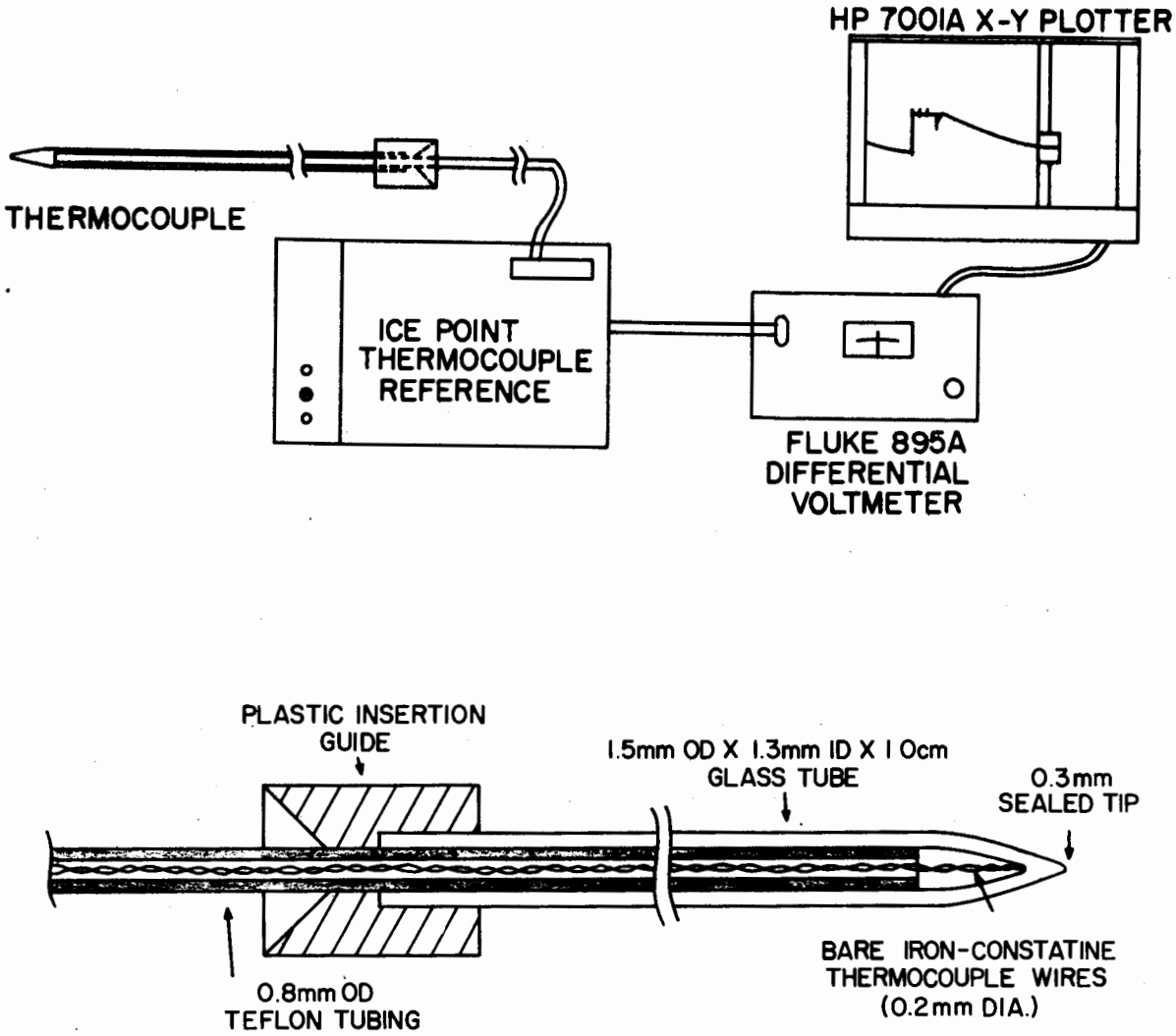


FIGURE 4 Glass probe and thermocouple combination for SAR measurements in biological tissue.

magnetic fields without producing any changes in the field configuration in the tissues. There are three different probes for the temperature range between 10 - 45° C. The maximum size of the probe is 3 mm in diameter, 10 cm long. This probe is commercially available.

Thermistor with High Resistance Lead

Bowman[25] has developed a probe using thermistor and high resistance leads for the measurement of tissue temperature during EM radiation. The probe consists of two pairs of very high resistance leads connected to a small high resistance thermistor. The thermistor resistance is sensed by injecting a constant current through one pair of leads and measuring the voltage developed across the thermistor by means of a high impedance amplifier connected to the other pair. The physical size of the probe is 1 mm OD. It has a response time constant of less than 0.2 sec., short term stability better than 0.01°C and a high resistance line heating error of less than 0.005°C for a heating rate of 1° C/min. This probe has been evaluated in several laboratories. However, it has not appeared on the market yet.

Other Temperature Probes

Larsen, *et al*[26,27] have developed a probe consisting of a Wheatstone bridge circuit, extremely fine electrodes connected to a thermistor and high resistance plastic leads. Thermographic methods verified very minimal temperature perturbation during exposure.

Cetas, *et al*[28] have developed a fiber-optic thermometer using a birefringent crystal as a sensor. Only a single optic fiber is needed to carry light to the sensor and back to the photodetector. Improvement of this probe is still needed.

Christensen[29] reported his work on an optical etalon (a small optical flat coated on opposite sides to form a cavity) temperature sensor. When the temperature of etalon varies, linear thermal expansion and changes in the index of refraction will cause a shift in the resonant wavelength, thereby shifting the wavelength positions of nulls of reflectivity from the etalon. A Fabry-Perot interfermometer was used to measure the wavelength shift. Some experimental tests have been made of this probe.

Deficis[30] designed a different temperature probe which does not measure the temperature rise in tissue. Instead the lossy material coated on the liquid crystal absorbs the energy. The heating is calibrated to give mW/cm^2 in tissue. Therefore, this probe measures power density in tissue, not SAR.

Microwave Diodes

This method measures the field in tissue instead of temperature rise. The same techniques involving microwave diodes and dipoles that are used for direct measurement of fields in air can also be used in tissues. There are difficulties, however, since the ratio of the dipole length to feedline separation must be kept large to maintain accuracy while at the same time the dipole must be sufficiently short to implant with a probe. Johnson and Guy[3] have used a microwave diode with pigtail leads cut to 1/2 cm as a dipole antenna to make field measurements at the brain surface of a cat. The major problem with this type of sensor is that it must be calibrated for each tissue to account for changes in dipole source impedance. With proper design, however, the impedance problem could conceivably be solved. Recently Bassen, *et al*[31] have used this microwave diode probe as described in the previous section to measure the field inside phantom tissues.

Measurement by Thermography

Guy[22], and Johnson and Guy[3] have described a method for rapid evaluation of SAR in tissues of arbitrary shape and characteristics when they are exposed to various sources, including plane wave, aperture, slot, and dipole. The method, valid for both far- and near-zone fields, involves the use of a thermographic camera for recording temperature distributions, magnitude of the electric field may then be obtained anywhere on the model as a function of the magnitude of the calculated heating pattern. The phantoms are composed of materials with dielectric and geometric properties identical to the tissue structures they represent. Phantom materials have been developed which simulate human fat, muscle, brain and bones. These materials have complex dielectric properties that closely resemble the properties of human tissues

reported by Schwan[32]. A simulated tissue structure composed of these modeling materials will have the same internal field distribution and relative heating pattern in the presence of an EM source as the actual tissue structure. Phantom models of various tissue geometries can be fabricated such as cylindrical structures consisting of synthetic fat, muscle, bone, and spheres consisting of synthetic brain to simulate various parts of the body. The models are designed to separate along planes perpendicular to the tissue interfaces so that cross-sectional relative heating patterns can be measured with a thermograph. A thin (0.0025 cm thick) polyethylene film is placed over the precut surface on each half of the model to prevent evaporation of the wet synthetic tissue. In using the model, it is first exposed to the same EM source that will be used to expose actual tissue. The power used on the model will be considerably greater, however, in order to heat it in the shortest possible time. After a short exposure, the model is quickly disassembled and the temperature pattern over the surface of separation is observed and recorded by means of thermograph. The exposure is applied over a 5 - 60 sec. time interval depending on the source. After a 3 - 5 sec. delay for separating the two halves of the model, the recording is done within a 5 sec. time interval, or less. Since the thermal conductivity of the model is low, the difference in measured temperature distribution before and after heating will closely approximate the heating distribution over the flat surface, except in regions of high temperature gradient where errors may occur due to appreciable diffusion of heat. The thermograph techniques described for use with phantom models can be used on test animals. The animal under test or a different animal of the same species, size and characteristic, must be sacrificed, however. The sacrificed animal is frozen with dry ice in the same position used for exposure conditions. It is then cast in a block of polyfoam and bisected in a plane parallel to the applied source of radiation used during the experiment. Each half of the animal is then covered with a plastic film and the bisected body is returned to room temperature. The same procedure used on the phantom model is then used with the reassembled animal to obtain SAR patterns over the two-dimensional internal surface of the bisected animal.

Twin-Well Calorimetry

Phillips, *et al*[33] have determined the average SAR in animals by measuring the amount of heat generated in a fresh rat carcass irradiated with microwaves by use of a differential, or twin-well calorimeter. The general procedure consists of placing a pair of freshly killed rats of equivalent body weight into a twin-well calorimeter and calculating the differential body heat content of the pair. Both carcasses are then removed from the calorimeter and placed in insulated containers constructed of expanded bead polystyrene. One animal is then exposed briefly to microwaves or RF fields in an anechoic chamber. The other animal serves as a sham-exposed control and reference heat source. Immediately after treatment both animals are put back into the calorimeter, and the heat added to one animal's body heat by irradiation is measured. Use of dead animals eliminates the problems of physiologic heat production and loss and requires only the assumption that death does not alter the lossiness of animal tissues for absorption of microwave energy. The accuracy of this technique for determining the absolute amount of energy absorbed by rats has been calculated to be 0.8%. This method does not give the two-dimensional SAR patterns as the thermographic technique. However, this method provides an alternative way for measuring average SAR accurarely for small animals like mice, in which the thermographic technique fails, due to the fast thermal diffusion in small objects.

Waveguide

A very effective and economical method for exposing small animals or *in vitro* preparation is through the use of a waveguide system. Chou[34] has designed a waveguide for exposing isolated tissues. The SAR in the tissue can be easily calculated by a simple mathematical equation. Ho, *et al*[35] have described an environmentally-controlled waveguide for exposing mice. The average SAR can be calculated simply by measuring incident and reflected power at the feed end of the waveguide and the transmitted power at the terminal end of the waveguide. Guy and Chou[36] have developed a cylindrical waveguide system for exposing rodents chronically to 918 MHz circulary polarized fields.

The average SAR in freely moving rodents has been determined by the simple measurement described above. Some results will be shown in the next section.

APPLICATIONS OF THE DOSIMETRIC TECHNIQUES

Rabbit Head Exposed to 2450 MHz Diathermy "C" Director[37]

The SAR pattern along the antereo-posterior axis of the eye and extending to the head of a rabbit exposed to a microwave diathermy "C" director was determined using the thermocouple micropipette technique. The animals were exposed to the near-zone of the applicator with horizontal polarization and the distance between the crossing point of the dipole feed and corneal surface of the eye was set at 5 cm. Incident power density at the same position as the right eye of the rabbit was measured with a Narda 8100 electromagnetic radiation monitor with the animal absent. The SAR patterns for five animals are shown in Figure 5. In all cases, the absorption reached peak values within the vitreous body about 1.5 cm behind the cornea, with a mean value of .92 W/kg based on a normalized 1 mW/cm^2 incident power level.

Rabbit Exposed to Approximate Plane Wave Field[13]

Figure 6 illustrates the SAR pattern measured in a rabbit exposed to 2450 MHz fields normalized to 1 mW/cm^2 as measured along the body axis of the rabbit. The rabbit was illuminated over the dorsal body surface by a standard gain horn spaced 100 cm away with the electric field polarized along the axis of the body. Thermograms taken on the rabbit by the techniques described previously were processed by computer and the iso-SAR lines were plotted as shown in the figure. SAR measurements were also taken along the antereo-posterior axis of the eye by the thermocouple micropipette technique. These measurements agree reasonably well with the thermographic measurements.

Cat Exposed to 918 MHz Aperture Source[3]

Figure 7 illustrates thermographic recordings taken to assess the SAR in actual cat head and a 6 cm diameter phantom spherical model of the head.

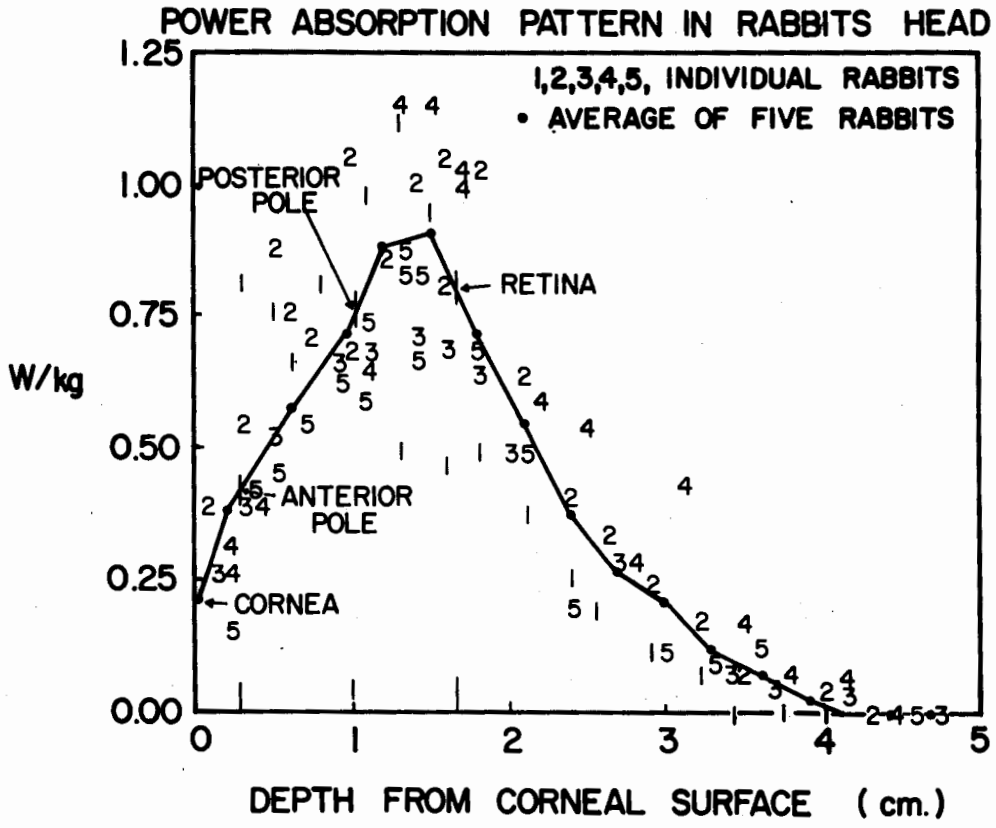


FIGURE 5 SAR in the eye and head of rabbit exposed to near zone 2450 MHz radiation (1 mW/cm^2 incident power density).

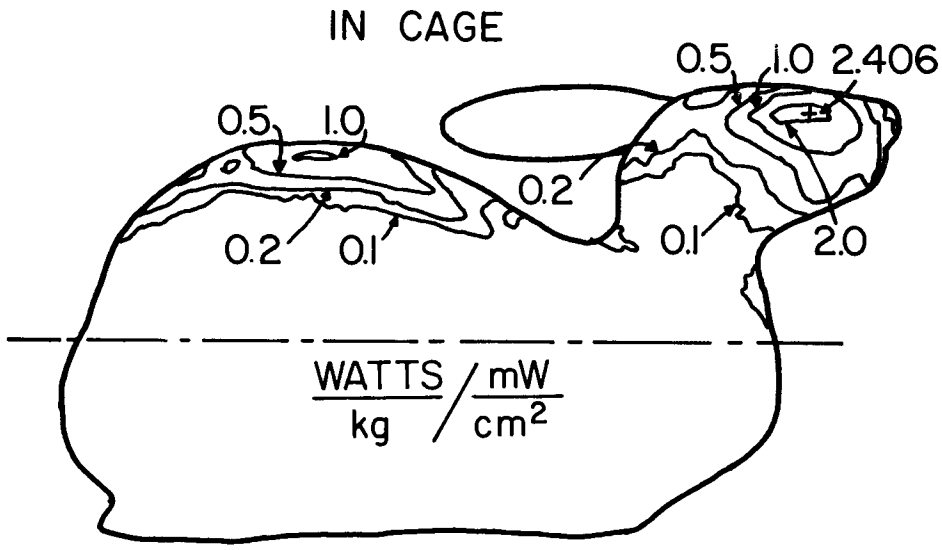


FIGURE 6 SAR pattern in rabbit exposed to 2450 MHz fields (normalized to measured incident power density at rabbit body axis).

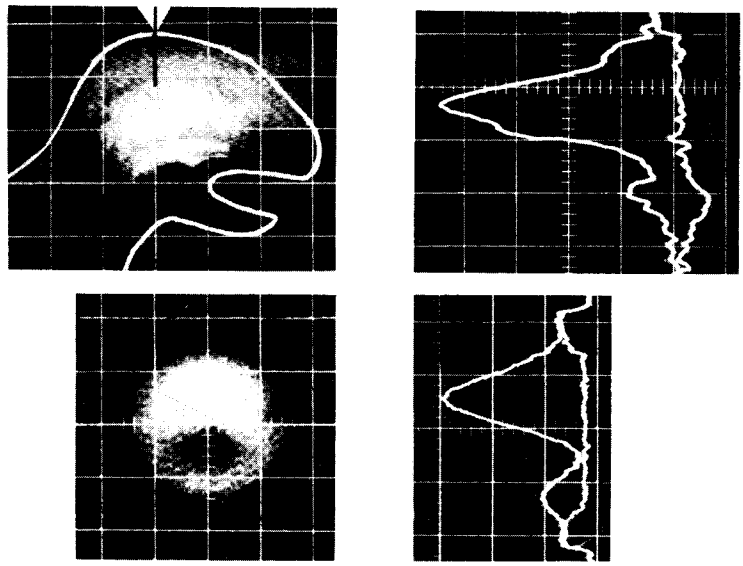


FIGURE 7 Comparison between SAR patterns in cat head and 6 cm diameter phantom sphere (brain tissue) exposed to 918 MHz operative source as measured with thermograph.

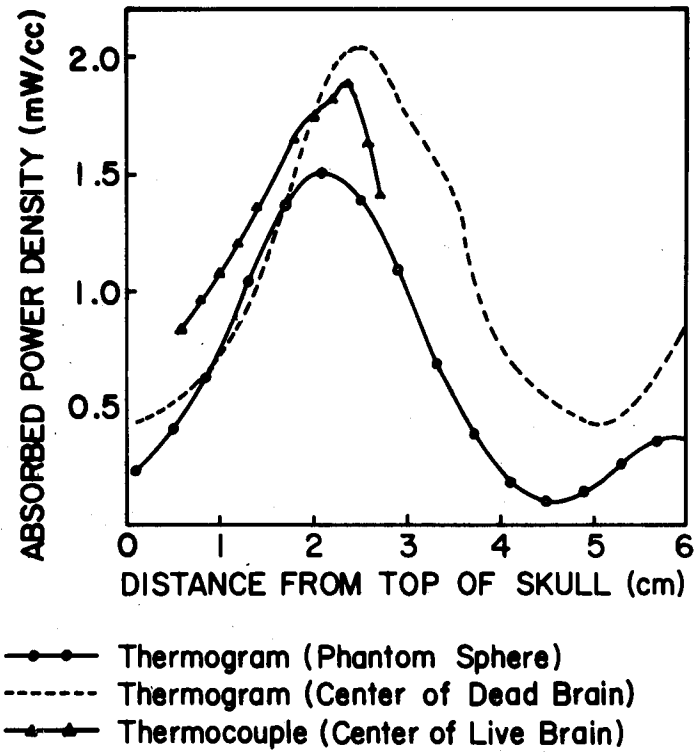


FIGURE 8 Measured SAR in cat brain and phantom sphere due to microwave radiation for 918 MHz aperture source (Spacing 8 cm with 1-W input power).

Thermograms were taken for exposure of the head to a 918 MHz 13 x 13 cm aperture source spaced the distance 8 cm from the dorsal surface. The results clearly show the presence of high absorption area or hot spots in the head of the exposed cat predicted from the theoretical calculations for a sphere. Both the theory and the measurements indicate approximately 0.8 W/kg peak SAR per mW/cm^2 incident power density. Figure 8 illustrates measured SAR in the head of the cat and the phantom sphere by different methods as a function of distance from the top of the exposed surface. The values are based on a 1 W input power to the 918 MHz aperture source under the same exposure conditons described for the previous figures. The curves illustrate thermograms taken on a phantom sphere and the center of the dead brain. They also illustrate thermocouple and micropipette measurements at the center of the live brain.

When conducting objects, wires or electrodes are brought in contact with or are implanted in biological tissues exposed to EM fields, high intensity fields may be induced locally where the conductors come in contact with the tissues. These fields can be many orders of magnitude greater than the fields that would normally be present without the presence of the conductors. This is clearly illustrated by Figure 9 showing thermograms taken of the head of the cat exposed to 918 MHz microwaves, both with and without the presence of a metal electrode inserted in the brain[3].

Rat Exposed to 918 MHz Aperture Source[38]

Figure 10 illustrates the thermograph of a study made on a phantom tissue model of the body of a rat exposed to 918 MHz 13 x 13 cm aperture source spaced 8 cm away from the animal. The results clearly illustrate unpredictable absorption peaks that may occur in the body and tail of the rat. The profound absorption 8.6 W/kg at the base of the tail is due to the increased current density resulting from the sharp change in tissue cross-section. The low absorption in the pelvic area is probably due to a standing wave null resulting from body resonance conditions since the rat model is approximately one wavelength long. Results indicate that one must be extremely careful in drawing conclusions from temperature measurements made with rectal thermo-

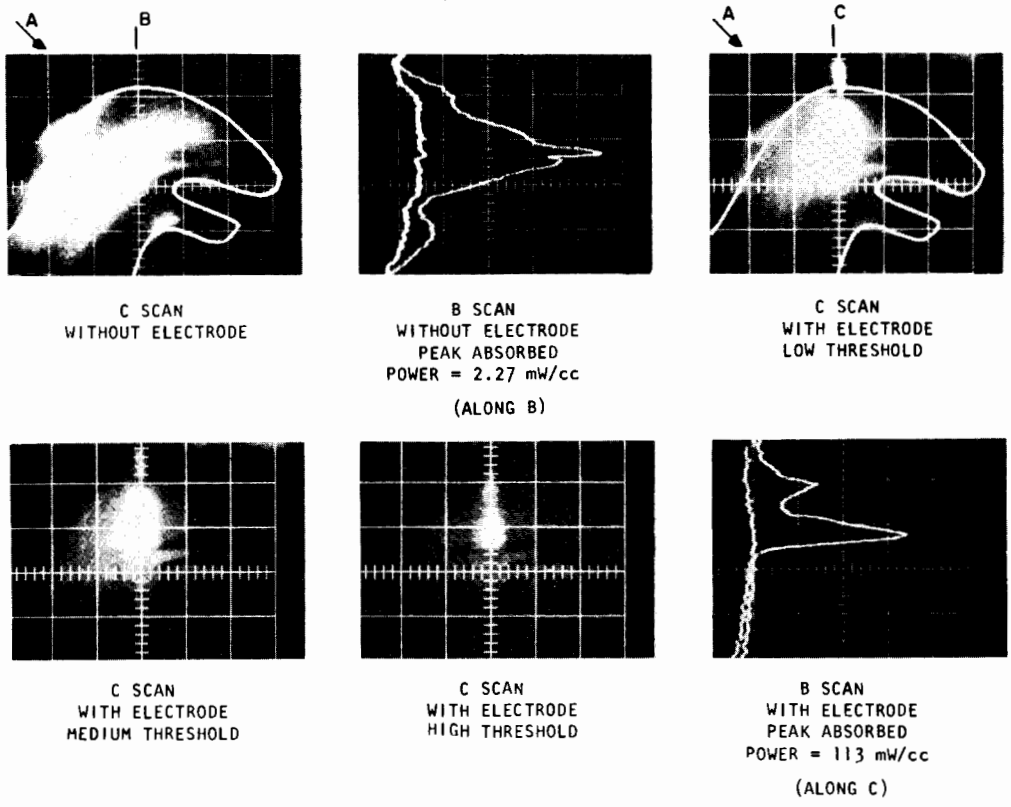


FIGURE 9 Thermograms showing the effect of implanted metal electrode on the SAR pattern in a cat brain exposed to 918 MHz aperture source (incident power density 2.5 mW/cm^2).

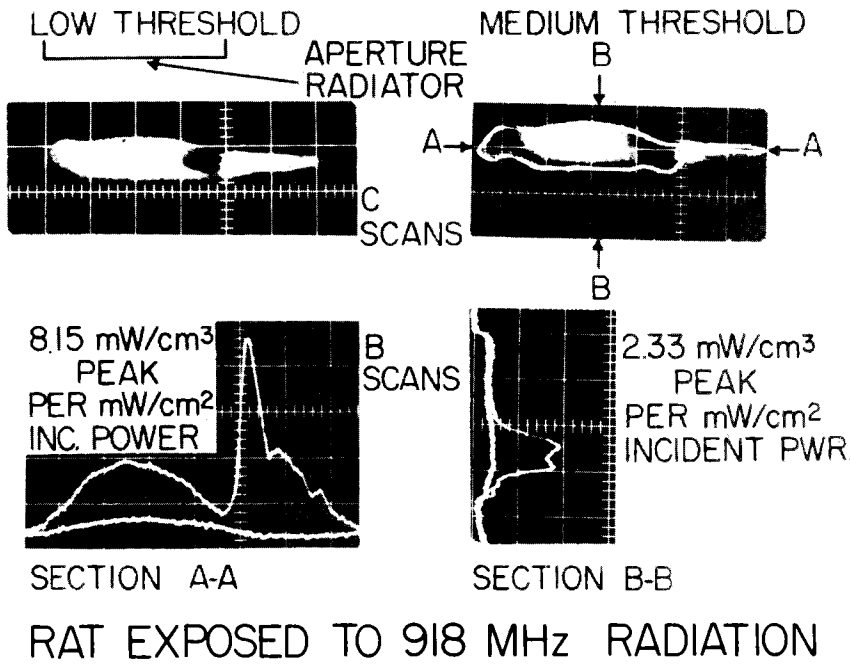


FIGURE 10 Thermograms of phantom rat exposed to 918 MHz aperture source.

meters. Also, one cannot make the easy assumption that keeping the tail or any portion of the rat out of the direct beam of radiation will insure non-exposure and, consequently, no absorption.

Phantom Man Exposed to Simulated 31 MHz RF Fields in Cavity[39]

Figure 11 illustrates thermograms taken for a scale model man exposed to an electric field oriented parallel to the long axis simulating a 1.74 m high 70 kg man exposed to a simulated 31 MHz electric field in a resonant cavity. Single profile scans were taken through regions of intensive absorption. The edges of the man for each scan are indicated by white vertical lines. The arrow indicates the position in which the peak SAR was calculated. Areas of maximum absorption occur in the smaller cross-section of the body such as the knees, ankles, and neck. The high absorption of the narrow cross-sections of the body is due to the constriction of the induced current along the length of the body, thereby increasing the current density and electric fields in those areas. The arms are not affected since they are parallel to the large cross-section trunk which shunts most of the induced currents. Figure 12 illustrates thermographs taken for the same man exposed to a magnetic field perpendicular to the frontal plane simulating a 31 MHz exposure. For this case, circulating eddy currents are produced. There is generally high absorption along the sides of the body in the area of the ribs of approximately 2.52 W/kg for 1 A/m incident magnetic field intensity. Peak absorption occurs in regions where the flow of the circulating eddy currents are forced into the smaller cross-sectional areas or are diverted by severe angular changes of the tissue such as the region near the axilla and the perineum. Since the maximum power absorption due to the electric field exposure occurs where there is minimal power exposure due to the magnetic field exposure, we can predict maximum SAR for a plane wave field from the values given in the previous two figures. Except for a change in magnitude, the resulting patterns are identical to those which would occur in actual full-scale subjects with homogenous dielectric tissue composition exposed to fields at any frequency below those indicated. Thus, the results can be extrapolated down to cover the entire RF frequency range. At lower frequencies, however, the nerve and muscle tissues

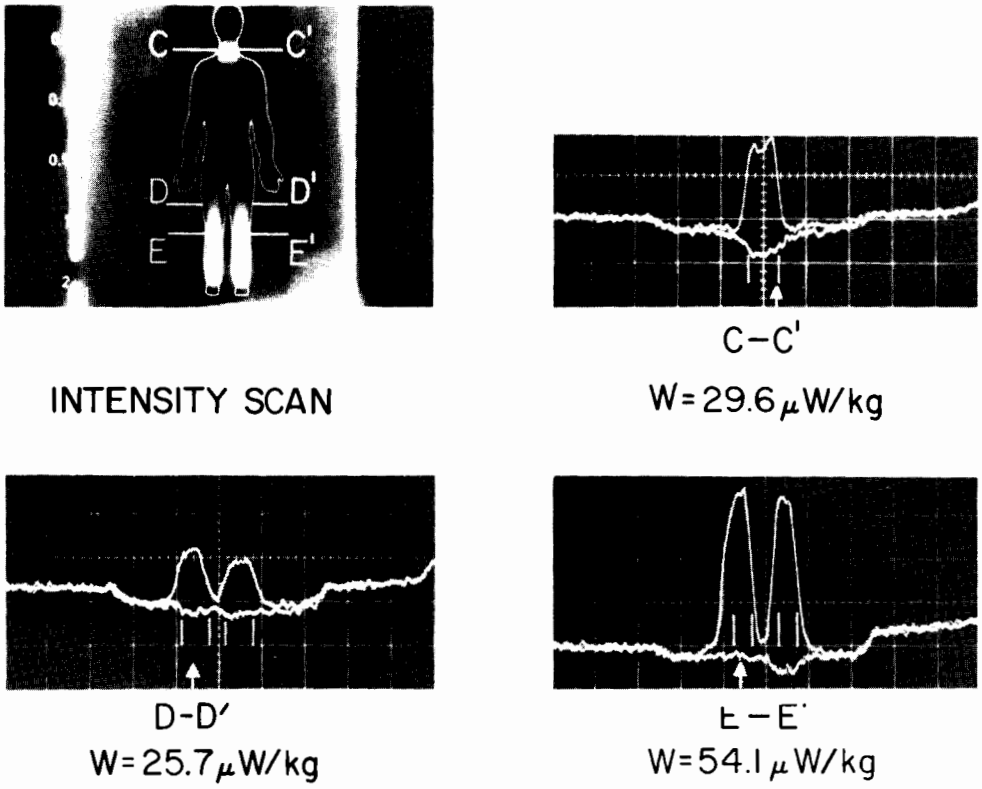


FIGURE 11 Thermograms and measured peak SAR for 70 kg., 1.74 cm height model man exposed to 31 MHz electric field; vertical divergence = 2° C, horizontal divergence = 4 cm. (sf=scale factor).

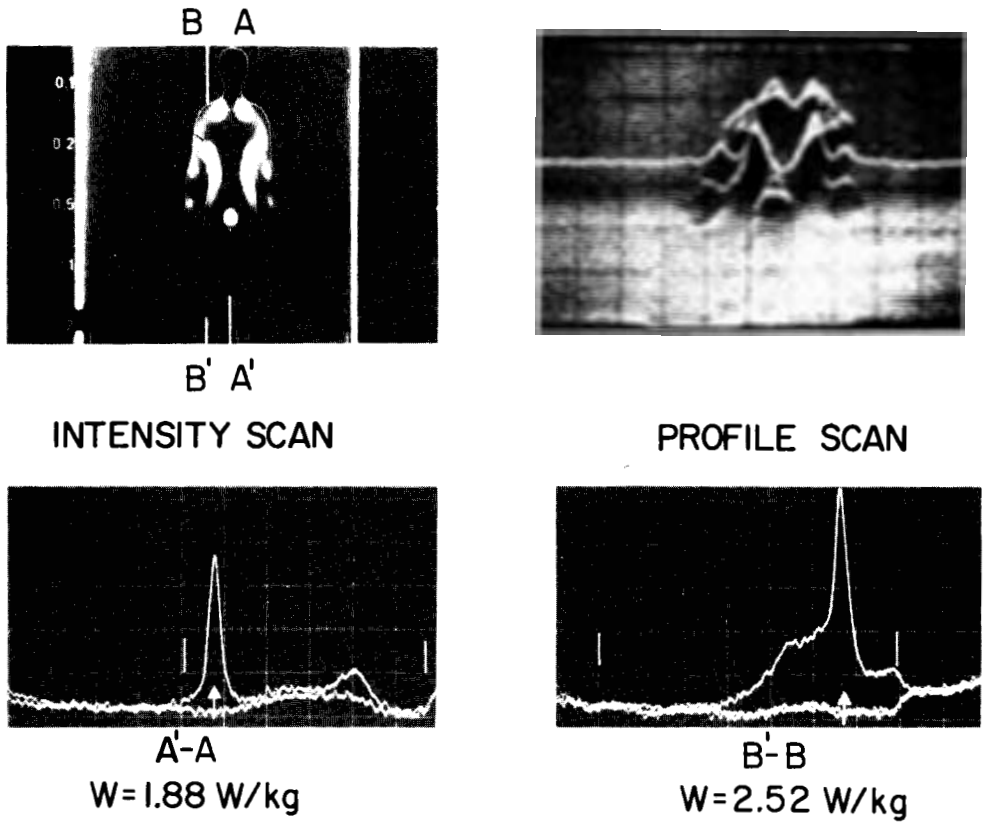


FIGURE 12 Scaled man model exposed to 31 MHz magnetic field (same scale as Fig. 11).

can become anisotropic requiring a much more sophisticated model.

Phantom Man Exposed to Simulated 198 MHz RF Fields in Free Space[40]

Figure 13 illustrates the exposure of the 70 kg, 1.74 m high man to 198 MHz (frequency near VHF television Channels 10 and 11) plane wave fields for EKH polarization[9]. This exposure provided the highest measured SAR obtained for all exposures conducted in this study. The scans show that the highest SAR occurs in the neck, wrist, and ankle regions on the exposed side of the subject. Note the peak SAR is 1.83 W/kg measured in the wrist. It is interesting to note that these regions of maximum measured SAR correspond to areas of the body with small cross-sections. Thus, the longitudinal electric currents induced along the long axis of the body by the parallel electric field are being constructed by the small cross-sections to produce high SARs. One may also note that these maximum SARs are more than an order of magnitude greater than the average values calculated for an equivalent prolate spheroidal model of the average man by Johnson, *et al*[9]. This would indicate that one should be very cautious about the use of averaged SAR when considering possible thresholds of biological effects of man exposed to VHF radiation. Though the total absorbed energy or averaged SAR might be small in terms of the total body mass, the fact that this energy can be absorbed in a relatively small volume could lead to effects that would not normally be observed if the energy were distributed uniformly over the body. Figure 14 illustrates the thermographic results of the model exposed to HEK polarization. For this exposure condition where the man was facing the horn (cross-polarized with the electric field), relatively intense hot spots were noted in the perineum area (.73 W/kg), in the axilla area (.41 W/kg), and in the wrists (0.63 W/kg). Again, these values of maximum SAR are more than an order of magnitude higher than averaged value predicted from a prolate spheroid model.

Comparisons of Heating Patterns of 2450 and 918 MHz Microwave Ovens

A number of models with the same electrical properties as human or beef muscle, including spheres 6 cm in diameter and 14 cm in diameter, ellipsoids with axes of 8.6 and 17.2 cm were tested in 2450 MHz and 918 MHz standard microwave ovens using the modified thermographic technique[41]. Models described

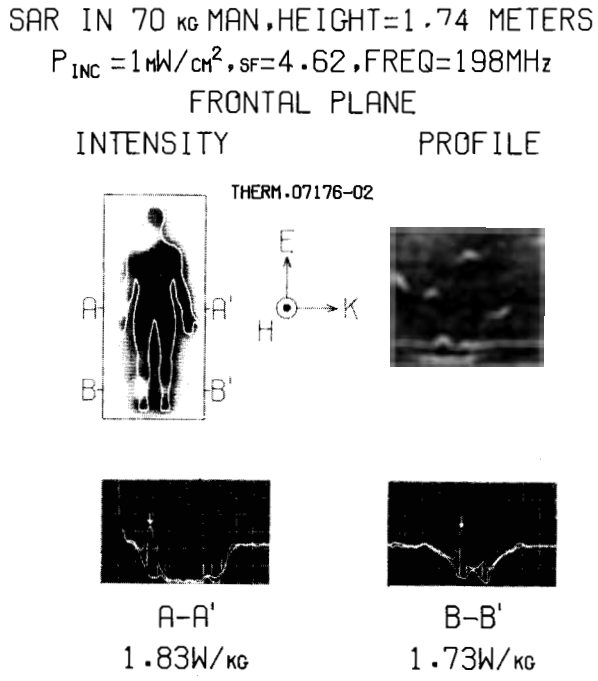


FIGURE 13 Peak SAR in scaled model man exposed to 198 MHz plane wave EKH polarization.

FIGURE 14 a

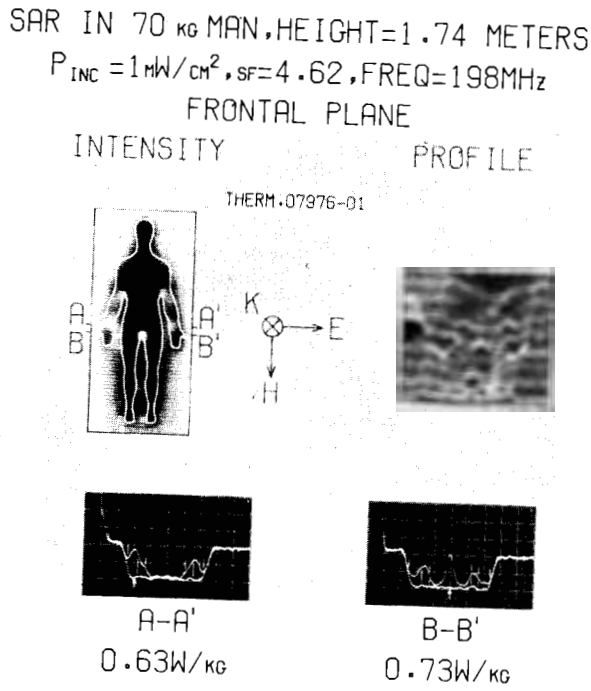


FIGURE 14 b

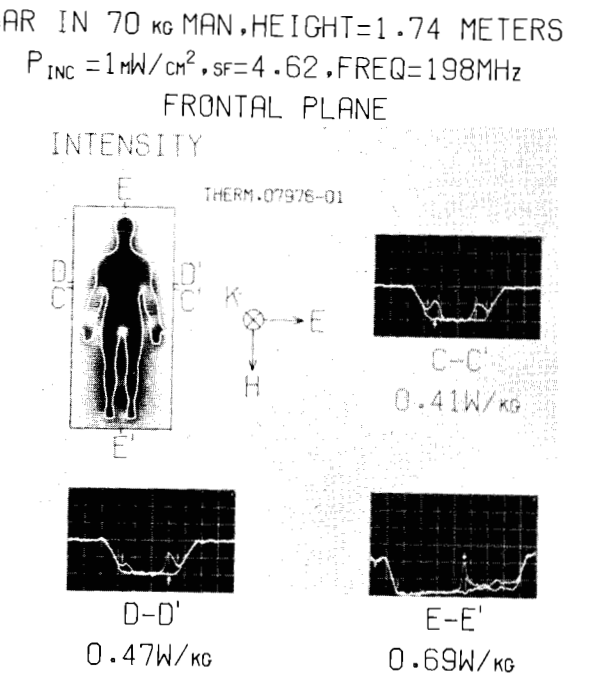


FIGURE 14 Peak SAR in scaled model man exposed to 198 MHz plane wave at HEK polarization.

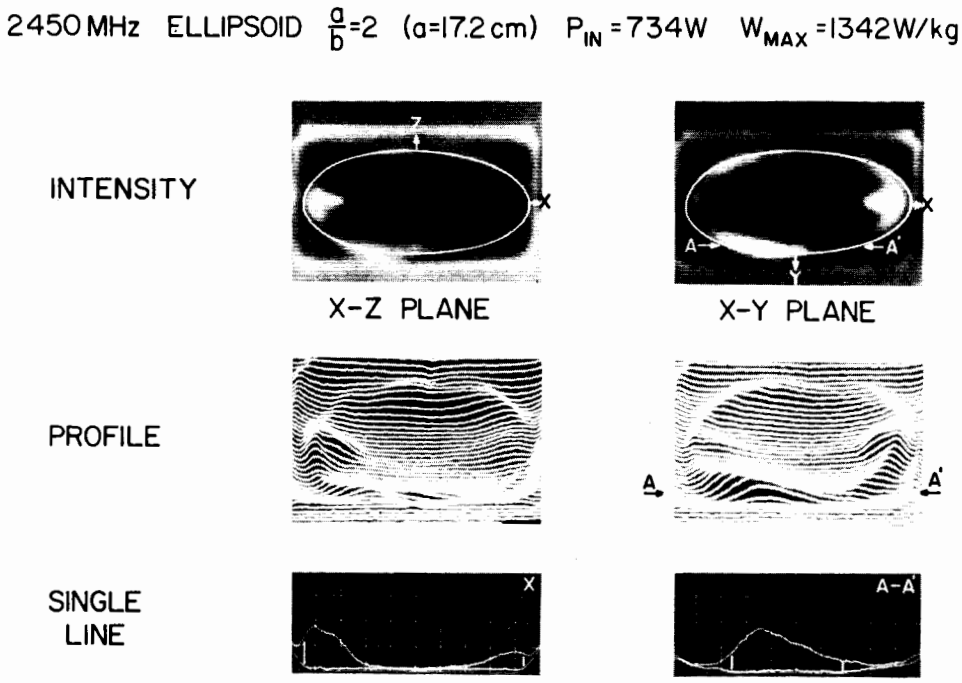


FIGURE 15a Thermograms illustrating SAR patterns for 17.2 cm 2:1 axial ratio ellipsoid with major axis along x axis exposed to 2450 MHz and 198 MHz microwave ovens (Scale: horizontal divergence = 2 cm, vertical divergence = 3.33° C).

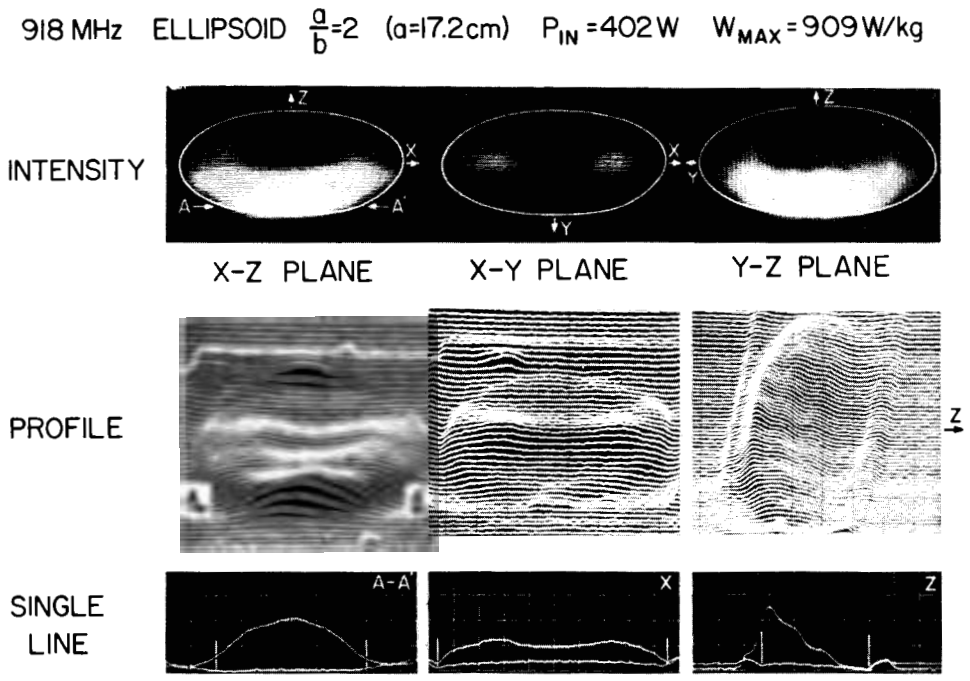


FIGURE 15b Thermograms illustrating SAR patterns for 17.2 cm 2:1 axial ratio ellipsoid with major axis along x axis exposed to 2450 MHz and 198 MHz microwave ovens (Scale: horizontal divergence = 2 cm, vertical divergence = 3.33°C).

previously were bisected along lines of symmetry with each half covered with a thin plastic film. Thus, the technique is only applicable to linearly polarized fields where the object can be oriented parallel to the field lines. For arbitrary-type polarization such as in cavities or in more general exposure conditions, a different technique has been developed. Instead of using a plastic sheet attached to each half of a model, a silk screen layer is stretched tightly over each half section. Animal tissue matter or modeling material will flow through the openings in the silk screen providing for good adhesion and electrical coupling between the two sections of the model. The models can easily be separated and rejoined repeatedly without loss of adhesion or electrical continuity.

The intact models were exposed to each oven for 5 - 60 sec. and thermograms of the plane of separation were taken before and after exposure in a manner similar to that described previously. Figure 15 illustrates the SAR patterns for the ellipsoids when exposed to 2450 and 918 MHz. The coordinate system was defined with the origin at the center of the exposed object such that the x axis was directed toward the front of the oven and the z axis in the vertical direction. Single scans were made over regions of maximum power absorption and along the major axis. The net power of the oven, p_{in}, and the maximum SAR, W_{max} as calculated from the thermograms are given in the figures. Since the object was rotated on the z axis on the standard platform in the 918 MHz oven, the patterns in the x-z and y-z planes are identical for that case. The data show a marked superiority of the 918 MHz oven in terms of power penetration and SAR uniformity in the larger objects.

Coupling of 918 MHz Microwave Oven Door Leakage to Human Subjects[42]

Full-sized human female and child phantom models with dielectric properties equivalent to muscle were exposed to 918 MHz near field leakage radiation from a microwave oven in order to obtain an approximate thermographic assessment of energy coupling between a leaky microwave oven and a human subject. With a leakage power density level of 5 mW/cm^2, as measured 5 cm from the door, approximate SAR as high as 2.28 W/kg in the nasal and 0.74 W/kg in the orbital regions of the child were measured when the head was 4.8 cm from

the oven door (Fig. 16). Significant values of SAR recorded at the neck are surprising since the region is so far from the oven leak and somewhat shielded by the chin and mouth. The same leakage level was found to produce approximate SAR values of 0.68 W/kg in the umbilical and 0.48 W/kg in the pubic regions of the female when the abdomen was 5 cm from the leaky microwave oven door (Fig. 17). The power distribution along the normal direction into the female model is similar in nature to that predicted for a plane slab of the same material.

Dosimetry Studies on a UHF Cavity

Guy and Korbel[43] have shown that when groups of animals are exposed to 500 MHz EM energy in cavities, it is extremely difficult to maintain a constant absorbed power relationship in each animal with respect to the power incident to the cavity. The results show variations as great as 1000 to 1 in SAR in the animal, depending on its position with the rest of the subjects or its position within the cavity. Contact with metallic walls or standard-type water dispensers can also produce serious problems (Fig. 18). Measurements with a standard power density meter sensitive only to electric fields cannot be used to predict the power absorption in a particular animal exposed in the cavity since absorption may also be highly dependent on the magnetic field strength which tends to be maximum in regions where the electric field strength is minimum (Fig. 19).

SAR Measurements in a Waveguide Chronic Exposure System

Guy and Chou[36] have developed a waveguide system for economically exposing a large population of rodents on a long term basis without disturbing their normal laboratory living patterns. The use of separate cells consisting of cylindrical waveguides excited with circularly polarized guided waves provides relatively constant and easily quantifiable coupling of the fields to each animal, regardless of their position, posture and moving patterns.

The averaged SAR can be measured by subtracting the reflected and transmitted power from the input power. Figure 20 illustrates the computer plot of the total absorbed power in a freely moving rat as a function of time

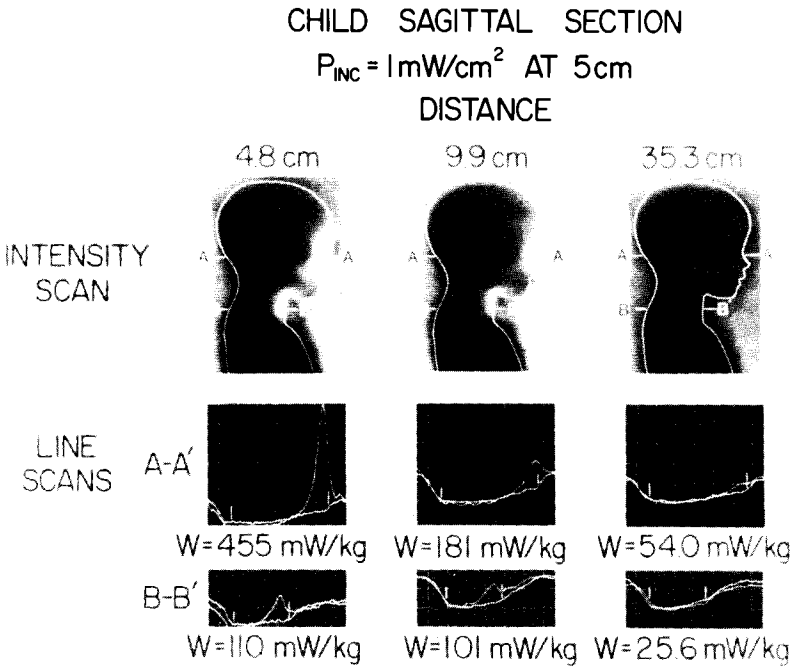


FIGURE 16 SAR pattern in phantom child model exposed to leaky 918 MHz microwave oven at the eye level.

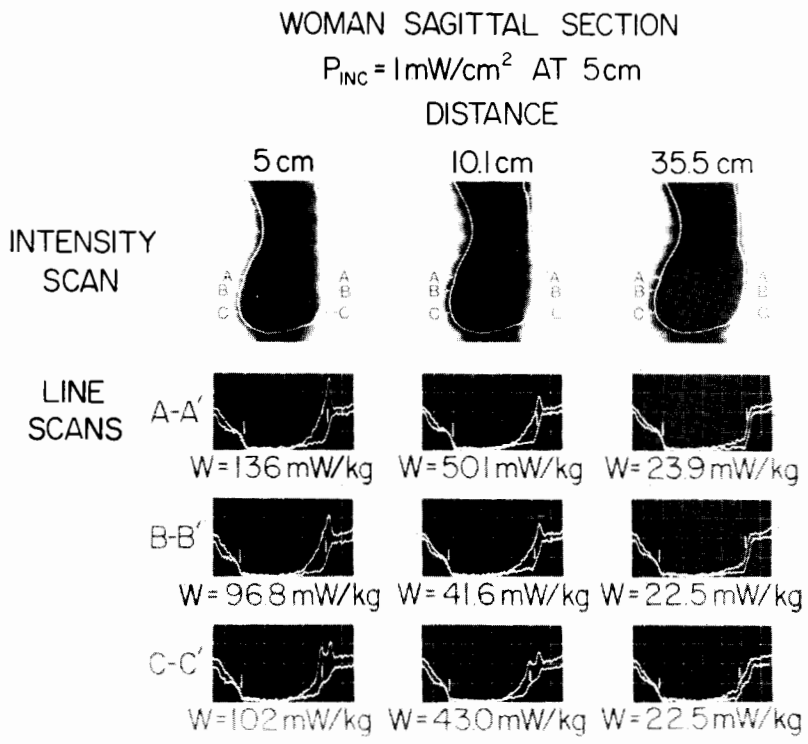


FIGURE 17 SAR pattern in phantom woman model exposed to leaky 918 MHz microwave oven at the pelvic region.

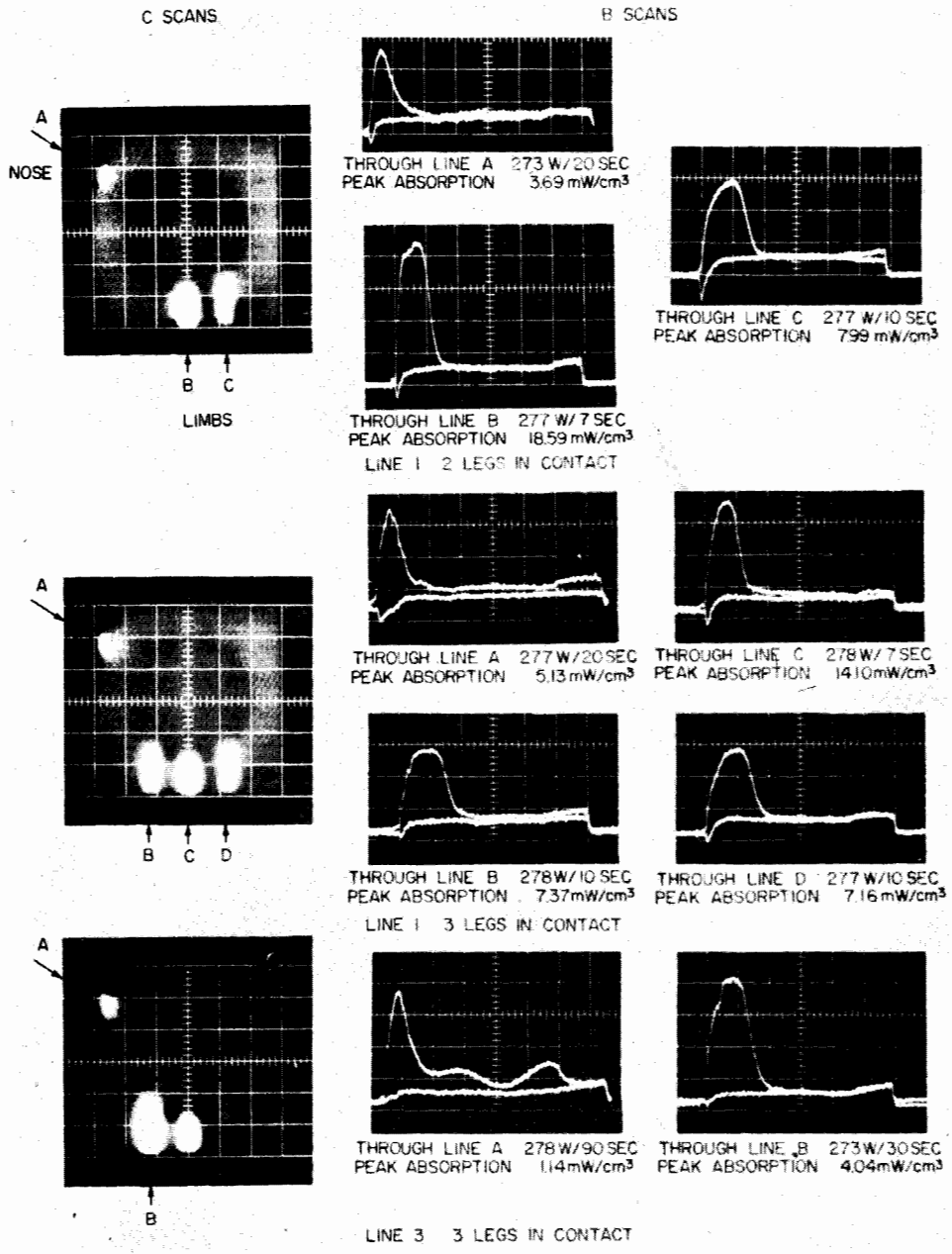

C SCANS
B SCANS
A
NOSE
B C
LIMBS
THROUGH LINE A 273 W/20 SEC
PEAK ABSORPTION 3.69 mW/cm3
THROUGH LINE C 277 W/10 SEC
PEAK ABSORPTION 799 mW/cm3
THROUGH LINE B 277 W/7 SEC
PEAK ABSORPTION 18.59 mW/cm3
LINE 1 2 LEGS IN CONTACT
A
B C D
THROUGH LINE A 277 W/20 SEC
PEAK ABSORPTION 5.13 mW/cm3
THROUGH LINE C 278 W/7 SEC
PEAK ABSORPTION 14.10 mW/cm3
THROUGH LINE B 278 W/10 SEC
PEAK ABSORPTION 7.37 mW/cm3
THROUGH LINE D 277 W/10 SEC
PEAK ABSORPTION 7.16 mW/cm3
LINE 1 3 LEGS IN CONTACT
A
B
THROUGH LINE A 278 W/90 SEC
PEAK ABSORPTION 1.14 mW/cm3
THROUGH LINE B 273 W/30 SEC
PEAK ABSORPTION 4.04 mW/cm3
LINE 3 3 LEGS IN CONTACT

FIGURE 18 SAR patterns in phantom rat exposed in cavity 60 cm from center of exposure chamber during drinking position with limbs in contact with metal screen. Intensive increase of SAR in legs is observed.

during its most active hours. The mean calculated absorption for the 16 hour period was 43% ± 7% standard deviation. SAR patterns in the rat when oriented in different positions in the waveguide are shown in Figure 21. Results show relatively constant power absorption for different orientation of rats in the waveguide.

The design of the water system was a major consideration in the development of this exposure system. When the nozzle of a standard waterbottle was in contact with an ellipsoid phantom, the peak absorption increased substantially at the point of contact (Fig. 22). A quarter-wavelength decoupling choke system consisting of double concentric metal sheath was placed around the water spout. Figure 23 illustrates that the double quarter-wave isolated system caused no detectable change in the SAR pattern when the ellipsoid was placed in contact with the water supply.

CONCLUSION

It has been shown that the power absorption in tissues exposed to microwave or RF radiation is determined by many factors. Meaningful research results can be obtained only through quantitative measurements of power absorption in tissues through proper microwave and RF dosimetric techniques.

ACKNOWLEDGEMENTS

This research was supported by the Bureau of Radiological Health, Food and Drug Administration Grant number R01 FD 00646, Air Force Grant number F 41609-76-C-0032, Rehabilitation Services Administration Grant number 16-P-56818 and a NIH Fellowship Grant number NIGMS-OADPA 1 F32GMCA 05681-01.

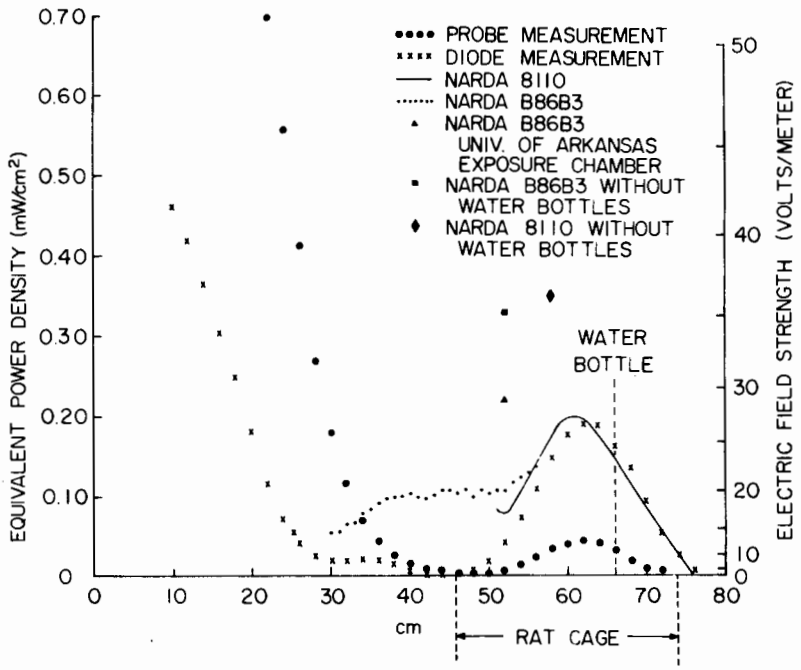


FIGURE 19 Electric field and "effective" power density along y axis in exposure chamber filled with 15 phantom rats (1 Watt input at resonant frequency of 500 MHz for degenerate TE_{501} and TE_{105} modes).

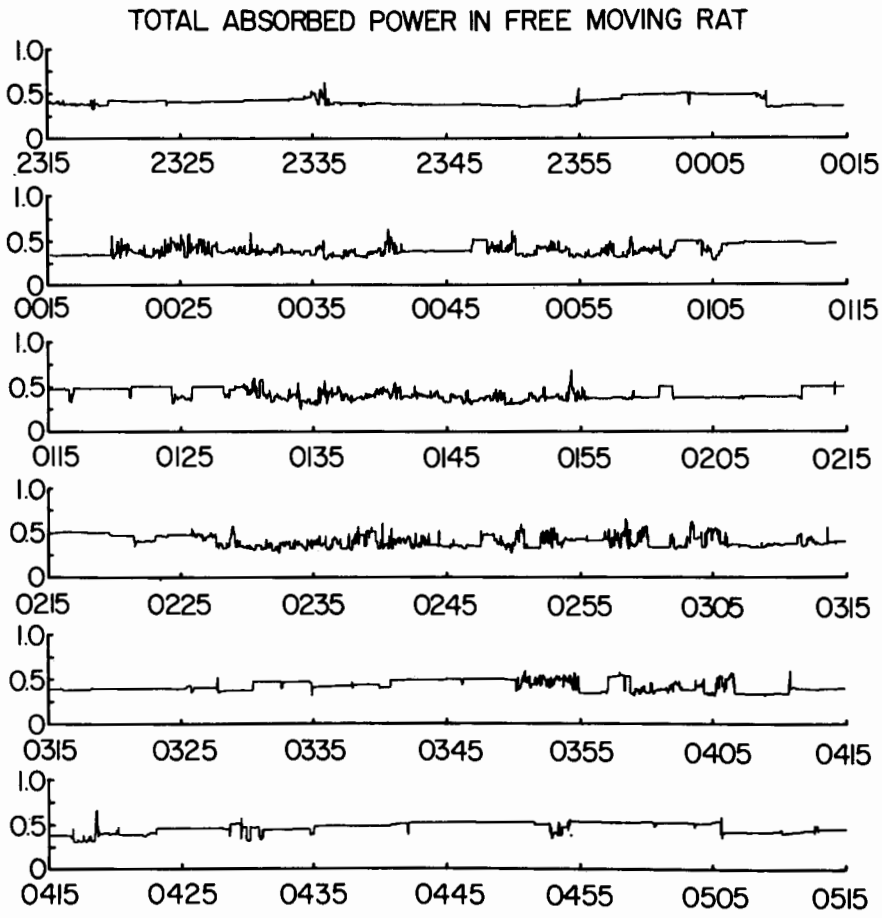


FIGURE 20 Total absorbed power in a freely moving rat (323 g) as a function of time in exposure chamber.

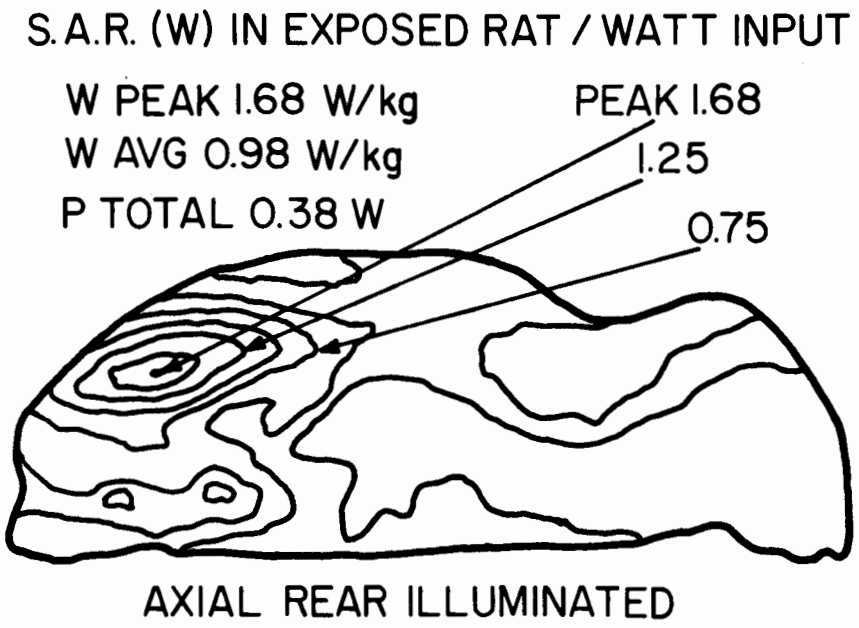


FIGURE 21 a

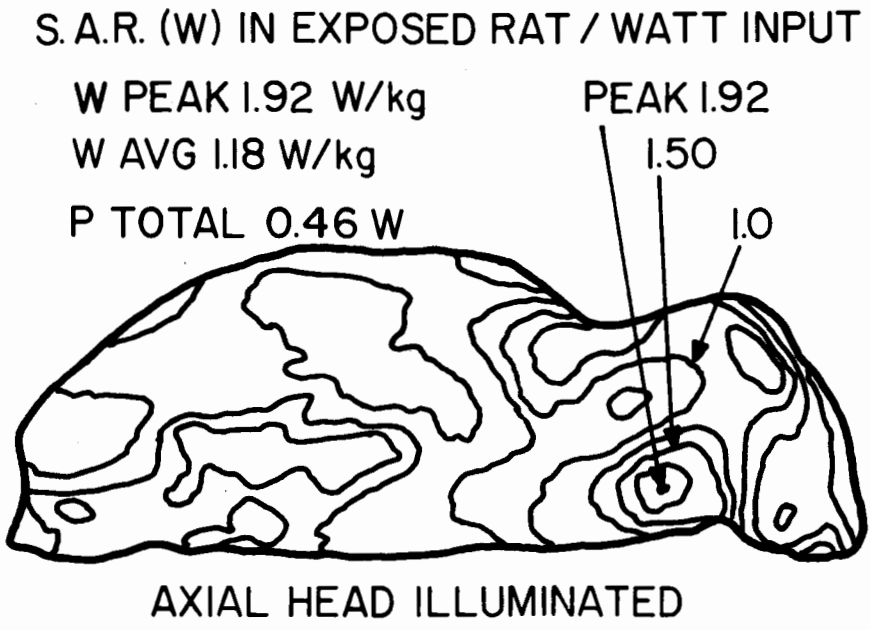


FIGURE 21 b

FIGURE 21 SAR patterns of sacrificed rat in exposure chamber at different exposure positions.

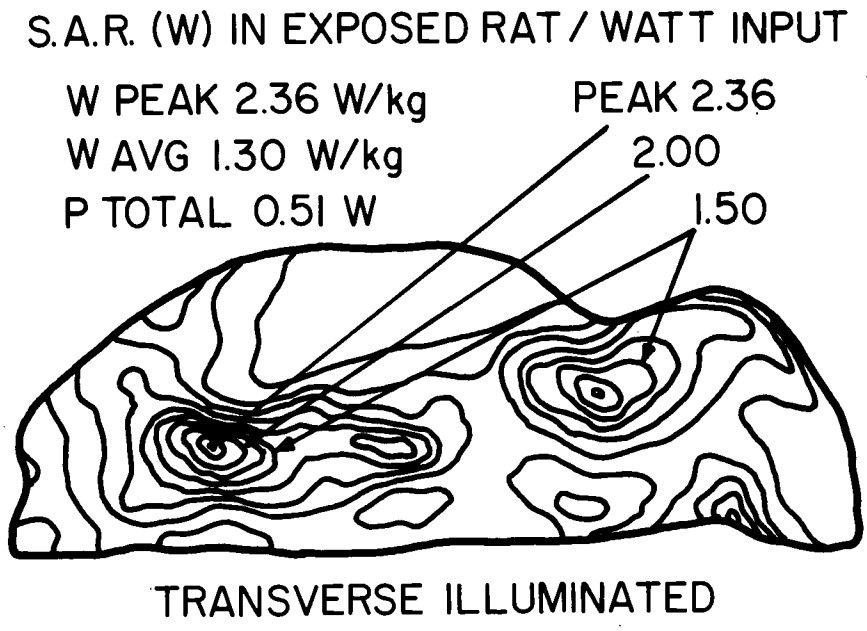


FIGURE 21 c SAR patterns of sacrificed rat in exposure chamber at different exposure positions.

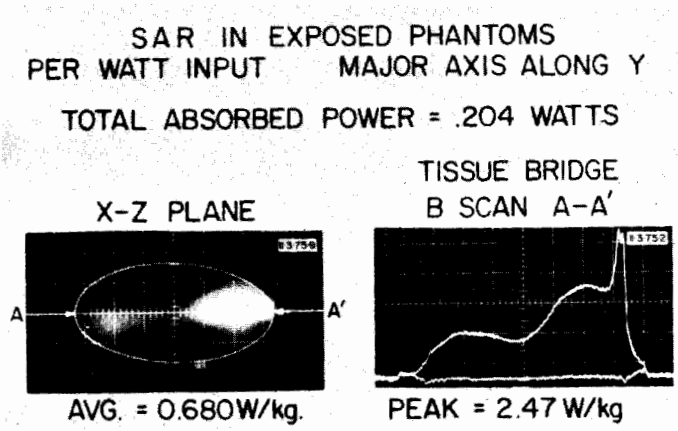


FIGURE 22 SAR patterns of a spheroid model simulating 300 g rat at drinking position from standard laboratory water bottle.

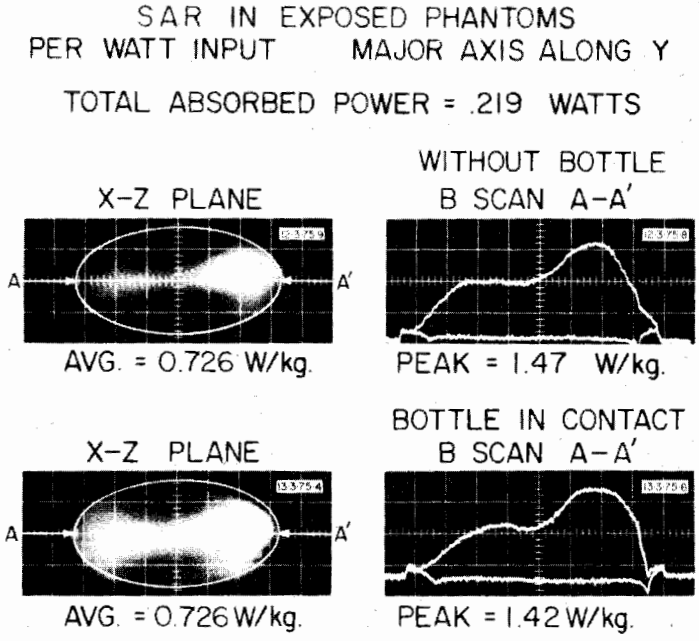


FIGURE 23 SAR patterns of a spheroid model simulating 300g rat at drinking position from the isolated choke water bottle.

REFERENCES

1. P. F. Wacker and R. R. Bowman, IEEE Trans. Microwave Theory Tech., MTT-19, 178 (1971).
2. H. P. Schwan, IEEE Trans. Microwave Theory Tech., MTT-19, 147 (1971).
3. C. C. Johnson and A. W. Guy, Proc. IEEE, 60, 692 (1972).
4. W. B. Coley, Amer. J. Med. Sci., 105, 487 (1893).
5. R. Cavaliere, *et al*, Cancer, 20, No. 9, p. 1351 (1967).
6. J. B. Block and C. G. Zubrod, Cancer Chemotherapy Reports, Part 1, 57, 373 (1973).
7. J. F. Lehmann, D. R. Silverman, B. A. Baum, N. L. Kirk and V. C. Johnston, Arch. Phys. Med. and Rehab., 47, 291 (1966).
8. J. F. Lehmann, C. G. Warren and S. Scham, Clin. Orth. and Related Res., 99, 207 (1974).
9. C. C. Johnson, C. H. Durney, P. W. Barber, H. Massoudi, S. J. Allen and J. C. Mitchell, *Radiofrequency Radiation Dosimetry Handbook*, USAF School of Aerospace Medicine, Brooks AFB, Tx., RPT. SAM-TR-76-35 (1976).
10. H. Massoudi, C. H. Durney and C. C. Johnson, IEEE Trans. MTT-25, 47 (1977).
11. O. P. Gandhi, IEEE Trans. BEM-22, 536 (1975).
12. O. P. Gandhi, E. L. Hunt and J. A. D'Andrea, Radio Science, Vol. 12 No. 6 (S), 39 (1977).
13. A. W. Guy, AGARD Lecture Series No. 78, *Radiation Hazards* (Non-Ionized Radiations - Biologic Effects and Safety Considerations) (1975).
14. E. E. Aslan, IEEE Trans. IM-19, 368 (1970).
15. E. E. Aslan, IEEE Trans. IM-21, 421 (1972).
16. R. R. Bowman, in *Biological Effects and Health Hazards of Microwave Radiation*, Polish Medical Publishers, Poland, p. 217 (1974).
17. K. Fletcher and D. Woods, *Non-ionizing Radiation*, p. 57 (1969).
18. H. Bassen, M. Swicord and J. Abita, N. Y. Acad. Sci., 247, 481 (1975).
19. G. K. Huddleston and D. I. McRee. N. Y. Acad. Sci., 247, 516 (1975).
20. T. M. Babij and H. Trzaska, URSI Meeting Abstract, p. 67 (1976).

21. G. Brengelmann and A. C. Brown, *Physiology and Biophysics*, 19th ed., T. C. Ruch and H. D. Patton, Eds., W. B. Saunders publisher, Philadelphia, p. 1050 (1965).

22. A. W. Guy, IEEE Trans. MTT-19, 205 (1971).

23. T. C. Rozzell, C. C. Johnson, C. H. Durney, J. L. Lords and R. G. Olsen, J. Microwave Power, 9.(3), 241 (1974).

24. C. C. Johnson, C. H. Durney, J. L. Lords, T. C. Rozzell and G. K. Livingston, Ann. N. Y. Acad. Sci., 247, 527 (1975).

25. R. R. Bowman, IEEE Trans. MTT-24, 43 (1976).

26. L. E. Larsen, R. A. Moore, and J. Acevedo, IEEE Trans. MTT-22, 438 (1974).

27. L. E. Larsen, R. A. Moore, J. H. Jacobi and F. Halgas, URSI Meeting Abstract, p. 68 (1976).

28. T. C. Cetas, D. Hefner, C. Snedaker and W. Swindell, URSI Meeting Abstract, p. 68 (1976).

29. D. A. Christensen, URSI Meeting Abstract, p. 276 (1975).

30. A. Deficis, *Fiberoptic Microprobe for Microwave Electromagnetic Field Measurements*, Proc. of Microwave Power Symposium, p. 162 (1975).

31. H. Bassen, P. Herchenroeder, A. Cheung and S. Nender, URSI Meeting Abstract, p. 67 (1976).

32. H. P. Schwan, Proc. 2nd Tri-Serv. Conf. on Biol. Effects of Microwave Energy, p. 127 (1958).

33. R. D. Phillips, E. L. Hunt and N. W. King, Ann. N. Y. Acad. Sci. 247, 499 (1975).

34. C. K. Chou, *The Effects of Electromagnetic Fields on the Nervous System*, Ph. D. Dissertation, University of Washington, Seattle (1975).

35. H. S. Ho, E. I. Ginns and C. L. Cristman, IEEE Trans. MTT-21, 837 (1973).

36. A. W. Guy and C. K. Chou, Proc. USNC/URSI Annual Meeting, Boulder, Col. 2, 389 (1975).

37. P. O. Kramar, A. F. Emery, A. W. Guy and J. C. Lin, Ann. N. Y. Acad. Sci., 247, 155 (1975).

38. A. W. Guy, in *Biologic Effects and Health Hazards of Microwave Radiation*, Polish Medical Publishers, Poland, p. 203 (1974).

39. A. W. Guy, M. D. Webb and C. C. Sorenson, IEEE Trans. BME-23, 361 (1976).

40. C. K. Chou and A. W. Guy, Symposium on Biological Effects and Measurements of RF/microwaves, Bureau of Radiological Health, 81 (1977).

41. A. W. Guy, M. D. Webb and J. A. McDougall, in Proc. Microwave Power Symposium, p. 36 (1975).

42. M. D. Webb, A. W. Guy and J. A. McDougall, J. Microwave Power, 11, 162 (1976).

43. A. W. Guy and S. F. Korbel, in Proc. IMPI Symposium, Ottawa, Canada, p. 180 (1972).

* *

DISCUSSION

Since your phantom model is smaller than the object, you scale the wavelength accordingly? [Illinger].

Chou: Yes. The conductivity is also scaled.

Your SAR concept is a very good one for determining the heating pattern, and the geometrical variations of some biological effects. I am particularly interested in thermal applications in which, generally, the time at some elevated temperature is quoted as the dose. Because of thermal dissipation, specific absorption and temperature elevation are not completely interchangeable. What is your view or experience as to which is the relevant dose? Will it be SAR that is more important, since thermal conduction allows you to spread out the energy of locally deposited power so that the temperature elevation is more uniform. Which will be more relevant in terms of treatment? The SAR is related to the energy absorption rate which can be integrated. That is different from the temperature produced. [Cetas].

Chou: The SAR measurement tells you where the energy is deposited in the exposed object. The final temperature in the object is modified by the blood flow and heat diffusion. For many biological effects, we do not know what the mechanisms are, whether they are due to heating or current induced in tissue, or what. However, one can calculate the field or current density from the measured SAR. Therefore, the SAR gives a common unit so that experiments using different animals can be compared and extrapolation to human is possible. In the biological effects research, the important concept is to have a quantifiable measurement not to measure the final temperature rise. For therapeutic heat treatment, of course, the final temperature pattern in the tissue is the most important parameter.

Since a metal probe would interfere with the heating, how did you measure the temperature? [Myers].

Chou: We used thermograms.

On the animal cut or on a model? [Myers].

Chou: We have used both phantom models and actual animals. When we use the actual animal, the animals were frozen in dry ice, cast in polyfoam blocks and bisected in halves.

This is a frozen animal then? [Myers].

Chou: The frozen bisected animal was returned to room temperature for thermographic measurement.

As I understand it, the animal was inside a high Q cavity. In other words, magnetic coupling was extremely strong. I wonder if you have comparable figures for semi-far field conditions at the same levels of incident radiation? Twelve years ago we completed a study for Walter Reed Hospital. They were interested in long spans, six to nine months, of daily radiation exposure to 10 milliwatts at S-band, using implanted electrodes. In this situation, the histology along the electrode tracks in the monkey brain showed absolutely no evidence of heating. For that reason I wonder how relevant a study of the type you have done may be to this field condition? [Adey].

Chou: The thermogram on cat head with a metal probe in the brain was taken in a near field situation. The animal's head was 8-cm away from the 915-MHz applicator, not in a high Q cavity. Theoretical calculations for far field radiation show field enhancement at the tip of metel electrodes can be in the order of 10^7. [Guy, A. W., AGARD Lecture No. 78, 1975]. For low level radiation, the field enhancement may not cause any observable heating damage. However, the micro-heating or micro-induced current can modify the electrophysiological activity of the neurons around the tip of the electrode. This field enhancement greatly affects the accuracy of dosimetry.

It really does not make much difference if we put an object such as a cat's head in the near field or the far field. The specific dosimetry is nearly the same. We know, according to the slides shown, you could at most increase by a factor of two in the near field. The question is what happens if you have a metal probe inserted into the brain tissue? I do not think that your statement that there is no difference between the near and the far field is correct. [Lin's comment to Adey].

In a cavity there are multi-lateral exposures, consequently can't the SAR be many times larger than for plane wave exposure? [Gandhi].

Chou: Yes, in a cavity the energy coupling is more complicated than in free field.

In the waveguide experiment you measure the input and output power. Doesn't the presence of the animal in the waveguide induce higher order modes? Does you experiment accurately measure the power in all modes? [Taylor].

Chou: There is only single mode propagation in the empty guide, when an animal is in there some higher modes may be induced but we can take this into account since we can measure the power absorbed by the animal by substrating the reflected power and the transmitted power from the input power.

ELECTRIC FIELD MEASUREMENTS WITHIN BIOLOGICAL MEDIA

A. Y. Cheung

Institute for Physical Science and Technology
University of Maryland, College Park, Maryland 20742

ABSTRACT

Theoretical and experimental analysis of the use of a miniature isotropic electric field probe developed by BRH for implantation electric field measurements within biological tissues is discussed. An analysis employing a transmission line model of a buried antenna as well as insulated dipoles was performed over the 0.9 to 10 GHz range. The antenna impedance modification due to interaction with the surrounging media was computed for a wide range of dielectric parameters typical of various biological materials, over a range of ambient temperatures. It was demonstrated analytically and experimentally that for deep implantation in muscle, very little change (± 10%) in probe response occurs with respect to the free space response of the probe over the frequency range of 0.915 GHz to 2.45 GHz. In addition, in very close proximity to the muscle-fat or even the muscle-air boundary, no observable change occurs in probe response due to dipole impedance variations. Calibration for electric field detection within muscular tissues has also been performed.

INTRODUCTION

Electrical field probes for the measurement of fields within biological media have been proposed and discussed[1-3]. No practical probe is available. For a probe to be suitable for implantation measurement, it has to satisfy the following requirements:

(1) The probe must be physically small and biologically compatible.
(2) The probe must not perturb the electromagnetic field significantly.
(3) The response of the probe should be independent of its surrounding medium.
(4) The probe should have isotropic detection characteristics.
(5) The probe should be insensitive to temperature variation over a wide range ($20\ C<T<50^{\circ}C$).
(6) The presence of junction and boundaries should create minimal perturbation to the probe response.

Bassen and co-workers at the U. S. Bureau of Radiological Health (BRH) have developed a miniature three dimensional electric field probe which has been demonstrated to have characteristics which satisfy some but not all of the above requirements[4]. The purpose of this paper is to describe the theoretical and experimental development leading to successful modification and calibration of the BRH probe for implantation electric field measurement.

The probe consists of an array of three orthogonal, electrically short dipoles (2.5 mm in length) each coated with a thin layer of epoxy shown in Fig. 1. Each dipole contains a microminiature beam lead diode detector chip placed directly across the center gap of the antenna. High resistance, thin film leads allow the detected voltage to be monitored by a high impedance DC amplifier, without the perturbation of the field under study due to microwave current flow on these leads Fig. 2. The detector is unique in several respects. Being a beam lead chip, it requires no inductive bonding wires for connection to the dipole antenna. This becomes very important at high frequencies, where a resonance of the diode and dipole reactances would seriously degrade the performance of the implanted probe. Secondly, this device utilizes a zero-bias Schottky diode, providing very high sensitivity while

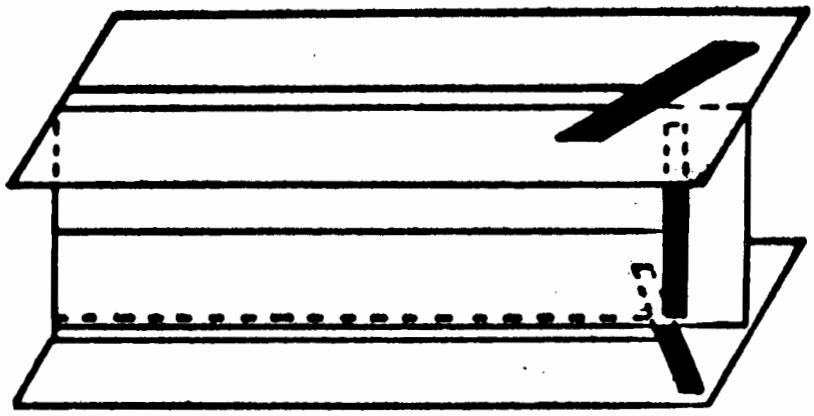


Figure 1. Array of Orthogonal dipole with colinear center.

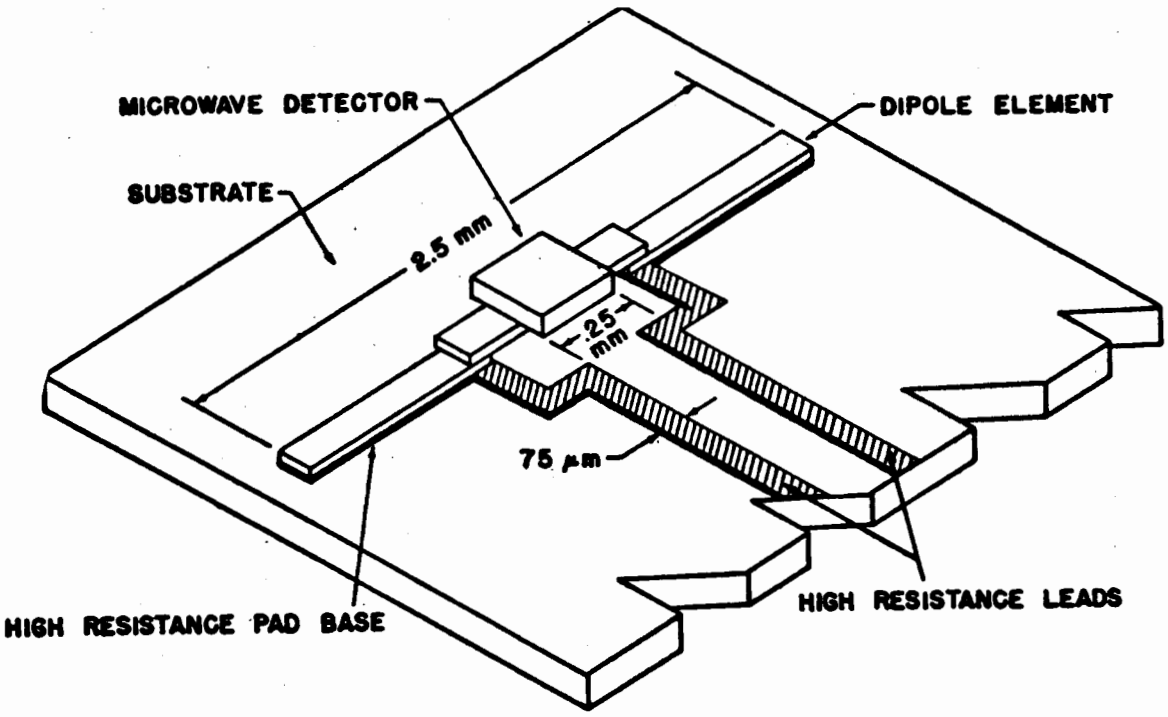


Figure 2. Miniature dipole-diode detector system.

eliminating the need for either DC biasing of the diode or the use of very high impedance (>100 MΩ) readout amplifier. The detector diode impedance at microwave frequencies is, however, very high with respect to the antenna impedance. The spatial resolution of this electrically small probe is also quite adequate even when measuring complex fields with steep gradients and short wavelengths within biological materials.

There are several important factors one must consider before attempting to calibrate this type of probe for electric field measurement within biological tissues. Upon implantation, the dipole antenna element is submerged in a medium with electromagnetic properties significantly different from those of free space. This may result in a modification of the dipole/diode detection characteristics. Second, local inhomogeneities within a single type of biological material as well as variations in the dielectric properties of a multilayered biological body may introduce severe limitations in a systematic calibration. Third, a change in the biological material's temperature can alter the dielectric properties of the media surrounding the antennas, resulting in a continuously changing electromagnetic environment. Finally, the problem of the mutual interaction between the antenna and boundaries of discontinuities formed by the interfaces between various layers of biological materials as well as the surrounding air (such as the muscle/fat/air or muscle/bone interface) must also be analyzed. Mutual interaction between each dipole element is eliminated by the orthogonal colinear array arrangement. It is important to establish the validity of electric field measurements performed close to boundaries. Boundary interaction problems also arise when external fields are measured in the close proximity of biological specimens. Ideally, a probe for implanted measurements should have a response to the local electric field (or square of the field) so that its detected terminal voltage V_D, as measured across the high resistance detection leads is as follows:

$$V_D = C|\vec{E}|^2 \tag{1}$$

where V_D = the square-law detected output voltage from the probe, $\vec{E}$ = local electric field, and C is a constant which should ideally be independent

of the constituent electromagnetic parameters of the surrounding medium. A probe with this kind of response not only will eliminate the need for a special calibration of the probe for use in a specific media, but also eliminates problems due to temperature variations and tissue inhomogeneity within the particular media, once it is calibrated in free space.

THEORETICAL ANALYSIS

Dipole Implanted within Biological Medium

A theorem in antenna modeling[5] states that the impedance of a short open antenna normalized to that of its surrounding medium takes on the same value at frequency ω in a medium of index n as it does at a frequency $n\omega$ in a medium of unity index. This theorem can be expressed mathematically as:

$$\frac{z(\omega,\varepsilon^*,\mu)}{\eta} = \frac{z(n\omega,\varepsilon_o,\mu_o)}{\eta_o} \tag{2}$$

where

ε^* = medium complex permittivity

μ = medium permeability

$\eta = \sqrt{\frac{\mu}{\varepsilon^*}}$ = medium intrinsic impedance

ε_o = free space permittivity

μ_o = free space permeability

$\eta_o = \sqrt{\frac{\mu_o}{\varepsilon_o}}$ = free space intrinsic impedances

$n = \sqrt{\frac{\mu\varepsilon}{\mu_o\varepsilon_o}}$ = relative refractive index

It is known that the impedance of a short, open antenna can be expressed as:

$$z = A\omega^2 + \frac{1}{j\omega c} \tag{3}$$

where A and C are constants determined by the antenna geometry. If the antenna is much shorter than the wavelength, the constant A can be neglected and the impedance of a short dipole is capacitive and given by:

$$z_d = \frac{1}{j\omega C_d} \tag{4}$$

where C_d = dipole capacitance. However, upon implantation in a biological medium, a short dipole is no longer capacitive as indicated by applying Eq. (2) to Eq. (4) to give

$$z_{d_m} = \frac{1}{j\omega C\varepsilon^*} = \frac{1}{C_d(\sigma+j\omega\varepsilon')} = R_m + \frac{1}{j\omega C_m} \tag{5}$$

where $\varepsilon = \varepsilon'(1 - \sigma/j\omega\varepsilon')$ is the complex permittivity.

Note that not only is the dipole no longer capacitive, but the impedance is also a function of the electrical properties of the medium (σ,ε'). However, by insulating the bare probe with a lossless dielectric, we can reduce the dependency of the antenna impedance on the medium.

Insulated Short Dipole in Biological Medium

For convenience, the dipole admittance parameter is used instead of the impedance parameter. Consider that an insulated cylindrical probe is formed by adding a concentric dielectric sheath of radius b and length h' over a wire of length h' and radius a, and the sheath is assumed to be lossless so that its electrical constitutive parameters are given by $\varepsilon_1, \sigma = 0$ and μ_0. This analysis is parallel to that of Smith and King[6]. The admittance for the bare probe in the medium and the capacitance of the insulating sheath are given by

$$Y_m = C_d(\sigma+j\omega\varepsilon') = G_m + j\omega C_m$$

$$Y_s = j\omega C_s \tag{6}$$

where C_d and C_s are capacitance of the bare probe in free space and of the insulation sheath given by Smith[7].

Figure 3 shows the circuit representation for the input admittance of the bare and insulated electric field probes. The admittance of the insulation capacitance in series with the bare probe yields an expression for the input admittance of an insulated probe in the medium to be

$$Y_i = C_d \left\{ \sigma \left[\frac{\gamma^2}{p^2+(1+\gamma^2)} \right] + j\omega\varepsilon_i' \left[\frac{p^2+(1+\gamma)}{p^2+(1+\gamma)^2} \right] \right\}$$

$$\gamma = \frac{\varepsilon_i'}{\varepsilon'} \frac{\log(h/a) - 1}{\log(b/a)}, \quad p = \tan\delta \tag{7}$$

and a and b are the radius of the antenna and insulation respectively. The design objective is to formulate a combination of antenna geometry such that Y_i is dominantly capacitive and independent of the biological medium.

First consider the case of the BRH probe. ($a = .01$ cm, $b \geq 2a$, $h = .25$ cm). For the range of $0 < \tan\delta < .5$ and $5 \leq \varepsilon' \leq 50$, the ratio of G_i and ωC_i is given by:

$$\frac{G_i}{\omega C_i} = \frac{P\gamma}{P^2+(1+\gamma)} \tag{8}$$

It can be shown that for the BRH probe operating at 1 - 10 GHz in materials with the above range of electrical parameters, G_i can be neglected so that Y_i is predominantly capacitive and is given by

$$Y_i = j\, C_d \varepsilon_i\, G(P,\gamma) \tag{9}$$

where $G(P,\gamma) = [P^2+(1+\gamma)]/[P^2+(1+\gamma)^2]$ is dependent on probe geometry, insulation geometry and electrical properties of the surrounding medium.

One primary requirement for a probe to be suitable for implantation measurement is that G varies insignificantly with changes from material to material. By proper antenna design this criterion can be met. Figure 4 shows the variation G as a function of the ratio of $\varepsilon_i/\varepsilon'$ for various insulation thickness ($b = 2a$, $3a$ and $4a$) for the BRH probe in a material with $\tan\delta = .2$. For $\varepsilon_i = 2$, the graph covers ε' from 5 - 50 which is typical of biological tissues. Figure 4 shows that for this particular case,

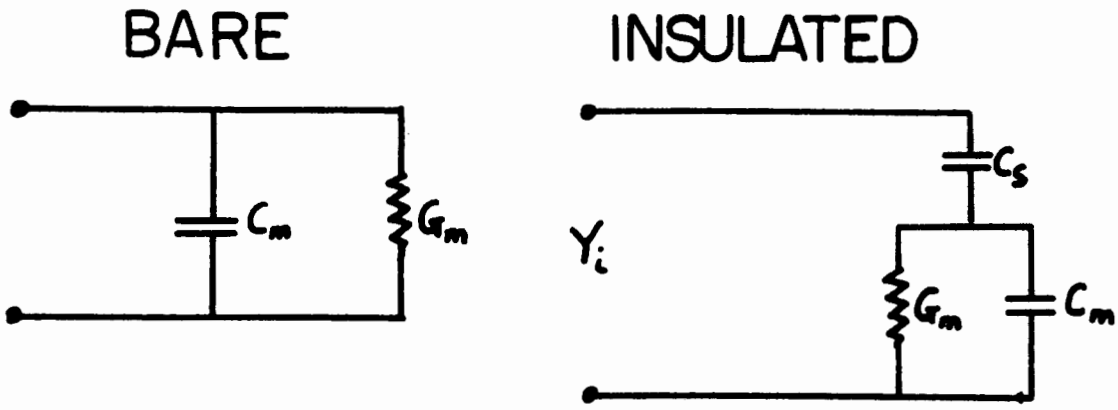


Figure 3. Input admittance circuit representation of bare dipole and insulated dipole in material media

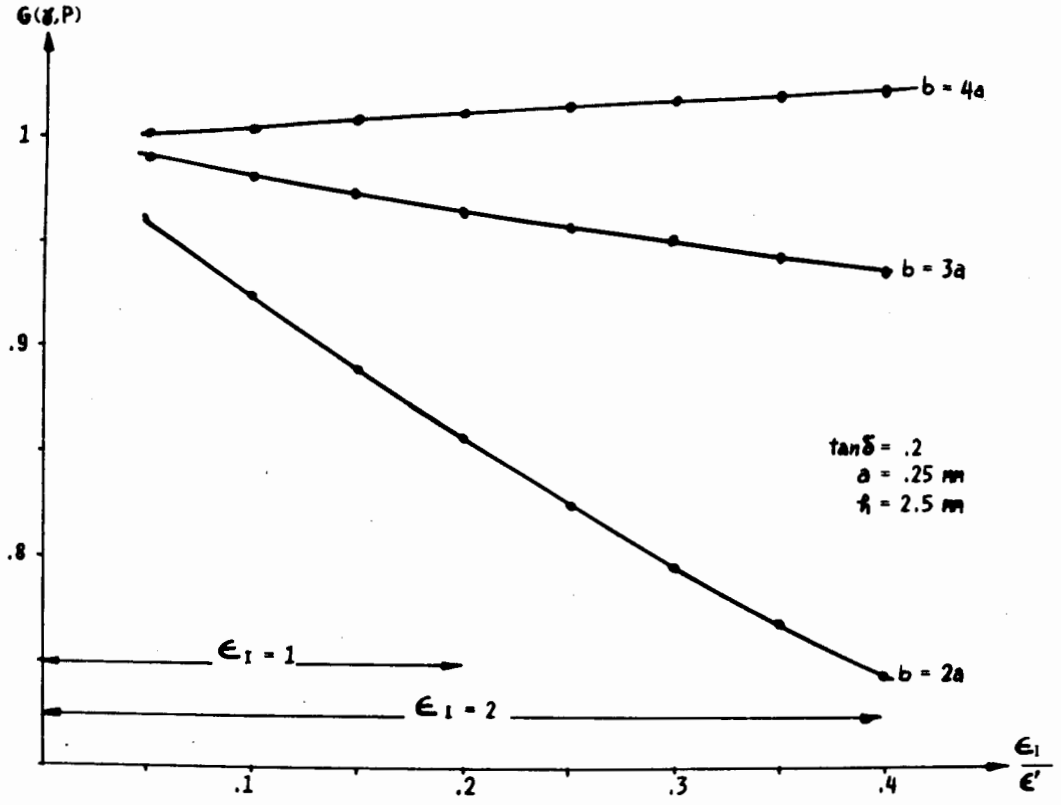


Figure 4. The variation of $G(\gamma,P)$ as a function of ϵ_I/ϵ' for various insulation thickness. Note that the full range of ϵ_I/ϵ' needed to cover the values of $5 < \epsilon' \quad 50$ depends on the value of ϵ_I used. In this case the falues of tan δ, a and h' are .2, .25 mm and 2.5 mm respectively.

an insulation thickness of $b \simeq 3.5a$ is the optimum design for a material independent probe. Figure 5 shows the variation of G as a function of $\varepsilon_i/\varepsilon'$ for $\tan\delta = .1, .3,$ and $.5$ for the BRH probe when $b = 2a$. If we limit our range to $15 < \varepsilon' < 50$ (typical of muscular tissues), then the error introduced due to changes in ε' will always be less than 10%. Note that if the insulation thickness is increased, our detection range capability for different ε' will be expanded as evidenced from the previous figure. Figure 6 shows a plot of variations in G as a function of ε' and ε_i for $\tan\delta = .2$, $a = .25$ mm, $b = .5$ mm and $h' = 2.5$ mm (which is the initial design of the BRH probe). The plateau-like dependence of G for $\varepsilon' > 20$ suggests that for implantation measurements in muscular tissues ($\varepsilon > 20$), the BRH probe is material independent.

Note that the above insulated dipole analysis is valid only for frequency ranges over which the dipole is short compared to the wavelength. In biological tissues, the wavelength is significantly shortened by a factor direc directly proportional to the square root of the dielectric constant which suggests, at a first glance, that 9 GHz ($\lambda_d \simeq .5$ cm) is the upper limit of the frequency capability of the BRH probe. Yet, the presence of insulation can reduce the wavelength shortening. Thus, in order to analyze the BRH probe response over a wider frequency range ($.5 \text{ GHz} \leq f \leq 10 \text{ GHz}$), the theory of buried transmission lines is used[8].

Theory of Buried Transmission Lines

For insulated antennas buried in a conducting medium, the buried transmission line theory can be used to obtain estimates of current distribution in the antenna and of the antenna impedance. The case we consider is an insulated dipole buried at a depth h inside an infinite planar slab of muscular tissue bounded on the outside by a fat layer as shown in Fig. 7. The insulated dipole can be modeled as an open-ended single wire transmission line of radius "a" coated with epoxy insulation of thickness (b-a). The wire is immersed in a lossy dielectric with dielectric constant $\varepsilon^* = \varepsilon' - j\varepsilon''$, $I = I_o \exp[-\Gamma z]$ along its axis and the resultant field is a superposition

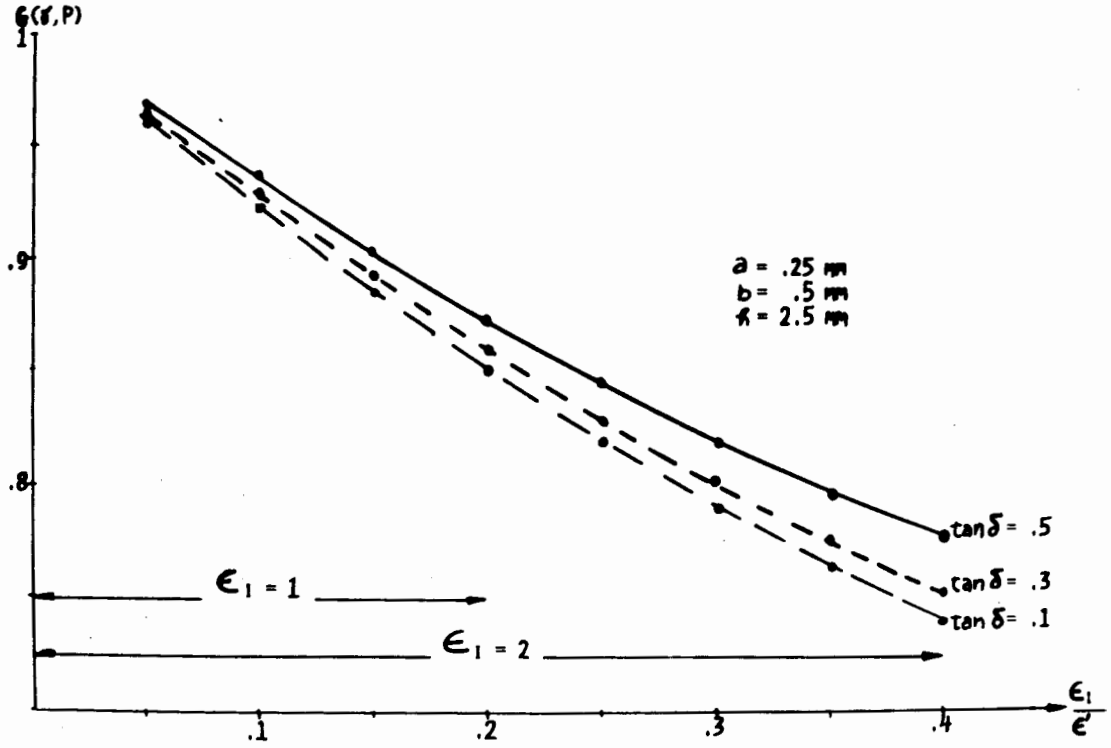


Figure 5. Variations of $G(\gamma,P)$ as a function of $\varepsilon_I/\varepsilon'$ for various values of loss tangent for a = .25 mm, b = .5 mm, and h' = 2.5 mm.

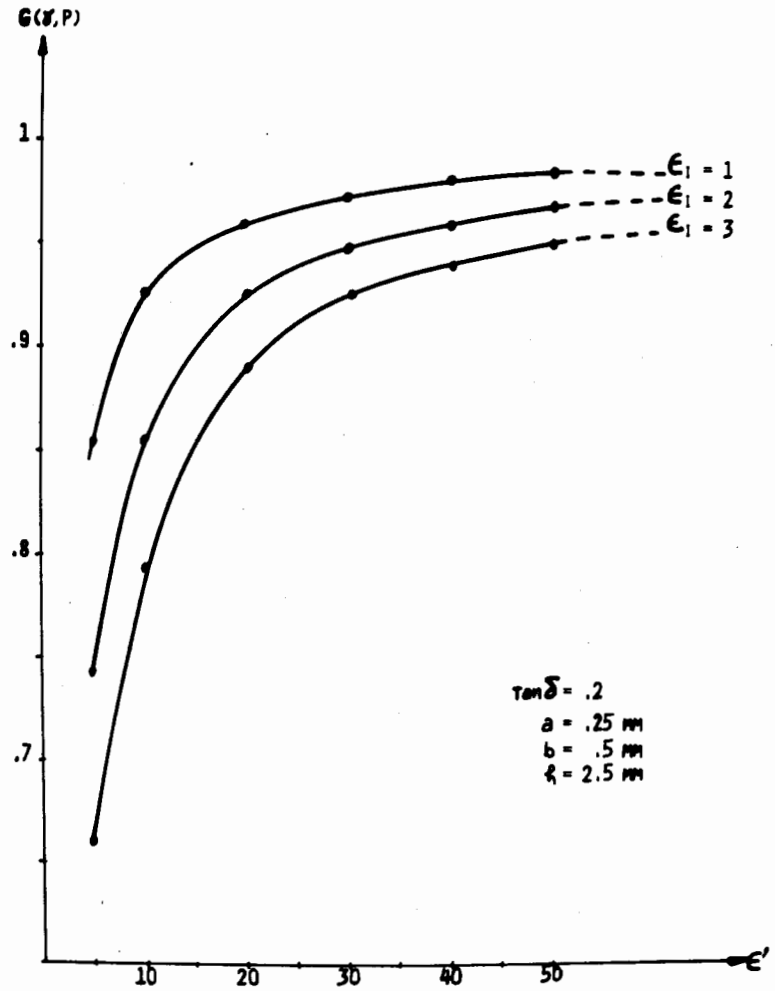


Figure 6. Variation of $G(\gamma,P)$ as a function of ε' for various insulation dielectric properties. Note that as ε_I increases, its shielding effectiveness decreases.

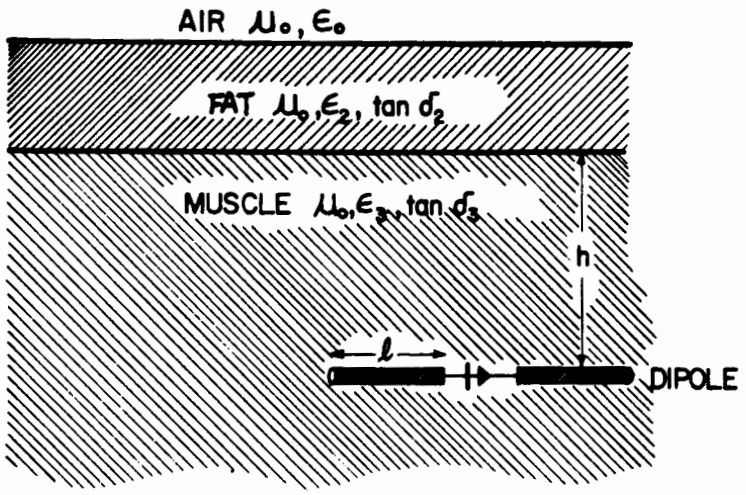


Figure 7. Diagramatic representation of dipole buried in a multi-layered infinite medium.

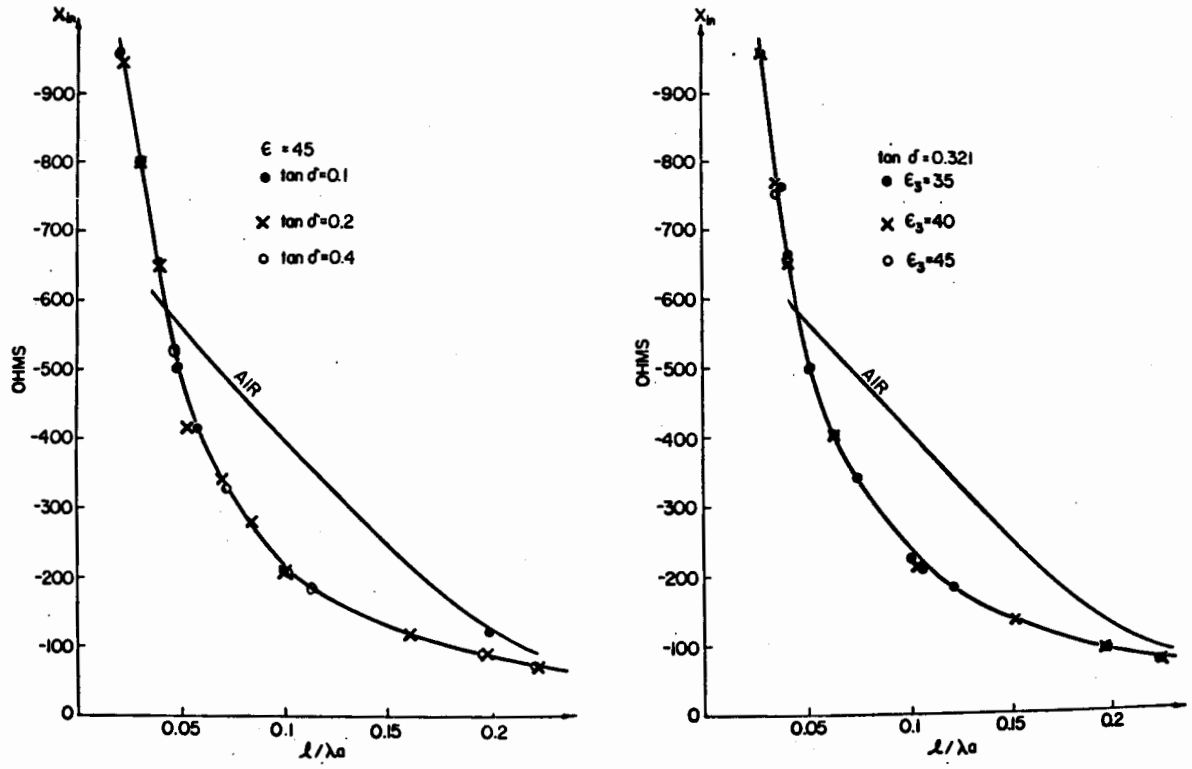


Figure 8. Antenna reactance for BRH dipole in various media (.1 < tan δ < .4; 35 < ϵ' < 45) as a function of electrical length. The range of .05 < $\ell/\lambda a$ < .2 covers .9 to 10 GHz.

of a primary field and a secondary reflection due to the boundary discontinuities between muscle and fat. This field is calculated with respect to matched boundary conditions so that a dispersion relation results. From the dispersion relation, one obtains Γ, which is the propagation constant along the wire. This constant is calculated[9] as:

$$\Gamma = i\, k_o \sqrt{\tilde{\varepsilon}_i'} \left[1 - \frac{1}{\log(b/a)} \left(\frac{-H_o^{(1)}(k_o\sqrt{\tilde{\varepsilon}^*}b)\ f(b,o,h)}{k_o\sqrt{\tilde{\varepsilon}^*}bH_1^{(1)}(k_o\sqrt{\tilde{\varepsilon}^*}b)} \right) \right]^{1/2} \qquad (10)$$

where

ε_r = relative dielectric constant of the muscle

k_o = free space wave number

$H_o^{(1)}$ and $H_1^{(1)}$ are Hankel Functions

and f(b,o,h) is a multiplying factor dependent on the properties of the boundary discontinuity and the burial depth "h".

Equation (10) was derived by assuming that the conductivity of the wire is infinite. Guy[9] has derived an expression for antenna resistance, R_A and reactance, X_A, using the relationship $\Gamma = \alpha - j\beta$ as follows:

$$R_A = \frac{120}{k_o\varepsilon_i'} \log\left(\frac{b}{a}\right) \left(\frac{-\beta\sinh\alpha\ell - \alpha\sin\beta\ell}{\cosh\alpha\ell - \cos\beta\ell}\right)$$

$$X_A = \frac{120}{k_o\varepsilon_i'} \log\left(\frac{b}{a}\right) \left(\frac{\beta\sin\beta\ell - \alpha\sinh\alpha\ell}{\cosh\alpha\ell - \cos\beta\ell}\right) . \qquad (11)$$

For the initial calculation, the burial depth is assumed to be infinite, so that $f(b,o,h) \to 1$. We generate values of R_A and X_A, at frequencies ranging from 1 - 10 GHz, with the BRH dipole geometry for values of ε' ranging from 35 - 45 and tan δ from 0.1 - 0.4 is shown in Figs. 8 and 9. During irradiation, temperature elevations may occur under high exposure situations. The change in the dielectric properties of simulated muscle has been experimentally measured at frequencies in the vicinity of 8.5 GHz over a range of 20°C to 50°C (Fig. 10). Very similar variations occur in the

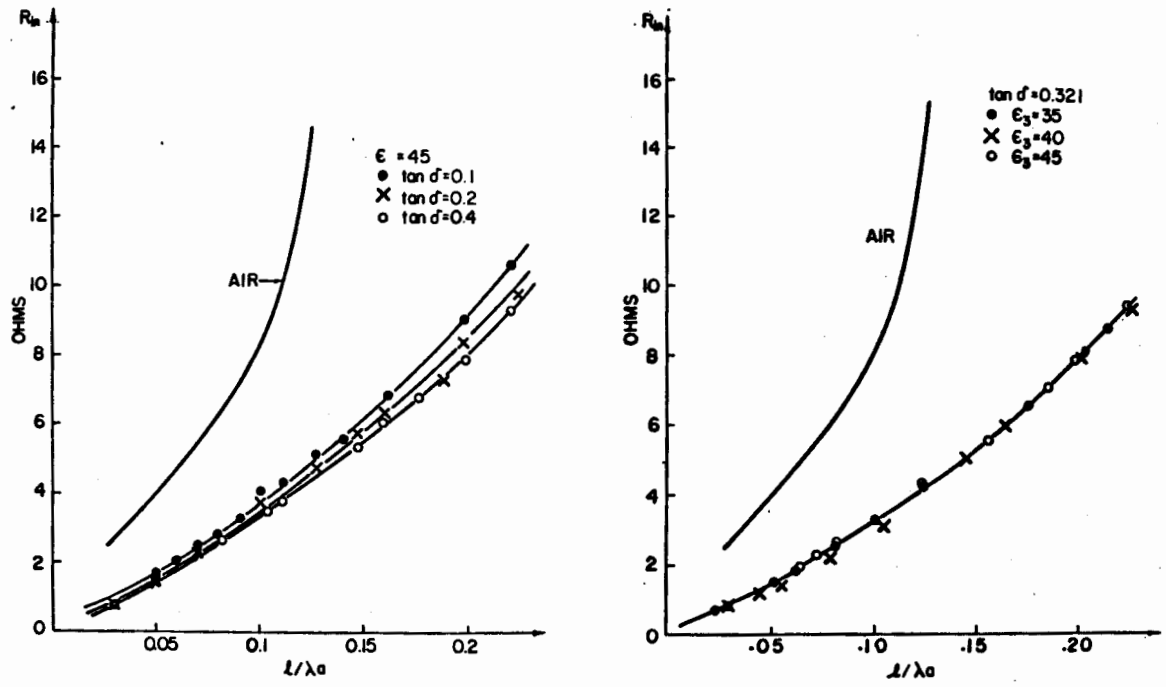


Figure 10. Temperature dependence of ε' and tan δ between the 20°C to 45°C range.

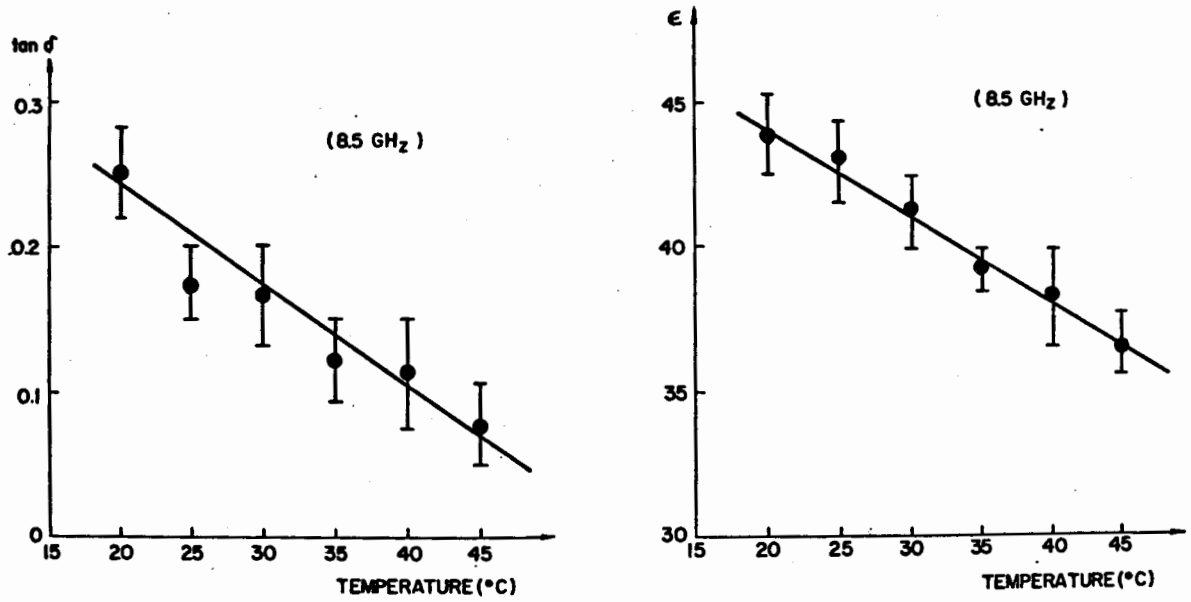


Figure 9. Antenna resistance of BRH dipole in various media (.1 < tan δ < .4; 35 < ε' < 45) as a function of electrical length.

1-3 GHz range. The findings suggest that these changes in the dielectric properties of biological materials must be considered when the impedance of an implanted antenna is computed. However, note that the range of ε' and $\tan\sigma$ considered in Fig. 8 overlaps with that due to temperature variation from $20^{\circ}C$ - $50^{\circ}C$. Thus, the response of the antenna can also be considered to be temperature independent for $35 < \varepsilon' < 45$, $0.1 < \tan\delta < .4$ and $20^{\circ}C < 50^{\circ}C$, as evidenced by Figs. 8 and 9.

BRH Probe Response

Now consider the practical detection characteristics of the BRH probe. Figure 11 shows the equivalent circuit representation of the antenna-diode detection junction. The following equations govern the detection characteristics of the BRH probe:

$$
\begin{aligned}
V_D &= -2h\,|\vec{E}|\,(Y_i/Y_i+Y_\ell) = K\,|\vec{E}| \\
V_{D_x} &= K_x \sin\theta\cos\phi\,|\vec{E}| \\
V_{D_y} &= K_y \sin\theta\sin\phi\,|\vec{E}| \\
V_{D_z} &= K_z \cos\theta\,|\vec{E}| \\
V_D^2 &= V_{D_x}^2 + V_{D_y}^2 + V_{D_z}^2
\end{aligned}
\tag{12}
$$

where

V_D = voltage across diode on each antenna

$|\vec{E}|$ = electric field strength along the antenna

V_D^2 = square of the sum of the detected voltage

and K_x,K_y and K_z are detection constant of the individual orthogonal antenna element.

In practice, K_x,K_y and K_z can be slightly different. However, the amplified detected voltage can be compensated by adjusting the gain of the external amplifier so that the effective gain of each channel is identical.

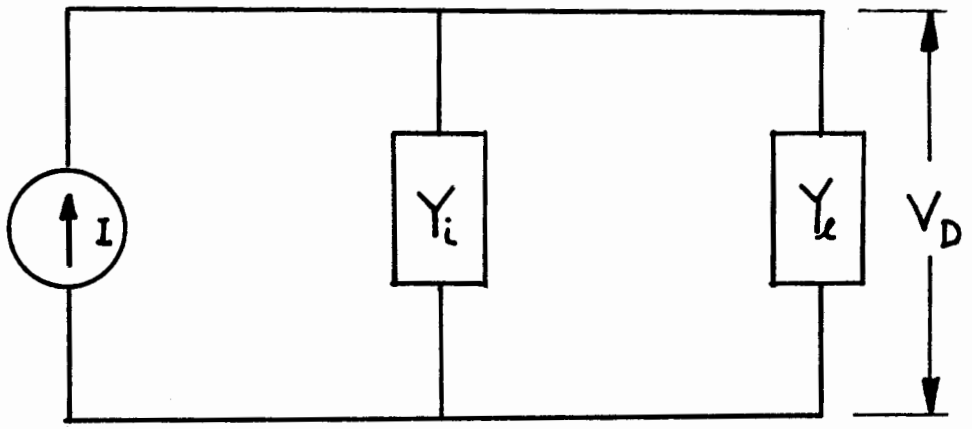


Figure 11. Equivalent circuit representation of the antenna diode-dipole detection junction.

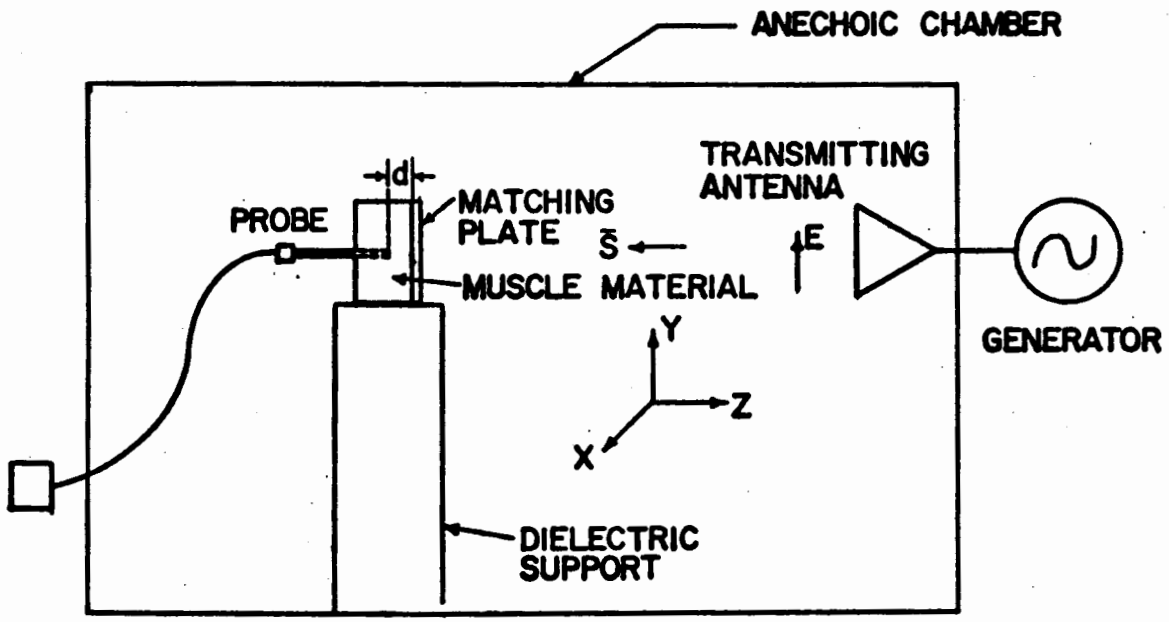


Figure 12. Experimental arrangement of system for calibration of BRH probe for E-field detection.

Under such conditions and if the diode is biased at the square law detection region, then the detected voltage measured at the output of the amplifier is given by:

$$V_P \propto V_D^2 = K^2 |\vec{E}|^2 \quad . \tag{13}$$

Satisfying Eq. (13) will guarantee isotropic detection characteristics of the probe. However, K^2 in Eq. (13) is a function of Y_i and Y_ℓ which are in turn functions of frequency and dielectric properties. An ideal probe should have K^2 independent of both change in frequency and change in electrical properties of the medium. We have demonstrated that for the BRH probe, Y_ℓ is relatively insensitive to change in ε' and tan σ for $\varepsilon' > 20$ over the frequency range of 1 - 10 GHz. Let us now examine the frequency dependence of K^2. The nominal capacitance of the Schottky diode given by the manufacturer is on the order of .1 picofarad. From results indicated in Fig. 8, Y_i is approximately 10^{-2} mhos at 10 GHz and 10^{-3} mhos at 1 GHz. In comparison, Y_ℓ is always much smaller than Y_i so that V_D can be written as

$$V_D = -2h' |\vec{E}| (Y_i/Y_i + Y_\ell) \simeq 2h' |\vec{E}| \quad . \tag{14}$$

Note that h' is totally independent of the frequency and electrical characteristics of the surrounding. Thus, when buried in an infinite muscular medium, the BRH probe satisfies conditions 1-5 which suggest that it is suitable for electric field detection within such tissues. However, as indicated by Chen and co-workers[3], junction effects can introduce significant modification of the antenna characteristics of the dipole, causing the measured values of electric field to be location dependent. The boundary effect was included in Eq. (10) by the modification factor f(b,o,h) given by:

$$f(b,o,h) = 1 + \frac{1}{\pi H_o^{(1)}(k_o\sqrt{\varepsilon^*}b)} \int_{-\infty}^{\infty} \frac{\sqrt{k_o^2\varepsilon^* - \xi^2} - \sqrt{k^2 - \xi^2}}{\sqrt{k_o^2\varepsilon^* - \xi^2} + \sqrt{k^2 - \xi^2}} * \frac{\exp(-2h\sqrt{k_o^2\varepsilon^* - \xi^2})}{\sqrt{k_o^2\varepsilon^* - \xi^2}} \, d\xi \tag{15}$$

where

$k^2 = k_o^2 \varepsilon_r$

ε_r = permittivity of the external medium

ε^* = permittivity of the tissue

Equation (15) can be analyzed numerically to generate information for a full assessment of planar boundary effects. However, note that the value of f given by the equation can never exceed two such that even under the worse case, (total reflecting boundary) the change in value of Y_i due to boundary interference is never expected to drop below half its original value. Thus, for detection within muscular tissues, the maximum error in V_D as indicated by Eq. (12) due to boundary effects can never exceed 17% for the BRH probe. ($Y_i \simeq 10Y_\ell$), and for implantation measurement in lossy medium such as muscular tissues, we expect that error due to junction should be minimal except very close to the boundary ($h << \lambda_o(\varepsilon^*)^{-1/2}$).

EXPERIMENTAL CALIBRATION

The antenna was calibrated within an "infinite" slab of simulated muscular tissue (30 cm x 30 cm x 15 cm) whose dimensions are large with respect to wavelength within the material. This material was formulated as specified by Guy with loss tangent values of 0.5 and 0.35 at the respective frequencies of 0.915 and 2.45 GHz and a dielectric constant of 50 at both frequencies. The antenna was inserted from access openings in the rear of the slab and the whole assembly was situated within an anechoic chamber with the front of the slab exposed to a known plane wave at 2.45 GHz and at 0.915 GHz. The incident and scattered fields in front of the slab were measured to allow the net internal field to be analytically computed. The experimental arrangement is shown in Fig. 12.

This "infinite" slab was placed directly behind a lossless matching plate (one quarter wavelength thick at 2.45 GHz) to minimize scatter from the dielectric body. To ensure that no standing waves existed within the slab in the transverse (X-Y plane) and the longitudinal directions (where the incident field is propagating along the longitudinal "Z" axis) and thereby demonstrating that the slab was "infinite", probe readings were measured along both X

and Y axes vs implantation depth. Figure 13 shows the measured probe response for various positions in the X-Y plane at 2450 MHz. Note that the plots of probe voltage outputs along the longitudinal direction in each transverse plane are virtually identical exponential curves which support the assumption that no standing waves exist within the media.

Probe output voltage data was taken at both 2.45 and 0.915 GHz for various incident power density levels within an anechoic chamber. Figure 14 shows the measured probe response versus theoretical values of the field existing within the infinite slab. The calculated theoretical field strength squared ($|\vec{E}|^2$ is plotted vs depth, h , and is shown as a continuous line along with the data generated from a typical calibration at 2.45 GHz within a muscular phantom. The same type of data was also obtained at 0.915 GHz. A comparison was made between the absolute response of a probe to a given, computed field strength within muscle equivalent material and the probe response obtained in a free space calibration at the same field strength. It was found that the experimental and theoretical response in muscle tissue agreed within ± 10% when the free space probe sensitivity coefficient was directly used. Thus, it was concluded that once calibrated in free space, this probe can be used for accurate measurements of E-fields within infinite slabs of muscular tissues. The response of the probe can be equated with the actual electric field strength existing in muscular tissue at frequencies ranging from 0.915 GHz to 2.45 GHz by simply using the free space calibration factor for the probe. Since multilayered, finite biological systems are of primary interest, further experiments were performed as follows to determine boundary effects on the probe calibration.

EXPERIMENTAL STUDY OF PROBE RESPONSE IN THE PROXIMITY OF BOUNDARIES

In order to study the effects of probe interaction with the multiple layers and their boundaries, which always exist in biological systems, a series of experiments was performed. The results were used in conjunction with the previous theoretical antenna analysis using the buried transmission line model in the proximity of the muscle-fat boundary. It was known that in the proximity of this or any boundary between different dielectric materials (including air)

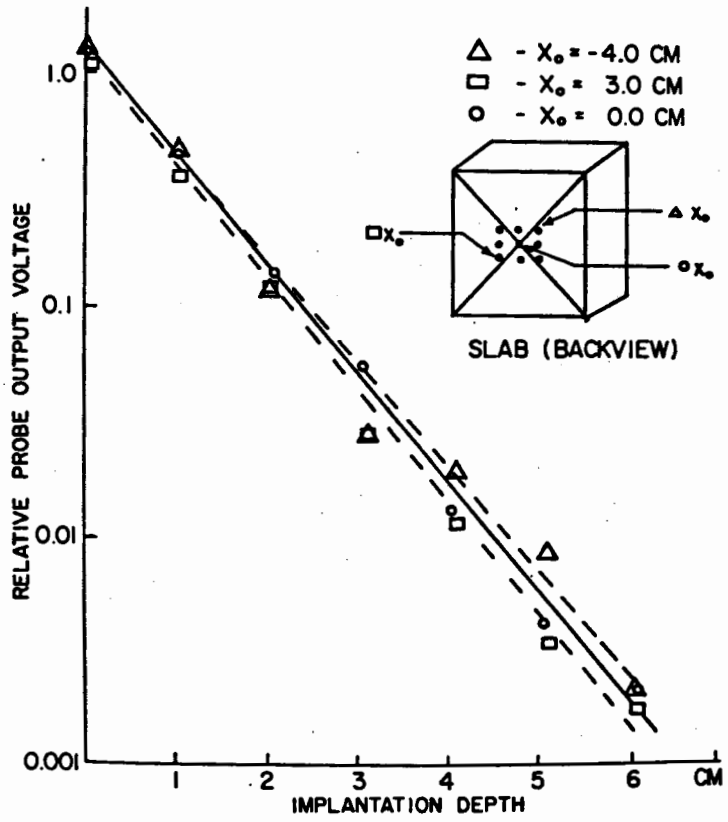


Figure 13. Probe output voltage as a function of depth along asymmetrical paths at 2450 MHz.

the currents induced in the probe antenna would reradiate microwave energy. When this reradiated energy was reflected from a boundary back to the antenna, the net current flow on the antenna, and hence its impedance would change. In very close proximity to the boundary, negligible attenuation occurs during the two-way travel of the reradiated energy. This proximity effect is accounted for by the parameter f(b,o,h) in Eq. (15). The increasing proximity to such a boundary would cause an exponentially increasing sinusoidal oscillation in antenna impedance, for probe travel toweard the boundary surface, along an axis which was normal to the surface.

The worst case condition of an air-muscle interface was chosen for the experimental evaluation of the probe-boundary interaction. At 0.915 GHz, the plane wave irradiation experiment with an "infinite" slab of muscle material was performed as previously described, except that the matching plate was removed and a low density styrofoam slab was placed on the front furface of the muscle material. Continuous probe scans were made from the rear of the slab to the front of the slab, with the probe body oriented parallel to the axis of propagation. The central probe dipole was oriented perpendicular to the axis of propagation and parallel to electric field. Using a mechanical positioner, well-covered with microwave absorber, the probe was slowly pushed through the entire muscle slab until it emerged in the styrofoam. The probe displaced muscle equivalent material during its travel, leaving a hole approximately 5 mm in diameter when withdrawn. The probe itself was found to be well coated in muscle material when withdrawn, ensuring complete emersion in the muscle-equivalent material during measurement. Similar data was taken at 2.45 GHz irradiator (a horn antenna, very close to the slab's front surface). Data is presented in Fig. 15 for both frequencies. As is evident, no significant oscillations occur in the probe output voltage as the distance of the probe to the boundary approaches and reaches zero. This qualitative data is conclusive proof that the diode impedance is high with respect to the antenna impedance, since the antenna impedance which is known to oscillate, has no effect on the probe output. Therefore, the probe may be used without concern for boundary effect errors in multilayered biological systems or for shallow implantation in non-infinite biological media. Bone and fat have a lower loss

tangent than muscle, and boundary interactions may be slightly more significant for the probe under discussion. Therefore, measurements of the electric field inside complex bodies composed of these materials can be accurately performed but some further measurement in low loss material is needed.

EXPERIMENTAL EVALUATION OF THE PERTURBATION OF FIELDS EXISTING IN SIMULATED BIOLOGICAL MEDIA BY THE IMPLANTED PROBE

To make certain that the electrically small probe did not perturb the electric fields being measured, and thus did not alter the distribution of energy within the previously unpenetrated system, an experiment was performed at 2.45 GHz. Using a TEM near-field applicator, the previously described muscle-equivalent slab with styrofoam front plate was irradiated while a probe was placed along the center axis of the slab, parallel to the axis of propagation. The center dipole was placed 2.5 cm from the front surface of the test "phantom". This dipole was aligned with the incident electric field and remained stationary while a second probe was inserted from the top of the slab, with its handle aligned with the electric field. This second probe was continuously pushed toward the first probe until the two tips touched. The output of the stationary probe was continuously monitored. No observable change in probe output was observed until the proximity between tips was less than 1 cm. Then the probe output increased to a value 10% higher than previously observed. This test demonstrated negligible perturbation by the probe body and its three orthogonal dipoles for implantation in lossy media. Again, further tests in low-loss material are needed.

CONCLUSIONS

The use of an electrically small three-axis dipole probe for direct measurement of electric fields at microwave frequencies (0.915 to 2.45 GHz) has been experimentally and theoretically explored with implantation in biological media as the goal. Using a well-established theoretical model, the antenna impedance has been analyzed with respect to various implantation situations. The use of a small insulated dipole as detection element enables

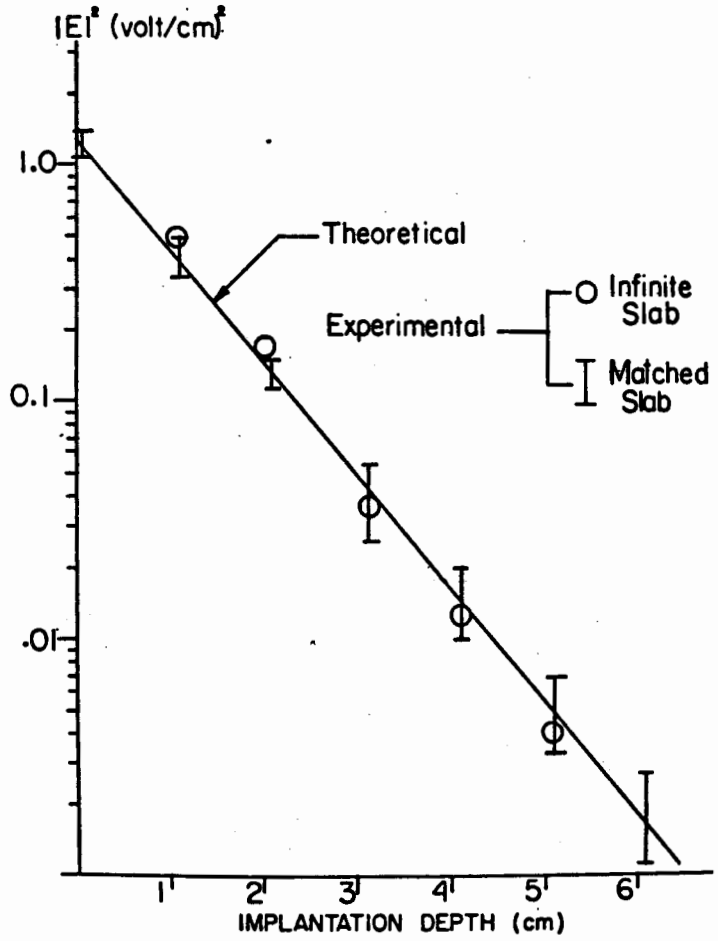


Figure 14. Comparison of absolute values of experimentally measured and predicted electric field strengths in Muscle-equivalent slab at 2450 GHz (normalized representation).

the probe's response to an electric field to remain relatively constant with regard to the electrical properties of the media surrounding the probe. Material inhomogeneities and temperature changes, therefore, do not affect this relationship, even though these produce significant variations occurring in the magnitude of the dielectric constant of the biological media. Therefore, a properly designed probe may be calibrated in free space, and then used as an implantable probe in "infinite" media without calibration. Using this approach, errors of less than ± 10% were encountered when fields experimentally measured in a large muscle-equivalent slab were compared with theoretically computed field strengths induced by plane wave irradiation of the slab at 0.915 to 2.45 GHz.

The problems associated with measurements performed in biological systems near the boundary layers between various biological materials (muscle-bone, muscle-fat-air) were also considered. Worst case (muscle-air) boundary conditions were experimentally measured with continuous scans along an axis normal to the boundary plane. The experimental findings demonstrated that no detectable probe-boundary interaction occurred during increasing proximity to the boundary. This is unique to the specific probe design utilized in which the diode detector impedance is much higher than the antenna impedance, thus eliminating dipole-boundary interaction as described in the theoretical analysis. The lack of significant electric field perturbation by the probe itself was also demonstrated in the muscle-equivalent slab.

The performance of this probe can be further improved by optimizing the design of the insulation thickness. A detailed numerical analysis of Eq. (15) for the variation of the factor, f, under all implantation conditions (especially in low-loss tissues) will give a full assessment of errors due to junction interference.

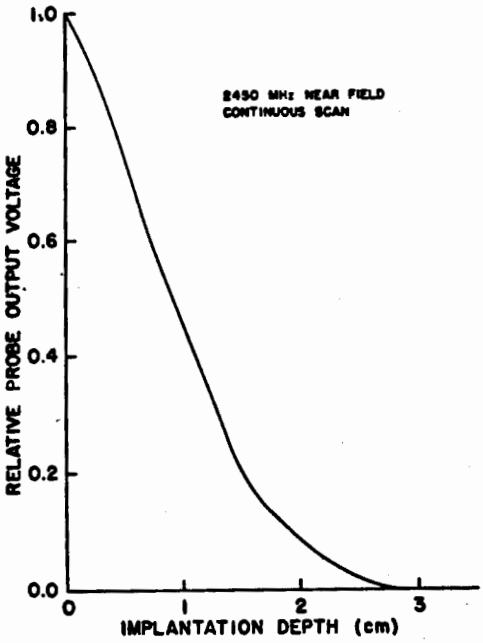


Figure 15a. Experimental probe output from continuous scan towards muscle-air boundary at 2450 MHz.

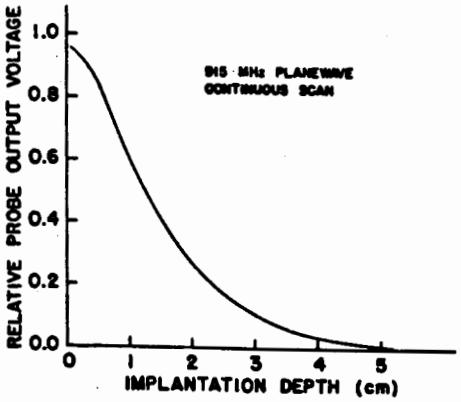


Figure 15b. Experimental probe output from continuous scan towards muscle-air boundary at 915 MHz.

REFERENCES

1. C. C. Johnson and A. W. Guy, Proc. IEEE 60, 692 (1972).
2. A. W. Guy, in *Conference on Precision Electromagnetic Measurements Digest*, IEEE, New York (1972).
3. B. S. Guru and K. M. Chen, IEEE Trans. MTT-24, 433 (1976).
4. H. Bassen, In *IEEE 1975 Electromagnetic Compatibility Symposium Record*, 5BIIa (1-5), IEEE, New York (1975).
5. G. A. Deschamps, IRE Trans. AP-10, 648 (1962).
6. G. S. Smith and R. P. King, IEEE Trans. EMC-17, No. 4, 206 (1975).
7. G. S. Smith, IEEE Trans. BME-22, 477 (1975).
8. J. Galejs, *Antennas in Inhomogeneous Media*, Pergamon Press 1969.
9. A. W. Guy and G. Hasserjian, IEEE Trans. AP-11, 232 (1963).

SOME RECENT RESULTS ON THE DEPOSITION OF ELECTROMAGNETIC ENERGY IN ANIMALS AND MODELS OF MAN [1]

O. P. Gandhi and M. J. Hagmann

Departments of Electrical Engineering and Bioengineering
University of Utah, Salt Lake City, Utah 84112

ABSTRACT

A realistic human model and improved numerical methods have been used for calculation of deposition of electromagnetic energy. Unlike earlier solutions both the average absorption and the distribution of absorbed energy within the model are in good agreement with experimental measurements made using phantom models. The distribution of absorbed energy is frequency-dependent and may be explained in terms of resonance of the various body parts. Numerical solutions for man near a ground plane and near reflectors are presented for the first time. At 10 MHz the specific absorption rate (SAR) of man standing on a ground plane is about seven times that for man in free space. Multibody effects have been predicted from antenna theory and observed with experiments using anesthetized rats. For two resonant targets separated by 0.65 λ an increased SAR, 170 percent of the free-space value, has been observed.

DESCRIPTION OF MODEL AND NUMERICAL TECHNIQUES

Solutions in electromagnetics are facilitated by choosing a model of simple geometry. Then an exact analytical solution may be possible, or a numerical solution may be expressed in terms of easily constructed whole-domain basis functions. We have rejected such methods since emphasis was placed on a realistic model of man. When simple geometries are not possible, one can always attempt a solution by "brute-force" using moment methods with a subsectional basis. We have used moment method solution of the electric field integral equation with a pulse function basis and delta functions for testing[1].

A total of 180 cubical cells of various sizes were used to obtain a best fit of the contour on diagrams of the 50th percentile standard man[2]. Sizes and placement of the cells is shown in Fig. 1. Anatomical cross sections[3,4] were used in partitioning bone, fat, skin, muscle, lung tissue, air, heart, brain, kidney, liver, and spleen through the cells. Whole-body volume fractions of each tissue type are in agreement with published values. Properties reported in the literature for the tissue types[5-7] have been used to calculate the volume-weighted complex permittivity of each cell.

Previously reported solutions for models of man have a ratio of 239.1 for energy deposition in one pair of adjacent cells at 10 MHz[8]. The arrangement and different sizes of cells in the present model cause the maximum ratio of energy deposition for a pair of adjacent cells to be 8:1 at the same frequency. The pulse function approximation is invalid if conditions force significant variation of $\vec{E}$ within the cells and a large difference between calculated energy deposition in adjacent cells suggests the existence of such variations.

If Δ is the side of a cubical cell and k represents the magnitude of the complex propagation vector within the cell, then substantial variation of the electric field must occur within the cell if $k\Delta > \sqrt{6}$ [9]. Thus the pulse function approximation may not be justified at frequencies above 200 MHz with the new model suggesting an increasing error at higher frequencies. Volume

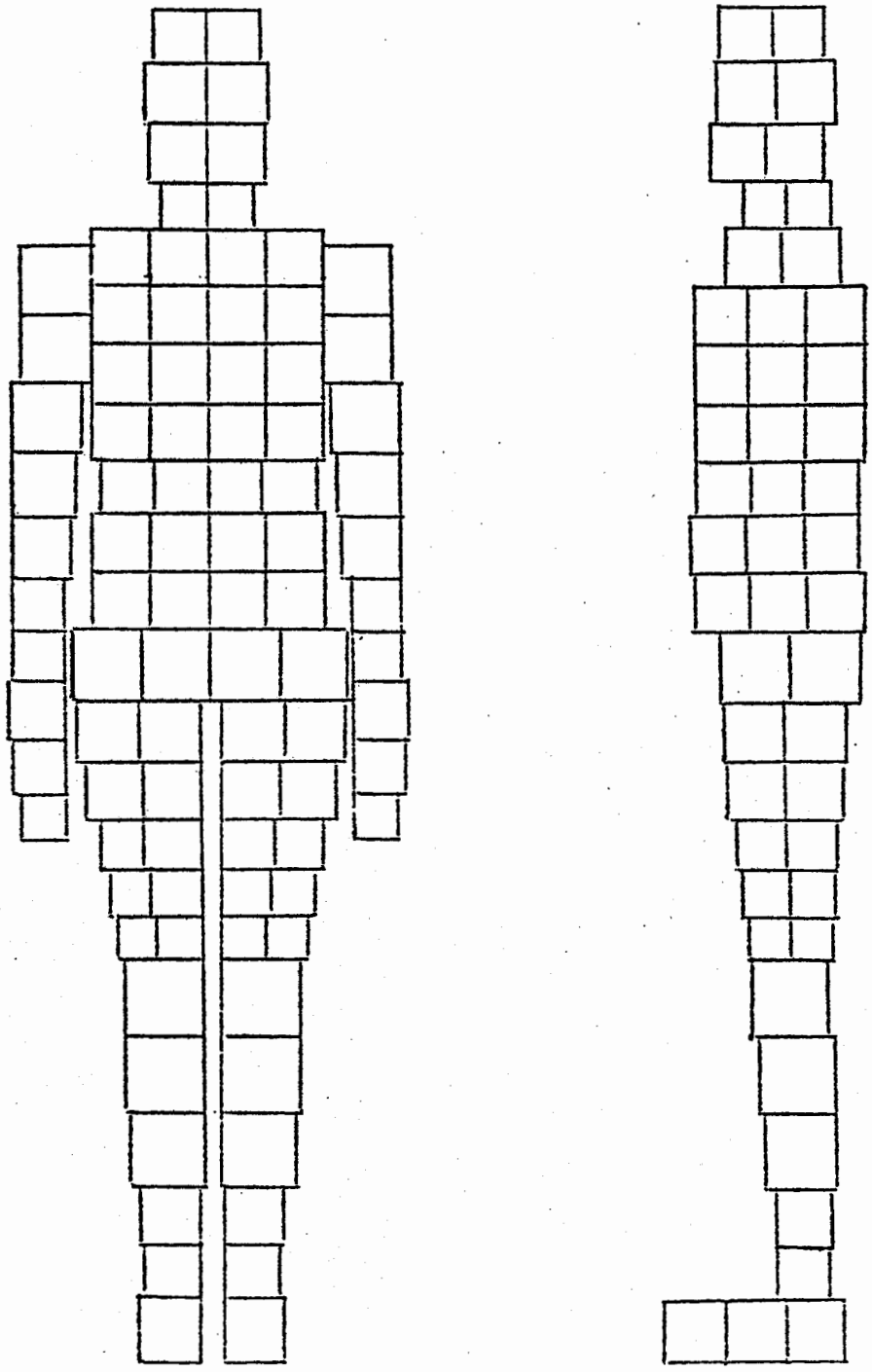


Figure 1.
An improved model of man for numerical calculations.

weighting of the complex permittivity within each cell may also be unjustified at frequencies above 200 MHz though the results appear reasonable to at least 500 MHz.

A numerical solution using a pulse function basis results in a single value representing $\vec{E}$ within each cell. It is possible to use the $\vec{E}$ values to calculate $1/2\ \sigma\vec{E} \cdot \vec{E}^*$ for each cell and use a volume average to estimate the specific absorption rate (SAR)[8]. Large numbers of cells must be used in order to find accurate values of SAR by such a procedure. For example, our calculations of the SAR of a 12cm muscle cube at 1 MHz show an error of 37% with eight cells, 26% with twenty seven cells, and 20% with sixty four cells. The delta functions used for testing enforce the integral equation at the center of each cell so that the calculated $\vec{E}$ values are most representative of the cell centers. Inspection of the solutions suggests that the local values of $\vec{E}$ have appreciably less error than occurs in the SAR. If there is much variation of $\vec{E}$ within a scattering body then even if we have exact values of $\vec{E}$ at the cell centers appreciable error would be expected in the calculated SAR. We have found that accuracy is improved by using a three-dimensional interpolant[10] with the $\vec{E}$ values initially calculated for each cell to account for some of the variation of E within each cell. Trilinear and triquadratic interpolants have both been used to estimate the variation of $\vec{E}$ between the cell centers. The interpolant is integrated in calculating the SAR. For the 12cm muscle cube at 1 MHz, the SAR found, using twenty seven cells with the triquadratic interpolant, has error comparable with the calculation using sixty four cells without the interpolant. The increase in cost due to use of the interpolant is about one percent. All values of energy absorption in this paper have been calculated using interpolants.

DISTRIBUTION OF ABSORBED ENERGY -- PART BODY RESONANCES

The principal contribution from the free space calculations is the distribution in energy deposition. Figure 2 shows the part-body and whole-body SAR for the homogeneous model of man with two-thirds the complex permittivity of muscle with $\vec{E} \parallel \hat{L}$ and $\vec{k}$ directed front-to-back. Calculated values of

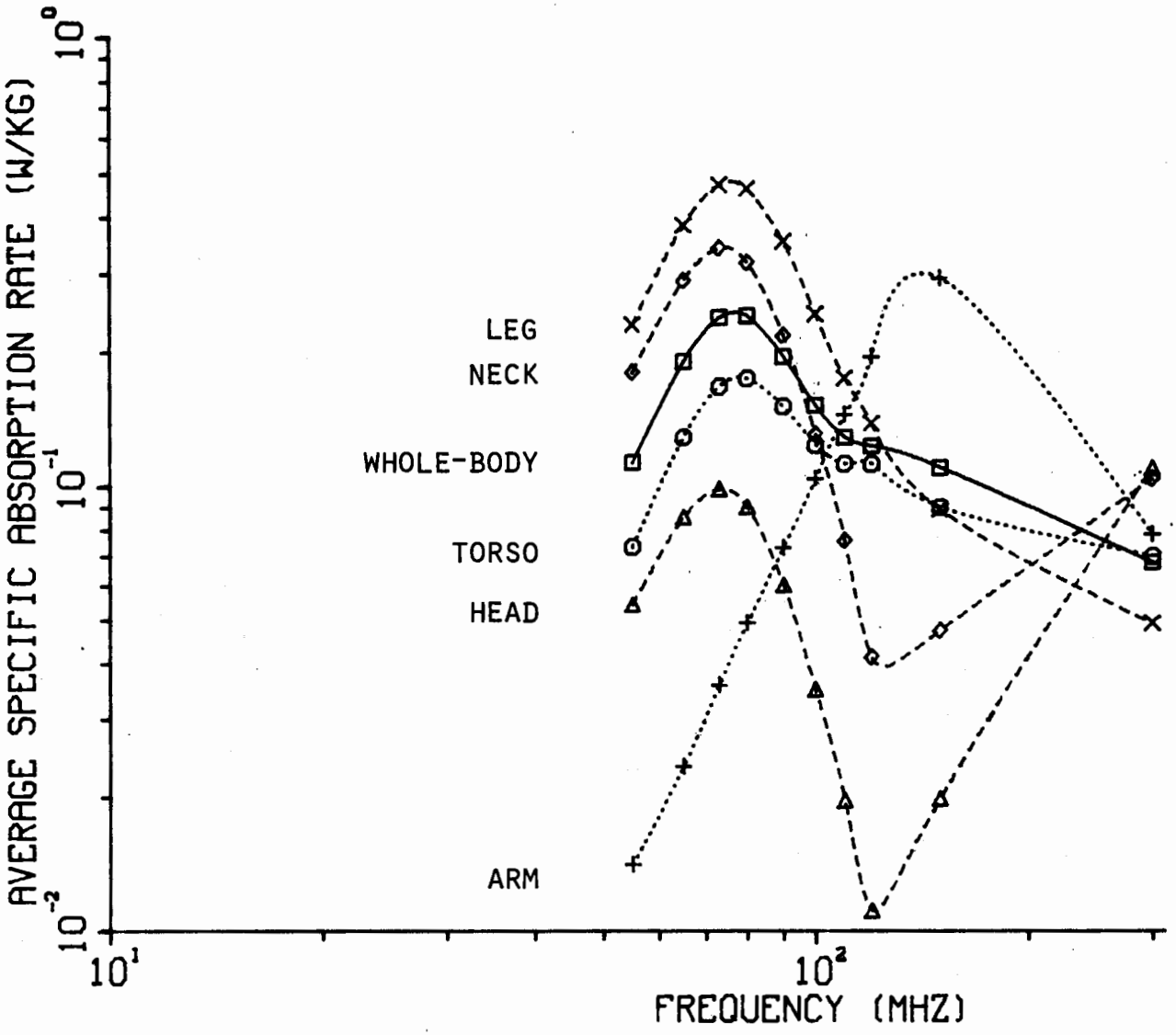


Figure 2.
Part-body SAR for homogeneous model of man. Incident intensity = 1 $mW.cm^2$.

whole-body SAR are typically within 20% of values found for prolate-spheroidal and ellipsoidal models[11]. Unlike earlier numerical models the distribution of absorbed energy within the model is in good agreement with that found experimentally for homogeneous phantom models[12]. For free space irradiation with this polarization near resonance, the local absorption in the legs and neck is considerably higher than the whole-body average while the torso has less than average absorption.

When the inhomogeneous complex permittivities are used with the model, a change of less than two percent occurs typically in the whole-body SAR, but a more significant change occurs in the distribution of energy deposition. Figures 3 and 4 illustrate the distribution of absorbed energy in man at 80 MHz in free space for the homogeneous and inhomogeneous models, respectively. One difference is that the inhomogeneous model has reduced absorption in regions with high bone content.

In previously reported experimental[13] results on whole body SAR for man, an anomalous increase in the rate of energy deposition was observed in the region of 470 MHz for $\vec{k} \parallel \hat{L}$ and $\vec{E} \parallel \hat{L}$ orientations. This has now been identified as the first (geometrical) resonance frequency of the head. Continuing experiments have given the absorption cross section for the head region as large as 3.1 times the physical cross section, perhaps on account of reflections from the nearby torso. At the head resonance frequency, an SAR 4.5 times the average value for the rest of the body has been experimentally observed.

Higher order resonances based on a multilayer formulation may exist for the head region at higher frequencies. Initial numerical results show one such resonance at frequencies of the order of 2000 MHz. It is, however, anticipated that the overall absorption cross section at these frequencies may not be as large as that for the first resonance, where an enhancement factor of 3.1 has been observed for the head region.

The frequency for maximum energy deposition in the arms is approximately 150 MHz (see Fig. 2) with an absorption cross section that is 2.3 times the physical cross section.

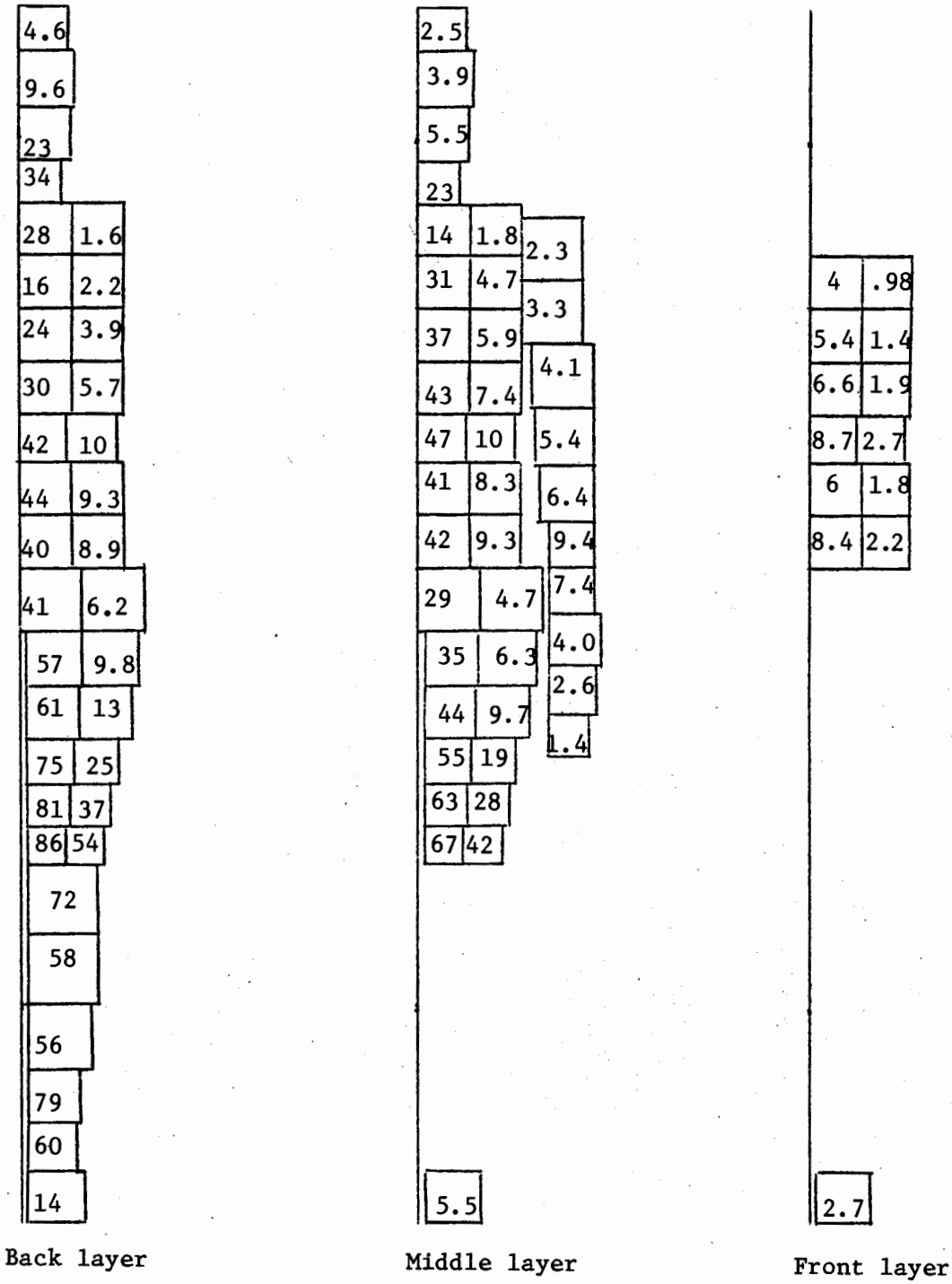


Figure 3.
Local SAR values (watts/kg per mW/cm^2) x 100 for homogeneous model of man with vertical polarization at 80 MHz.

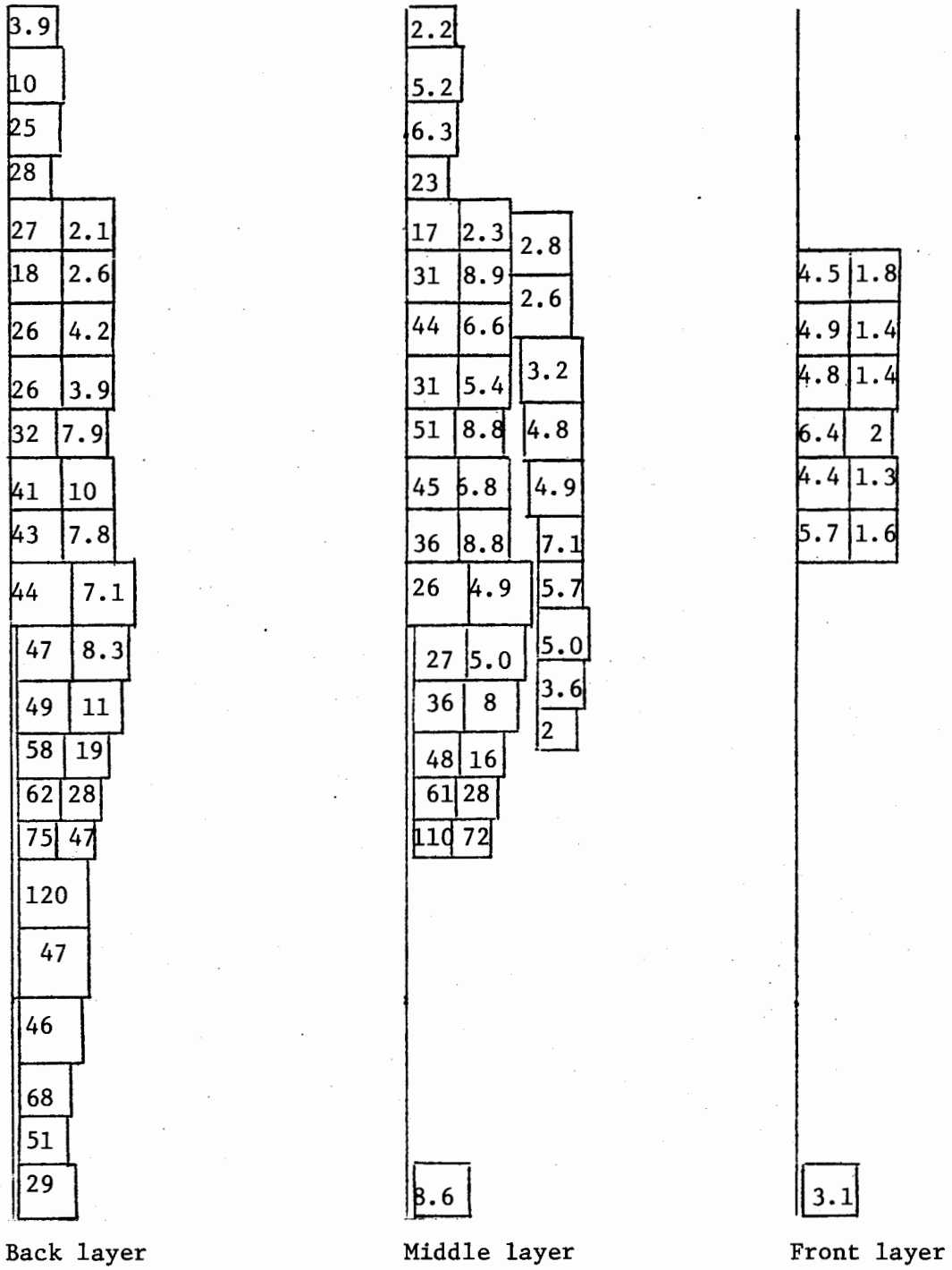


Figure 4. Local SAR values (watts/kg per mW/cm^2) x 100 for inhomogeneous model of man with vertical polarization at 80 MHz.

GROUND EFFECTS

Experimental observations of ground and reflector effects[13] have been reported previously but numerical methods have not been available to explain the observations. We have used image theory to reduce the problem of man above ground or in front of reflectors to a multibody problem in free space. Symmetries have been used to reduce the matrix size.

All calculations of ground effects have assumed that man is standing on or above a perfectly conducting ground plane that is infinite in extent. The incident field is vertically polarized with k directed front-to-back on the man. Internal fields in the model are the same as those in one half of a double-man consisting of the model and its image in free space.

The resonance frequency of man standing on a ground plane is one half that for man in free space. The SAR of man on the ground plane at the reduced resonant frequency is within 2 percent of the SAR for man in free space at the free-space resonance frequency.

At 10 MHz the SAR of man standing on a ground plane is 0.0163 watts/kg per mW/cm^2, which is about seven times that found for the same model in free space. The enhancement in SAR due to the ground effect is found since the frequency of 10 MHz is much closer to the grounded man resonance frequency ($\approx$35 MHz) than to the free-space resonance frequency ($\approx$70 MHz).

Figures 5 and 6 illustrate the distribution of absorbed energy in man at 10 MHz in free space and in contact with the ground plane, respectively. The enhancement factor in local energy deposition due to the ground effect is about 60 in the heel area.

Figure 7 shows the part body and whole body SAR for the inhomogeneous model of man with different spacings from the ground plane at 10 MHz. A small small separation that breaks electrical contact with the ground plane is sufficient to eliminate much of the ground effect.

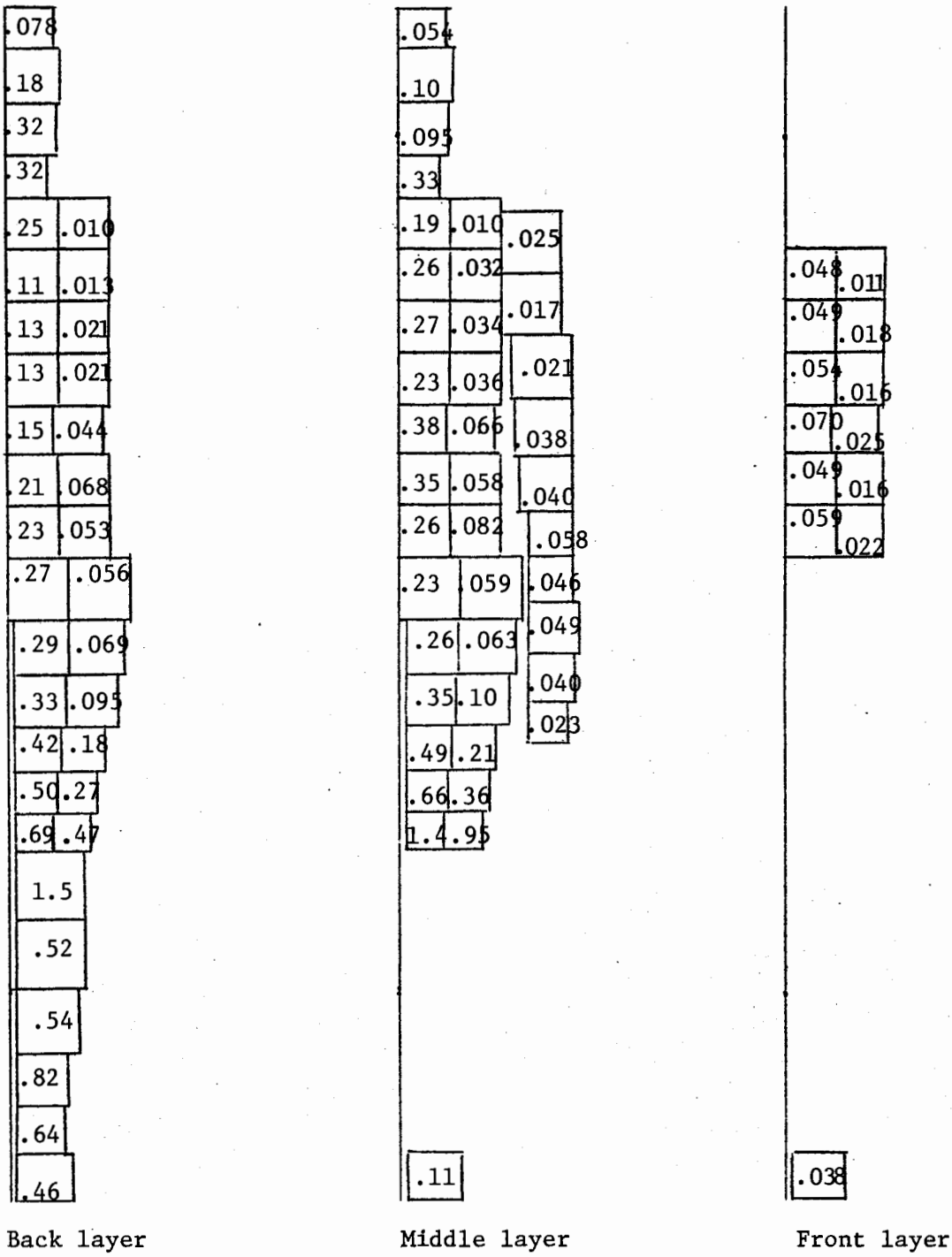


Figure 5.
Local SAR values (watts/kg per mW/cm^2) x 100 for inhomogeneous model of man in free space at 10 MHz.

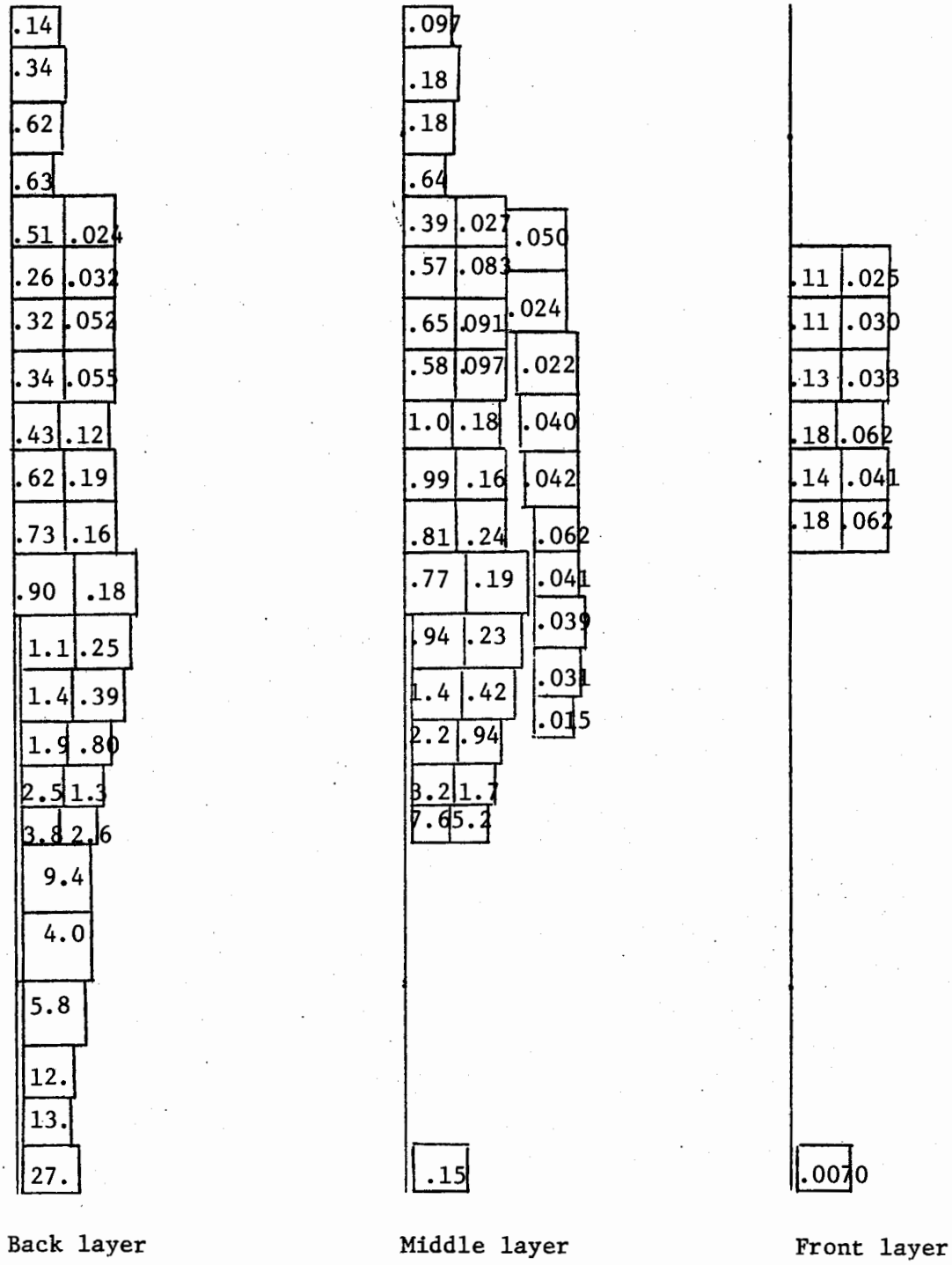


Figure 6.
Local SAR values (watts/kg per mW/cm^2) x 100 for inhomogeneous model of man standing on a ground plane at 10 MHz.

REFLECTOR EFFECTS

All calculations of reflector effects have assumed that man is standing in front of a reflector that is perfectly conducting and infinite in extent. The incident field is vertically polarized with $\vec{k}$ directed front-to-back on the man. One image is required for a flat reflector and three are needed for a 90° corner reflector.

At 65 MHz the computed SAR is 4.87 times the free-space value when man is 0.1875 λ in front of a flat reflector and 16.6 times the free-space value when man is 1.5 λ in front of the axis of a 90° corner reflector.

Antenna theory may be used[13] to calculate the ratio of effective area of a half-wave dipole with a reflector to that of the dipole in free space. Such ratios are within 16% of the above calculated factors of enhancement of SAR due to reflector effects.

For certain length-to-width ratios, the experimentally[13] observed enhancement in energy deposition is 30 to 40% higher than that anticipated from antenna theory and calculated numerically for reflectors of infinite dimensions. This phenomenon is, once again, in agreement with experimentally obtained antenna gains for finite size[14] corner reflector antennas. Significantly enhanced rates of energy deposition are projected for all kinds of corner angles (not just the values corresponding to $180^{\circ}/n$, where n is an integer) and for reflector lengths and widths that are no more than a fraction of a wavelength at the resonance frequency.

MULTIBODY EFFECTS

Driving point inpedance values for a broadside array of two half-wave dipoles[15] have been used to prepare Fig. 8 which shows the variation of effective area per dipole with spacing. If the two dipoles are tangent, each will receive approximately one half the energy it would receive if isolated in free space. For separations greater than two or three free space wavelengths, the antennas have little coupling so that each has an effective area approximating the isolated free space value. At a spacing of 0.65 λ, each dipole will receive about 56% more energy than it would if it were isolated.

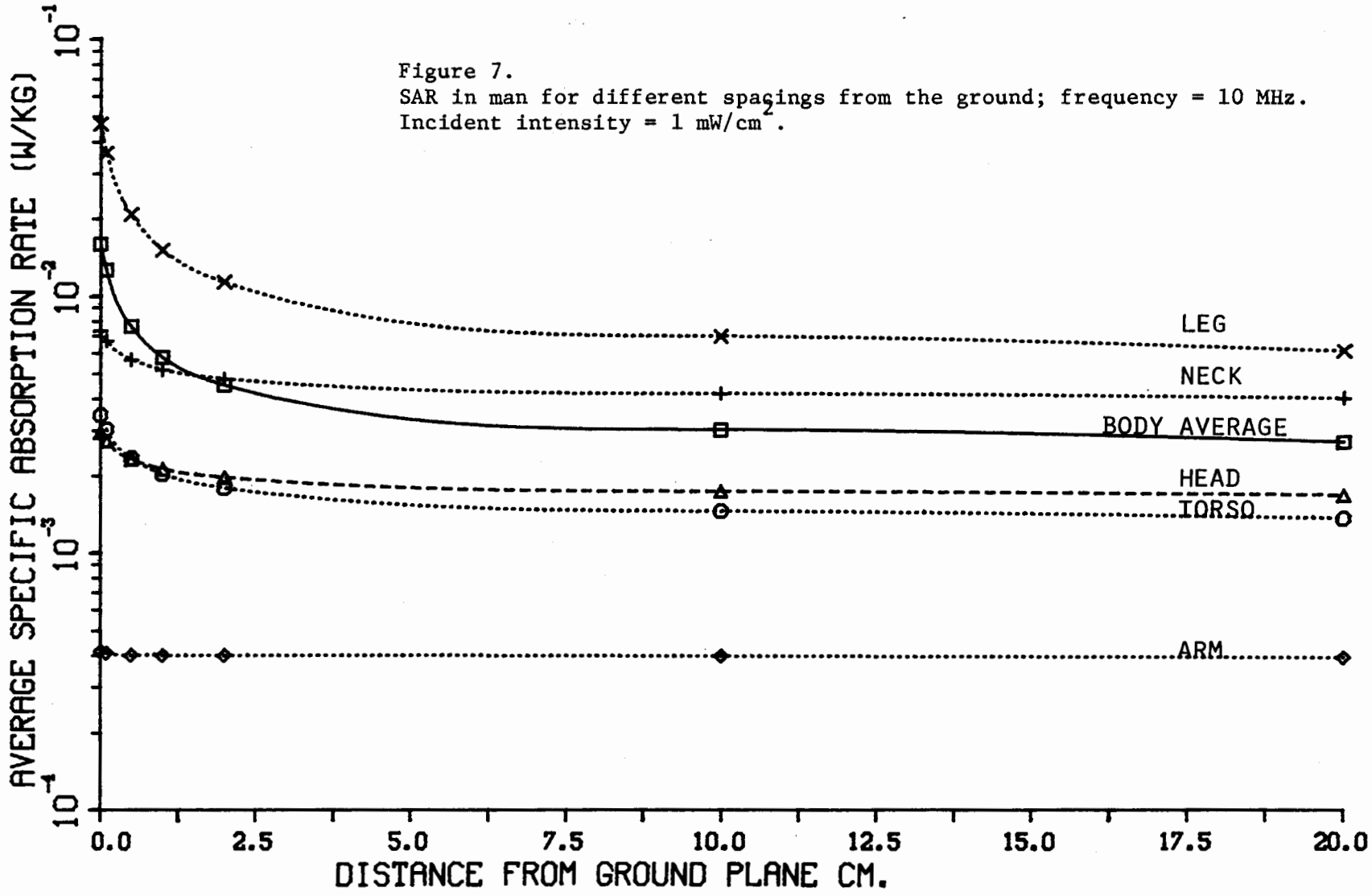
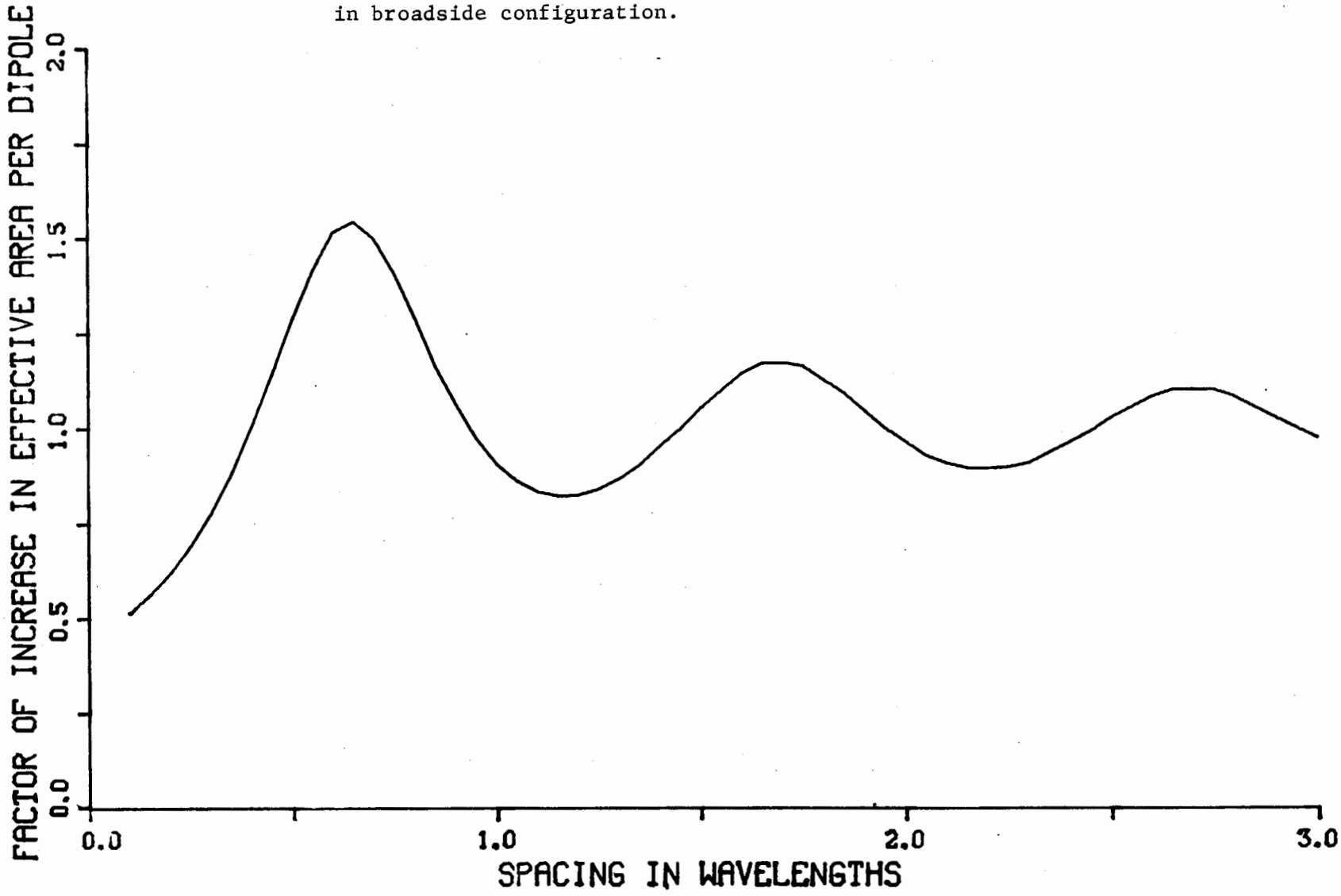


Figure 7.
SAR in man for different spacings from the ground; frequency = 10 MHz.
Incident intensity = 1 mW/cm^2.

Figure 8.
Variation of effective area with spacing for a pair of half-wave dipoles in broadside configuration.



It has been shown[13] that the energy absorbed by man at resonance corresponds to the energy received by a half-wave dipole of length approximately equal to the height of the man. Mutual impedance, and hence driving point impedance, values are dependent upon the shape of the antenna elements, but we may expect that the variation of SAR with spacing for two men near resonance is similar to Fig. 8.

Preliminary experiments using animals have confirmed the existence of multibody effects. We have used anesthetized adult rats with $\vec{E} \parallel \hat{L}$ orientation and frontal (broadside) incidence. In tests with 480 ± 50 gram rats at 600 MHz with an incident intensity of 100 mW/cm^2, isolated animals had an average temperature increase of 0.675° C/min. For two animals placed 0.65 λ apart, the monitored animals had an average temperature increase of 1.14° C/min. A 70 percent increase in SAR was caused by the presence of the second animal.

Antenna theory suggests similar enhancements in SAR for targets in the subresonance and supraresonance regions, also for spacing on the order of 0.65-0.7 λ. Furthermore, a greater enhancement in the SAR by a factor as large as 2.5 is anticipated for the inner targets with three or more elements.

REFERENCES

1. G. W. Hohmann, Geophys. 40, 309 (1975).
2. N. Diffrient, A. R. Tilley and J. C. Bardagjy, *Humanscale 1/2/3*, MIT Press, Cambridge, 1974.
3. D. J. Morton, *Manual of Human Cross Section Anatomy*, Williams and Wilkins, Baltimore, Second Edition, 1944.
4. A. C. Eycleshymer and D. M. Schoemaker, *A Cross-Section Anatomy*, D. Appleton and Company, New York 1911.
5. C. C. Johnson and A. W. Guy, Proc. IEEE 60, 692 (1972).
6. C. C. Johnson, C. H. Durney and H. Massoudi, IEEE Trans. MTT-23, 739 (1975).
7. H. P. Schwan, *Advances in Biological and Medical Physics*, Vol. V, (ed. by J. H. Lawrence and C. A. Tobias) Academic Press, 1957.
8. K. M. Chen and B. S. Guru, *Induced EM Field and Absorbed Power Density Inside Human Torsos by 1 to 500 MHz EM Waves*, Technical Report No. 1, NSF Grant ENG 74-12603, April 1976.
9. M. J. Hagmann, O. P. Gandhi and C. H. Durney, IEEE Trans. MTT-25, (1977).
10. M. J. Hagmann, O. P. Gandhi and C. H. Durney, *Improvement of Convergence in Moment-Method Solutions by the Use of Interpolants*, IEEE Transactions, to be published.
11. C. C. Johnson, C. H. Durney, P. W. Barber, H. Massoudi, S. J. Allen and J. C. Mitchell, *Radio Frequency Radiation Dosimetry Handbook*, USAF Report SAM-TR-76-35, September 1976.
12. O. P. Gandhi, K. Sedigh, G. S. Beck and E. L. Hunt, USNC/URSI Meeting Summary of Papers, 201 (1975).
13. O. P. Gandhi, E. L. Hunt and J. A. D'Andrea, *Deposition of Electromagnetic Energy in Animals and Models of Man*, USNC/URSI Meeting, Amherst, Massachusetts (1976).
14. H. V. Cottany and A. C. Wilson, IRE Trans. AP-6, 366 (1958).
15. R. W. P. King, *Tables of Antenna Characteristics*, IFI/Plenum, New York, 1971.

* *

DISCUSSION

One of your human model measurements, where the radiation came from the right showed higher absorption on the left leg. Do you have an explanation for that? [Chou].

Gandhi: Usually the radiation has been uniform within experimental levels of no more than eight to ten percent. Occasionally, however, the placement of the corner reflector has not been exact. That may have been the reason for that distribution.

I would like to comment that a casual inspection of the universal function which was derived by Fock shows that the frequencies at which one could use geometrical optics to estimate these patterns are very high X-band. Longer wavelengths result in a number of half-shadow or diffraction regions around the body. [Taylor].

Gandhi: I think multi-layered models are going to effect resonances at frequencies in the lower microwave band, that is, some of these minor resonances of the kind seen at lower frequencies, will still exist at much higher frequencies and, indeed, because of the skin layer, may go well into the X-band.

THERMOMETRY IN STRONG ELECTROMAGNETIC FIELDS

T. C. Cetas

Radiation Oncology Division, University of Arizona
Arizona Health Sciences Center, Tucson, Arizona

ABSTRACT

We report on the progress of several new developments in thermometry designed to meet the need for measurements in the presence of strong electromagnetic fields. The requirements for calibration facilities for probe thermometers and for thermographic systems are also described.

INTRODUCTION

Thermometry in the presence of strong electromagnetic fields has been recognized as difficult for many years. At the most basic level, fields emanating from the power mains interfere with nearly all measurements. Precision measurements in many places are plagued by radiofrequency interference from nearby radio and television transmitters. Careful shielding and grounding of equipment or even entire rooms eliminates most of the problems caused by environmental radiofrequency fields. The problem addressed by many investigators now is far more complex in that not only is accurate thermometry required, but it must be attained without significantly perturbing intense applied fields. Furthermore, in cases of interest to those addressed by these proceedings, biological constraints are imposed as well.

The nature and significance of the perturbing effect of thermometers in strong fields, especially in relation to electromagnetic heating, has been demonstrated graphically with a thermographic camera by Guy, *et al*[1,2], and by others[3]. Conversely, some have claimed that their data were only minimally affected by the presence of electromagnetic fields. The discrepancy lies in the fact that many factors influence the magnitude of the perturbation. Some of these are the field strengths and the magnitude of the power broadcast, the orientation and position of the thermometer leads with respect to field orientation and phase, the degree of shielding, including that due to tissue, and the geometry of the subject and the radiator. For example, in one test we performed using 3 MHz current fields to heat a man's arm, no measurable artifact appeared in temperatures monitored with a needle mounted thermistor. However, when the same treatment was applied to an eleven-year-old girl with osteogenic sarcoma, much poorer electromagnetic coupling to the arm was achieved and a thermometry artifact of about $1^{\circ}C$ resulted.

In this paper, the status of thermometry in microwave fields is addressed. Basically, it represents a progress report on several new developments that are under way to meet these thermometric needs. The requirements of a calibration

facility are addressed as well, both for probe thermometers and for thermographic systems. Most of the material discussed is taken from portions of other recent manuscripts[4,5,6,7]. It is included here in the interest of completeness for these proceedings.

PROBLEMS WITH CONVENTIONAL THERMOMETER PROBES

The difficulty of making reliable temperature measurements in the presence of strong electromagnetic fields stems from three types of interaction between the thermometer and the field. The first is the familiar problem of electromagnetic interference due to broadcasting by the source and pickup by the electronic measurement system. The second is the self-heating of the thermometer element resulting from direct absorption of the energy from the electromagnetic field. The third is the perturbation of the electromagnetic field caused by reflection or shunting by the thermometer or its sheath.

Several techniques can be used to reduce the magnitude of these effects. The instruments should be well shielded and grounded, with special care taken to avoid ground loops, especially those involving capacitive coupling. Radiofrequency filters in the sensing circuitry and in the power lines help as well. The thermometer leads should run perpendicular to the electric field vector and they should be tightly twisted to reduce magnetic induction pickup. When possible, extraneous fields radiating from the source should be eliminated.

With respect to interference in the sensor itself, the thermometer should be isolated electrically from the electromagnetic field. For example, if thermistors mounted in hypodermic needles are used to measure temperatures in tissues heated by radiofrequency currents, the needle should not be electrically continuous with the thermistor leads. Guy[2] has shown that smaller temperature reading errors result for thermistors mounted in dielectric catheters if the leads extend slightly beyond the bead so that it is not in the fringing fields at the end of the conductors. Frequently, adequate temperature information can be obtained by shutting off the power periodically, in order to read the thermometer. For some experiments, reentrant wells can be

prepared in the subject prior to heating and thermometer probes inserted immediately after the field is extinguished. The maximum temperature attained can be determined by extrapolation of the cooling curve back to the instant heating ceased. In other cases, the sensor can be inserted such that the tissues electrically shield most of the sensor leads. Practically, the magnitude, in degrees celsius, of any temperature artifact is proportional to the power levels which produce the artifact. We have found in our laboratory that insignificant perturbations occur when small volumes, say 50 cm^3 or less, are heated and maintained approximately $10^{o}C$ above the initial temperature, using low power (≈10W) radiofrequency current fields in the region of 1 MHz. However, when larger volumes are heated requiring powers greater than about 50 W, themometer artifacts tend to become significant.

These solutions are not entirely satisfactory for a number of reasons. First, they frequently are not adequate; significant interference remains. Shielding a sensor may reduce electromagnetic interference but also may produce a substantial reflection or shunting of the electromagnetic field. The near field of an antenna can have electric field components in all directions and thus it may be impossible to place the leads normal to the field. The fields are especially complex in regions of curved interfaces which can focus the fields. Hot spots caused by the presence of the probe may occur where no probe is located. Thus the common technique of momentarily switching off the field and distinguishing between the fast jump in the sensor reading which is attributed to electromagnetic interference and the slower change which is attributed to a real temperature change will not necessarily reveal localized tissue heating caused by the presence of the thermometer. Many situations occur for which continuous monitoring of the temperature is necessary for precise control of heating fields. Even switching the field off for a few seconds will result in a substantial temperature drop if a large blood flow rate exists in the region being heated. Finally, in a given experiment, biological or physiological constraints frequently take precedence over physical considerations. Nevertheless, the above techniques must be used until new thermometers specifically designed for use in strong electromagnetic fields become available.

MINIMALLY PERTURBING PROBE THERMOMETERS

To meet the problems of thermometry in strong electromagnetic fields several new thermometer probes are under development (see Table 1). Five of these avoid electromagnetic absorption and reflection effects by going to optical fibers rather than electrical conductors. Two others use thermistors as sensors and reduce the electromagnetic interactions through very high lead resistivities to minimize dipole currents and small enclosed loop areas to reduce magnetically induced currents. Another uses the viscosity of a fluid as the sensitive parameter and so by-passes electromagnetic interactions. It is unfortunate that, in spite of the developers' enthusiasm and the clear need for the probes, only one is available commercially at the time of this writing. Most of the other investigators are pursuing that objective for their thermometers.

Optical Probes

Liquid crystal optical fiber (LCOF)[8-12]: Two optical fiber bundles carry light from the source, a red light-emitting diode (LED), to the sensor and from the sensor to a photodetector, a photodiode. The sensor tip is composed of a liquid crystal mixture which exhibits strong temperature dependence in its reflectance of red light. Various temperature ranges of about 14°C width can be selected by varying the liquid crystal mixture. A precision of 0.1°C is quoted. The standard tip is 3mm in diameter, although the manufacturer indicates that smaller units are available. The principal advantage of this device (apart from its electromagnetic immunity which is common to all of the probes described in this section) is that it is commercially available now. Some problems remain in that the liquid crystal mixture is not stable[12]. Hysteresis effects are evident when the sensor temperature is cycled and the calibration tends to drift throughout the day. These can be overcome by a calibrate-use-calibrate routine. The probes have been used in ionizing radiation beams without calibration changes greater than those posed by the liquid crystal instability. The probe must not be allowed

TABLE I

THERMOMETER PROBES DESIGNED FOR USE IN ELECTROMAGNETIC FIELDS

SENSOR	LEADS	PHYSICAL PARAMETER SENSED
Liquid Crystal[8-12]	Optical Fibers	Light Intensity
Liquid Crystal[13,14] (Microencapsulated)	Optical Fibers	Light Intensity
Liquid Menicus Variation[13,14]	Optical Fibers	Light Intensity
Optically Birefringent Crystal ($LiTaO_3$)[3,15,16]	Optical Fibers	Light Intensity
Optical Etalon[18]	Optical Fibers	Light Wavelength Change Light Intensity
Semiconductor Optical Absorption (GaAs)[19]	Optical Fibers	Light Intensity
Thermistor[20,21]	Carbon Loaded PTFE	Resistance
Thermistor[22,23]	Microminiature Integrated Circuitry	Resistance
Fluid Viscosity (Orifice)[24]	Dielectric Tubing	Fluid Pressure Difference

to heat beyond the mesomorphic transition point (~54°C). A variation of this probe has been used for electric field measurements[10] by coating the tip with absorbing material and calibrating the probe heating rate versus the applied field.

Microencapsulated Liquid Crystal Probe

Another style of liquid crystal has been described by Deficis and Priou[13] in which microencapsulated liquid crystals are used for the sensors. The temperature range quoted by the authors is narrower than that above. They also specify smaller dimensions (0.5 mm if the tip is bare and 2 mm if protectively sheathed). The same authors describe a probe which uses the thermal expansion of a liquid as the sensor. The meniscus acts as a reflector with its position and shape being temperature dependent. The quoted temperature range is from -30 to 10°C with a resolution of 0.2 to 1.0°C, depending on the temperature.

Birefringent Crystal Optical Thermometer

This optical thermometer[3,15,16] uses a solid single crystal of lithium tantalate as a sensor and hence avoids the instabilities associated with a liquid crystal mixture. The basic principle is that the indices of refraction along the optic axes of the crystal differ and this difference is temperature dependent. Following a standard optical treatment[15,17], the measured signal, I, which is proportional to the intensity of light passing through a polarizer-crystal-analyzer sandwich, is given by:

$$I = I_o \left\{1 - \alpha \sin^2 \beta(T - \theta)\right\}$$

where

$$\beta(T - \theta) = \frac{\pi}{\lambda} h \, (n'' - n') \, .$$

The thickness of the crystal is h, the wavelength of the sensing light is λ, the indices of the refraction are n" and n', T is the temperature and I_o, α β and θ constants determined from a calibration. The constant I_o depends on the intensity of the light source, the sensitivity of the photodetector,

and their associated electronics. The other constants are defined principally by the initial construction of the tip. The response function I(T) is sinusoidal, but the temperature range between successive extrema can be made sufficiently broad (for example 40°C) by choosing a thin crystal and the proper wavelength of sensing light that no ambiguity exists. A sensor is constructed by plating one side of the crystal with a dielectric mirror and cementing a polarizing film to the other side. The sensor (crystal plus polarizer) then is cemented onto the end of an optical fiber light conduit. A crystal of lithium tantalate 0.1 mm thick will result in a thermometer with a useful temperature range of 18 to 49°C and a resolution of better than 0.1°C.

The initial prototype used optics and electronics similar to those of the liquid crystal thermometer. While the solid crystal sensor is stable, the light emitted by the LED and the sensitivity of the photodiode are not. Thus a new prototype has been constructed which provides for a reference signal from the LED directly to the photodiode. More sophisticated electronics are required to sample both the signal from the sensor and from the reference and then to compute the ratio. (This is equivalent to dividing the expression for I(T) by I_o.) The advantage of this probe is that it is much more stable than the liquid crystal device and can be miniaturized. The present probe has a 1 mm diameter, but construction of smaller sensors will be attempted soon. The important disadvantage is that only one prototype exists at the time of writing.

Optical Etalon Sensor

An etalon is an optical flat coated on both sides to form a resonant optical cavity. Light striking the etalon is reflected from both surfaces and for appropriate wavelengths, destructive interference produces a null in the net reflected intensity. The thickness of the etalon varies due to thermal expansion and, hence, the resonant wavelength will vary also. The resonant wavelength can be measured by varying the incident wavelengths with a tunable Fabry-Perot interferometer, and noting the null in the reflected signal. The technique[18] has the distinct advantage of no longer calibrating the analog

intensity of the reflected light as a function of temperature. Consequently, many sources of error are eliminated. The range and sensitivity depend on the precision with which the null can be resolved by the monochrometer source and the thermal expansion coefficient and thickness of the etalon. One of the initial prototypes was tested from 22° to 70°C (expected range was 154°C) and resulted in a resolution of 0.5°C. The sensor was made from 0.145 mm thick crown glass. Another prototype made from fused silica (3.2 mm thick) had a range of 11.1°C and a sensitivity of 0.05°C. The chief disadvantage is that the measuring electronics appear to be more expensive, and again, the device is not ready for distribution.

Christensen[19] also has constructed a prototype thermometer which uses the semiconducting absorption edge of a crystal of GaAs as a sensor. The measurement system would be similar to that used in the liquid crystal or birefringent crystal probes. This probe also looks quite promising, but is still in its early stages.

Thermistor Sensor

Two other thermometer probes[23] are based upon thermistor sensors. In these cases, the thermometric characteristics are reasonably well understood or at least familiar. Both thermometer developments capitalize on the ability to control the power absorption in the leads and, hence, match the probe properties to those of the material (tissue) to be measured. This is an advantage in that the probe will not act as either a heat source or sink and so, in some cases, would not have to be made quite as small and fragile. The thermistor resistance is determined using conventional four-terminal techniques in order to eliminate the substantial lead resistance (of the order of megohms). Care must be taken to minimize the noise in circuits with such large impedances and to avoid current leakages which would affect the accuracy. Nevertheless, these are manageable. The principal difference between the two developments is in the manner of construction, especially in relation to the leads.

Bowman[20] used carbon-impregnated PTFE leads which are cut from sheet material. Each insulated lead is attached to the thermistor and four are fed

through a 1 mm outer diameter plastic tube. Larsen, *et al*[22,23], have taken advantage of thin film and integrated microcircuit technology to construct small, glass encapsulated probes. Both systems have been tested thermographically to determine the degree and significance of both electromagnetic heating and field perturbation.

Viscometric Sensors

Chen, *et al*[24], have proposed the use of the temperature dependence of the viscosity of a fluid as a probe. The viscosity is proportional to the pressure difference that can be sustained across an orifice. This pressure difference, as measured across the dielectric tubing leads, is then the parameter measured and calibrated as a function of the temperature of the fluid at the orifice. The net fluid transport can be kept negligibly small for sufficiently small orifices. The authors indicate that a wide variety of working fluids with differing fluid and dielectric properties can be used, and the system could be operated open-ended in which body fluids could be used. The device is in its early development stages, however, and time will be required to establish an accurate and stable measurement system.

CALIBRATION FACILITIES

Various biological studies, such as hyperthermia for cancer therapy, require that temperatures be recorded to 0.1 C. In some cases, this is more stringent than can be achieved at present, but it represents a realistic goal. However, interchangeable, direct-reading systems with this accuracy do not exist and it is quite expensive to purchase individual calibrations for all the practical probes to be used. Furthermore, both the probes and the measuring electronics systems are subject to drift with time. Thus, a thermometer calibration facility is essential as part of the physical support for research involving heating and thermal monitoring.

The first requirement of a calibration facility is the presence of at least one, preferably three, stable thermometers which have been calibrated absolutely to 0.02°C. This accuracy limit provides sufficient reserve that calibration errors which are propagated into practical measurements will not

be significant. Furthermore, it permits monitoring of the drift characteristics of the thermometers at levels below those which are biologically significant. Standard laboratory quality precision mercury-in-glass thermometers are quite inexpensive and satisfy these stability and accuracy requirements. Wise[25] at NBS has prepared a very useful monograph on their use and the care which is necessary to obtain this accuracy.

Other types of standard thermometers include specially-designed and tested standard thermistors, industrial platinum resistance devices, the acoustic quartz thermometer and finally, the standard platinum resistance thermometer (SPRT) which is the defined interpolation instrument for the International Practical Temperature Scale of 1968 (IPTS-68)[26]. We are using a standard thermistor thermometer principally because it is compatible with other instrumentation in our laboratory. In checks in an ice point cell, this thermometer has remained stable for a year to better than 0.002°C, which is our limit of resolution.

The second requirement of a calibration laboratory is to have a means of producing several stable temperatures for calibrating the practical thermometer against the standards. A well-stirred liquid bath is most commonly used. If the temperature of the bath fluctuates either spatially or temporally, the indications of the small probes (short time constants) will vary more than will those of more massive standard thermometers (long time constants). We have constructed a large aluminum calibration block which averages out these variations and permits calibrations of the order of a few millidegrees Celsius while the bath fluctuates by a few tenths of a degree. We also have used a similar block insulated with polystyrene and temperature-controlled electrically to calibrate probes to better than 0.01°C.

An interesting alternative to temperature-regulated blocks or baths is the use of thermodynamic fixed points. The most familiar is the ice point[25]. Distilled water should be used for both the liquid and to make the ice. The major pitfall in constructing an ice bath is insuring the water level is low enough that the mass of crushed ice does not float. This leads to thermal stratification and increased temperatures (~0.5°C) near the bottom of the cell. Recently Sostman[27,28] as well as Mangum[29] and Thornton[30] have described

the use of the melting point of gallium as a fixed point (29.77°C). The National Bureau of Standards (NBS) is selling gallium-fixed point cells (SRM 1968), under their Standard Reference Materials program. Magin and Statler[31] have been studying the dissociation temperatures of hydrated salts for use as fixed points. They indicate that eventually a collection of these will be described with temperatures spaced about 10°C apart. In particular, they suggest sodium sulphate (32.37°C) as one and sodium thiosulphate (48.04°C) as another.

Several sources of error exist in thermometric measurements. One, for which we have recent data[4], arises from heat conduction along the shaft of a needle-mounted thermistor. The temperatures of water flowing through two plastic tubes was monitored with thermistors. A needle probe was passed through one tube at 23.7°C, through insulation and into the second tube at 41.75°C. The difference between the indicated needle temperature and the actual temperature of the warm tube was plotted as a function of the depth of insertion. For the error in the indicated reading to be less than 0.1°C, the insertion depth must be 3 to 4 mm, as measured from the tip. This is the case for flowing water. The error in a still mass (such as tissues) would be greater and also much harder to evaluate. It would depend upon the thermal conductivity and heat capacity of the surrounding mass. Robinson, *et al*[32] have looked at this error from the viewpoint of apparent temperature asymmetries caused by the insertion of a needle probe into a heated mouse tumor.

THERMOGRAPHY

In recent years, scanning infrared thermographic cameras have been employed for observing and measuring thermal variations across exposed surfaces. Guy[1,33] initiated their use in conjunction with tissue equivalent electromagnetic phantom materials in studies concerned with power absorption properties in biological media. The effects of antenna and subject geometries, of heterogenic electromagnetic properties of tissues, of interfaces between electromagnetically discontinuous materials and of the frequency of the radiation are graphically portrayed by this method. Furthermore, the thermal artifacts which can result from inserting conductive probes into samples in strong

electromagnetic fields can be observed. Studies such as these added strong emphasis to the development of the probes discussed in the preceding section.

Thermography is also useful for monitoring surface temperatures of tissues subjected to electromagnetic heating when the antenna or electrode configuration leaves part of the surface exposed. Observation of temperature variations across at least one section of the treatment region is helpful even if that section is not the ideal one. In many heating configurations, hot or cold regions slightly below the surface produce irregularities on the surface as well and so serve as qualitative warnings of difficulties, if not quantitative measures. Skin temperatures in the vicinity of a tumor frequently are the normal tissues that restrict a hyperthermia treatment. Either pain is sensed and the treatment temperature at depth is limited or non-uniformity of heating results in excessive skin temperatures and burns.

In many cases quantitative temperature data is required, rather than just qualitative determinations of thermal irregularities. Some knowledge is necessary of the radiometric characteristics of thermographic cameras such as the wavelength band to which it is sensitive, the minimum detectable temperature, the spatial resolution, the frame rate and the sources of systematic errors. For precise work, each thermographic camera must be calibrated individually. The radiometric characteristics such as emittance and transmittance of the surface to be monitored must be determined as well. Procedures and facilities needed for obtaining this information are discussed in detail in earlier papers[6,7]. Some of the results are summarized here.

Thermographic Camera Calibration

The response, I, of a thermographic camera to a temperature, T, is typically given in units close to degrees Celsius. However, the relationship between the temperature of an object and the radiation it emits, (Planck's distribution if the source is a blackbody) is non-linear and so a linear correspondence between the camera units and actual temperatures can hold only for a narrow range of temperatures. In one thermographic system which was calibrated, the ratio of camera units to temperature units, $\Delta I/\Delta T$ ranged from $0.8/^{o}C$ near $24^{o}C$ to $1.2/^{o}C$ near $37^{o}C$. In other words, if the camera

response units, ΔI, were assumed to be reading directly in degrees Celsius, 20% errors in temperature differences, ΔT, would result near room temperature or near body temperature.

The total camera response i_1 to a specific subject s_1 at temperature T_1 is the sum of the radiation emitted, reflected, and transmitted by the subject:

$$i_1 = \varepsilon_1 \, I(T_1) + \rho_1 \, I(T_a) + \tau_1 \, I(T_b) \quad . \tag{1}$$

Here ε_1, ρ_1, and τ_1 are the emittance, reflectance and transmittance characteristics of the subject and T_1, T_a and T_b are the subject, ambient and background temperatures. The I(T) represents the response of the thermographic camera to radiation which it receives from an ideal blackbody source. The laws of radiometry[34,35] will apply to this function. The characteristics of the source are treated explicitly in this formula. A second object will have a similar response, i_2. The camera is frequently and most accurately used to measure temperature differences between two sources or to measure temperature gradients on a single object; thus, the difference Δi_{12} can be represented as:

$$\Delta i_{12} = i_1 - i_2 = \varepsilon_1 \, [I(T_1) - I(T_2)] + (\varepsilon_1 - \varepsilon_2) \, [I \, (T_2) - I(T_a)] \, . \tag{2}$$

Here we have assumed that the object is sufficiently thick that no radiation from behind the object is transmitted ($\tau_1 = \tau_2 = 0$). We have also set $\rho = 1 - \varepsilon$. This is a familiar expression which involves both conservation of energy for radiation and the Kirchhoff relation which states that the absorption of incident radiation by an object equals the emittance of radiation by that object (under certain restrictions). Some features of this expression must be noted. Only temperature differences are given, such as $I(T_1) - I(T_2)$, so an absolute calibration of the camera is not necessary. Ambient temperature must be recorded in order to account for the radiation that is reflected from the surface. In the derivation of Eq. (2), only diffuse background radiation is permitted. No provision is made for specular reflection of radiation emitted from a nearby localized hot source. If the camera is calibrated, that is, if the function I(T), or more particularly its derivative $\Delta I/\Delta T$, is known,

we can determine $T_1 - T_2$.

The limiting accuracy of the measurements is determined by the minimum detectable temperature plus the magnitude of any systematic errors that may be present. For two systems we have used, the resolvable temperature difference is approximately $0.2^{\circ}C$. One of these systems introduces an error of $+0.2^{\circ}C$ for an object appearing at the edge of the field of view compared to an object of the same temperature appearing in the center. The absolute calibration of another system depends slightly on the distance from the source to the camera.

The calibration of the camera consists of interpreting the camera display, ΔI, as a function of the temperature difference, ΔT. The procedure is to view two black reference sources at temperatures T_1 and T_2 and measure the corresponding difference $\Delta i_{12} = I(T_1) - I(T_2)$. (Set $\varepsilon_1 = \varepsilon_2 = 1.0$ in Eq. 2). In order to eliminate errors associated with the source, it is important that blackbody sources ($\varepsilon = 1.0$) be used.

A few other sources of error must be recognized in measurements with thermographic camera. The first is to verify that the source is large compared to the spatial resolution of the camera. One procedure for testing this is to blacken the knife edges of vernier calipers and place them in front of a hot source. The slit width, for which the apparent temperature difference between ambient and the hot source is one-half the true difference, is a measure of the spatial resolution at the objects distance from the camera. This width, divided by the distance to the camera, gives the spatial resolution in terms of milliradians, typically 1.3 milliradians for the systems we have used. This question has been considered in more detail by Macey and Oliver[36].

Another error can arise from viewing the sources at an oblique angle. Watmough, Fowler and Oliver[37] have shown that for diffusely emitting materials, the error is not significant ($0.1^{\circ}C$) for angles less than 30° but becomes important (several degrees Celsius) for angles greater than 50°. Finally, care must be taken to insure that the camera optics are clean and that no localized hot sources shine on the object surface. Incandescent lights, instrumentation racks or even the observer himself can reflect specularly from the surface of the object and be detected by the camera.

Radiometric Properties of Materials

Knowledge of the infrared properties of materials such as emittance, reflectance, penetration depth and transmittance is important for determinations of the temperature of the object. Reflectance and emittance are related by the expression $\varepsilon = 1 - \rho$, for opaque objects in the absence of specular reflections, so these parameters can be treated together. Penetration depth is a measure of the surface "thickness" of the object. The term transmittance is used in reference to the fraction of incident radiation which penetrates windows placed in front of the object to be measured.

If a sample is not at a uniform temperature, and if, for example, the bulk is warmer than the surface, then a fraction of the radiation emitted from the bulk of the material may be transmitted to the surface, enter the thermographic camera and cause an error in the temperature reading associated with the surface. The depth from which 37% of the emitted thermal radiation reaches the surface is referred to as the penetration depth. A simple experiment was set up to determine maximum limits of the surface "thickness." A thin sample of the material was placed in front of a hot source and was viewed with a thermographic camera. Muscle equivalent electromagnetic phantom material[33] was placed between two thin sheets of polyethylene; the thickness was established by a spacer in the sample holder. (For the case of bone phantom material, the holder was merely a clamp.) The temperature of the sample was that of the ambient air. The signal detected by the camera was compared for the case when the hot source was behind the sample to that after it was removed. No differences were seen for sample thicknesses down to as small as 0.5 mm, the thinnest that was measured.

Occasionally, a plastic window is placed over the source to prevent evaporative or convective cooling. The transmittance of the window then must be determined in order to compensate for infrared radiation absorbed within it. Calculations of these effects are very difficult[38,39] because of the multiple reflections within the window and because of the radiation emitted by the window material. Nevertheless, practical experiments can be performed to evaluate the effective transmittance especially if the transmittance is high ($\tau \sim 0.9$).

The transmittance, τ_ρ, of a film window was determined by covering half of a blackbody source with the film and measuring with the thermographic camera the difference in signal, (Δi), between the two halves. Room temperature was recorded with a mercury-in-glass thermometer, although it could have been found through use of the thermographic camera and the reference source. The equation relating these measurements to the transmittance is:

$$\tau_\rho = 1 - \frac{(\Delta i)}{I(T_1) - I(T_a)} \quad . \tag{3}$$

$I(T_1) - I(T_a)$ is found through use of the camera calibration. The transmittance of a film of polyethylene 0.05 mm thick was found to be 0.90 ± 0.01 for a camera sensitive to the 2-5.6 μm wavelength band. Thus, if the film is used as a window, true temperature differences are about 11% greater than apparent ones.

Equation (2) shows that a temperature difference [or, $I(T_1) - I(T_2)$] on a surface is directly proportional to the emittance of that surface. A direct measurement of the emittance is to compare the amount of radiation emitted by a surface at a given temperature to the radiation of a blackbody source at the same temperature. However, it is difficult to determine the surface temperature. Measurements with a thermometer in the bulk of the material will not give surface temperature because of the presence of steep thermal gradients across the exposed surface. Another approach is to compare the emittance of a surface to the known emittance of a reference material coating half of the surface. The object is placed in an insulated and temperature-controlled oven. When the sample is brought to a given temperature and observed with a thermographic camera, the temperature line profile will exhibit a sharp step which is proportional to the difference in emittance between the bone phantom surface and the reference coating. The emittance of the bone can be calculated from this difference through use of Eq. (2), where $I(T_1) = I(T_2)$,

$$\varepsilon_2 = - \frac{\Delta i_{12}}{I(T_1) - I(T_a)} + \varepsilon_1 \quad . \tag{4}$$

The subscripts 1, 2 and a, refer to reference material, unknown material and ambient. The temperature of the surface can be determined radiometrically by comparison of the blackbody source to the black reference coating. $I(T_1) - I(T_a)$ can be found directly with a second thermographic measurement.

If the thermographic camera has been calibrated and if proper account is taken of the radiometric properties of the source, then according to Eq. (2), reliable temperature measurements can be made within the noise specifications of the instrument.

ACKNOWLEDGEMENTS

Mr. David Cooper assisted with most of the measurements that have taken place in our laboratory. Mr. Charles Snedaker, Mr. R. Dale Hefner and Dr. William Swindell are principals in the refinements of the birefringent crystal thermometer. Dr. Gideon Kantor of the Bureau of Radiological Health, Electromagnetics Branch, collaborated on the thermographic camera calibration. Partial support was provided by grants CA-17343, FDA 03189-76-J and FDA 221-76-0189 (NEG).

REFERENCES

1. C. C. Johnson and A. W. Guy, Proc. IEEE 60, 692 (1972).
2. J. F. Lehman, *et al*, Arch. of Phys. Med. and Rehab., 49, 193 (1968).
3. T. C. Cetas, Proc. Inter. Symp. on Cancer Therapy by Hyperthermia and Radiation. American College of Radiology, Bethesda, Md.(1976).
4. T. C. Cetas and W. G. Connor, "Thermometry Considerations in Localized Hyperthermia." Submitted to Medical Physics 1977.
5. T. C. Cetas, W. G. Connor, and M. L. M. Boone, Proc. Inter. Symp. on Cancer Therapy by Hyperthermia and Radiation, Essen, (1977).
6. T. C. Cetas, "Practical Thermometry with a Thermographic Camera: Calibration, Transmittance and Emittance Measurements." Rev. Sci. Instrum. (In Press).
7. T. C. Cetas and G. Kantor, Proc. Symp. on Biological Effects and Measurements of RF/Microwaves, Bureau of Radiological Health, Rockville, Md., (1977).
8. T. C. Rozzell, *et al*, J. Microwave Power 9, 241 (1974).
9. C. C. Johnson, *et al*, Ann, New York Acad. Sci. 247, 527 (1975).
10. C. C. Johnson, O. P. Gandhi, T. C. Rozzell, Microwave J. 18, 55 (1975).
11. Ramal, Inc., P. O. Box 275, Sandy, Utah 84070.
12. G. K. Livingston, *et al*, in *Biological Effects of Electromagnetic Waves*, Proc.1975 USNC/URSI Symposium. HEW Publication (FDA) 77-8011.
13. A. Deficis and A. Priou, J. Microwave Power 11, 148 (1976).
14. A. Deficis and A. Priou, Microwave J. 20, 55 (1977).
15. T. C. Cetas, in *Biological Effects of Electromagnetic Waves*, Proc. 1975 USNC/URSI Symposium. HEW Publication (FDA) 77-8011.
16. T. C. Cetas, *et al*, in Proc. 1976 USNC/URSI Meeting on Biological Effects of Electromagnetic Waves, Amherst, Mass.
17. M. Born and E. Wolfe, *Principles of Optics*, Fourth Edition, Oxford, Pergammon, 1970, pp. 694-696.
18. D. A. Christensen, Proc. 1975 USNC/URSI Meeting on Biological Effects of Electromagnetic Waves, Boulder, Col.
19. D. A. Christensen, Proc. 1977 IEEE-MTTS International Microwave Symposium San Diego, Cal.
20. R. R. Bowman, IEEE Trans. MTT-24, 43 (1976).

21. R. R. Bowman, Proc. 1975 USNC/URSI Meeting on Biological Effects of Electromagnetic Waves, Boulder, Colo.

22. L. E. Larsen, R. A. Moore, and J. Acevedo, IEEE Trans. MTT-22, 438 (1974).

23. L. E. Larsen, *et al*, Proc. 1976 USNC/URSI Meeting on Biological Effects of Electromagnetic Waves, Amherst, Mass.

24. C. A. Cain, *et al*, Proc. of the Workshop on the Physical Basis of Electromagnetic Interactions with Biological Systems, College Park, Md. (1977).

25. J. A. Wise, NBS Monograph 150, U. S. Government Printing Office. (1976).

26. International Practical Temperature Scale of 1968, Metrologia 5, 35 (1969).

27. H. E. Sostman, Clin. Chem. 23, 725 (1977).

28. H. E. Sostman, Rev. Sci. Instrum. 48, 127 (1977).

29. B. W. Mangum, Clin. Chem. 23, 711 (1977).

30. D. D. Thornton, Clin. Chem. 23, 719 (1977).

31. R. L. Magin and J. A. Statler, Personal Communication.

32. J. E. Robinson, D. McCulloch and E. A. Edelsack, J. Microwave Power 11, 87 (1976).

33. A. W. Guy, IEEE Trans. MTT-19, 205 (1971).

34. J. C. Richmond, in *Mechanical and Thermal Properties of Ceramics*, ed. J. B. Wachtman, NBS Special Publication 303, Superintendent of Documents, U. S. Government Printing Office, Washington, D. C. (1969).

35. W. L. Wolfe and F. E. Nicodemus, in *Handbook of Military Infrared Technology*, ed. W. L. Wolfe, Superintendent of Documents, U. S. Government Printing Office, Washington, D. C. (1965).

36. D. J. Macey and R. Oliver, Phys. in Med. and Biol. 17, 563 (1972).

37. D. J. Watmough, P. W. Fowler and R. Oliver, Phys. in Med. and Biol. 15, 1 (1970).

38. J. D. Klein, in *Proceedings of the Symposium on Thermal Radiation of Solids*, NASA Sp-55, Superintendent of Documents, U. S. Government Printing Office, Washington, D. C. (1965).

39. J. C. Richmond, J. Res. NBS 67C, 217 (1963).

* *

DISCUSSION

What is the spatial resolution of these cameras; how small are the areas being resolved at these temperatures? [Edelsack].

Cetas: As a blackbody, the source becomes smaller. Its image on the detector eventually becomes less than the size of the detector and the temperature reading is not accurate. We define the spatial resolution as equal to the size of an object such that the measured temperature difference between the object and its background is half the true difference. This was about 1.3 milliradians for the cameras I used. In other words, a source 1.3 millimeters wide, one meter from the camera would show a temperature error of 50 percent. To make an accurate temperature measurement one meter from the camera, you would need an object about three times that, or four millimeters wide.

Is it possible to do the thermographic measurements at other wavelengths? [Illinger].

Cetas: The only commercially available cameras that I am familiar with use either InSb detectors (2 to 5.6 μm wavelength band) or HgCdTe detectors (8-14 μm). Pyroelectric detectors are under development, but they are not available yet for these purposes.

What is the accuracy of the commercially available liquid crystal thermometer? [Mangum].

A tenth of a degree, approximately. [Rozzell].

Over a long or short time? [Mangum].

Over several hours. [Rozzell].

NON-PERTURBING MICROPROBES FOR MEASUREMENTS IN ELECTROMAGNETIC FIELDS

A. Deficis and A. Priou

Microwave Department, ONERA - CERT
Toulouse, France

ABSTRACT

A new generation of non-interfering microprobes is under development. It consists of dielectric microthermometers, named the M.T.D. probes; their specific temperature range cover $-40^{\circ}C$ to $+150^{\circ}C$ in several steps. The introduced perturbation is very low, less than 0.1 db whatever the frequency range. The M.T.D. probe's medical and industrial applications are widespread and significant.

INTRODUCTION

The use of microwave energy could solve a certain number of problems pertaining to the fields of industrial processes or of medical applications with a saving of energy. It is therefore necessary to study exactly the conditions for using microwave energy and also the means to best couple this energy into materials. Research, in every domain, is being carried out on microwave irradiator design, but it seems very difficult to define a suitable optimum irradiator if dosimetry sensors are not available. These sensors must be "non-interfering probes" with respect to electromagnetic waves.

Two main problems are met therefore: The first relative to the knowledge of power density or temperature gradients in microwave irradiated material, according to purpose, the respective temperature ranges could be between $-50^{\circ}C$ to $+150^{\circ}C$ for industrial applications, and from 20° to $45^{\circ}C$ for room and body temperature range in which we find the studies on biological effects; The second concerns the measurement of fields or power in an unloaded microwave oven, or in an oven loaded with the material to be heated, or in free space when studying biological effects.

Our department has studied both problems. In the first case, our studies have progressed well, but, in the second case, we are only now making the first microwave energy studies for medical applications (cancer therapy, diathermy, microwave thawing of organs, etc...). This paper is a synthesis of the results we obtained in designing these probes and in finding their possible applications.

NON-INTERFERING PROBES

We first studied the feasibility of realizing dielectric microprobes which are non-interfering with electromagnetic waves. Two types of probes were then defined; The first operating exclusively in the range of $10^{\circ}C$ to $40^{\circ}C$, named the cholesterical crystal probe; The second pertaining to industrial application of microwaves which would cover a temperature range of $-40^{\circ}C$ to $+150^{\circ}C$ in steps of $40^{\circ}C$, and also the range of $20^{\circ}C$ to $40^{\circ}C$. The

name of this probe is the dielectric microthermometer (or M.T.D.) and is essentially a French invention. Each probe includes a head (different according to the temperature range or density to be measured) containing the essential thermosensitive dielectric material, dielectric light conductors (optical fiber set) and associated electronics system.

Cholesterical Crystal Probes

This first microprobe, still called "cholesteric crystal[1-4] and optical fibers probe" has been the subject of several papers. Without further explanation we comment that: Such probes relate only to the measurement of temperature in narrow band in the range of 10 to 40°C, and, therefore, this kind of probe is to be devoted to the study of biological effects and cannot give any information in lower or higher temperature range; the very narrow temperature range of this probe is inherently due to the physical proprieties of the liquid crystal used.

An important propriety of the cholesterical crystal is a very high rotatory power which is variable from one crystal to another. This rotatory power of about 18.000° per mm, varies in amplitude and sign with wavelength and temperature. This very high rotatory power is due to an ordered shifting of the molecular axis of each thin film. Statistically, in these conditions, it seems impossible that such crystal arrangements could again find exactly the same position during a temperature cycle. This explains the main difficulties encountered in designing such probes which need to be recalibrated due to liquid crystal aging and instability[5]. We then obtain microprobes presenting problems in crystal shift variations and hysteresis effect and it is difficult to obtain reliable industrial units. It is for all these reasons that we stopped this activity in France.

M.T.D. Probes[6-7]

This second probe is, in fact, a dielectric microthermometer operating within a range of -40°C to +150°C in steps of 40°C. The principle of the probe operation is based on the reflection of a light beam by a thermodilatable liquid contained in a capillary glass pipe of small dimensions. In the

glass pipe, the liquid forms a concave reflector meniscus whose position and shape vary versus temperature (Figure 1). The quantity of liquid is very small (a few mm^3). Therefore, the probe thermal inertia is low and the temperature readout is rapidly accomplished without any disturbance of the medium.

Accordingly, the head of this probe is composed of a conical glass pipe with, at the end, a small bulb containing the liquid, a dielectric thermodilatable liquid and an optical fiber set lighting up the meniscus. The cone aperture is calculated versus the liquid volume at $0^{\circ}C$ and the sensitivity to be obtained. The head of the probe and the optical fibers are within a thermoretractable sheath.

In a first step, we designed a microprobe working from $-30^{\circ}C$ to $+20^{\circ}C$; we are now able to design microprobes in every range within steps of $40^{\circ}C$ covering the $-40^{\circ}C$ to $+150^{\circ}C$ temperature range. Measurements effected within the ranges 900 to 915 MHz, 2400 to 2500 MHz and 8.2 to 12.4 GHz show that the perturbation caused by the thermometer is very low (less than or equal to 0.1 db) whatever the orientation of the probe in terms of the electric field. Furthermore, the VSWR due to the probe is less than 1.1. The microprobe contribution is therefore negligible and we can say that it does not disturb the electromagnetic waves, being transparent in the microwave spectrum. Figure 2 shows a response curve for one of these probes in the range 5° to $45^{\circ}C$. This device has been the object of a patent registered by ANVAR (ANVAR n° 9211, Deficis probe) and extended to several foreign countries.

Electronic Units

The electronics are similar and relatively simple for each probe described above. In the first step, we used a white light source to light up the dielectric meniscus. The reflected light is collected by a photomultiplier driven by a power supply. The analysis of the reflected light is then done either by recording on a plotter or by any other process. We are using a phototransistor followed by its amplifier as the light receptor. This allows us to try to integrate both the white light source and the phototransistor on the same support and reduce the cost of the device.

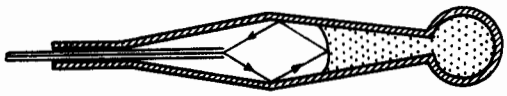


Figure 1. Dielectric Thermometer Probe.

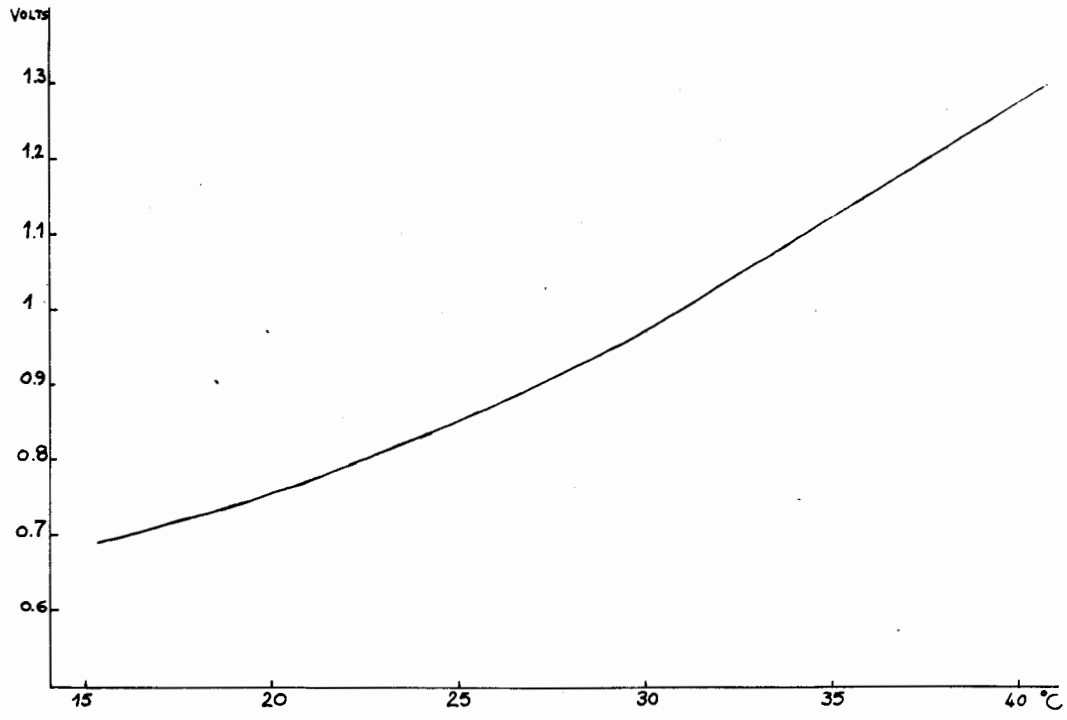


Figure 2. Response Curve Versus Temperature.

The M.T.D. Probe Performance

In experimental tests of the unit operating in the range of -30°C to +20°C, we have obtained records of a microwave thawing process of a chopped beef piece weighing about 2 kilos, then of another of about 50 kilos. Figure 3 shows one of these curves, indicating that we can record continuously the microwave thawing process. This fact is very important in industrial applications as well as in medical applications of microwave energy. By using such probes, we can know exactly where microwave power is deposited in biological materials. We can think of many applications for such probes in dosimetry related to diathermy or cancer therapy process, for example. In all cases, these probes, working alone or cooperatively, can be used for exact temperature mapping during a microwave process.

The principal microthermometer characteristics are presently as follows:

Temperature ranges: -40°C to +150°C by steps of 40°C.
Special series in 10°C to 40°C.
Sensitivity: about 0.5°C, presently.
Response time: < 15 seconds.
Electronics output voltage: 0 to 5 V, (average sensitivity: 200 mV/d°, electronic noise: < 20 mV).
Dimensions:
Probe length: from centimeter to some meter lengths
Probe diameter: 2 mm
Sheath diameter: < 3 mm.
Performances between DC to 12 GHz:
VSWR = 1.1, Insertion loss = 0.1 db.
Presentation: rack: 5/25 3 U.
Analog output with B.N.C. connector.
Possibility of many units driven by microprocessor.

The future developments envisaged in our microwave department in liaison with an industrial firm are the design of microprobes with $\Delta T = 60°C$, 100°C, 200°C respectively with average sensitivities of about $\pm 1.5°C$, $\pm 2.5°C$ and $\pm 5°C$ respectively. Figure 4 shows a photograph of the M.T.D. probe with the electronic unit.

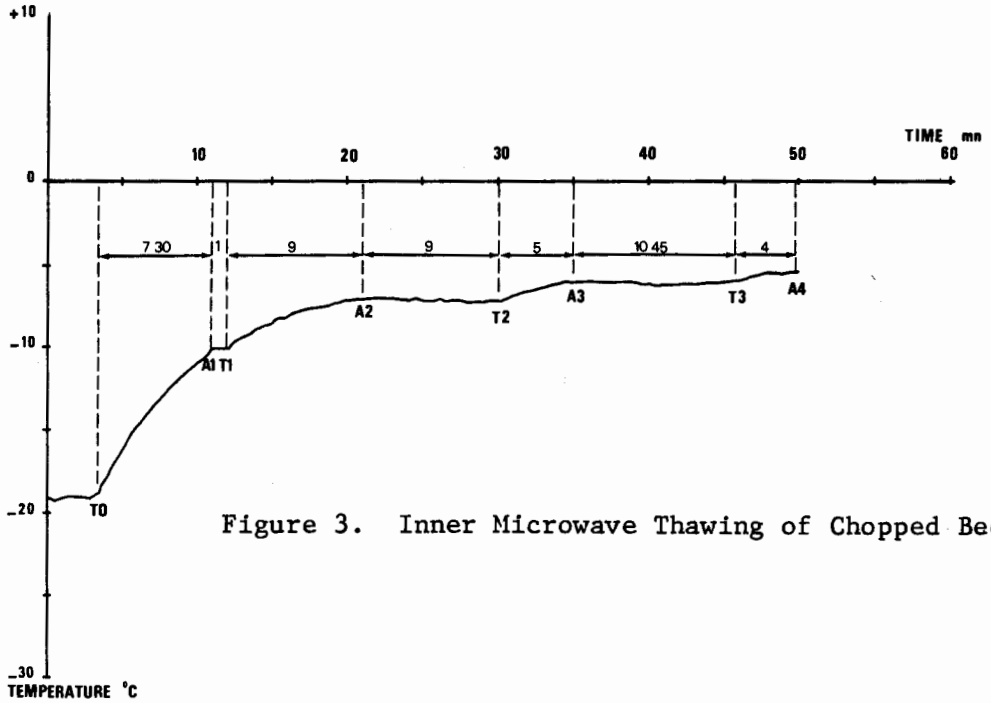


Figure 3. Inner Microwave Thawing of Chopped Beef.

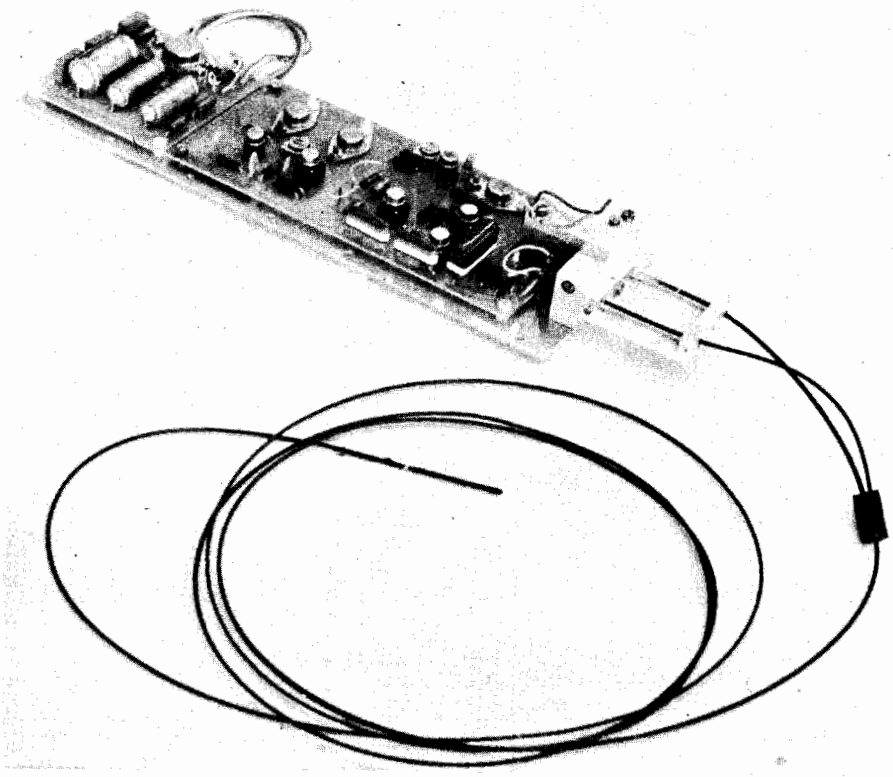


Figure 4. M.T.D. Probe with the Electronic Unit.

PRACTICAL APPLICATIONS OF THE M.T.D. PROBES

Medical Field

We foresee applications from +20°C to 40°C with high sensitivity of ± 0.1°C in the 10°C range, including studies of EM penetration and absorption by biological media, local dosimetry applications such as diathermy and studies of microwave thawing of frozen organs or granylocytes and applications in places where the measurement of the temperature is difficult (small areas, etc...), as well as continuous control and regulation processes of microwave penetration in hyperthermia for cancer therapy and the detection of overheated points.

Industrial Applications

We would also like to remark about the usefulness of such probes. In the temperature range of -40°C to +150°C, it is now possible to control exactly microwave penetration into large pieces of beef, for example, to assist processing simulation (such as thawing simulation), to obtain continuous control and regulation of processes such as pasteurization, sterilization and lyophilization of food products, and to insure a continuous control of distribution of microwave power.

The large range of applications leads us to forecast a very good market and we think that these probes or their successors will become important laboratory and industry tools.

CONCLUSION

We believe that the M.T.D. probes can be considered as the second generation of non-interfering microprobes following the cholesterical crystal probes. They can operate from -40°C to +150°C in steps of 40°C and they can be used in the range of 10° to 40°C with good accuracy. We also believe that we will need considerable effort in the next years to either improve this kind of probe or to develop new types of probes devoted to specific temperature

range measurements. Furthermore, it seems very useful to proceed to design field or power density probes that can be used near a microwave applicator, such as those employed in the medical applications, in the near-field zone.

REFERENCES

1. C. C. Johnson, T. C. Rozzell and O. P. Gandhi, Part I: Microwave Journal, p. 55 (August 1975).
2. A. Deficis, 1975 IEEE MTT International Symposium, Palo Alto, p. 300 (May 1975).
3. A. Deficis, 5th European Microwave Conference Digest, Hamburg (September 1975).
4. A. Deficis and A. Priou, "Non-perturbing Microprobes for Measurement in Electromagnetic Fields" (to be published in Microwave Journal, April 1977).
5. D. Mennie, IEEE Spectrum, p. 4 (January 1977).
6. A. Deficis and A. Priou, IMPI Louvain Digest (1976).
7. A. Deficis and A. Priou, Journées d'Electronique de Toulouse (March 1977).

* *

DISCUSSION

What was the method used to observe the perturbation due to the probe?

Priou: A rectangular guide or coaxial line is used. One measures the perturbation due to the probe when it enters into the wet tissue.

Was that measurement also made with a metallic probe in place instead?

Priou: In that case, with a 0.2 mm diameter, the perturbation is perhaps 3 or 4 db.

What is the diameter of your probe? [Harris].

Priou: Presently the diameters of the probes are from 2 to 3 millimeter.

What is your temperature resolution? What is the smallest ΔT *that I would have to produce for your probe to give me an accurate representation?* [Olsen].

Priou: It depends on the temperature range of the probe.

At what noise level can one determine $0.1^{\circ}C$ *?* [Olsen].

Priou: The noise level is about 30 to 50 milliwatts on top of 3 volts of signal.

THE VISCOMETRIC THERMOMETER

Charles A. Cain, Michael M. Chen
Katherine Loh Lam, and Jeffrey Mullin
University of Illinois, Urbana-Champaign, Illinois

ABSTRACT

A new technique for temperature measurement without artifacts in microwave environments is described. The instrument, called the viscometric thermometer, is based on the variation of fluid viscosity with temperature. The sensing element is simply a flow restriction at the end of the probe containing fluid supply and return lumens. A suitable fluid is pumped through the system at sufficiently low speed that the temperature of the fluid at the sensing tip is in equilibrium with the surrounding media, and the fluid flow is in the viscous (Stoke's flow) regime. If the sensing capillary represents the dominant flow restriction, the pressure difference for a given flow rate is directly proportional to the fluid viscosity at the probe tip and can be calibrated in temperature. Since the viscosity of many fluids is highly temperature dependent, a wide variety of fluids can be used. It may be possible to construct probes which more closely match the electrical properties of tissue, thus rendering the probes non-perturbing, not just non-absorbing. In production the probes could be relatively inexpensive and perhaps even disposable.

INTRODUCTION

The accurate measurement of temperature and power deposition in biological tissues is often essential in research on the biological effects of non-ionizing electromagnetic (EM) radiation. Conventional thermometric methods are not suitable for use in strong EM fields at radiofrequency or microwave frequencies because of either perturbations in the fields caused by metallic components of the sensor and associated instrumentation or by direct heating of the sensor by the incident fields[1]. This problem has seriously hampered research on the biological effects and medical applications of non-ionizing EM fields. Recently, the problem has become even more acute with the beginning of clinical trials of electrically-induced hyperthermia as a cancer therapy.

A number of temperature sensors designed to minimize sensor-EM field interactions have been reported. One method is to adapt a conventional thermometer technique (*e.g.*, thermistors or thermocouples) by the use of high resistance leads and by minimizing electrical loop areas[2,3]. The other method is to use optical fibers to transmit information about temperature-dependent physical properties of some sensing material in the probe tip. Thermometers in the latter category include devices based on temperature-dependent changes in the intensity of light reflected from a liquid crystal[4-7] or upon temperature induced changes of optical rotary power in a liquid crystal[8]. Other optical probes include one based on a temperature-dependent birefringent crystal sensor [$LiTaO_3$][9], an optical etalon[10], and temperature-dependent changes in the optical reflectance of certain semiconductors[11]. Another optical probe is based on changes in intensity of light reflected from a meniscus formed by a thermodilatable fluid in a capillary[12]. The relatively large number of attempts to produce truly non-perturbing temperature probes is illustrative of both the need for such a device and the frustration in not having a suitable instrument available to researchers in the area.

Adaptations of conventional techniques have certain limitations. Since conducting leads are necessary, it is impossible to completely eliminate

artifacts due to probe field interactions. Optical thermometers have the advantage of being non-absorbing and relatively non-perturbing in an electromagnetic environment. However, the liquid crystal versions suffer from drift problems due to instability of the liquid crystal sensor. Such probes require periodic calibration to maintain acceptable accuracy. In addition, they are not thermally rugged, and care must be taken not to cycle them through large temperature changes in either direction beyond their limited operating range. However, since all optical probes are constrained to use optical fibers, they share the disadvantage that their dielectric and thermal properties will, in general, be different from the surrounding media. Hence, in principle, they will not be truly nonperturbing in an EM environment.

The viscometric thermometer, discussed in this paper, may have a number of advantages for temperature measurements in EM environments. As we shall see, the technique imposes surprisingly few constraints on probe material and geometric configuration.

THE VISCOMETRIC THERMOMETER

Description

A schematic representation of a typical viscometric probe is shown in Fig. 1. The thermometer is based on the measurement of temperature-dependent viscosity of a fluid flowing through a small sensing capillary in the probe tip. Since the change in viscosity of most liquids is in the range of percents per degree Celsius, very high temperature sensitivities are possible. The viscosities of a number of fluids at different temperatures are given in Table I.

TABLE I

Temperature-Dependence of Viscosity for Several Common Liquids (Ns/m^2)

^{o}C	Water	Castor Oil	Petroleum Oil (Heavy)	Ethyl Alcohol
20	1.002×10^{-3}	0.986	0.799	1.200×10^{-3}
30	0.798×10^{-3}	0.451	-----	1.003×10^{-3}
40	0.653×10^{-3}	0.231	0.210	0.834×10^{-3}

A large number of pumping and measuring arrangements can be made to measure the flow resistance and, indirectly, the viscosity in the probe tip. These include: a constant flow pump with measurements of the pressure difference; a constant pressure-rise pump with measurements of flow; and systems representing intermediaries of these two examples. In analogy to electrical systems, either unidirectional or alternating flow could be used. The pressure and/or flow readout could also be either mechanical (*e.g.*, using bellows or Bourdon gages) or electrical (employing suitable transducers and signal processing components). The pumping and measuring devices are connected to the probe through flexible tubes much like the flexible electrical leads used in thermistor or resistance thermometer circuits. A schematic of a typical pumping and measuring arrangement is shown in Fig. 2.

Physical Principles

Viscosity is one of the most stable and reproducible properties of matter. It is immune to mechanical and thermal shock and the presence of electrical fields[13]. These characteristics facilitate the design and construction of stable instruments with high sensitivity. Furthermore, since the operating principle does not involve a peculiar property of a special material, but is based on a basic property shared by many fluids, the working fluid can be chosen to fit special needs. Note that aside from dimensional stability and biocompatability, the properties of the solid material forming the body of the probe have very little influence on the operation of the device.

Viscosity is a measure of a fluid's resistance to continuous shear strain. As a macroscopic property, viscosity is a function of the molecular structure of a liquid and, under normal pressures, is generally insensitive to environmental conditions except temperature. Although the prediction of viscosity from molecular physics is still not a reality, the general forms of the temperature dependence are well known and in agreement with current qualitative understanding of the physics of liquids[13].

In general, the pressure drop of fluids flowing in conduits depends on both inertial and viscous effects. It is known, however, that the inertial influence is negligible when the Reynolds number is small. The latter, a

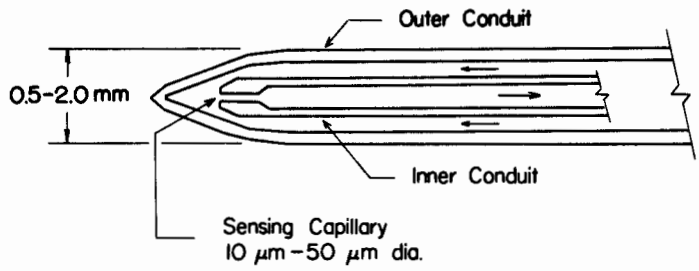


Figure 1. A Typical Viscometric Thermometer Probe.

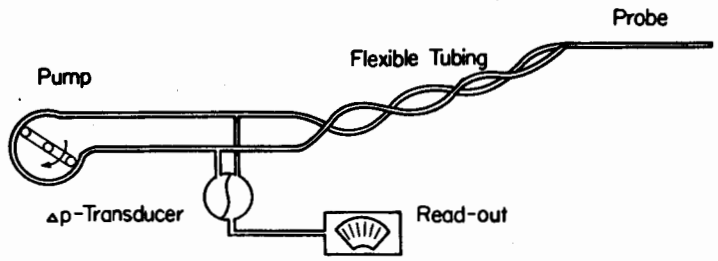


Figure 2. Schematic of a Viscometric Thermometer System Including Pumping and Measuring Arrangements.

dimensionless measure of the ratio of inertial forces to viscous forces, is defined as

$$Re = \frac{\rho u D}{\mu} \tag{1}$$

where ρ denotes the fluid density, μ the viscosity, u the mean velocity, and D, a characteristic dimension of the containing vessel, the capillary diameter. The magnitude of the marginal Reynolds number which permits the neglect of inertial effects depends on the flow configuration. For steady flow in straight tubes, it is as high as 2,000. For conduits with rapid diameter changes, it could be unity or below. When the neglect of inertial effects can be justified on this basis, the partial differential equation governing the flow of fluids in conduits with only slowly changing cross sections can be integrated to yield the following relationship[14] for the pressure drop Δp between two points, x_1 and x_2:

$$\Delta p = 128\pi^{-1} \mu Q \int_{x_1}^{x_2} D^{-4} \, dx \, . \tag{2}$$

It is clear that, for straight conduits with a constant diameter, Eq. (2) reduces to the following simple formula for flow resistance

$$R = \frac{\Delta p}{Q} = 128\pi^{-1} L \mu D^{-4} \tag{3}$$

where L and D denote the length and diameter of the sensing capillary, respectively.

The factor D^{-4} appearing in the integrand indicates that for a conduit with varying cross sections, it is the length with the smallest cross section which makes the greatest contribution to the total pressure drop. It is this property which makes it possible for the viscometric thermometer to sense only the viscosity at the probe tip. If the diameter of the sensing capillary is much smaller than the diameter (or equivalent diameter as the case may be) of the connecting conduits, then the latter would make essentially no contribution to the total pressure drop. Accordingly, the viscosity and temperature of the fluid in the connecting conduits have no influence on the measurement. In essence, the fluid in the conduits serves merely as the signal transmitting

media. Operation of the viscometric thermometer is thus analogous to the electrical resistance thermometer. The main difference is that a viscous fluid, rather than electrical current, is the flowing medium.

A Practical Example

Preliminary studies have indicated that for optimal results L and D should be of the order of 1 mm and 10 μm respectively. Because of the D^{-4} dependence, the supply and return conduits, with much larger flow passages, would have negligible resistances. This consideration of the pressure drop in the connecting conduits is of practical importance. In many applications, it is necessary to locate the pumping and measuring devices away from the probe. Long flexible tubing must be used to connect them. In addition, the tubes in the probe body, although short, must also be considered since it is generally desirable to make them as small as possible. If the pressure drop of any of these conduits constitutes a measurable fraction of the total pressure drop, then the total pressure drop would become sensitive to the temperature of the connecting tubes. In order to have a quantitative appreciation for the relative pressure drops involved, a specific example will be considered. The assumed parameters and results are shown in Table II.

Table II

Relative Pressure Drops for Typical Conduits

	Capillary in Probe Tip	Conduits in Probe Stem	External Conduits
Assumed Parameters:			
Diameter	10 μm	300 μm	1 mm
Length	1 mm	10 cm	10 m
Results			
Pressure Drop (relative to capillary)	1	10^{-4}	10^{-4}

The dimensions assumed are quite conservative and representative of those to be encountered in potential applications. It can be seen that the conduits can be constructed with practically negligible influence on the accuracy of the instrument.

PROTOTYPES

Several prototypes of the viscometric thermometer probes were constructed and tested to verify the practicality of the concept. These consisted of both rigid probes and flexible probes. The rigid probes were made of concentric glass tubes with sensing capillary diameters ranging from 10 to 50μm. Probe outer diameters ranged from 1.5 to 2.0mm and were approximately 50mm long. The flexible probes were made of commercial polyethylene tubing with a glass microcapillary fitted to the end of the inner tubing. The finished probe had a uniform outer diameter of 1.2mm. The probes were driven by a constant-flow fluid supply. A differential pressure transducer was used to measure the pressure drop. A number of fluids, including distilled water, castor oil, mineral oil, and ethylene glycol, were used as the sensing media. Flow rates varied from 3×10^{-4} to 2×10^{-3} ml/s. Note that compared to water, mineral oil does not absorb microwave energy whereas ethylene glycol is highly absorbing. A mixture of two or three fluids could be used to obtain any desired loss characteristics.

For calibration, the probe was taped to a mercury thermometer and both were immersed in a stirred water bath as the water temperature was increased or decreased slowly at a rate of approximately 10 to 20°C/hr. A typical calibration curve is shown in Fig. 3. It should be pointed out that the sensitivity of the instrument, measured in units of pressure change per degree temperature change, can be varied over very wide ranges depending on the capillary diameter, the working fluid, and the flow rate. Much greater or smaller sensitivities than those shown in Fig. 3 can be easily obtained by choosing the appropriate operating parameters. The sensitivity shown, however, suffices to indicate that the signal levels are more than adequate to effect accurate, noise-free readout. Using a standard coupler for medical pressure transducers, outputs of the order of 10^{-1}V/°C were obtained. The small amount of scatter in the data was to be attributable to the inconstancy of the fluid pumping system employed. Further testing employing improved pumping and readout procedures is currently in progress.

To test the time response, the probe was removed from one bath and quickly

inserted into another bath at a different temperature. The observed exponential time constants were about two seconds. This corresponds roughly to the order of magnitude of the thermal time constant for the equilibrium of the probe with surrounding temperatures. In other words, with proper hydraulic systems, the time response of the viscometric thermometer is not limited by the hydraulic processes involved. Note that the thermal time constant of all probes of the same diameter are essentially the same.

DISCUSSION

The above results demonstrate that the viscometric thermometer can be a useful instrument for temperature measurement in electromagnetic wave environments such as those encountered in microwave or radiofrequency induced hyperthermia. The concept appears to have a number of advantages over other existing temperature measurement techniques, including:

a) Stability: The viscometric thermometer is thermally and mechanically rugged. Since the viscosity of the fluids is a basic materials property, the calibration of the viscometric thermometer is not affected by exposure to temperature extremes. Thus, frequent recalibration is not necessary. In addition, the probes should be autoclavable. This is of considerable importance in clinical use.

b) Non-perturbing: While many of the existing thermometers are transparent to microwaves, they are not truly non-perturbing in the sense that their dielectric and thermal properties are not identical to those of the surrounding tissue. In contrast, for the viscometric thermometer, the probe body materials and the sensing fluid can be chosen so that their electrical and thermal properties match closely those of the tissue, thus minimizing any electrical and thermal perturbations. In other words, a viscometric thermometer probe of a given size can be made less perturbing than other probes of even smaller sizes.

c) Simplicity: The simplicity of the operating principles of the viscometric thermometer should lead to more reliable and less expensive instruments. Another possible consequence is the potential feasibility of disposable probes which would be valuable for clinical applications.

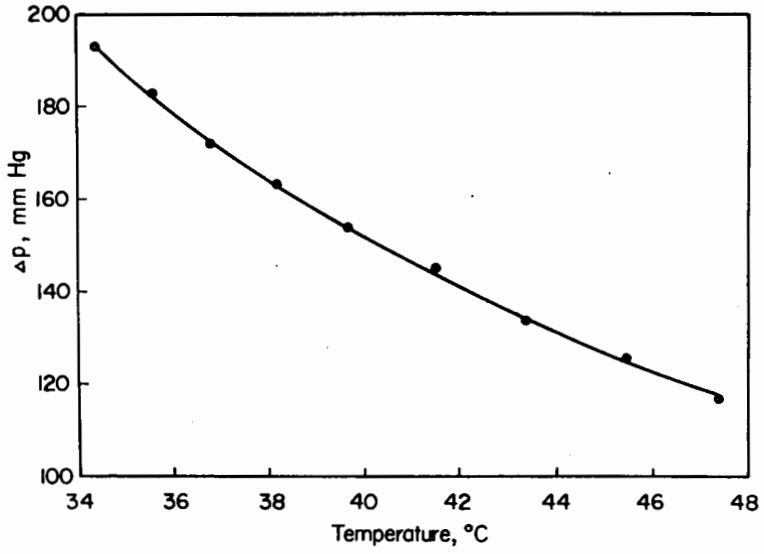


Figure 3. Sample Calibration Curve for a Viscometric Probe.

REFERENCES

1. C. C. Johnson and A. W. Guy, Proc. IEEE 60, 692 (1972).
2. L. E. Larsen, R. A. Moore and J. Acevedo, IEEE Trans. MTT-22, 438 (1974)
3. R. R. Bowman, IEEE Trans. MTT-24, 43 (1976).
4. C. C. Johnson, *et al*, in *Biological Effects on Non-ionizing Radiation*, Ann. New York Acad. Sci., ed. E. Tyler, (1975).
5. T. C. Rozzell, *et al*, J. Microwave Power 9, 241 (1974).
6. C. C. Johnson and T. C. Rozzell, Microwave J., p. 55 (1975).
7. O. P. Gandhi and T. C. Rozzell, Microwave J., p. 58 (1975).
8. C. W. Smith, *et al*, Appl. Phys. Lett. 24, 453 (1974).
9. T. C. Cetas, in *Biological Effects of Electromagnetic Waves*, Vol. II, Selected Papers of the USNC/URSI Annual Meeting, Boulder, Colorado, (1975).
10. D. A. Christensen, Abstracts USNC/URSI Annual Meeting, Boulder, Colorado, (1975).
11. D. A. Christensen, presented at Workshop on Electromagnetics and Cancer, June 1977 MTTS International Microwave Symposium, San Diego, California.
12. A. Deficis and A. Priou, Microwave J., p. 55 (1977).
13. R. Reed and T. Sherwood, in *The Properties of Gases and Liquids*, McGraw-Hill, New York (1958).
14. C. Yeh, *Fluid Mechanics*, McGraw-Hill, New York (1969).

* *

DISCUSSION

In your design equation, you claimed only the viscosity changes with the temperature. What about the probe? [Chou].

Cain: One could also make a thermometer based upon dimensional changes in the probe. For a particular probe, such changes would be reflected in the calibration curve.

What are possible sources of error of your measurement errors? Secondly, how well can you measure your pressure reproducibly? That is, given $\delta P/P$, *what does this incur in terms of* δT? [Cetas].

Cain: I did not give some data that we obtained from the prototype models. Just using fluids that one can get from any chemical store shelf we obtained sensitivities on the order of ten millimeters of mercury per degree Celsius. Although we really have not optimized the design so far, our prototypes certainly do not discourage us. As to some of the sources of error: Obviously, if one dpends on the fact that the flow rate is constant, then one must have some technique for maintaining a constant flow rate. We have tried several ways of doing this. We first tried one of the tubing pumps that revolve very slowly, and also a syringe pump. It turns out that a syringe pump has a time-average flow rate which is quite uniform, but evidently there is some play in the gear systems which can cause considerable measurement error. Another way of obtaining constant flow is to use two flow constrictions in the path. If one constriction is made quite a bit smaller than the other and the smaller constriction is placed in a constant temperature bath and is connected to a high pressure head, then the flow is determined by this reference constriction. Whatever you do out at the larger sensing constriction is not going to make much difference in the flow rate. This is analogous to using a constant current source in a resistance thermometer. I would say that coming up with a good way of getting a constant flow is probably one of the more difficult design problems of the system.

I believe another source of error is the length of the tubes you use. Although the pressure drops over the constriction in proportion to the flow radius, I think the tube length to radius ratio will also have some effect on the sensitivity. [Lin].

Cain: It depends. We are talking about flow constriction on the order of microns.. Whereas, the diameter of the tubes themselves are much larger.

What is the whole conceptual design going from one phase of the instrumentation to another? My concern is this: The sensor is excellent but what about the transition? Where are you going to make the pressure measurements? And how are you going to interpret that pressure as a temperature? That is, I am concerned about the pickup problem. [Lin].

Cain: The output of the pressure transducer can be calibrated as temperature. The pressure transducer can be placed at the end of the conduits away from the sensor.

Shouldn't you be concerned about the possible direct pickup by the wires that are used to measure the pressure? [Lin].

Cain: Well, all of these probes that we have considered have the same problem in the sense that someplace some electronics is introduced. The problems would not be any more difficult here than there.

What is the response time of this probe? [Priou].

Cain: This probe has a response time of about two seconds. Of course, response time must be defined in terms of the measurement procedure. Here I mean that if you take two glasses of water at different temperatures and switch the probe from one to another, in a very simple experiment, the thermal time constant is of the order of two seconds. The time constant might be optimized, as I mentioned, by flattening the whole structure so that the contact between the constriction and the fluid whose temperature is being measured is optimized.

In your system, a fluid is being pumped from a source which is at ambient temperature, and then is going through a small orifice. How does the temperature become localized at that orifice when it is bathed, so to speak, in a thermal reservoir? [Bassen].

Cain: I tried to make the point that we are using very small flow rates, on the order of microliters per second. It has to be small because the constriction is small. Moreover, although the first probes that we constructed used continuous flow, one can use an alternating flow, so that one would actually be exchanging a small volume of fluid right at the tip of the probe.

I think that the question is, that one could have an effect on the temperature of the fluid along the pathway until it reaches the constriction. [Rozzell].

Cain: If you are exchanging fluid right at the tip, that fluid does not flow there.

No, but it is thermally connected through the fluid. [Taylor].

Cain: That is a long thermal path.

But shouldn't the temperature be only that of the medium being sensed? [Rozzell].

Cain: If the flow rate is such that the fluid has a chance to reach thermal equilibrium, it will work. As I said, there are ways to design the probe so that can be achieved.

I have an idea about the use of physiological saline as the fluid and I wondered if it has occurred to you. With that fluid one could greatly simplify the device; instead of having a closed system, one could have an open system which would simply be a cathode with a tiny hole in the end. [Friend].

Cain: We have in fact tried that. If you wish to measure temperature in a fluid where it is feasible to inject physiological saline, yes, one could do it that way.

If you are injecting microliters per second, it would usually have no effect on it. [Friend].

Cain: Although I illustrated the operation as a closed loop, one can operate open loop. In the latter case, the fluid would flow through and out. If you have a bidirectional flow, you do not even have that problem, hwoever.

If you had a bidirectional flow you would be sampling the fluid inside the animal. [Friend].

MICROWAVE THERMOGRAPHY: PHYSICAL PRINCIPLES AND DIAGNOSTIC APPLICATIONS

Philip C. Myers and Alan H. Barrett

Department of Physics and Research Laboratory of Electronics
Massachusetts Institute of Technology, Cambridge, Mass.

ABSTRACT

Microwave thermography is the application of the techniques of microwave radiometry to the mapping of microwave emission from human tissue. This emission has a thermal spectrum for frequencies $\gtrsim$10 kHz. The relative transparency of human tissue at microwave frequencies permits sensing of the average temperature within a volume, extending to depths 1-5 cm, depending on frequency and tissue type. Receiver temperature sensitivity is of order $0.1^{\circ}C$. Lateral resolution is of order 1 cm^2, and depends on depth, frequency, and antenna aperture size. Frequency-dependent tradeoffs exist between lateral resolution and depth resolution, and between temperature sensitivity and depth resolution. Microwave thermography is similar to infrared thermography in its noninvasive detection of tissue temperature, but is different in its coarser resolution and in its ability to sense the temperature of deeper tissue. Potential applications in diagnostic medicine require the presence of temperature variation $\simeq 1^{\circ}C$ on spatial scales $\simeq$1 cm, with favorable tissue geometry. These include detection of cancerous tumors, peripheral vascular disease, incipient strokes, and local inflammations. Clinical trials of application to breast cancer detection indicate true-positive and true-negative rates $\simeq$70%, which are comparable to the rates for infrared thermography. Combined microwave and infrared true-positive rates are $\simeq$90%, giving performance comparable to mammography but with no associated risk to the patient.

INTRODUCTION

Recently, several investigations of microwave emission from human tissue have been made. These show that: the emission spectrum of live human tissue appears thermal over the frequency range 10^4-10^{10} Hz[1,2]; at centimeter wavelengths microwave radiometry is capable of detecting variations in subsurface temperature[3-8]; and this technique may have diagnostic value in detection of breast cancer and other pathological conditions with associated thermal structure[9,10].

We have called this measurement technique microwave thermography in analogy with the well-known infrared method. In this report we describe the relevant physical principles, instrumentation, and initial results of a clinical study of breast cancer detection.

PHYSICAL PRINCIPLES

Microwave thermography is possible because: human tissue emits thermal radiation, whose intensity at microwave frequencies is proportional to tissue temperature; several medical problems, including cancer and vascular occlusions, are accompanied by local changes in temperature of order 1° C; microwave radiation can penetrate human tissue for e^{-1} distances of several cm; and present-day radiometers can easily detect intensity changes corresponding to emitter temperature changes of less than 1° C. The underlying physics is, therefore, the physics of thermal radiation, and its transfer in a lossy, inhomogeneous medium. In recent years, attention has focussed on the possibility of nonthermal effects of absorbed electromagnetic radiation, and to a lesser degree on the possibility of nonthermal mechanisms of emission by biological tissue. However, there is no evidence that nonthermal mechanisms play any role in the measurements we shall describe; we shall therefore discuss thermal emission only.

Thermal Radiation

All media with absolute temperature $T > 0^{\circ}$ K emit electromagnetic radiation toward, and absorb electromagnetic radiation from their surroundings. This thermal emission is a result of the accelerations experienced by individual charges in the course of their thermal motions. The specific intensity I of this thermal radiation is given by Planck's law:

$$I(\nu,T) = \frac{2h\nu^3}{c^2} \left(e^{h\nu/kT} - 1\right)^{-1} \varepsilon(\nu) \ . \qquad (1)$$

Here ν is the frequency, T is the temperature of the medium, and h, c, and k are, respectively, Planck's constant, the speed of light, and Boltzmann's constant. $I(\nu,T)$ is the emitted power passing through a unit area, into a unit solid angle about a particular direction, in a unit interval of frequency about ν. The emissivity, $\varepsilon(\nu)$, is a dimensionless parameter which depends on the dielectric properties of the emitting and receiving media. A 'black body' or perfect emitter has $\varepsilon = 1$. For radiation by human skin into air at a 10-μm wavelength, $\varepsilon \simeq 1$. For radiation by skin and muscle into air at a microwave frequency of 3 GHz (10-cm) wavelength, $\varepsilon \simeq 0.5$.

Figure 1 shows the intensity spectrum of black-body emission for $T = 100^{\circ}$ K and $T = 1000^{\circ}$ K. At human body temperature $T = 300^{\circ}$ K, maximum intensity occurs at a wavelength $\lambda = 10$ μm. This has led to the operation of infrared thermographs at wavelengths near 10 μm. At a typical microwave frequency of 3 GHz ($\lambda = 10$ cm), I is reduced by a factor of $\simeq 10^8$ from its maximum; but microwave radiometers, developed primarily for radio astronomy, can easily detect radiation with this intensity.

At microwave frequencies, $h\nu \ll kT$, one may expand the exponential in Eq. (1) to obtain the Rayleigh-Jeans law,

$$I(\nu,T) = \frac{2kT\nu^2}{c^2} \varepsilon(\nu) \ . \qquad (2)$$

Thus, at microwave frequencies, the emitted power is proportional to the temperature of the emitting material. If one takes $\varepsilon = 1$, then Eq. (2) defines the *brightness temperature*, T_B, of an emitter.

$$T_B \equiv \frac{c^2}{2kT\nu^2} \; I(\nu,T) \qquad (3)$$

Here $I(\nu,T)$ is the observed specific intensity, regardless of emitter properties. Thus, T_B is the physical temperature which a black body must have to emit the intensity observed at a particular frequency.

Radiative Transfer

In order to relate the emergent brightness temperature at the skin surface to the underlying distribution of tissue temperature, it is necessary to make a specific tissue model and to make several simplifying assumptions. These give a highly idealized picture which should be considered a first approximation only. We model a tumor in breast fat, in accordance with our current clinical work. We assume that the tissue is composed of planar layers of fat, skin, and muscle, with a single inhomogeneity in the fat layer. We ignore all other inhomogeneities such as blood vessels. We ignore all scattering except that which occurs at layer interfaces. We assume that the tissue is isothermal at temperature T, except for the source in the fat layer, which is hotter by ΔT ^{o}C. The background radiation incident on the source has brightness temperature $T_B = T$. The dielectric tissue properties are assumed to be the bulk properties summarized by Johnson and Guy[11].

The radiation transfer depends strongly on the absorption properties of high- and low-water tissue. These properties are shown in Figure 2 in terms of the e^{-1} penetration depth for power. At 3 GHz (free-space wavelength 10 cm) the penetration depth is ≃5 cm (≃1 tissue wavelength) in fat and ≃0.8 cm (≃0.5 tissue wavelengths) in muscle or skin. The penetration depth decreases with increasing frequency. At frequencies above 10 GHz, escaping thermal emission originates in a skin layer <1 mm deep. This suggests that thermography at millimeter wavelengths may be expected to give results very similar to those of infrared thermography.

The presence of parallel tissue layers makes it necessary to consider possible interference effects due to multiple reflections. Standing waves in the fat layer have been shown to be significant at 2450 MHz in the case of microwave diathermy, where one transmits power from the skin through the fat

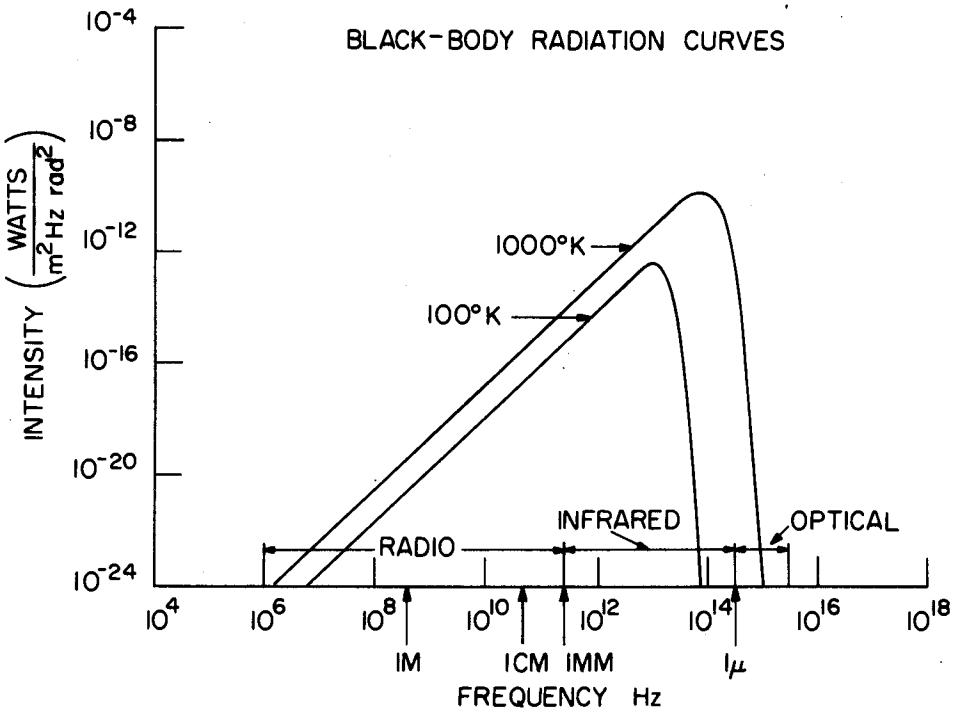


Figure 1. Specific Intensity of black-body Thermal Radiation with Frequency, for T = 100° K and 1000° K.

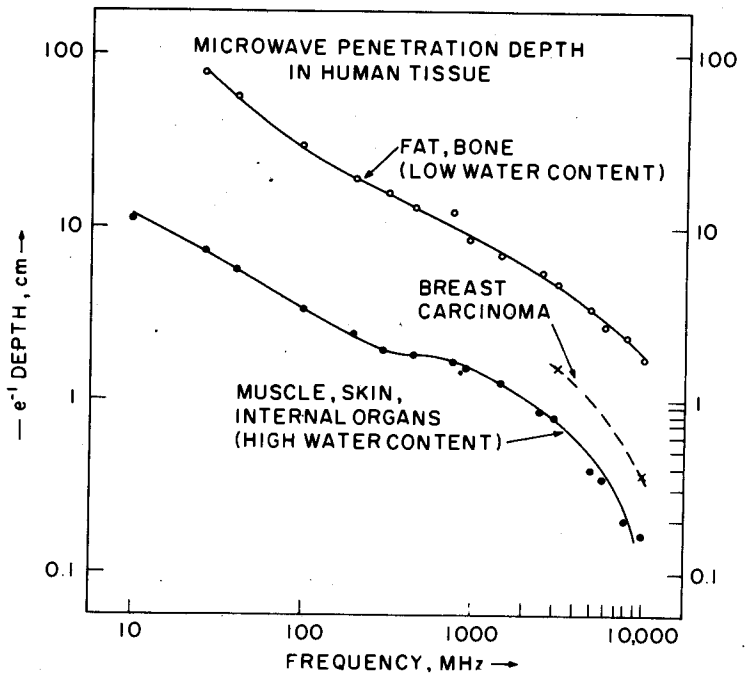


Figure 2. Penetration Depth versus Frequency for Typical Human Tissue of "high" and "low" Water Content.

into the deep muscle tissue[12,13]. In the present case, a tumor imbedded in the fat layer radiates from the fat through the skin into a receiving antenna at the skin surface. Standing waves may, therefore, arise in the skin layer. We estimate the magnitude of this effect by considering the case of maximum interference, which occurs if the layer is $\lambda/4$ in thickness. This condition is met at 3.3 GHz for a skin thickness of 3.4 mm. If the antenna is matched to the skin-fat combination, the transmission-line equations indicate that the twice-reflected wave entering the antenna interferes constructively with the zero-reflected wave, and adds approximately 9% to its amplitude. Since this is the maximum contribution, we neglect this effect in the following discussion.

Neglect of interference effects permits the discussion of radiative transfer in terms of power, and, therefore, at microwave frequencies in terms of temperature. The excess brightness temperature due to the tumor, ΔT_B, incident on the skin-antenna interface is given by the plane-parallel solution to the equation of radiative transfer[14]

$$\Delta T_B = \Delta T(1 - e^{-\kappa_t \Delta z_t}) \, e^{-\kappa_f \Delta z_f} \, t_{fs} \, e^{-\kappa_s \Delta z_s} \quad . \tag{4}$$

Here ΔT is the mean excess temperature of the tumor above ambient, κ_t, κ_f and κ_s are the power absorption coefficients (inverse penetration depths) of the tumor, fat, and skin tissue; Δz_t, Δz_f, and Δz_s are the sizes of the tumor, overlying fat layer, and skin layer; t_{fs} is the power transmission coefficient from fat to skin. For illustration, we evaluate Eq. (4) for tissue properties at 3 GHz: $\kappa_t = 0.65$ cm^{-1} [15], $\kappa_f = 0.21$ cm^{-1}, $\kappa_s = 1.2$ cm^{-1}, $t_{fs} = 0.75$[11], and for representative dimensions $\Delta z_t = 2$ cm, $\Delta z_f = 2$ cm, $\Delta z_s = 2$ mm. We obtain

$$\Delta T_B = 0.28 \, \Delta T \quad . \tag{5}$$

Thus for a typical temperature elevation associated with breast carcinoma, $\Delta T = 1.5^{\circ}$ C[16], one may expect $\Delta T_B \simeq 0.4^{\circ}$C.

Measurement

In microwave radiometry, measurements are made in terms of *antenna temperature*, T_A, which takes into account the finite resolution of the receiving antenna, and dissipative or reflective antenna losses:

$$T_A(\Omega) = \eta \int d\Omega' \; G(\Omega' - \Omega) \; T_B(\Omega') \quad . \tag{6}$$

Here G is the power gain of the antenna, Ω and Ω' are coordinates of solid angle, with origin at the antenna, and η is the antenna efficiency. $T_A(\Omega)$ is thus an average of the brightness temperature incident from all directions surrounding the antenna axis, weighted by the antenna gain or beam shape, and multiplied by an efficiency factor, η.

One generally measures the difference between T_A at the position of interest, and T_A at a suitably chosen reference position. In measuring the excess power of a source, one ideally measures the reference T_A in the same direction with the source replaced by normal tissue. In practice, T_A is measured at another position, where one may expect that the temperatures and opacities are similar, but where no source is present (*e.g.*, a symmetrically opposite position on the body). The resulting antenna temperature difference, ΔT_A, is related to the mean excess brightness temperature due to the source, ΔT_B, by

$$\Delta T_A = \eta \Phi \Delta T_B \quad . \tag{7}$$

Here Φ is the "beam-filling factor" which results from evaluation of the integral in Eq. (6). If the source angular size $\Delta\Omega_s$ is greater than the beam size $\Delta\Omega_b$, $\Phi = 1$. Then one may conclude the estimate of the preceding paragraph by adopting a representative antenna efficiency value $\eta \simeq 0.8$; the expected increase in antenna temperature due to a typical breast cancer tumor is then $\Delta T_A \simeq 0.3^{\circ}C$. On the other hand, if $\Delta\Omega_s/\Delta\Omega_b \ll 1$, then

$$\Phi \simeq \Delta\Omega_s/\Delta\Omega_b \quad .$$

For a diffraction-limited beam this factor is proportional to $(\Delta z/z)^2$, where Δz and z are, respectively, the source size and depth. Then the expected signal is reduced accordingly.

The resolution properties of any antenna depend upon the frequency, the antenna aperture dimensions, the source-aperture distance, and the dielectric properties of the medium being viewed. In general, the limiting factors are diffraction and inhomogeneities in the medium. We discuss here only the rectangular waveguide antenna in direct contact with the skin surface. The antenna response pattern is a combination of the near- and far-field patterns of each aperture dimension. At each depth z, the antenna resolution can be described by the area inside the half power contour of its response pattern. For a 3.3 GHz antenna of dimensions 1.0 x 2.3 cm viewing fatty tissue, the resolution area is approximately 2.5 cm^2 for $z < 0.3$ cm, broadens linearly with z for $0.3 \lesssim z \lesssim 1.3$ cm, and broadens as z^2 for $z > 1.3$ cm. The response pattern thus resembles a funnel whose cone opens away from the antenna with a half angle of about 50°. For $0 < z < 1.5$ cm, the average resolution area is about 10 cm^2. This depth range contains over 60% of the breast volume, assuming a hemisphere of radius 5 cm.

For fixed aperture size and tissue type, the far-field resolution area decreases as frequency increases, due to diffraction. Therefore, if a source occupies a fraction of the antenna beam area, that fraction will increase with increasing frequency, as the beam narrows. Then the beam filling factor Φ in Eq. (7) increases with frequency. However, the penetration depth of the overlying tissue decreases with increasing frequency; then ΔT_B in Eq. (7) also decreases with increasing frequency. Thus a"tradeoff" occurs: two factors which contribute to ΔT_A vary in opposite directions with increasing frequency. If $\Phi < 1$, estimates indicate that Φ increases faster than ΔT_B decreases. In that case detection should be more advantageous at high frequencies. However, it is unclear whether $\Phi < 1$ is typical. This is due to uncertainties in the true antenna pattern in a complex tissue medium, and to uncertainties in the temperature distribution in the tumor environment.

INSTRUMENTATION

We have built three radiometers for use at 1.3, 3.3, and 6.0 GHz. The 1.3 and 3.3 GHz instruments are in clinical use; the 6.0 GHz unit is in our laboratory. All have design similar to the block diagram in Figure 3, which

illustrates the 3.3 GHz radiometer. It is a conventional Dicke-switched, or comparison, superheterodyne radiometer, with 100 MHz intermediate frequency bandwidth, centered at 60 MHz. The input to the first stage tunnel-diode amplifier is switched at 8 Hz between the antenna, and a matched load maintained at 22.0 $\pm$ 0.1^{o} C by a thermoelectric refrigerator. The resulting square-wave signal is detected at the intermediate frequency by a square-law crystal detector, whose output is synchronously demodulated. The output signal is fed in parallel to an analog strip-chart recorder, and to a digital processor which converts the incoming voltage to a L.E.D. display of temperature in degrees C. Gain calibration is provided by a solid-state noise diode, attenuated to produce a signal equivalent to a temperature increase of 8.5^{o} C at the antenna input. The rms temperature sensitivity is approximately 0.1^{o} C for an integration time of 6 sec.

The antenna is a straight section of rectangular waveguide, with aperture dimensions 1.0 x 2.3 cm, and filled with a low-loss solid, with dielectric constant = 11. The dielectric reduces the waveguide dimensions required to propagate the TE_{10} mode above cutoff at this frequency. The radiation is transformed to the TEM mode for transmission through coaxial cable in the usual way, by a probe in the waveguide. During data-taking, the antenna aperture is placed flush against the skin, in order to eliminate reflective loss at the tissue-air interface, and in order to permit minimum spatial resolution for the given antenna size. Most of the detected power thus originates in the near field of the antenna. Impedance matching between the tissue and the radiometer input is achieved by placing a suitable length of coaxial line, and quarter-wave coaxial transformer, between the antenna and the radiometer input. The antenna is maintained at a temperature of 32° C in order to minimize thermal conduction effects at the antenna-tissue interface.

DIAGNOSTIC APPLICATIONS

There are many potential medical applications of microwave radiometry. By analogy with infrared thermography, we may expect these to include detection of subsurface thermal anomalies such as malignant tumors, especially in

the female breast; localized inflammations, such as appendicitis; and vascular insufficiency in the limbs and in the brain.

For the initial clinical investigation, we have sought to use microwave radiometry to detect breast cancer. The need for a reliable means of early detection is indicated by the fact that approximately one woman in 15 in the United States will get breast cancer in her lifetime. The potential danger of x-rays as a diagnostic method has been underscored by recent claims[17] that each examination involving a dose of 1 rad may increase a woman's lifetime breast cancer incidence risk by approximately 1%, for example, from 7% to 7.07% The value of infrared thermography in breast cancer diagnosis has also been questioned recently by Moskowitz,*et al*[18].

A 3.3 GHz radiometer was installed in Faulkner Hospital, Boston, in November 1974. Space was provided through the efforts of N. L. Sadowsky, M.D., Radiologist-in-Chief. Our goal was to examine patients who are examined as part of the Sagoff Breast Cancer Detection Clinic. Most women examined are outpatients having family history of breast cancer, a lump in the breast, or other complaint. Each patient receives a clinical examination, xeromammography and infrared thermography. The xeromammography and infrared thermography films are judged by staff radiologists. A medical technician operates the equipment full-time at the hospital, and examines approximately 30 patients per week.

The examination lasts about 10 minutes from start to finish. The patient opens her robe above the waist, and lies supine on an examing table. A technician places the antenna on the first position to be measured, usually the right nipple, and holds it in place for about 15 seconds. The measured temperature is indicated on the L.E.D. display, and recorded on a mapping form. The antenna is placed on the symmetrically opposite position on the other breast for another 15 seconds; the process is continued until two nine-point grids have been mapped out, one on each breast. The spacing between adjacent grid points depends on the breast size, but is typically 3 cm. The mapping form is completed by adding information about the patient's medical history, and the results of the xeromammography and infrared thermography.

The goal of the data analysis has been to find a quantitative test which can be applied to the measured temperatures, in order to produce high true-

positive (TP) and true-negative (TN) detection rates. [The TP rate, or sensitivity, is the fraction of cancers which the criterion identifies correctly; the TN rate, or specificity, is the fraction of normals which the criterion identifies correctly.] The test should be quantitative and objective, to permit rapid assessment of the patient's thermal pattern; and to avoid the training, time and variability in judgment which accompany the requirement of a skilled "reader". The microwave data are well suited to construction of such a a test, because they are in numerical form. This contrasts with the usual pictorial data format for mammography or infrared thermography.

We have tested eleven mathematical combinations of the measured temperatures with the "F-test" for significance in discriminating between the population of cancers (proven by biopsy), and the population of "normals" (all other cases)[19]. Each measure, M_i, is a simple function of the 18 observed temperatures for each patient. Each measure has an associated threshhold value, T_i. Then if $M_i > T_i$, a detection is indicated. For those measures, M_i, with F-values greater than 8, thresholds T_i have been varied in order to optimize the corresponding true-positive and true-negative rates. After optimizing TP and TN for individual M_i, it was found that TP and TN could be increased by combining two M_i in a logical "or" function.

Thus we define

$$M_1 = |\bar{T}_R - \bar{T}_L|, \qquad T_1 \simeq 0.3^\circ \text{ C}$$

Here $\bar{T}_R$ ($\bar{T}_L$) is the mean right (left) breast temperature over the nine measured values. This measure indicates large-scale temperature asymmetry. T_1 is given in approximate terms only, because it may be varied according to the relative priority assigned to TP and TN. The second measure is

$$M_2 = \max \left\{ \begin{array}{l} \max\,(T_R(j) - \bar{T}_R) \\ \\ \max\,(T_L(j) - \bar{T}_L) \end{array} \right\}, \qquad T_2 \simeq 1.3^\circ \text{ C}$$

Here j indicates one of the nine data points on each breast. This measure finds the hottest spot on each breast, relative to the mean temperature of

that breast; it then picks the larger of the two temperature differences. The combined detection criterion is then

$$M_1 > T_1 \quad \text{or} \quad M_2 > T_2 \rightarrow \quad \text{"cancer"}$$

$$M_1 < T_1 \quad \text{and} \quad M_2 < T_2 \rightarrow \quad \text{"normal"}$$

The TP and TN rates obtained with measures M_1 and M_2 depend upon the chosen thresholds T_1 and T_2. Figure 4 shows this dependence, and the relative performance of the microwave, infrared, and xerographic techniques with the same patient sample (3400 normals, 56 cancers). The lower curve labeled M(1) shows the TP and TN performance of microwave thermography with criterion M_1 only, as T_1 varies from .17 (upper left) to .35 ^{o}C (lower right). The curve labeled M(1,2) corresponds to criteria M_1 and M_2, as described earlier, with $T_2 = 1.2^{o}$ C and $.19 \leq T_1 \leq .47^{o}$ C. We note that the mid-range value $T_1 = 0.3^{o}$ C agrees well with the detection estimate made previously. The curves labeled I and X show the individual performance of infrared thermography and xeromammography. Again, the TP and TN rates vary as the detection criteria are varied. The upper curves show the effect of combining tests, as the corresponding criteria are varied. These are important because each method detects some tumors which the other methods miss. The curves IX and MIX respectively show the effect of combining infrared thermography and xeromammography together, and these together with microwave thermography. The TP rates are very high; but these tests are subject to the criticism that they expose many normal patients to x-rays. If the additonal risk estimates[17] are correct, a study of the present size, with 1 rad dose per patient, would cause two new cases of breast cancer. However, two combinations are possible which reduce patient exposure to x-rays. The curve labeled MI is the result of microwave thermography [M(1,2)] and infrared thermography combined. This has TP > 90%; there is no radiation exposure risk; but there is a relatively low TN rate. The curve labeled MI; IX is the result of a) giving all patients an MI test, and b) giving an x-ray exam only to those indicated positive by a). The x-ray results are then combined with the previous

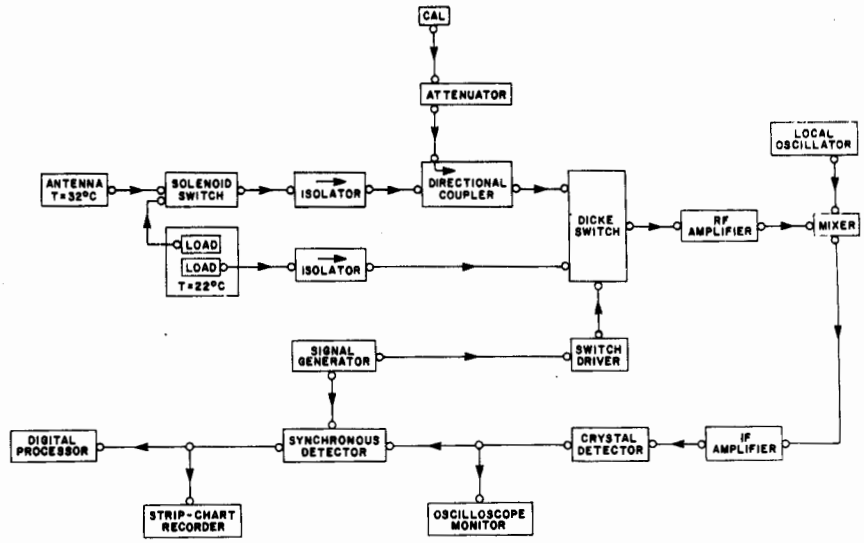


Figure 3. Block Diagram of the 3.3 GHz Radiometer currently in use in Faulkner Hospital.

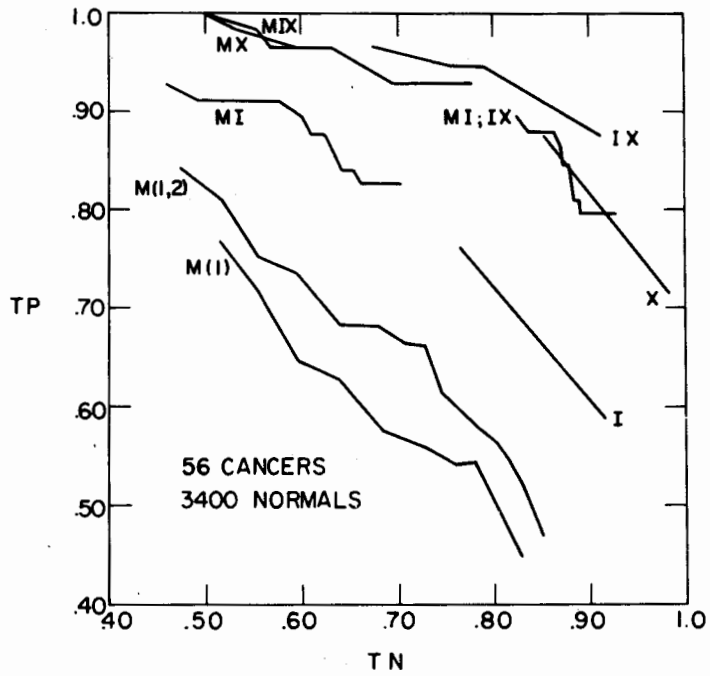


Figure 4. The True-Positive (TP) versus True-Negative (TN) Detection Rates for Various Combinations of Microwave Thermography (M), Infrared Thermography (I), and Xero-Mammography (X), as Detection Criteria are Varied.

infrared results to give a second-pass judgment. This two-phase process gives TP and TN performance as good as xeromammography alone, and exposes only about half the incident patients to x-rays.

In summary, the present 3.3 GHz results indicate that: by itself, microwave thermography gives TP and TN rates slightly inferior to those of infrared thermography; in combination with infrared thermography or with xeromammography, microwave thermography makes a significant improvement in the TP rate; and microwave thermography may provide a means of screening which reduces the risk of exposure to x-rays in the detection of breast cancer.

We have also examined over 600 normals and 14 cancers with a 1.3 GHz radiometer, but a thorough analysis of the data has not yet been performed. A 6 GHz radiometer is now operational in the laboratory; this will also be tested clinically to aid in determining the optimum frequency for detection. Schemes for improved antenna resolution are also under investigation. Extension of these methods to the diagnosis of other medical problems, such as cerebrovascular occlusions, and peripheral vascular occlusions, is anticipated within the next two years.

ACKNOWLEDGEMENTS

We are indebted to J. W. Barrett, J. Orenstein, and D. C. Papa for engineering assistance; to N. L. Sadowsky for cooperation in making the Faulkner Hospital facilities available to us; to E. M. King for operation of the equipment at Faulkner Hospital; to S. Bauer for assistance with data reduction. This research was supported in part by the U.S.N.I.G.M.S. Grant 5 R01 GM20370-04.

REFERENCES

1. J. Edrich and P. C. Hardee, Proc. IEEE, 62, 1391, (1974).
2. B. Enander and G. Larson, Trita-Tet-7701 (Royal Institute of Technology, Stockholm) (1977).
3. A. H. Barrett and P. C. Myers, M.I.T. Research Laboratory of Electronics Quarterly Progress Report No. 107, 14 (15 October 1972).
4. A. H. Barrett and P. C. Myers, M.I.T. Research Laboratory of Electronics Quarterly Progress Report No. 109, 1 (15 April 1973).
5. A. H. Barrett and P. C. Myers, M.I.T. Research Laboratory of Electronics Quarterly Progress Report No. 112, 39 (15 January 1974).
6. A. H. Barrett and P. C. Myers, Bibl. Radiol., 6, 45, (1975a).
7. A. H. Barrett and P. C. Myers, Science, 190, 669, (1975b).
8. B. Enander and G. Larson, Electronics Lett. 10, 317 (1974).
9. A. H. Barrett, P. C. Myers and N. L. Sadowsky, in *Proceedings, Third International Symposium on Detection and Prevention of Cancer* (in press; Marcel Dekker, New York) (1977a).
10. A. H. Barrett, P. C. Myers and N. L. Sadowsky, Radio Science, in press, (1977b).
11. C. C. Johnson and A. W. Guy, Proc. IEEE, 60, 692 (1972).
12. A. W. Guy and J. F. Lehmann, Trans. IEEE, BME-13, 76 (1966).
13. A. W. Guy, Trans. IEEE, MTT-19, 214 (1971).
14. S. Chandrasekhar, *Radiative Transfer* (Oxford University Press) (1950).
15. T. F. England, Nature 166, 480 (1950).
16. M. Gautherie, Y. Quenneville and Ch. Gros, Functional Explorations in Senology, 93 (1975).
17. B.J. Culliton, Science, 193, 555 (1976).
18. M. Moskowitz, J. Milbrath, P. Gartside, A. Zermeno and D. Mandel, New England Jour. Med., 295, 249 (1976)
19. C. Jung, unpublished BS thesis, M.I.T. Department of Electrical Engineering (1976).

* *

DISCUSSION

First, if you have the option of making one internal temperature measurement, what would be the critical place? Would it be the muscle tissue? Secone, how much can your resolution be improved?

Myers: You would like to make it where the abnormality is located, if you know where the abnormality is located, as an aide to the diagnostic measurement, but I don't think a single measurement would help very much. It should be clear we really are measuring an average temperature of very large volume, and if we add an exact temperature measurement at one location with a spatial resolution of less than a cubic millimeter, it may serve to calibrate the absolute scale of our measurement, but it will not tell us too much differentially. As to our resolution, we are never going to improve our resolution very much. I think a factor of two or three improvement in resolution, that is about as good as we will ever get. We are simply limited by the laws of diffraction with apertures of these sizes. We have been looking at the possibility of using a waveguide which propagates the TE_{20} and TE_{10} modes. If we subtract the patterns obtained by radiating these modes we get a different pattern which is narrower than the TE_{10} pattern alone, by a factor of about two.

When I heard of the work this group was doing, I thought it was most exciting. However, in talking with our physicians, some of them have really serious doubts about the validity of infrared or microwaves as a means for detecting breast cancer. They tell me that many of the breast cancers could be detected by self-examination by the individual or by palpitation by the physician. My question is, are we going to find additional breast cancers that could not be detected by self-examination by the individual or by physicians' present techniques? Are the very sophisticated techniques going to be really useful in the detection of breast cancer? [Robinson].

Myers: I think that is a fair question, and I really can't say that I know the answer. We are not doing as well with small tumors which is where the need is greatest, obviously, for your early detection. We have been able to rate the detection success of each of the three methods, microwave, infrared and x-ray, in cases where we know the tumor size or we have a very reliable estimate of the tumor size from the pathology report or from the x-ray itself.

Now the fact that both infrared and microwave methods are having a problem detecting small tumors may mean that the tumors of that small size are not hot enough. If they are not hot enough, then we are really in trouble, and we are not going to do any better no matter how much we improve our resolution. On the other hand, if it is a combination of inadequate resolution and low temperature, we may do better by improving our resolution We are attempting to determine this through the use of an antenna of higher

resolution. I don't think that it is likely that we are going to drastically improve detection statistics by adding microwave thermography in its present form to the arsenal of equipment that now exists. We may, however, be able to reduce risk to x-ray exposure and still have good detection.

Are you considering inverting your routine such that you can obtain a spatial temperature profile, perhaps using multiple scanning and different frequencies? [Cetas].

Myers: The thermal distribution is not a nice simple hot spot. We know now that because of the blood vessel structure around the tumor the isotherms look like octopi with tentacles going out to each blood vessel. It is not a simple thermal structure. Secondly, it is very difficult to adequately model our resolution in a tissue which is filled with inhomogeneities. In other regions of the body which are simpler to model, such as the arms or legs, we might be able to have more accurate localization of the temperature profile to determine vascular insufficiency. But for this application, all we can really do is indicate the presence of a tumor.

In the studies of hyperthermia they are trying to localize heating into confined regions. Could your methods be used to determine the success of these techniques? [Cetas].

Myers: No, we have a volume average, and I think deconvolving that volume average is going to be difficult. The best way to measure hyperthermia is with a scan probe.

DESIGN AND STANDARDIZATION OF EXPOSURE SYSTEMS FOR RF AND MICROWAVE EXPERIMENTATION

Mays L. Swicord and Henry S. Ho

Bureau of Radiological Health, Food and Drug Administration
Rockville, Maryland 20857

ABSTRACT

A discussion of currently used microwave and RF animal and cellular exposure systems is presented. This includes descriptions of systems using anechoic chambers, parallel plate transmission lines, Crawford cells, and waveguide systems for whole body exposure. Exposure systems utilizing waveguide or coaxial lines to expose cell cultures, and systems designed for selective or partial body exposure are also discussed. An appeal is made for the design of exposure systems which will aid in determining biophysical mechanisms rather than demonstrating the existence of another biological effect of microwave radiation. These systems, in most cases, should be designed to selectively expose parts of the animal. In addition, biological considerations may dictate cellular or whole-animal experiments. In all cases a complete description of internal exposure fields should be made and temperature and humidity are to be controlled and reported.

INTRODUCTION

In the recent past, microwave exposure system design was dictated by the equipment immediately available to the experimenter. This often resulted in the use of modified microwave ovens, diathermy machines, and various other makeshift equipment. An outcry from the engineering community concerning the uncertainty of levels of exposure and its results brought about the age of the defined exposure system. Consequently, the better exposure systems presently in use define either external unperturbed fields or absorbed dose. Absorbed dose in this instance is defined as the total power absorbed divided by the weight of the animal.

The better designed systems have provided fairly well-defined exposure levels at which biological effects have been observed. This statement does not imply that threshold levels have been defined, but that various effects have been observed at various defined and repeatable exposure levels. These biological experiments have not, however, provided the basic information for understanding the chain of events relating cause and effect. Neither the physical nature of the absorption or interaction process (a major subject of this workshop) and whether its importance lies on the molecular, cellular, membrane or organ level nor the biochemical process leading from excitation to observed effect are understood.

The question to be raised for discussion today is whether the current design criteria for exposure systems and the practice of reporting exposure fields or average absorbed dose is adequate for providing information to aid in the understanding of mechanisms relating cause and effect. A review of current practice will aid in considering this question.

CURRENT IN-USE EXPOSURE SYSTEMS

Free Space-Whole Body Exposure Systems

A common and often desired system is one which makes use of an anechoic chamber. Figure 1 shows the interior of a chamber at the Bureau of Radiological Health (BRH). Similar designs of varying size are employed in several laboratories around the country. The basic system uses a horn antenna or parabolic reflector to expose animals with a well-characterized, uniform field.

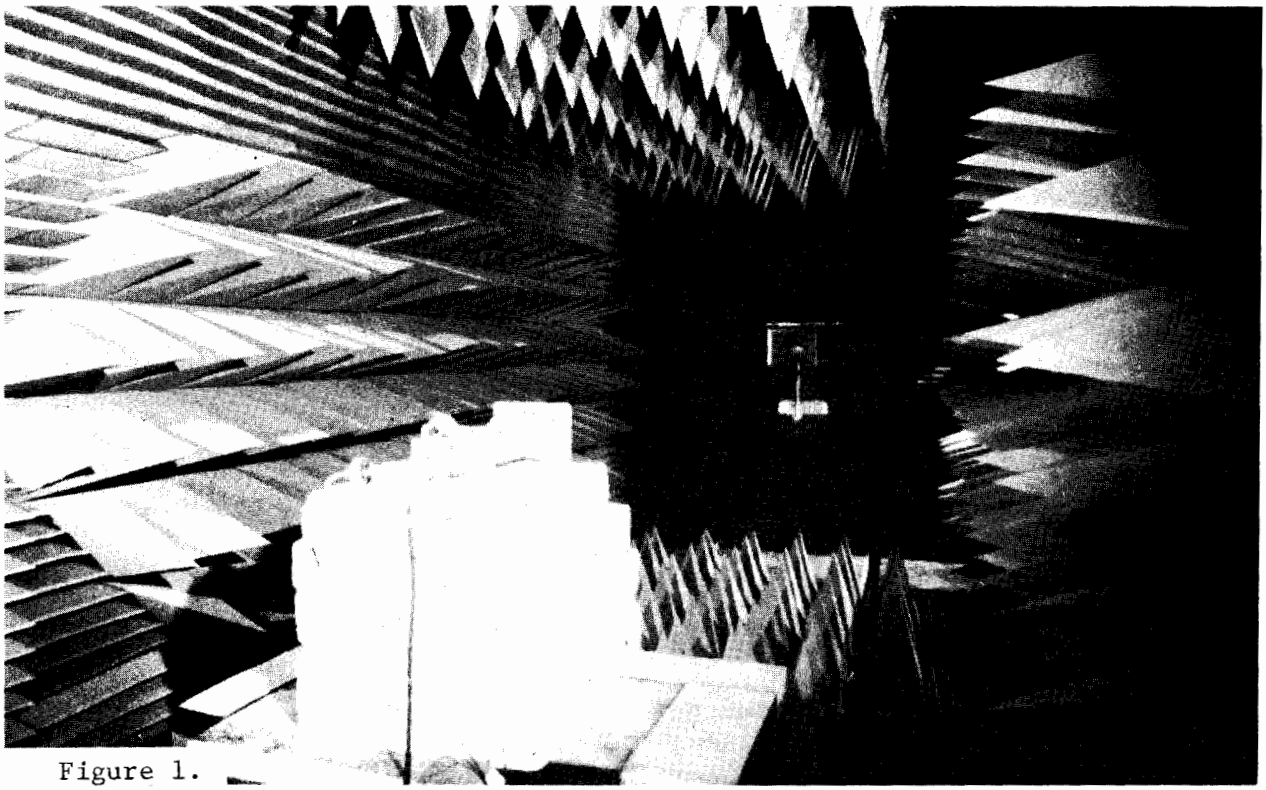


Figure 1.

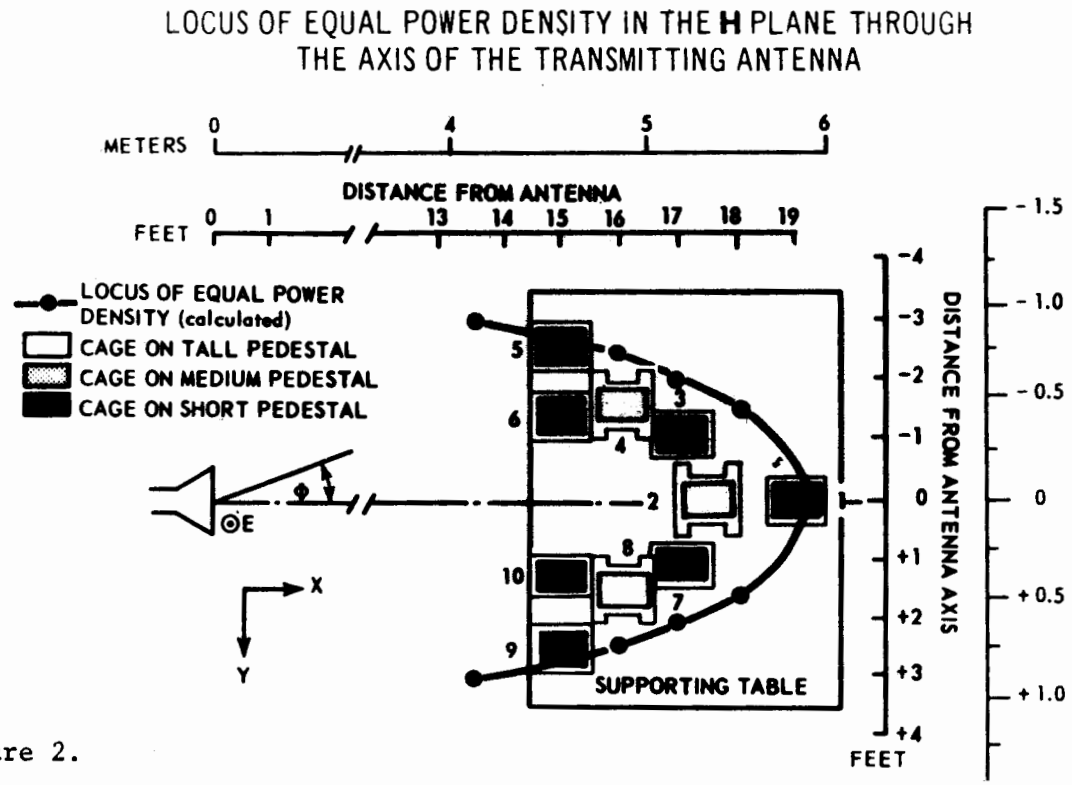


Figure 2.

Animal holders, restrainers, or cages are made of low loss, low dielectric constant material. Anesthetized animals can be simply placed on styrofoam blocks, such as that supporting a receiving antenna shown in Fig. 1. Multiple exposure arrangements can be accomplished by spacing animals appropriately in front of the radiating element as done by Oliva[1] and shown in Fig. 2. Three-dimensional placement has been incorporated (Fig. 3) so as to move animals as far apart as possible to minimize scatter from one animal to the next and yet achieve an approximately equal level of exposure to all animals. Figure 4 shows the free-field exposure chamber of the Bureau of Radiological Health[2]. The radiating element is a waveguide flare (truncated horn) mounted in the top of the chamber. The overhead mounting allows placement of several animals on a styrofoam block for multiple exposure. A truncated horn or waveguide flare is used rather than a standard gain horn in order to achieve field uniformity closer to the antenna, thus conserving the space and transmitted power required for the exposure facility. The latter results from the relation of power density, S, with distance, r, gain, G, and radiated power, P, given by

$$S = \frac{GP}{4\pi r^2}$$

and the customary rule-of-thumb of field uniformity of some multiple of D^2/λ, where D is the larger dimension of the antenna aperture. If ND^2/λ is substituted for r, and the gain is assumed proportional to D^2 then

$$S \propto \frac{P}{D^2} \quad .$$

Thus, the same degree of uniformity of field can be achieved at a closer distance and at reduced power through the use of the smaller antenna. The animal holders used for rat experiments in the Bureau of Radiological Health's chamber are shown in the lower portion of Fig. 4. The individual animal holders are arranged so that all animals will receive approximately the same exposure, but half will have their bodies aligned with the E-field and half will be perpendicular to the E-field. An individual holder is shown in Fig. 5. A considerable amount of compromise has been made in the design of these

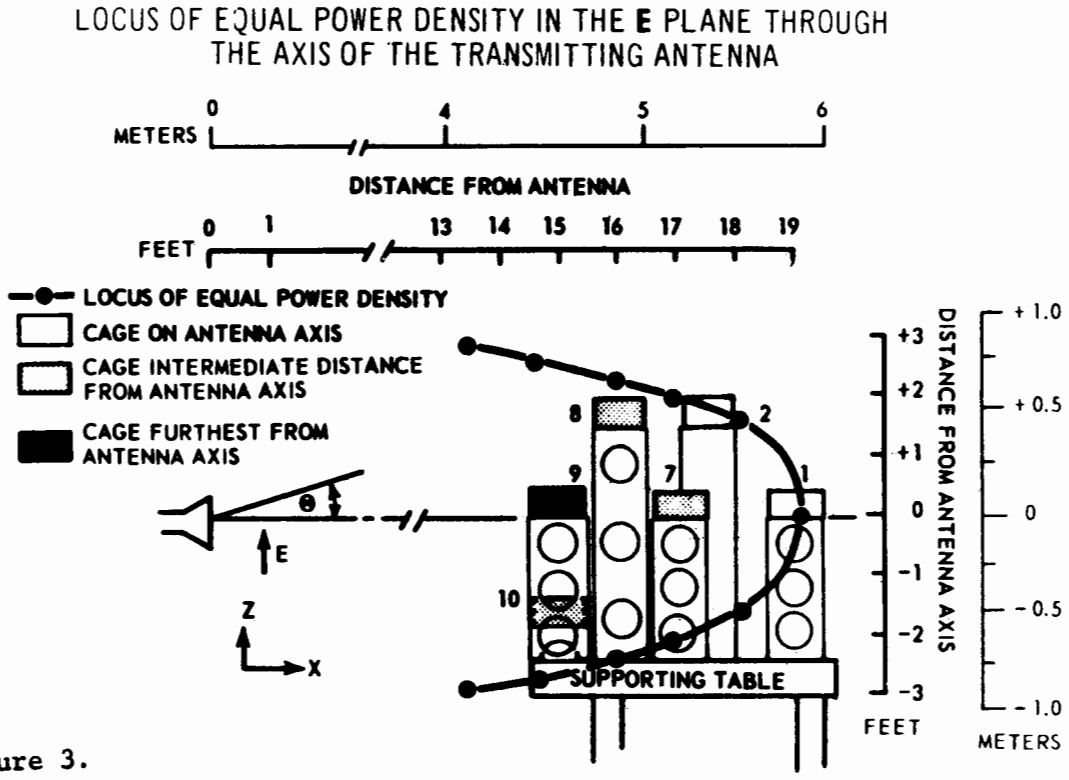

LOCUS OF EQUAL POWER DENSITY IN THE E PLANE THROUGH THE AXIS OF THE TRANSMITTING ANTENNA
METERS
0
4
5
6
DISTANCE FROM ANTENNA
FEET
0
1
13
14
15
16
17
18
19
LOCUS OF EQUAL POWER DENSITY
CAGE ON ANTENNA AXIS
CAGE INTERMEDIATE DISTANCE FROM ANTENNA AXIS
CAGE FURTHEST FROM ANTENNA AXIS
θ
E
Z
X
8
9
7
2
1
10
SUPPORTING TABLE
+3
+2
+1
0
-1
-2
-3
FEET
DISTANCE FROM ANTENNA AXIS
+ 1.0
+ 0.5
0
- 0.5
- 1.0
METERS

Figure 3.

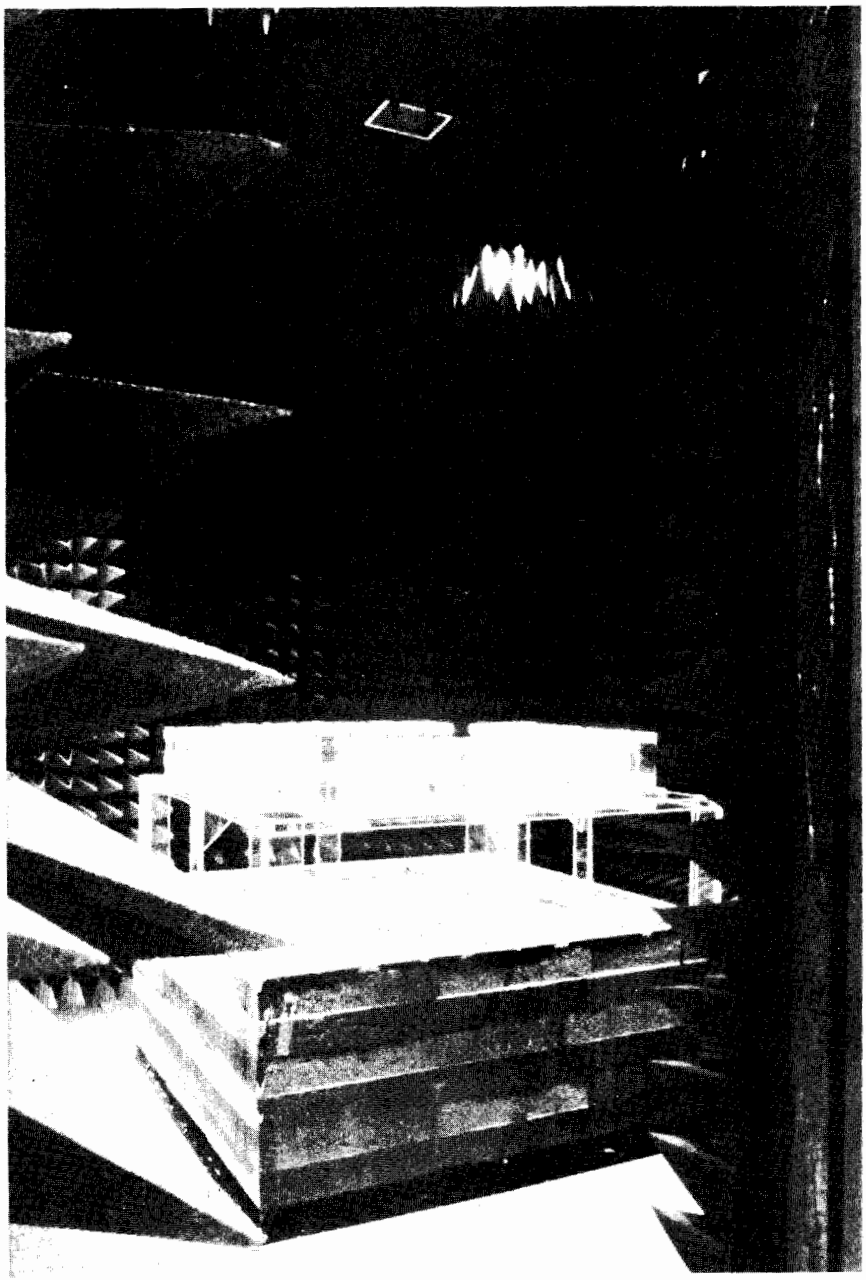


Figure 4.

holders for several reasons. First, these animals have a tendency to attack any restraining holders. Animals contained in Teflon holders in early trial-run experiments chewed their way out in five to ten minutes. The present design avoids this problem by using a hard Plexiglas holder. The four vertical walls are made of a solid sheet of Plexiglas 1/8" thick. The top and bottom are 1/16" plastic made into grids with 1/2" spaces, originally used as fluorescent-lamp-fixture diffusers. These holes provide ventilation for the animals and the general construction does not present a solid surface normal to the incident field.

Such designs are often criticized for the perturbation the holder effects on the exposure field. The fact is that such holders do perturb the field, but the criticism may be overemphasized. Lin, *et al*[3] have shown theoretically and experimentally that Plexiglas sheets mounted in the plane of the electric vector (where one might expect minimal perturbation) can still cause significant scattering of the field. However, Ho[4] has shown theoretically that for lossy infinitely long cylindrical objects such perturbations have a minimal effect on the field within the irradiated subject and, in turn, on the absorbed dose. The critical factor is the ability to characterize the field and not its lack of uniformity. Proper dosimetry can be achieved regardless of the field distribution. Measurements of the exposure field, the external and/or internal field, total absorbed energy of phantom models, and point-by point temperature distributions can be made by methods which have been discussed in other papers of this workshop. In addition, methods of calculating internal fields are widely available for plane wave exposure of symmetrical, regular-shaped objects[5,6,7]. Recently, Neuder[8] of the Bureau of Radiological Health and others[9,10] have been successful in developing programs to handle irregular-shaped objects. These programs can calculate the fields inside and outside animal and animal holders provided a plane wave is defined at some point outside the holder/animal system. An extension of the BRH program to handle other than plane wave exposures is expected.

There are many methods for restraining animals in anechoic chambers, most of which attempt to minimize field perturbations and minimize excitation of the animal. Another example developed by Herman and reported by Everts, *et al*[11] is

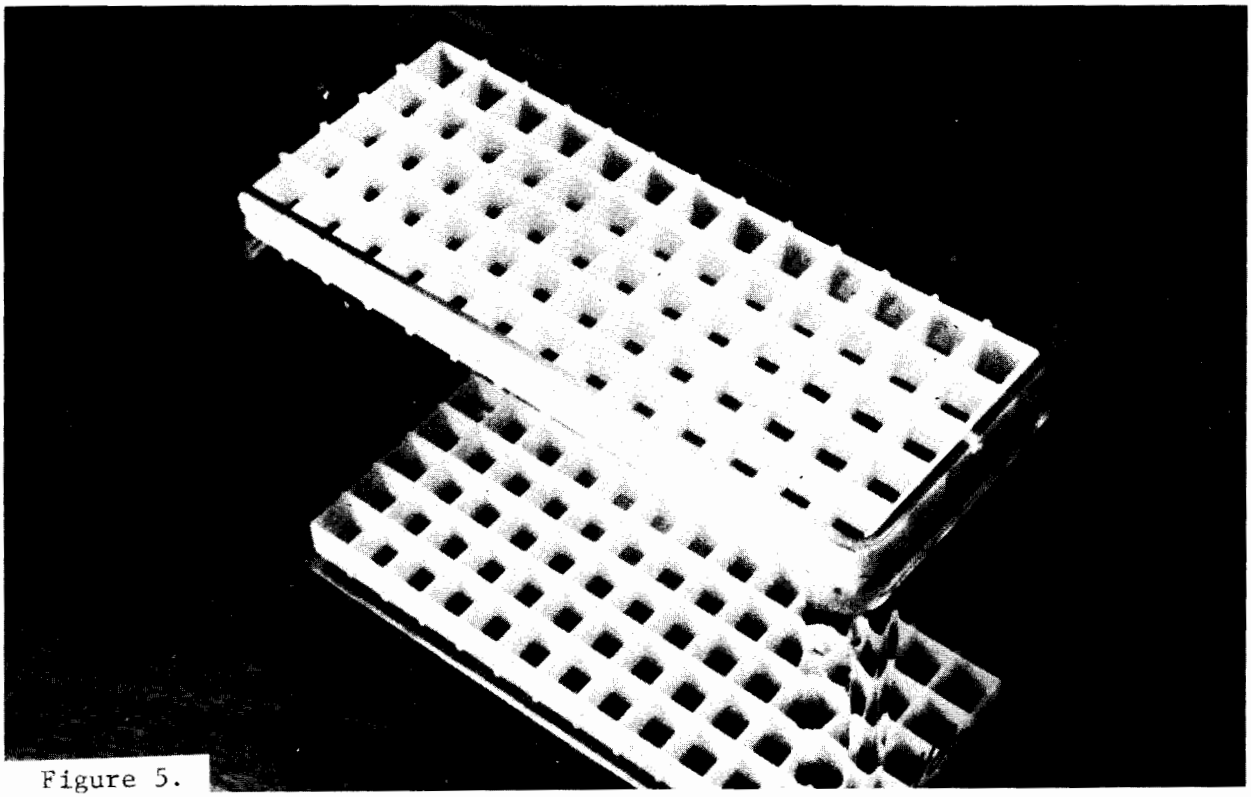


Figure 5.

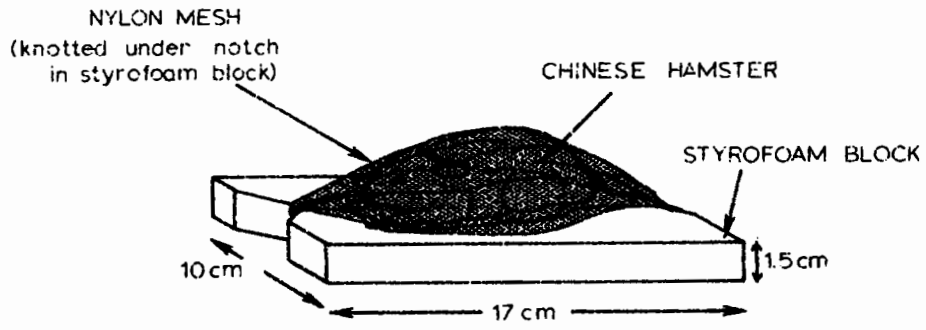


Figure 6.

shown in Fig. 6. Here the animals are restrained by thin nylon netting. Exposure is again from above. Animals can be held on a styrofoam block with the netting. The degree to which this or any other type of restraint would excite the animal would depend on the type of animal used. This is a point where the engineer and biologist must consult in order to determine all necessary parameters of the experiment.

Parallel Plate Animal Exposure Systems

A second type of whole body exposure system which is occasionally used is a parallel plate transmission line. Such a system is shown in Fig. 7. This particular line was developed for BRH for probe calibration and measurement purposes[12]. It uses an E-plane sectorial horn array to launch the wave and terminate the line. Space is saved and immediate uniformity of field is achieved through this technique. The dimensions of the line are 61 cm x 1.52 meter x 1.83 meter. If the line is terminated in its characteristic impedance, a TEM mode propagates. An open-circuit termination simulates a capacitor and provides a dominant E-field. Shorting the line simulates a loop antenna and provides a dominant H-field. Not only is such a line versatile in providing various well-characterized exposure fields, it also can provide a means of determining total absorbed dose. One merely needs to measure forward, reflected and transmitted power to determine the power absorbed by the animal. The line must be operated within its designed frequency range in order to avoid loss due to radiation from the sides. For the line shown, this is below 10 MHz. A similar line in use which operates up to 600 MHz is shown in Figs. 8 and 9. This exposure facility was developed and is in use at the University of Utah[13]. The dimensions are 6.35 x 15.9 x 92 cm.

A variation and possible improvement of this design is the TEM-Cell[12], developed by Crawford of the National Bureau of Standards[14]. A commercial version of this design[15] is shown in Fig. 10. The usable exposure area is enclosed by a solid rectangular outer conductor and flat inner conductor running down the center which can be seen in the figure through the open access door. This particular line has dimensions of 45 cm x 45 cm x 30 cm with a 12 cm x 15 cm access door. The line is usable below 500 MHz. A ± 1 dB uniform field

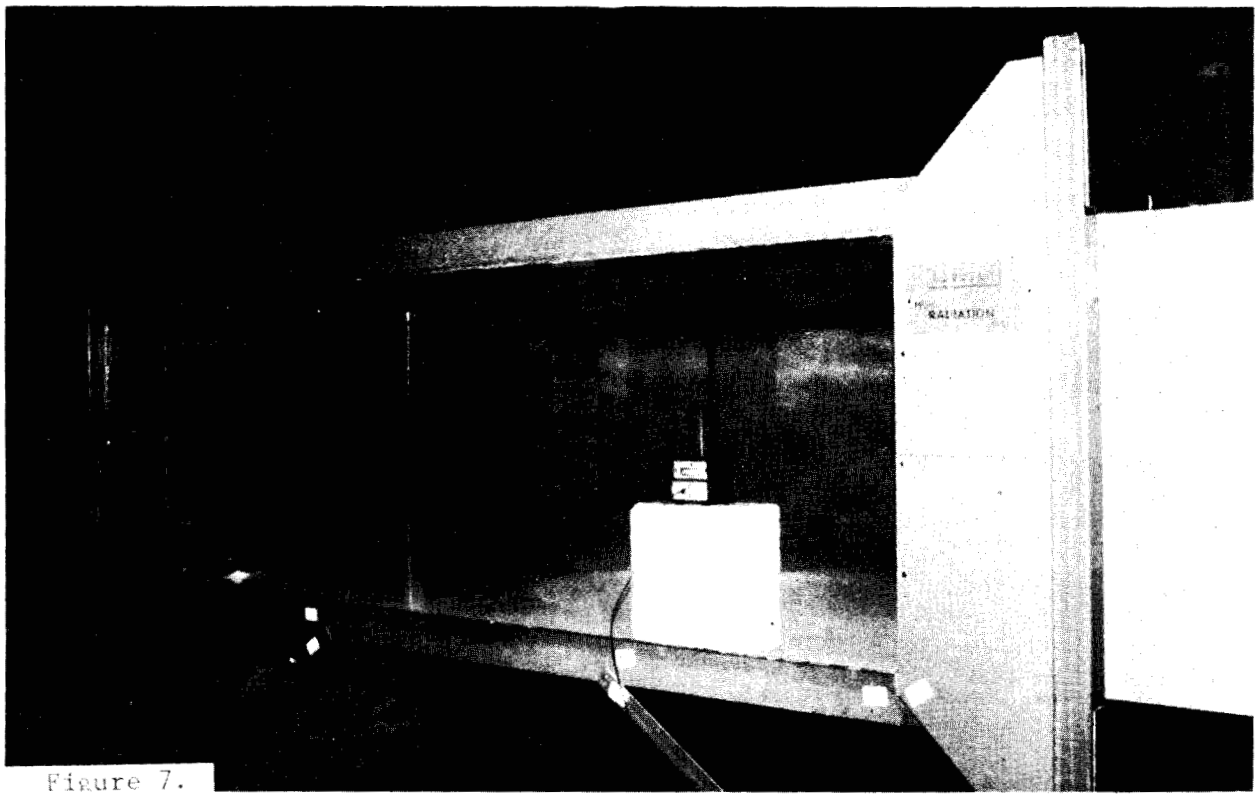
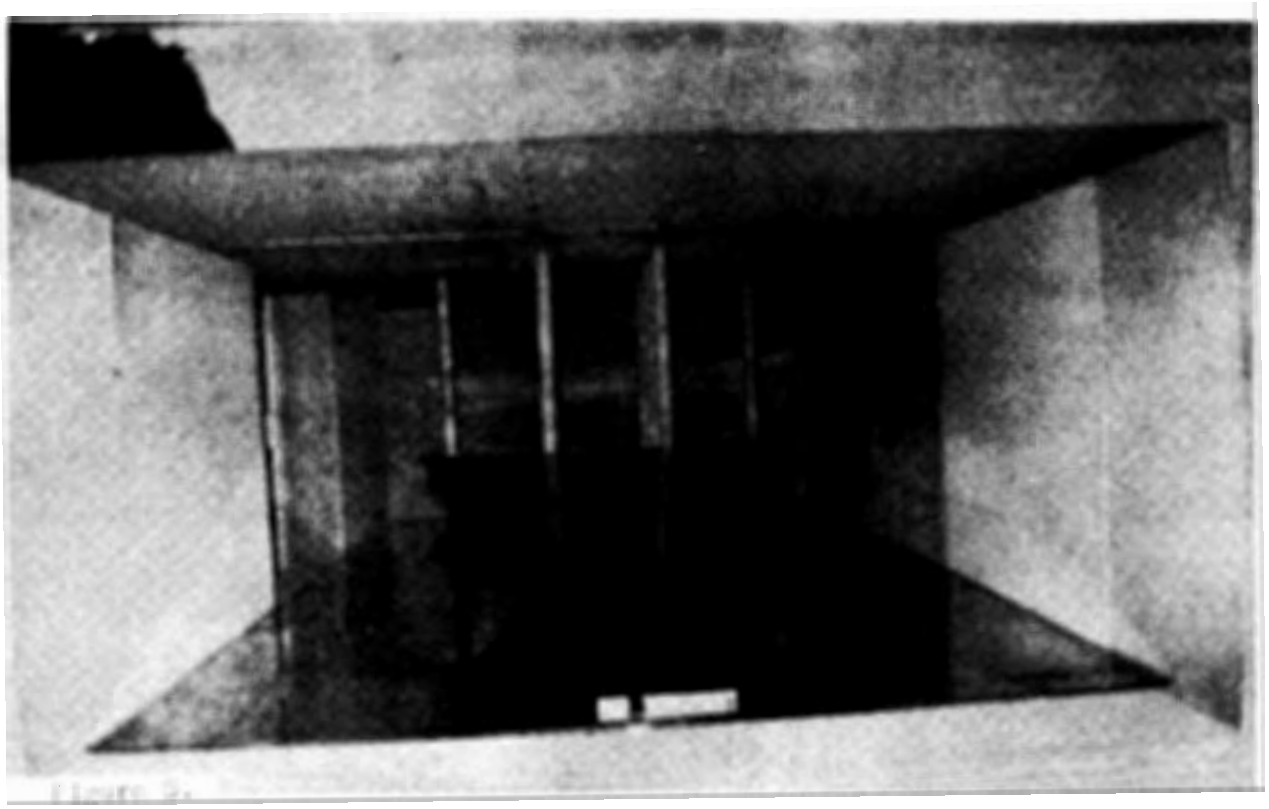


Figure 7.



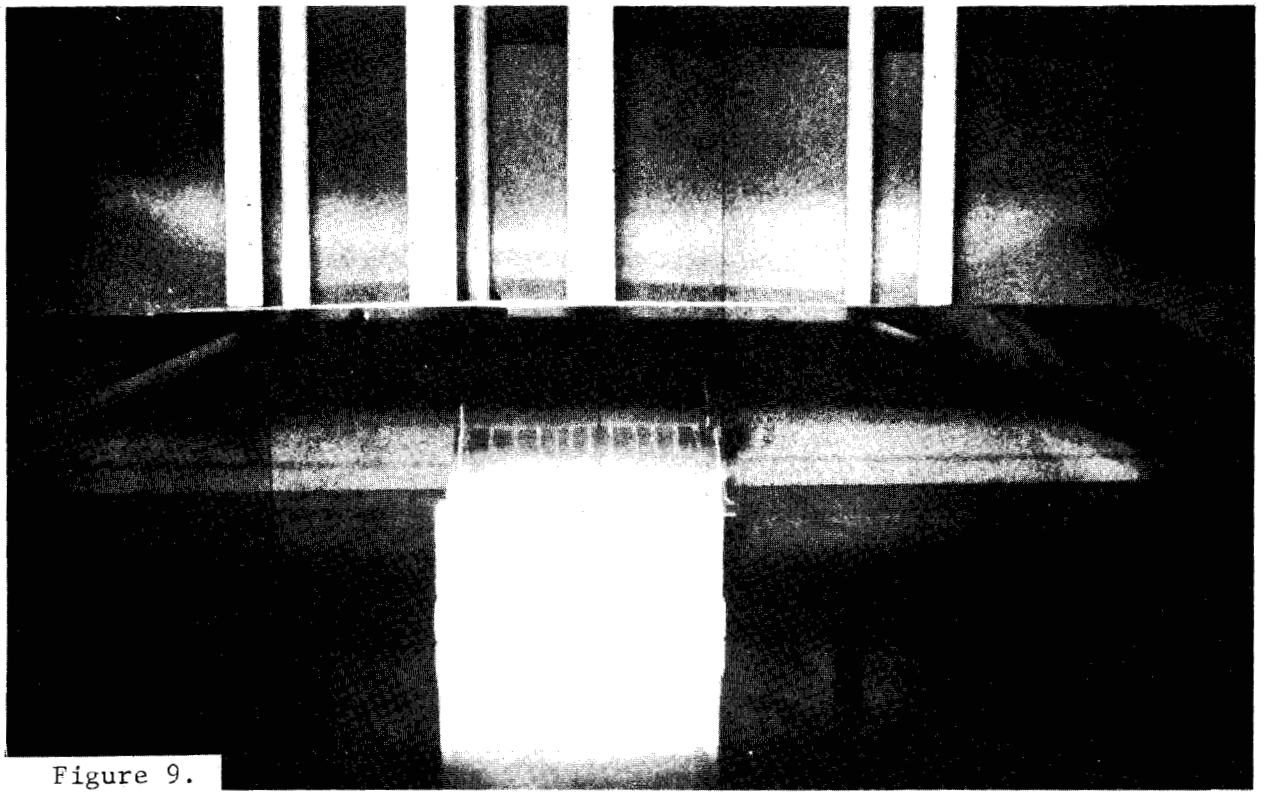


Figure 9.

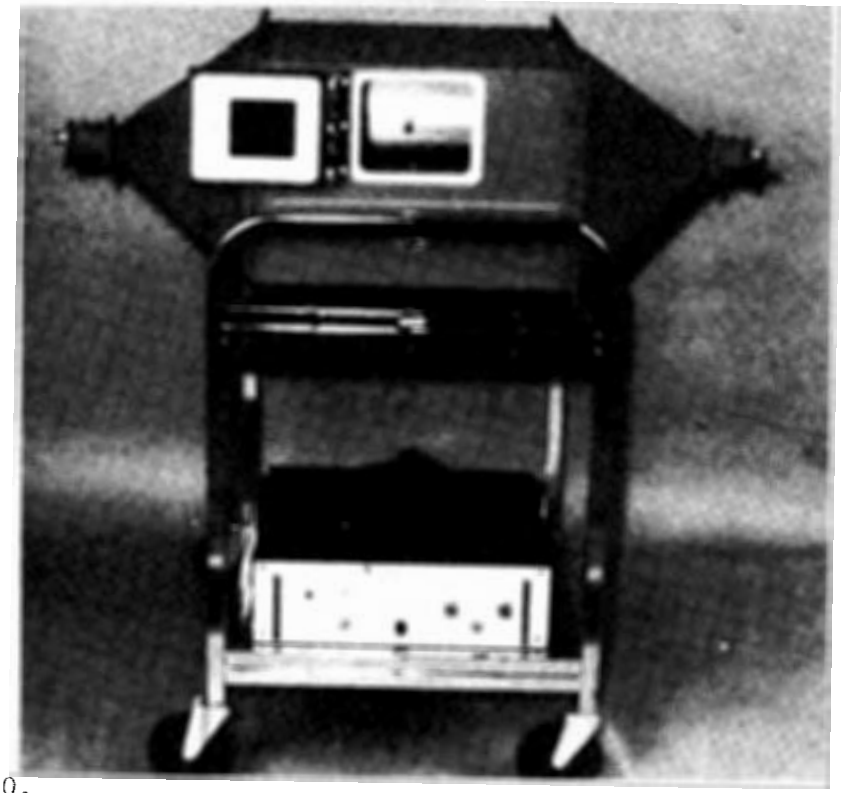


Figure 10.

exists in a 1.5 cm cube in the geometric center of the cell on either side of the center plane.

Figure 11 shows a larger version of such a design in use at Brooks Air Force Base with dimensions of 1.45 meters x 2.82 meters x 9.14 meters. Such a large design is operable at RF and lower frequencies only (DC-30MHz). In this line, as well as the open transmission line, one should not distort the field by putting too large an object in the cell for exposure relative to the size of the line. Details of design and use have been published by Crawford[14] and by Mitchell[16] of Brooks Air Force Base.

Waveguide Animal Exposure Systems

Figure 12 shows an exposure system using S-band waveguide (WR 430) in use at BRH[17]. Such a closed system provides exposure capabilities at microwave frequencies similar to the Crawford Cell at RF frequencies. It provides a well-defined exposure situation in which total absorbed dose is determined through measurement of forward, reflected and transmitted power. This system is shown schematically in Fig. 13. The waveguide is opened to allow insertion of a small animal in a styrofoam holder. The integration of each of the three power signals is necessary due to power fluctuations resulting from movements of the animal. The fact that total absorbed dose varies with animal position has been made use of in behavior studies in which rats were observed to minimize their absorbed dose after a short period of exposure[18].

Figure 14 shows dose distribution for phantom models of rats in fixed position as determined through the use of a thermographic camera. Animals could be restrained in these positions through the use of Plexiglas holders.

A second type of waveguide exposure system was developed by Guy[19]. This circular waveguide system is depicted in Fig. 15. The system is designed to operate at 918 MHz. The dual RF feed system launches a circularly polarized wave providing a means for exposing the animal to a constant field resulting in a constant dose regardless of the position of the animal. Another advantage of this system, which is constructed of screen mesh, is the ability to observe the animal during exposure. In addition, the system contains devices by which the animal can be fed and watered during exposure without apparent

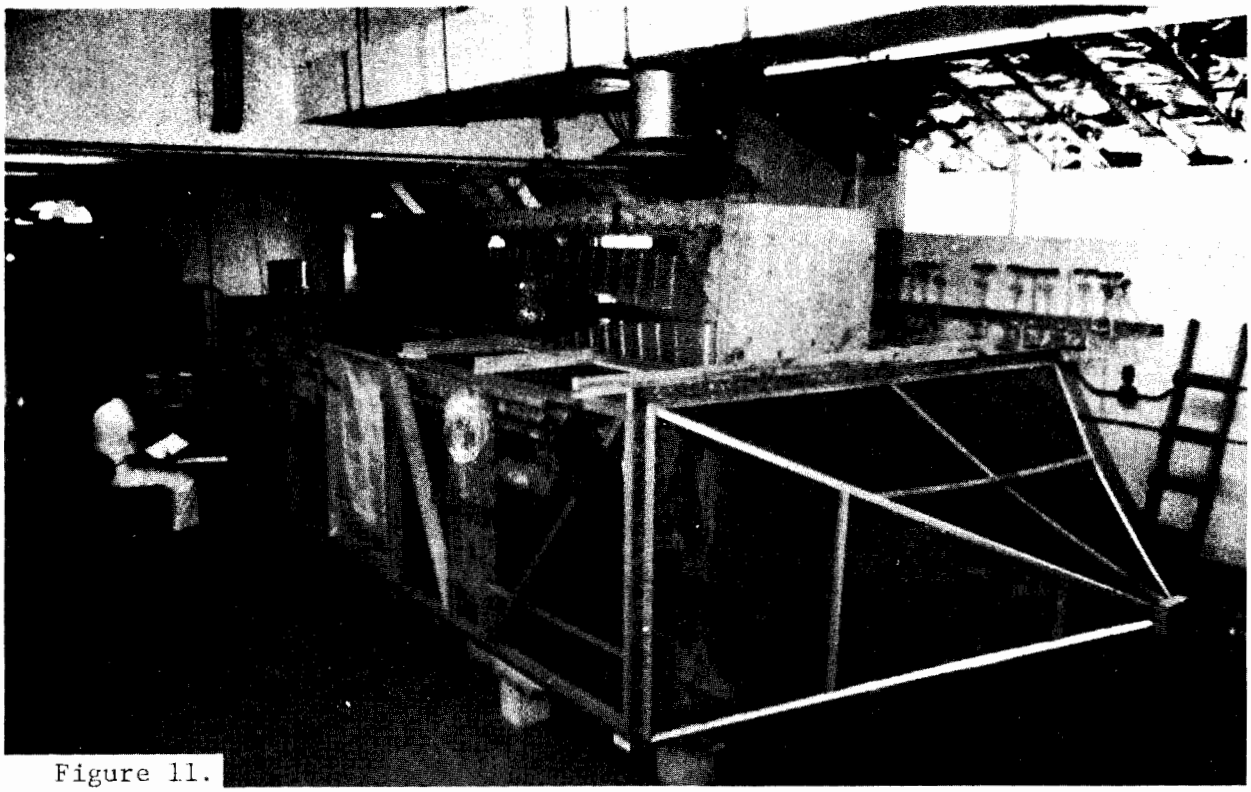


Figure 11.

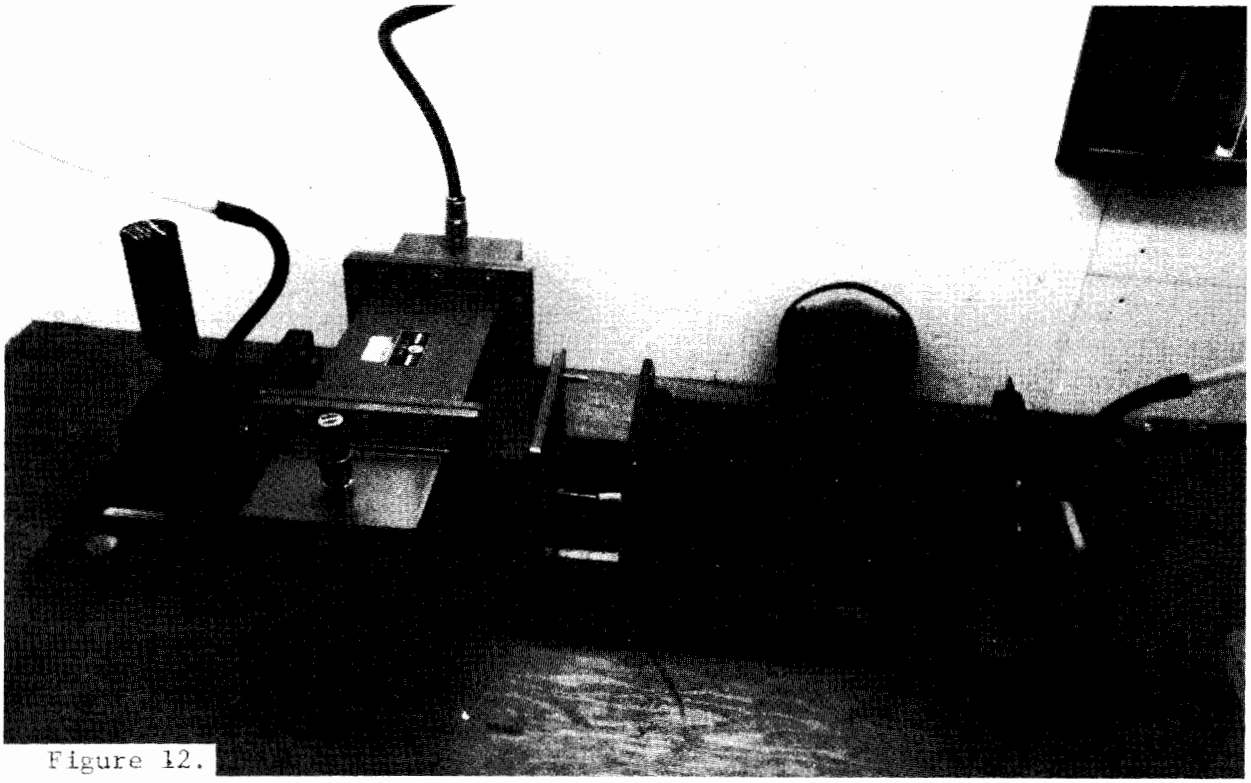


Figure 12.

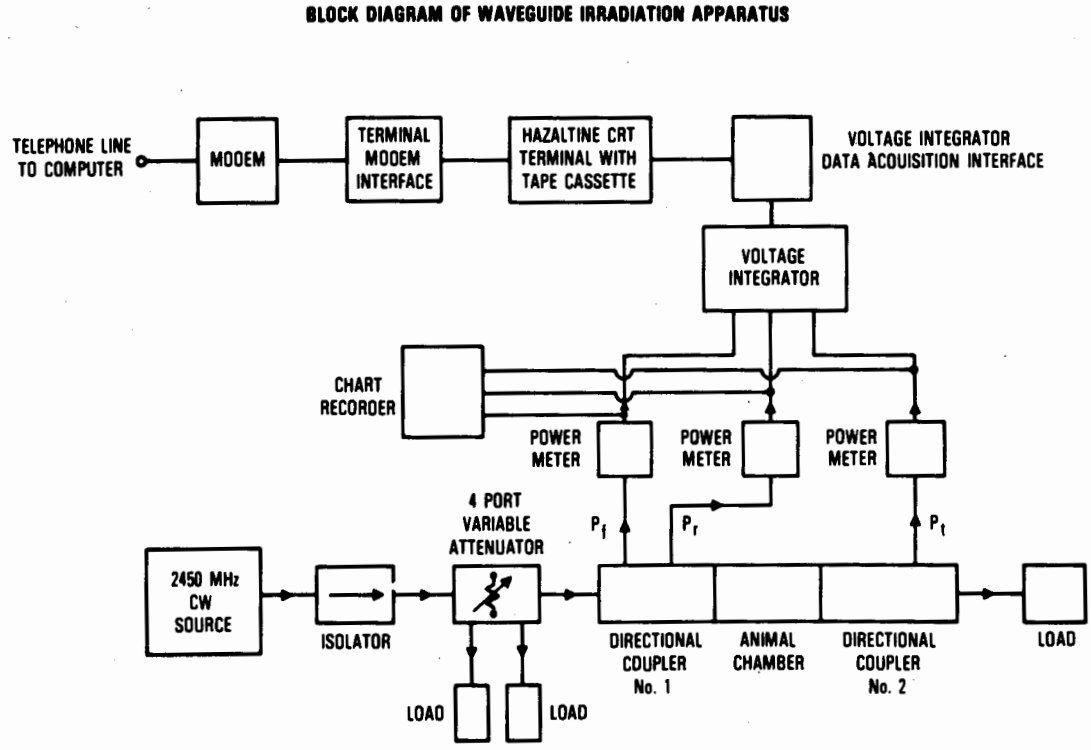

BLOCK DIAGRAM OF WAVEGUIDE IRRADIATION APPARATUS
TELEPHONE LINE TO COMPUTER
MODEM
TERMINAL MODEM INTERFACE
HAZALTINE CRT TERMINAL WITH TAPE CASSETTE
VOLTAGE INTEGRATOR DATA ACQUISITION INTERFACE
VOLTAGE INTEGRATOR
CHART RECORDER
POWER METER
POWER METER
POWER METER
4 PORT VARIABLE ATTENUATOR
P_f
P_r
P_t
2450 MHz CW SOURCE
ISOLATOR
DIRECTIONAL COUPLER No. 1
ANIMAL CHAMBER
DIRECTIONAL COUPLER No. 2
LOAD
LOAD
LOAD

Figure 13.

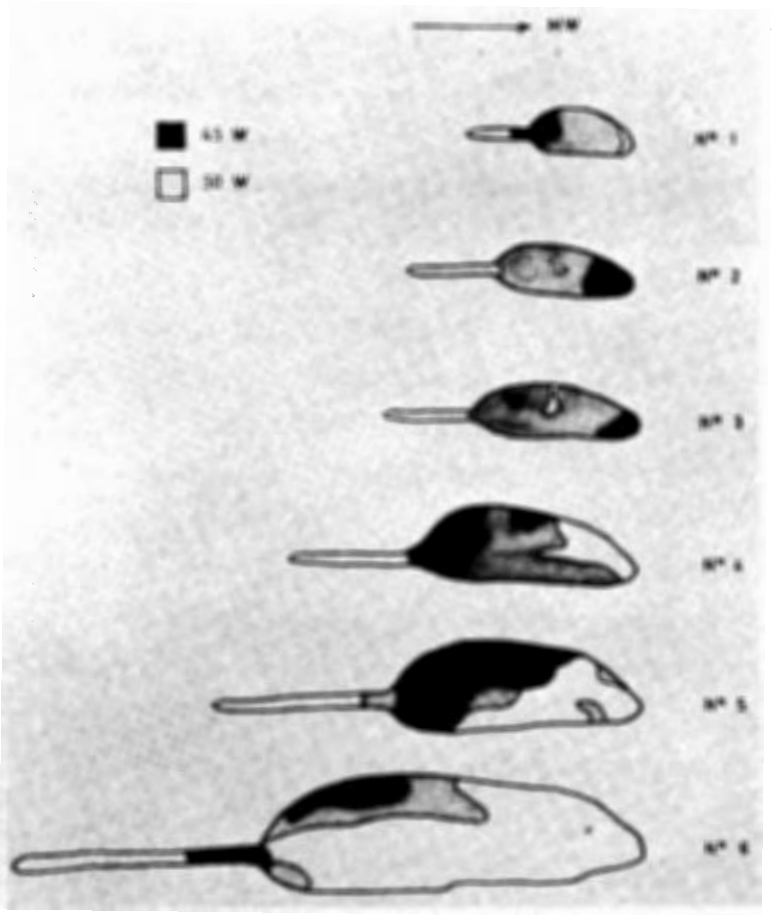


Figure 14.

significant effects on the absorbed dose. For nonselective, constant-dose exposure, this system is perhaps the best engineered design. However, as most of the previously discussed whole-body exposure systems, this system lacks the ability to selectively expose a specified portion of the animal.

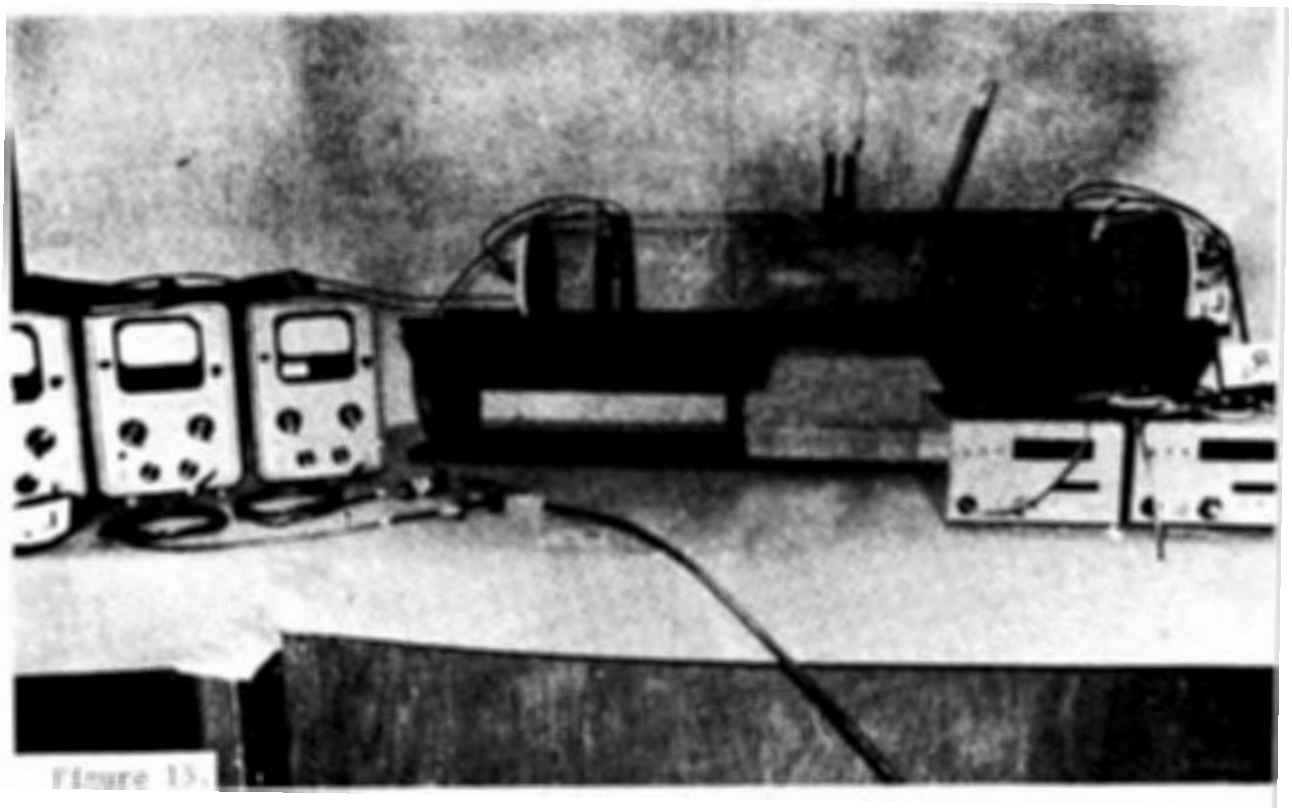
Environmental Control of Whole Body Exposure Systems

A slight digression at this point is appropriate to discuss environmental control using the BRH waveguide system as an example. It has been known for some time that environmental conditions influence the extent of stress on a subject in a microwave field. To ensure reproducibility in experiments, the outer chamber shown schematically in Fig. 16 was constructed to contain or enclose the microwave apparatus. Temperature, relative humidity, and airflow past the animal are specified during an exposure. As seen from Fig. 16, the environment within the chamber is obtained by mixing two air streams, one which has been cooled and dehumidified and one which has been heated and humidified.

The air temperature in the waveguide is measured with a protected thermocouple probe (thermocouple telethermometer) located at the center of the chamber just above the waveguide. The fluctuation in temperature during an exposure is less than $\pm$ 0.5°C. The variation in relative humidity (measured with a membrane hygrometer at the air inlet of the waveguide) is $\pm$ 1.5% during an exposure. The range of relative humidity that can be obtained within the chamber is 25-70% over the temperature range of 15-40°C.

The temperature-and moisture-conditioned air within the environmental chamber is drawn through the waveguide by a low-pressure (vacuum) system attached to one end of the waveguide. The 0.25" air inlets and outlets at the ends of the waveguide have no effect on dosimetry. Airflow rates (past the animal being irradiated) of up to 38 ℓ/min (measured with an air-calibrated flowmeter) are possible. The front of the chamber is fitted with gloves that permit access to the interior of the chamber without disturbing the controlled environment.

This exposure system lends itself very nicely to a high degree of control of environmental conditions. Similar controls should be placed on all systems



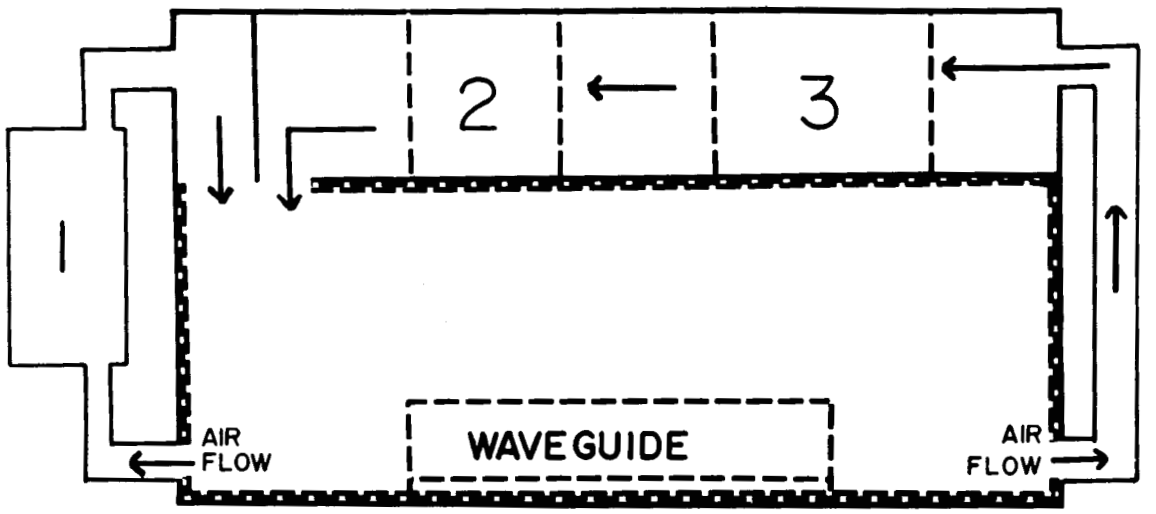


Figure 16.

large and small, and conditions should be specified in all experiments. The literature is filled with descriptions of experiments in which the environmental conditions are uncontrolled and often unreported. The importance of multiple stresses in biological experimentation cannot be overemphasized. The free field exposure system at our Bureau is also being equipped with such an environmental control system. Air is cooled by a continuously running air-conditioning compressor and reheated and humidified to the desired levels.

Cellular Exposure Systems

Cell cultures, blood samples, and solutions of bio-materials have been exposed in free field systems. Although the fields may be well known, the true absorbed dose may be most difficult to ascertain due to the relative size and shape of the containers in comparison to the solution or culture itself. Again, this may be a case of the experimenter using what is available, but may not lead to reproducible results. Another difficulty is the temperature control of a solution in a petri dish sitting in a large anechoic chamber in front of a standard gain horn.

Several systems have been developed and are in use employing waveguide or coaxial sample holders, thus eliminating these problems. A simple system employed at the Bureau of Radiological Health is shown in Fig. 17. Directional couplers are employed to determine forward and reflected power. The reflected power is minimized by means of a stub tuner.

The sample holder is simply a shorted section of 14mm air line or waveguide. Thus, knowledge of forward and reflected power yields knowledge of total power absorbed by the sample. The temperature of the holder is controlled by immersion of the entire sample holder in a large water bath. Such a system is shown in Fig. 18. Temperature gradients can, of course, exist in the sample. However, the small sample volume (3 cc), the high thermal conductivity of the broth, and the presence of a metallic wall combined with the large thermal capacity of the water bath, greatly reduce the temperature gradient in the sample. Note also that the inner and outer conductors of the coaxial holders are in thermal contact through the short circuit termination.

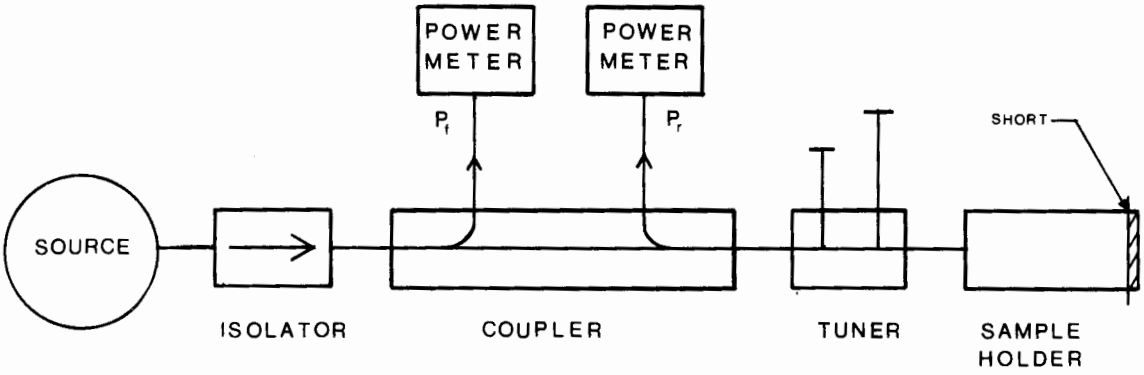


Figure 17.

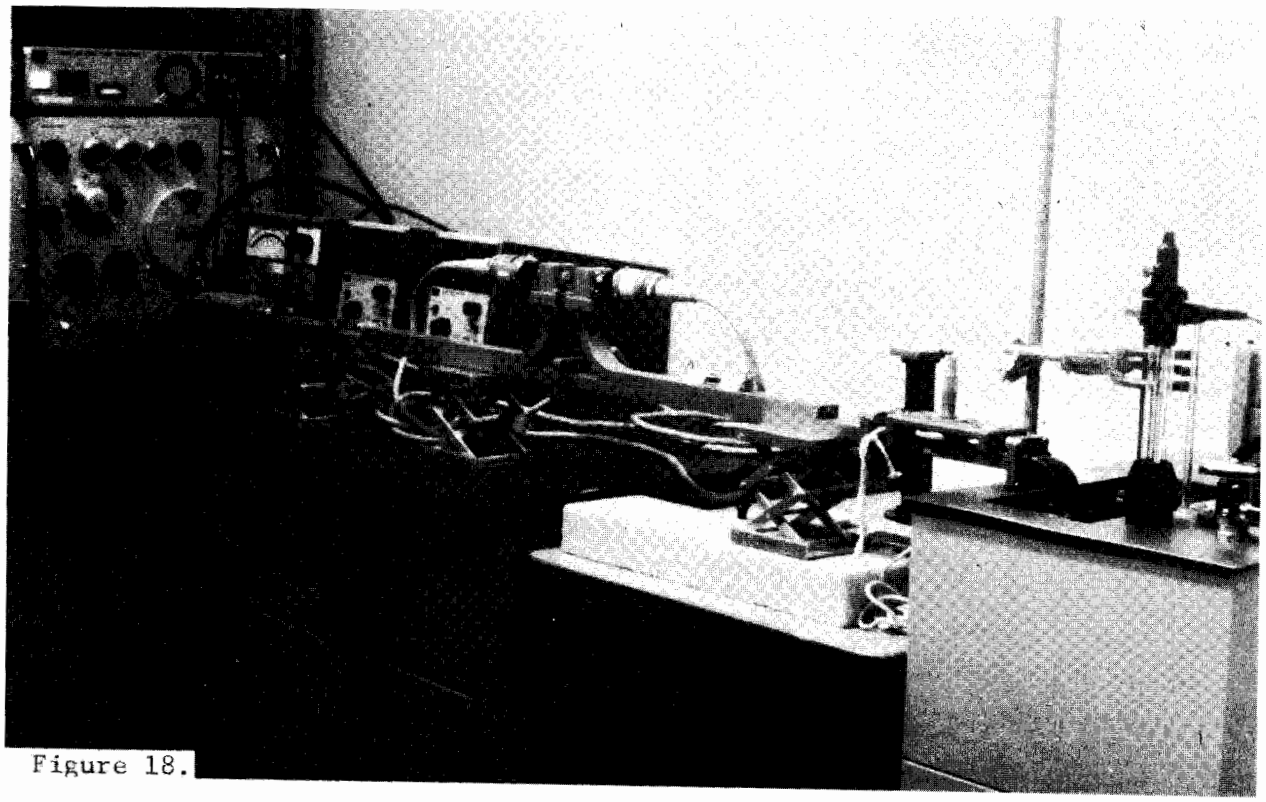


Figure 18.

Nevertheless, for high dosages (above 200 mW/g), the importance of these temperature gradients increases with the size of the sample, and may require temperature measurements to determine the temperature gradient in the solution. Control experiments may be needed to rule out effects due to a rise in temperature of the broth and of temperature gradients in the broth.

Consideration should be given to the magnitude of the electric field at the location of the cell during design of the experiment. For example, a cell culture growing in a broth will settle to the bottom of the solution during extended exposure periods. Due to absorption, standing waves in the medium, and the fact that the electric field is zero at the shorted end, the settled cells may be receiving little or no exposure. Periodic shaking can re-suspend cells. However, one should realize that non-uniformity of absorption still exists and results should be analyzed accordingly. Reporting of total absorbed dose (mW/gm) for this type of experiment is, therefore, inadequate. Calculations of the field and absorbed energy distribution in the holder can and should be made.

The problems of non-uniformity due to cell suspension, and uncertain exposure due to settling of cells against a short-circuit termination has been minimized by experimenters in the BRH laboratories by filling the slotted waveguide with agar to a thickness of one-fourth wavelength and then putting a concentrated solution of cells on top of the agar[20]. Cells are allowed to either settle to the one-fourth wavelength point, or cells of certain types may be grown over the surface of agar in this configuration. An alternate solution to the problem is to use a holder (commercially available) that is electrically (but not physically) "open" at one end.

A third system is depicted in Fig. 19. The overall system is much the same as shown previously, except this system was designed to operate at millimeter wave frequencies. This system is shown schematically in Fig. 20. Forward power is not measured using directional couplers because of the high degree of error in the coupler measurement. Instead, the power is measured with a terminating power meter at the point of sample placement. The sample is then inserted and the ratio of forward to reflected power is determined with the slotted line. The transmitted power is measured using the terminating power

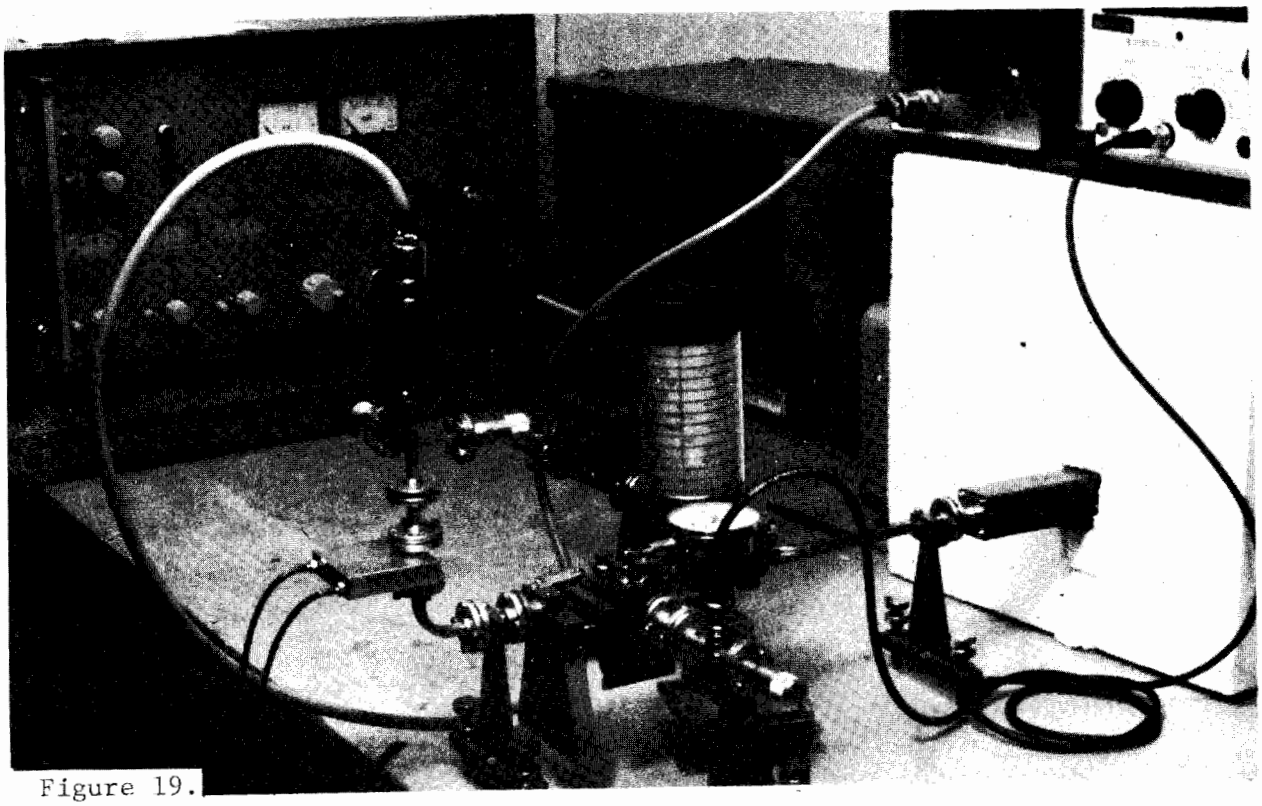


Figure 19.

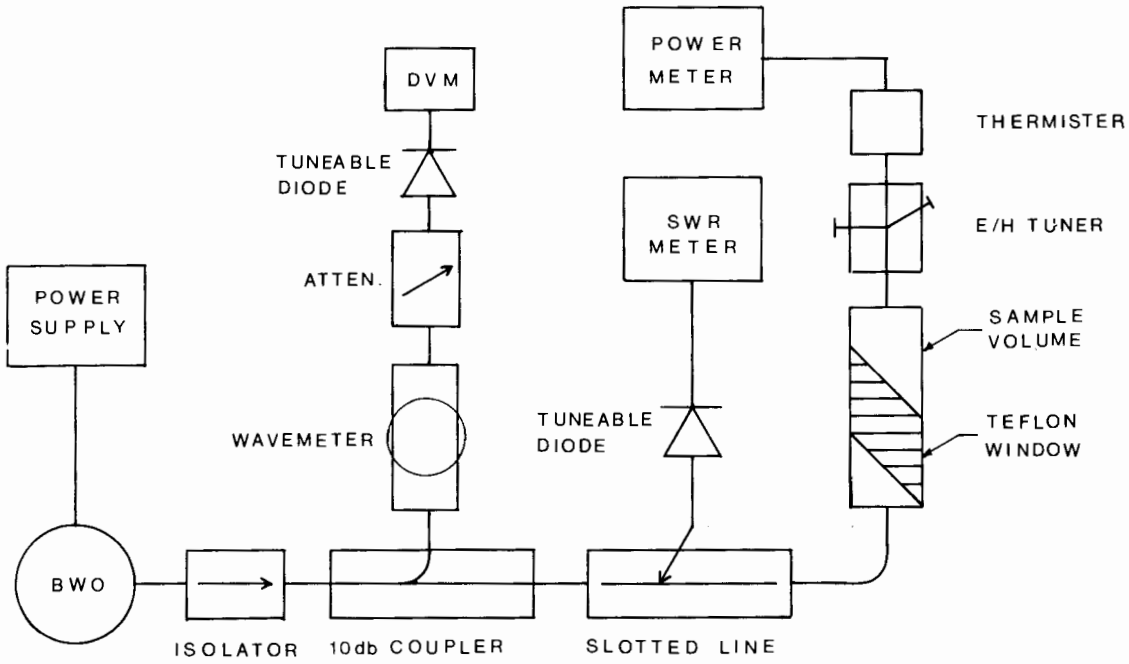


Figure 20.

meter. A tapered section of teflon is inserted into a waveguide and functions as an impedance-matching device to the sample as well as the bottom of the sample holder. Cells settling to the bottom of the holder will now be on the front surface of sample holder and be exposed to maximum field strength. Temperature is controlled by attaching the short section of waveguide to a heat sink through which water is circulated at a constant temperature.

A coaxial system for cellular exposure has been developed by Guy[21] and is shown in Fig. 21. This system provides means of controlling temperature within the center conductor as well as outside the outer conductor. Temperature gradients should be reduced through this method, particularly for large coaxial systems. The system is operable over a frequency range from dc to 3GHz, and can provide exposure fields as high as 100 V/cm. without significant temperature rise. The apparatus is diagramed in Fig. 22.

SELECTIVE EXPOSURE SYSTEMS

A lot of early work in bioeffects, particularly that directed towards cataractogenesis, used selective or contained exposure systems, such as a diathermy applicator. These "off-the-shelf" type systems often provided a complex field with strong radial components (E-field normal to subjects surface) which were difficult to characterize with the instrumentation available at that time. An unjustified criticism of this work was that it did not simulate actual exposure conditions. This line of reasoning in some bioeffects research led to the development of many of the free field, plane-wave exposure systems and other systems which vary the ratio of electric and magnetic field to simulate various near-field exposures. These sophisticated systems may have placed an emphasis in the wrong direction. The following are examples of the selective exposure systems (as opposed to the sophisticated free field systems).

Dielectric Lens

Carpenter[22], with theoretical assistance from Ho[23], has made use of a dielectric lens to focus energy on the eye of a rabbit. This system is shown in Fig. 23. The Luneburg lens which is shown here is commercially available from Emerson and Cummings, Inc. The dielectric sphere is exposed to a plane wave

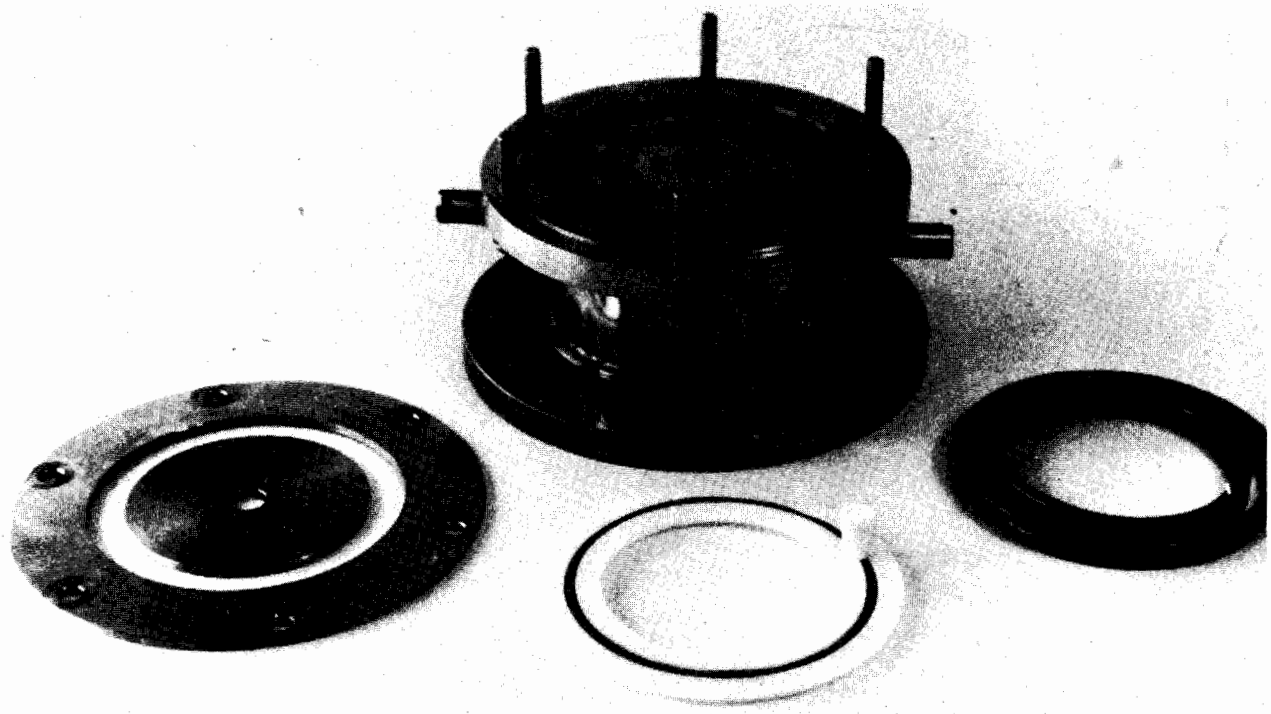


Figure 21.

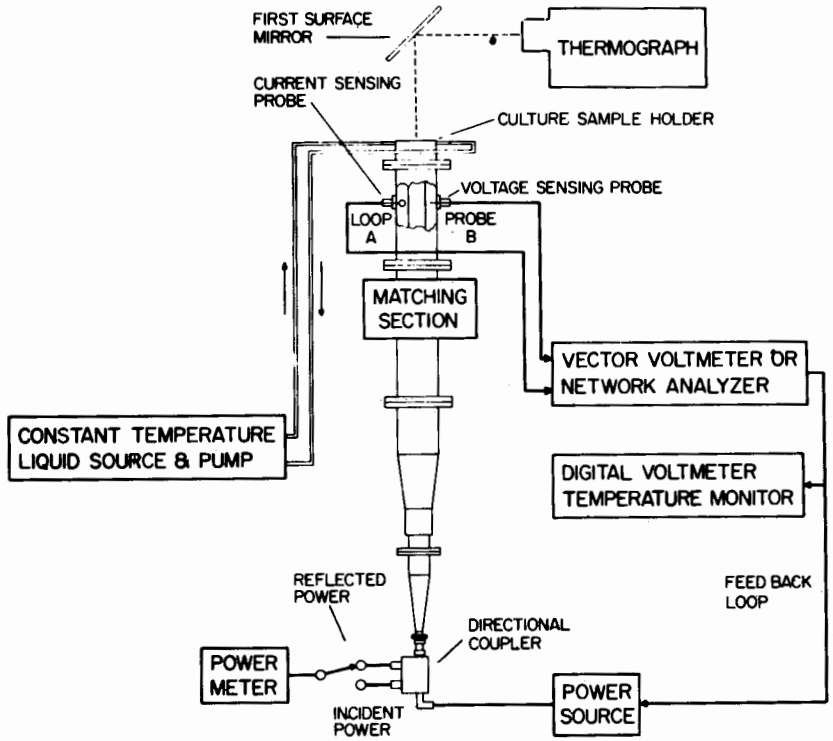


Figure 22.

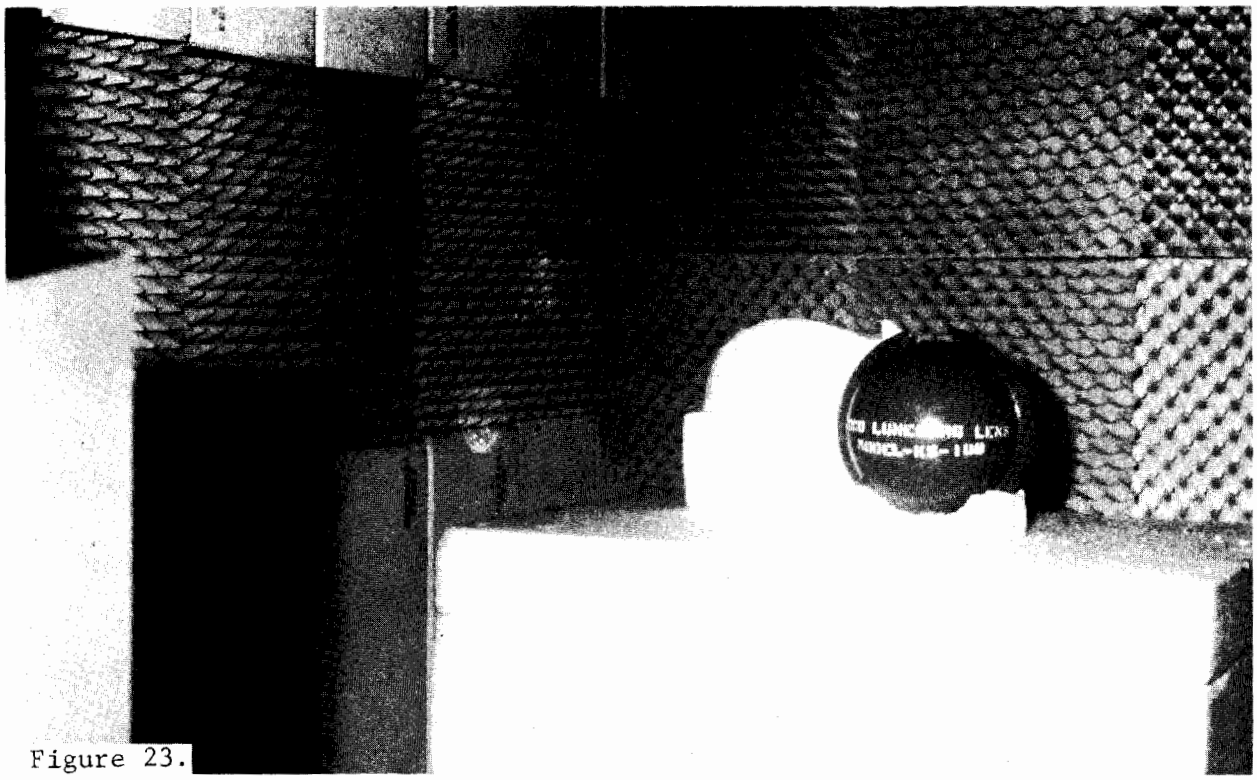


Figure 23.

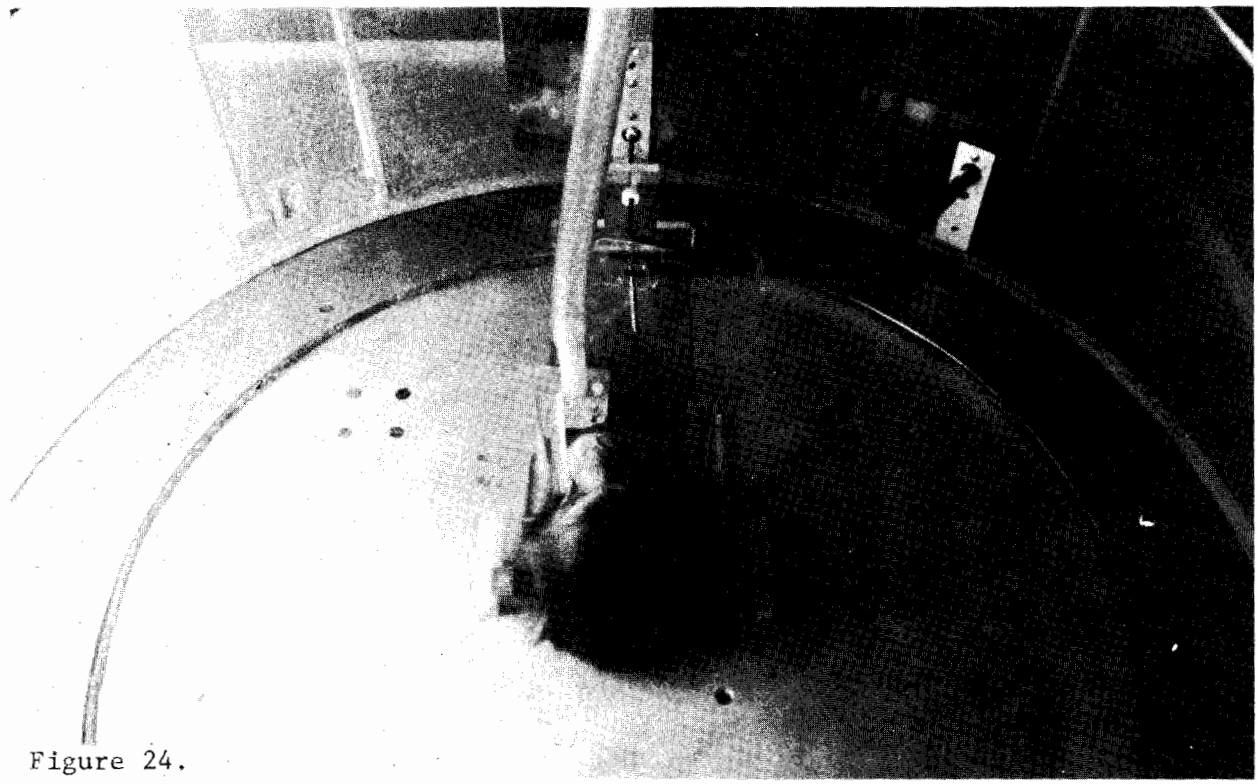


Figure 24.

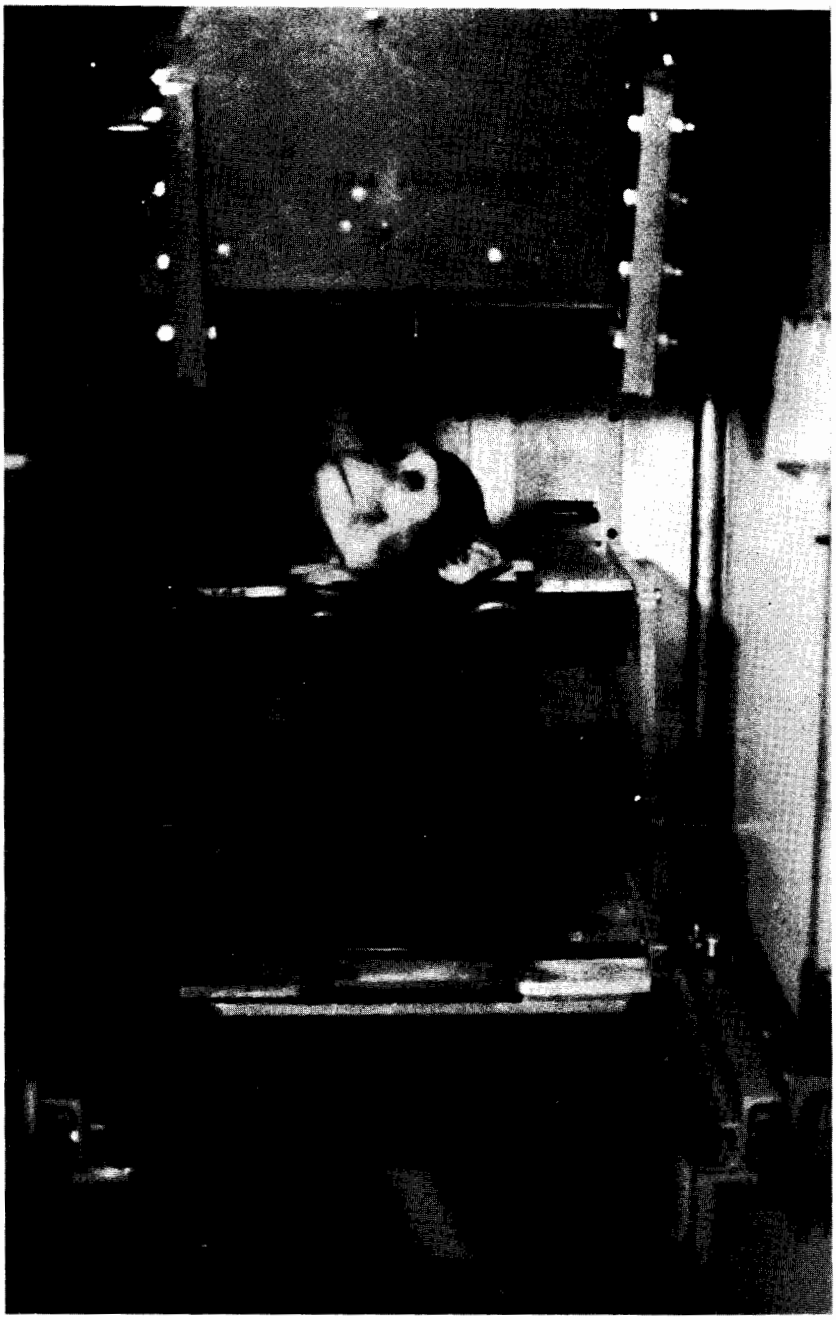


Figure 25.

DISCUSSION AND FUTURE DIRECTION

An experiment describing another observed biological effect is always interesting and in the past has been helpful in establishing the fact that various kinds of biological effects of microwave radiation can and do exist. It is, however, time to cease looking only for just another effect and begin to design and direct future experimental work toward the more basic and fundamental questions relating to the chain of events between cause and effect. The random exposure of whole animals may be incapable of resolving such questions. For example, whole-body exposure of pregnant mice will not allow the experimenter to distinguish between primary fetal effects, due to growth of fetal cells in an externally applied electric field, or secondary effects due to a disruption of the metabolism of the mother. A second example is the reported work on the effects on the blood-brain barrier system[29,31]. In one instance[29], radioactive-labelled molecules were injected into the animal after irradiation, and then samples of the brain of the animal were analyzed by counting tagged molecules. The animal was sacrificed 15 seconds after injection. The question of whether the permeability of the membrane is directly affected by melting or distortion, or whether the metabolic system has been affected by some effect on another organ, is not answered by this experiment, since the whole animal was exposed under free-field conditions. The complexity of the biological system may not allow such differentiation even with selective exposure systems. This may then indicate that the system selected for study is inappropriate, and that the results of such an experiment will aid only in arousing interest in the subject of biological effects of microwave radiation. They may not aid in the understanding of the mechanisms relating cause and effect.

The biological effects researcher must be made aware of the dosimetric tools at his disposal. First, we have previously mentioned the ability to measure or calculate internal fields. These statements are not meant to imply that these measurements or calculations are easily accomplished. Nevertheless, this can be done and must be done in order to compare experimental results,

or make any attempt to extrapolate from levels obtained with animal experimentation to possible safe levels for humans. Secondly, the experimenter must be aware of the ability to control energy deposition so that the desired area or organ receives a maximum exposure while deposition in other parts of the body is minimized. An example can be taken from the work on hyperthermia. To selectively heat cancerous tumors, Taylor[32] developed the antenna array shown in Fig. 26. This particular experimental design is a two-element antenna array made from double-cladded PC board using stripline techniques. Multiple-element arrays are possible. Proper phasing of the array elements allows focusing within the tissue at the location of the tumor. This provides a means of minimizing or avoiding overheating of the skin or subcutaneous tissue while exposing the tumor to a high level of radiated power. The design shown has undergone engineering testing only and has not been clinically tested. However, it demonstrates the concept of selective exposure.

CONCLUSION

Exposure systems must be designed through the joint efforts of the engineer, biologist and/or biophysicist after the objective of the experiment has been established and possible mechanisms of expected effects have been considered. Such consideration may dictate selective or whole-body exposure. In either case, the standard universal exposure system does not exist. There are, however, standard procedures and measurements that should be incorporated. First, temperature and humidity should be controlled and held at a fixed, agreed-upon value unless variation is desired, or other extenuating circumstances exist. These values could appropriately be 28°C and 40% humidity for whole-body exposure and 37°C for cell exposure. Secondly, internal fields throughout the exposed animal or cell system should be described through measurement or calculation, so that an appropriate comparison of experimental results can be made. Hypotheses concerning mechanisms can only be tested if a detailed knowledge of energy deposition exists. Thirdly, the exposure field characteristics of frequency and modulation must be monitored and controlled.

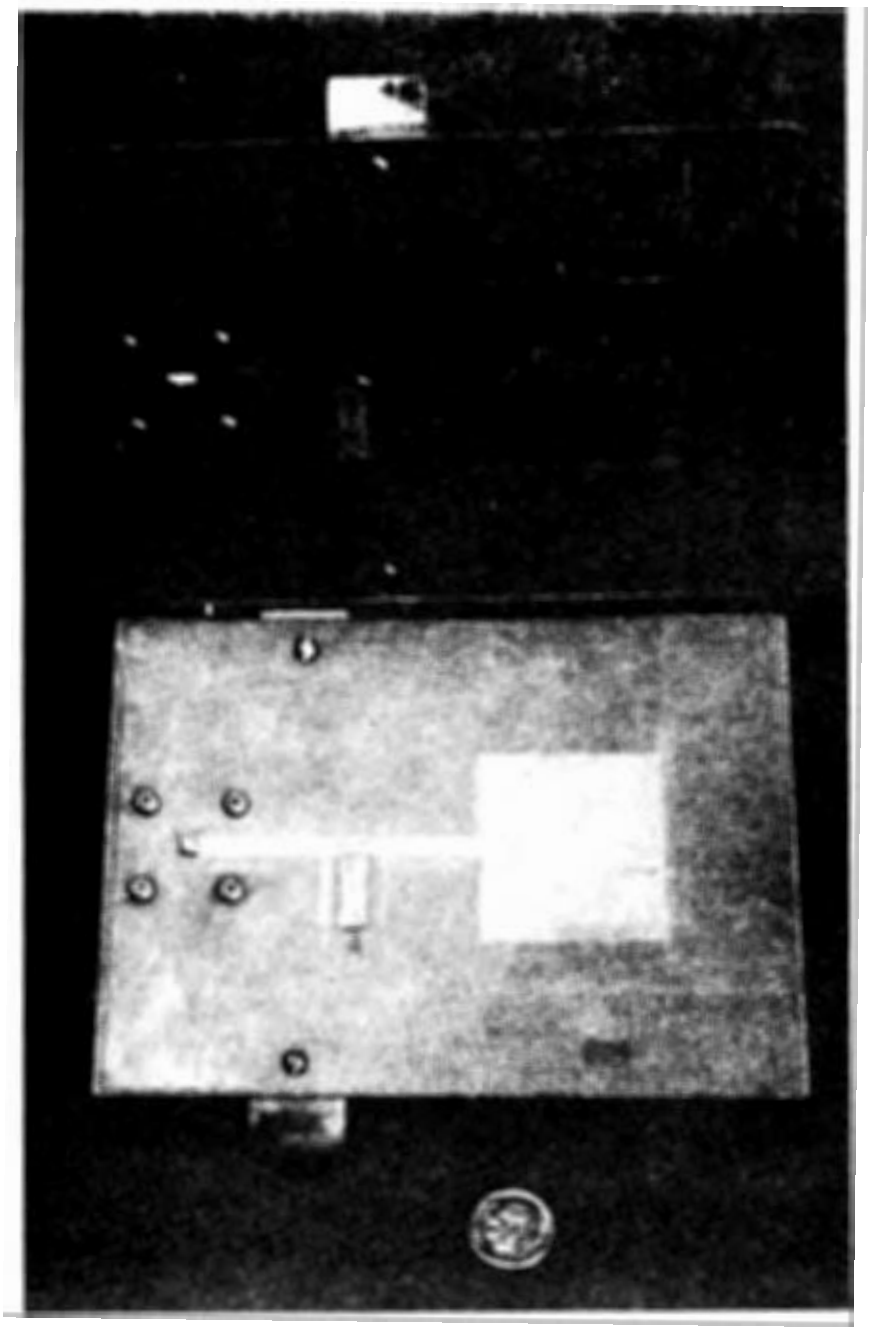


Figure 26.

REFERENCES

1. S. A. Oliva and G. N. Catravas, *Microwave Exposure Facility: Multiple Animal Exposure at Equal Power Density*. AFRRI Scientific Report 76 (April 1976).
2. H. S. Ho, M. R. Foster and M. L. Swicord, Selected Papers of the USNC/URSI Annual Meeting, Vol. II,423, Boulder, Colorado, (October 1975).
3. J. C. Lin, H. I. Bassen and C. L. Wu, IEEE Trans. Biomed. Eng., 80 (1977).
4. H. S. Ho, Effect on Plexiglas Animal Holders on Microwave Energy Absorption. Submitted for publication in IEEE Transactions on Biomedical Engineering.
5. A. R. Shapiro, R. F. Lutomirski and H. T. Yura, IEEE Trans. MTT-19, 187 (1971).
6. S. M. Neuder, R. B. Kellogg and D. H. Hill, in *Biological Effects of Electromagnetic Waves*, Selected Papers of the USNC/URSI Annual Meeting, Vol. II, Boulder, Colorado, (October 1975). December 1976 DHEW Publication (FDA) 77-8011.
7. H. S. Ho, Ann. N. Y. Acad. Sci. 247, 454 (1975).
8. S. M. Neuder and P. H. E. Meijer, in *Biological Effects of Electromagnetic Waves*, Selected Papers of the USNC/URSI Annual Meeting, Vol. II, Boulder, Colorado, (October 1975).
9. D. E. Liversay and K. M. Chen, IEEE Trans. MTT-22, 1273 (1974).
10. S. K. Chang and K. K. Mei, IEEE Trans. AP-24, 35 (1976).
11. J. Everts, W. Herman, M. Colvin, C. Phillips and R. Porter, presented at 1972 Symposium on Microwave Power, Ottawa, Canada.
12. P. S. Ruggera, in *Biological Effects of Electromagnetic Waves*, Selected Papers of the USNC/URSI Annual Meeting, Vol. II, Boulder, Colorado, (October 1975).
13. O. P. Gandhi, IEEE Trans, BEM-22, 536 (1975).
14. M. Crawford, Generator of Standard EM Fields Using TEM Transmission Cells, IEEE Trans. EMC-16, 189 (1974).
15. Instruments for Industries, New York.
16. J. C. Mitchell, *A Radiofrequency Radiation Exposure Apparatus*. USAF School of Aerospace Medicine Report SAM-TK-70-43.
17. C. L. Christman, H. S. Ho and S. Yarrow, IEEE Trans. MTT-22, 1268 (1975).

18. J. C. Monahan and H. S. Ho, in *Biological Effects of Electromagnetic Waves*, Selected Papers of the USNC/URSI Annual Meeting, Vol. II, Boulder, Colorado, (October 1975).

19. A. W. Guy and C. K. Chou, in *Biological Effects of Electromagnetic Waves*, Selected Papers of the USNC/URSi Annual Meeting, Vol. II, Boulder, Colorado, (October 1975).

20. F. Buchta, private communications.

21. A. W. Guy, Presented at 1976 Annual Meeting, URSI, Amherst, Mass. (October 1976).

22. R. L. Carpenter, E. S. Ferri and G. J. Hagan, in *Biological Effects of Nonionizing Radiation*, Ann. N. Y. Acad. Sci. 247, 142 (1975).

23. H. S. Ho, Gary J. Hagan and M. R. Foster, IEEE Trans. MTT- (1975).

24. W. D. Galloway, in *Biological Effects of Nonionizing Radiation*, Ann. N. Y. Acad. Sci. 247, 410 (1975).

25. H. S. Ho, in *Biological Effects of Nonionizing Radiation*, Ann. N. Y. Acad. Sci. 247, 454 (1975).

26. H. S. Ho and J. Faden, Health Physics 32, (1977).

27. A. Z. Smolyanskaya and R. L. Vilenskaya, Sov. Phys. USP 16, No. 4, 571 (Jan. Feb. 1974).

28. S. M. Bawin, R. J. Gavalas-Medici and W. R. Adey, in *Biological and Clinical Effects of Low-Frequency Magnetic and Electric Fields*, Charles C. Thomas, Springfield, Ill. (1974).

29. K. J. Oscar and T. D. Hawkins, *Electromagnetic Radiation Effects on the Blood-Brain Barrier System of Rats*. Proc. 1975 Annual Meeting, USNC/URSI, Boulder, Colorado, (October 1975). Also to be published Published in Brain Research.

30. P. Czerski, in *Biological Effects of Nonionizing Radiation*, Ann. N. Y. Acad. Sci. 247, 232 (1975).

31. E. N. Albert, L. Grau and J. Kerns, *Microwave Effects on the Blood-Brain Barrier of Hamsters*. Presented at 1976 Annual Meeting USNC/URSI, Amherst, Mass.

32. L. S. Taylor, private communications.

* *

DISCUSSION

The directional coupler which you are using to measure the power will not perform correctly if there is multimoding. Thus the modes created by the presence of the animal in the guide disturb the system. [Taylor].

Swicord: One should try to operate the system at the lower frequency end of the waveguide in order to minimize the multimoding. Secondly, there should be a long enough section of the waveguide between source and subject to minimize any multimode interactions.

What I mean is that the presence of the animal creates higher modes, which are evanescent in the same section of waveguide. Consequently, some of this power goes into waveguide losses and you overestimate the amount of power which is being absorbed by the animal. [Taylor].

Swicord: The evidence for such modes is not present, and one might argue that they are certainly going to be small in comparison to the amount of energy that is absorbed into the animal.

We have made calormetric comparative measurements, using whole bodies and water loads to directly measure average absorption. Comparison with the power measurements is excellent. Thus such effects must be small. [Chou].

Your philosophical leaning here is away from the whole measurement - am I correct? [Olsen].

Swicord: Yes.

This appears to assume that the question of hazard has been answered. We are whole bodied receptors. What is your reply to that? Has the question of hazard been answered? [Olsen].

Swicord: Quite the opposite. All that has really been done to date is catalog a number of effects, and we could continue with the cataloging of effects *ad infinitum*. Unless we are ready to introduce and test hypotheses, we are not going to make any more progress toward finding out what are the causal relationships. Until these are really established, the degree of hazard or what is hazardous will be difficult to ascertain.

Just a comment; I think it is the extrapolation from animal to man that is very difficult. If one could localize the effect and understand the effect on the organism being studied it would be much better than just a linear extrapolation to man. [Bassen].

Swicord: Clearly, a great deal of thought must go into determining what sort of exposure measurements should be made.

CALIBRATION TECHNIQUES FOR MICROWAVE AND RF EXPOSURE MEASUREMENT DEVICES

Howard I. Bassen

Bureau of Radiological Health, U.S. Food and Drug Administration
Rockville, Md.

ABSTRACT

Several methodologies have been recently developed by various laboratories which allow isotropic "hazard probes" to be calibrated under "free-space" conditions with an overall uncertainty of less than ± 1 db, traceable to primary electrical power standards. One technique, most suitable above 500 MHz, involves the use of an anechoic chamber and a waveguide horn antenna whose gain is precisely calibrated under "far-field" conditions. To ensure the most precise calibration of system mismatches and the accurate transfer of electrical power standards to the radiated power-density calibration system, the power equation techniques developed by Engen of NBS are utilized by BRH. Special measures must be taken to eliminate artifacts from various multipath reflections which exist in the anechoic chamber. A complementary technique is employed below 500 MHz to calibrate isotropic hazard probes. It involves the use of a rectangular TEM transmission line cell originally developed by Crawford of NBS. In addition to providing accurate calibrated field strengths from D.C. to 500 MHz, these "cells" require only a moderate amount of RF power to generate fields of sufficient strength to calibrate hazard probes over their intended range of operation. The evaluation of probe performance with respect to temperature, antenna pattern, field modulation, and other parameters is also discussed. In addition, radiofrequency interference (RFI) in the probe's output cable and readout instrumentation package is discussed as a significant source of error.

INTRODUCTION

A variety of calibration methodologies have been developed by various researchers to permit the accurate calibration of hazard probes that are used to measure leakage from microwave ovens, microwave and RF diathermy machines, radar systems and other electronic products emitting electromagnetic radiation. In addition, these probes are extensively used to evaluate the levels present in near-and far-field exposure systems used by biological effects researchers. An important aspect of such calibration systems is the accurate transfer of primary electrical power standards to electromagnetic field strength. Therefore, an overall calibration methodology which deals with direct traceability to a primary electrical standard is required, with particular emphasis on the minimization of cumulative errors or uncertainties. Both plane wave (far-field) and guided wave calibration systems will be discussed.

MICROWAVE PLANE WAVE CALIBRATION SYSTEM

A large body of literature exists[1,2] which deals, both analytically and experimentally, with the determination of the gain of standard horn antennas. Additional problems arise when an electrically small antenna such as a hazard probe is introduced into the overall measurement procedure. The many near-field measurement problems, unique to specific leakage probes and their inherent antenna/sensor design, require special consideration.

In the BRH plane wave calibration systems, extensive use is made of the power equation techniques developed by Dr. G. Engen of the National Bureau of Standards, allowing the basic quantities of power and mismatch in a waveguide to be transferred to the calibration of radiated power. Accurate measurement of the path loss between two truncated waveguide horn antennas is performed in an anechoic chamber, facilitating antenna gain determination. A high-power directional coupler, in series with the transmitting antenna, is calibrated to allow absolute transmitted power to be monitored. A small isotropic probe may be placed at a point in the chamber and calibrated, using a television camera with telephoto lens to observe the instrument's indicated power density Fig. 1. Evaluation of multipath reflections and other error sources allows the precise prediction of plane wave power density at this specific point in the chamber.

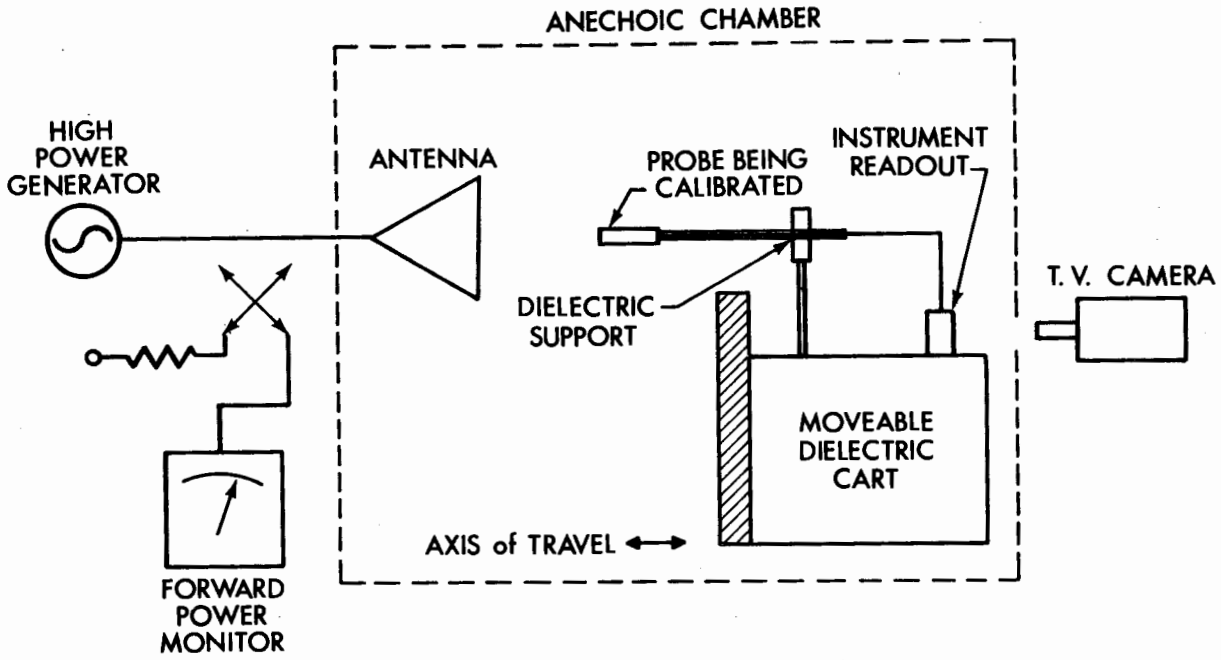


Figure 1. Probe Calibration System.

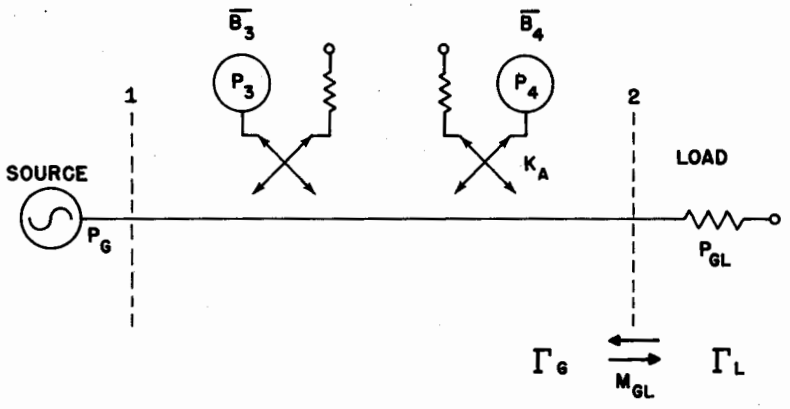


Figure 2. One Port Power Equation Measurement System.

POWER EQUATION CONCEPTS

The use of power equation concepts permit fast, accurate measurements of the total system mismatch, insertion loss, and absolute power without the restrictive requirements of precision connectors. During these measurements the entire system is treated as a unit, eliminating the characterization of each component with respect to an arbitrary "standard impedance." Cumulative errors associated with the multiple measurements of VSWR, complex impedance, or s-parameters are reduced significantly in the specific application to be discussed. The power equation theory and various application techniques have been well-documented[3-5]. In considering the evaluation of mismatch, it is useful to examine the question of power transfer from a generator/directional-coupler combination to a one-port device Fig. 2. In this case, using power equation terminology, we have the relationship[4]

$$P_{g\ell} = P_g M_{g\ell} . \tag{1}$$

In the above equation, $P_{g\ell}$ is the net power delivered by the generator to the load, P_g is the available power (the maximum power that can be delivered to a passive load by the generator) and $M_{g\ell}$ is a matching factor, which may have any value between zero and unity. P_g, $P_{g\ell}$, and $M_{g\ell}$ are all positive and real. Further, $M_{g\ell}$ is only a function of the coupler/load combination and is independent of the actual signal source[4]. In more conventional terminology[3]

$$M_{g\ell} = 1 - \left| \frac{\Gamma_\ell - \Gamma_\ell^*}{1 - \Gamma_\ell \Gamma_g} \right|^2 . \tag{2}$$

The parameters used in Eq. (2) are complex reflection coefficients defined as follows:

Γ_ℓ is the reflection coefficient of the load, and Γ_g is the reflection coefficient of the equivalent generator associated with the directional coupler. It should be emphasized that Γ_g is dependent upon the directivity of

the coupler, among other factors. Furthermore,

$$P_g = P_4 k_a \quad . \tag{3}$$

Power P_4 represents the coupler sidearm power and k_a is a property of the coupler/sidearm-detector combination. P_g, P_4, and k_a are all positive and real. It should be noted that k_a is independent of the load at port 2, irrespective of the coupler directivity. In general, P_g is not equal to the power associated with the forward-propagating (generator-to-load) component of the signal in the coupler main arm.

Engen[3] has shown that if the generator/coupler combination is terminated in a sliding short such that $\Gamma_\ell = e^{j\theta}$, the complex voltage ration, b_3/b_4, is described by a circle having a center at R_c and a radius R (Fig. 3), where $b_n \propto P_n^{1/2}$. Thus:

$$\left| \left(\frac{b_3}{b_4}\right)_{max} \right| = \left(\frac{P_3}{P_4}\right)^{1/2}_{max} = R + |R_c|$$

$$\left| \left(\frac{b_3}{b_4}\right)_{min} \right| = \left(\frac{P_3}{P_4}\right)^{1/2}_{min} = R - |R_c| \tag{4}$$

Therefore, by attaching a sliding short to port 2 (Fig. 2) and measuring b_3/b_4, the above equations may be solved to obtain values of R and R_c for the particular configuration measured. Furthermore, it has been shown that, for any passive load:

$$M_{g\ell} = 1 - \left(|w - R_c|^2 / R^2 \right) \tag{5}$$

where $w = b_3/b_4$ for the load of interest.

The parameter $M_{g\ell}$ in Eq. (1) can be unambiguously determined by values of w, R_c, (complex quantities), and R. If phase measurement capabilities are not available, a tuner must be used to eliminate either w or Rc. In the present BRH application, offset waveguide shorts together with phase and amplitude

data provide the capability for rapid multi-frequency measurements in each ISM band. Computation of $M_{g\ell}$ is performed from this data. When measuring the path loss between antennas (Fig. 4) via power equation techniques, the magnitude of the loss is large enough (>15dB) to allow a one-port mismatch measurement to be performed independently on both transmitting and receiving antenna. Path loss (η_a) may be computed from the relationship

$$\eta_a = \frac{P_{g\ell}}{P_4 k_a M_{ga} M_{a\ell}} \tag{6}$$

where M_{ga} and $M_{a\ell}$ are matching factors of the transmitting and receiving antennas respectively. The effects of chamber surface and antenna support structure reflections are included in the measurement of matching parameters. Other parameters are illustrated in Fig. 4 for the path loss measurement.

ANTENNA GAIN MEASUREMENT

The relationship employed in the calibration of far-field power density, S, is:

$$S = \frac{P_T G_T}{4\pi r^2} \tag{7}$$

where the transmitted power, P_T, and distance, r, from an antenna with far-field gain, G_T, are measured quantities[6]. For finite separations between the pair of antennas, a "near-zone correction factor" must be applied to the far-field gain of the antennas[7]. This factor has a value of less than one and increases with separation distance, approaching unity as a limit. As long as antenna separations are greater than many units of a^2/λ (where a is the maximum aperture dimension of the larger antenna and λ is the wavelength of the transmitted signal) plane wave power density may be computed using Eq. (7) where G_T is the product of the constant far-field gain and the near zone correction factor. (G_T is a function of distance.) This separation criterion ensures that no transmitting antenna reactive fields are intercepted by the receiving antenna and only second-order field curvature effects are corrected.

Using a total of three antennas in three combinations of two antennas per path loss measurement, individual antenna gains may be computed from the relationship:

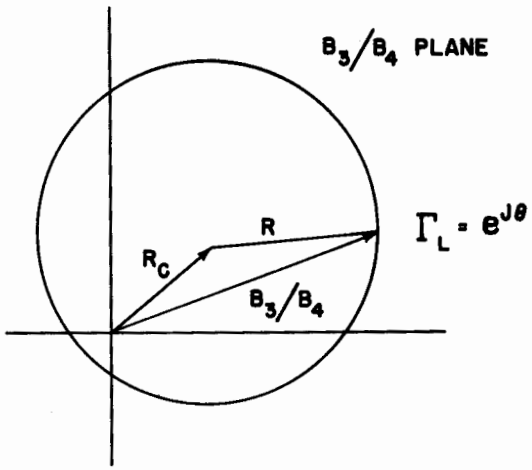


Figure 3. Power Equation Relationships.

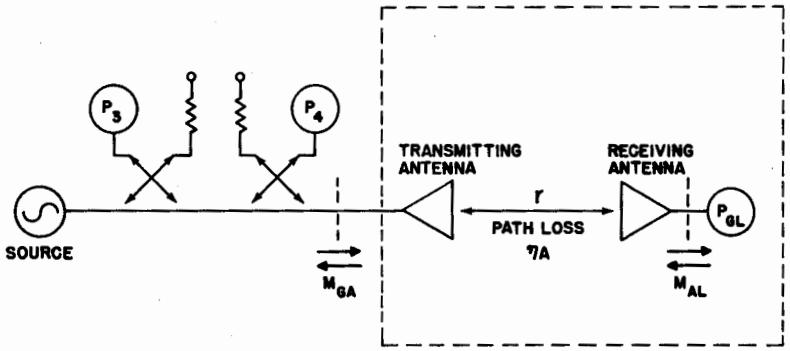


Figure 4. Path Loss Measurement System.

$$G_T G_R = \frac{P_R}{P_T} \left(\frac{4\pi r}{\lambda}\right)^2 \qquad (8)$$

where $(P_R/P_T) = \eta_a$ as previously defined. Antenna reciprocity is assumed, implying that gain is not dependent upon the role of the antenna (transmitting or receiving) or its physical environment (assuming sidelobe reflections are negligible). Experimental tests were performed to ensure that the separation distances between antennas were sufficient to justify the "plane-wave" and the reciprocity assumptions.

ABSOLUTE TRANSMITTED POWER CALIBRATION

It is required that plane-wave power densities be generated with magnitudes sufficient for the calibration of typical microwave hazard survey instruments (1-10mW/cm^2) at distances from the transmitting antenna which satisfy previous theoretical assumptions. Therefore, high powers (up to 1 KW) must be transmitted. A convenient and highly accurate secondary standard of absolute microwave power is the coaxial bolometer, calibrated as a function of dc substituted power for a given net microwave input power (1mW) with a self-balancing bridge. To establish a high power density level in the far field of a horn antenna, much larger amounts of power must be accurately measured with respect to this reference. A cascaded directional coupler technique[8] may be used to obtain accurate 100-1000 watt calibrated power measurements. A unitized "high-power meter", separate from the power density calibration system, was created for use as a high power reference standard. This "high-power meter" serves as a transfer standard, tying the power density calibration system to the precisely calibrated 1 mW reference bolometer previously mentioned. When used in conjunction with power equation techniques, a minimum amount of cumulative error exists in the transfer of calibration procedures from the electrical standards laboratory to the power density calibration facility. These coupler/bolometers have been precisely calibrated by the National Bureau of Standards for effective efficiency (the ratio of dc substituted power in the bolometer to net microwave power). The calibration of transmitted power involves the use of the subsystems shown in Fig. 5. The

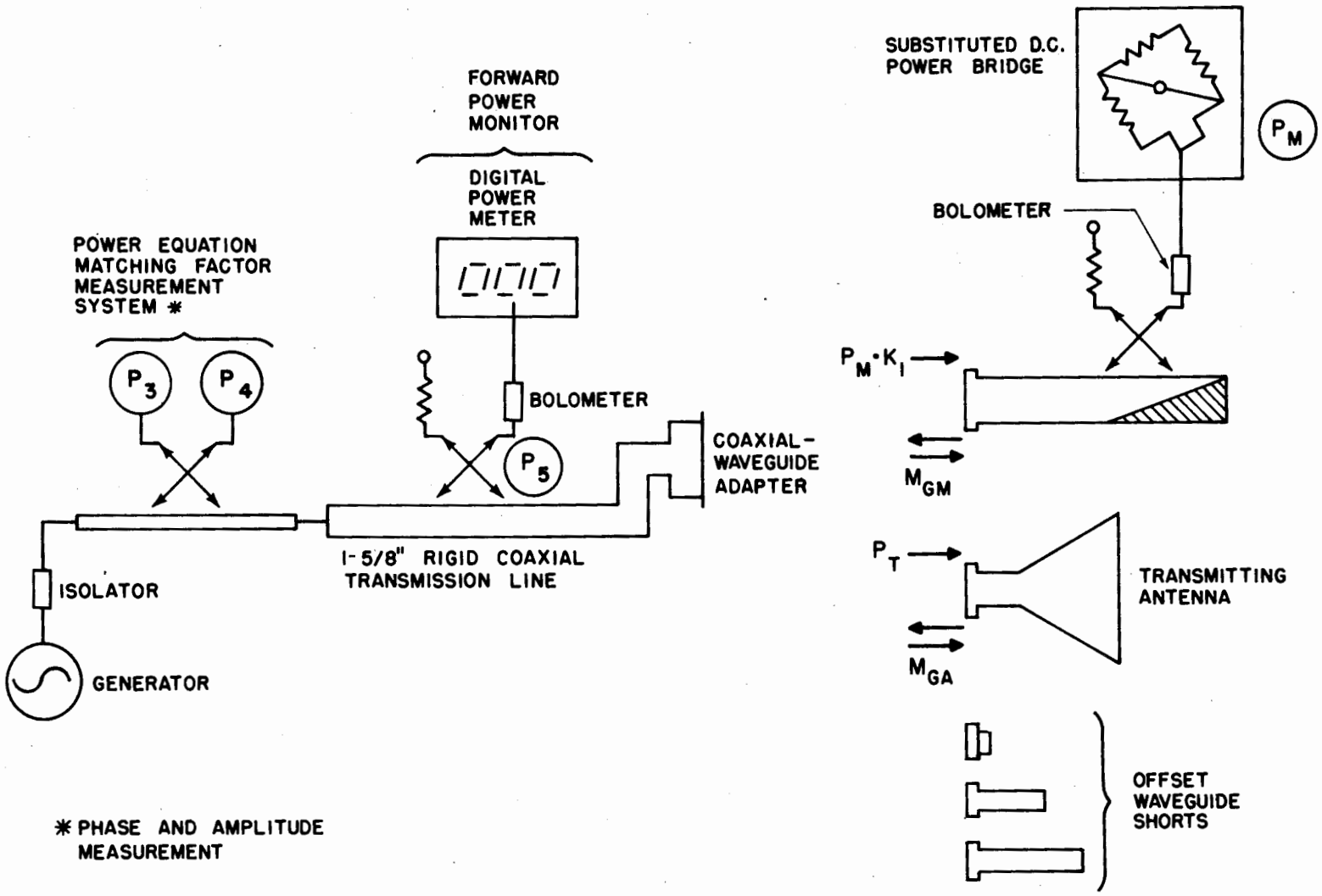


Figure 5. Absolute Transmitted Power Calibration.

subsystems are: a transmitting antenna, the calibrated coupler/bolometer, a forward power monitor (consisting of a rigid, high-power transmission line with an integral directional coupler, sidearm power meter, and waveguide output port), a set of three waveguide offset short circuits, and an additional pair of directional couplers to measure matching factors. Only the antenna and forward power monitor are used in the final system operation, Fig. 1.

During the calibration procedure, the forward power monitor is first terminated by the calibrated coupler/bolometer. The reading of power meter, P_4, on the first set of directional couplers and the value of substituted dc power applied to the previously calibrated reference coupler/bolometer are simultaneously recorded. The coupler/bolometer's matching factor, M_{gm}, is measured next via power equation techniques involving the use of the offset shorts. The next step is to terminate the system with the transmitting antenna and to measure M_{ga}, the match to the antenna. Finally, simultaneous values of P_4 and P_5 (where P_5 is the meter reading of the forward power monitor) are also recorded with the antenna in place. The linearity of P_4 and P_5 must be accounted for when various power levels are to be transmitted. The net power fed to the transmitting antenna, P_T, is expressed as:

$$P_T = \frac{P_m k M_{ga}}{M_{gm}} \tag{9}$$

where P_m is the substituted dc power applied to the bolometer to restore its original resistance (as measured before microwave generation). In addition, k is defined as the effective efficiency of the coupler/bolometer. Parameters M_{ga} and M_{gm} are matching factors which were previously defined. During this procedure the power P_4 is held constant while the coupler/bolometer and then the antenna terminate the system, implying that P_G is constant from Eq. (3).

LABORATORY MEASUREMENT TECHNIQUES

Power equation matching factor measurements were performed on transmitting and receiving antennas using the one port power equation model for each antenna. The lack of significant mutual interaction between antennas was verified experimentally by placing a sliding short circuit on the output of the transmitting antenna (outside of the anechoic chamber). The minimum possible antenna

separation was established and the receiving antenna matching factor, $M_{a\ell}$, was measured. Continuous movement of the sliding short over several wavelengths produced variations of less than one percent in $M_{a\ell}$. This test was more severe than the actual situation where both antennas are terminated in well-matched loads.

The receiving antenna measurement configuration is shown in Fig. 6 as described by Engen[4]. It was mounted on foam blocks several wavelengths above a dielectric cart in the anechoic chamber. Reflections from the transmitting wall of the chamber as seen by the receiving antenna were significant because of their close proximity of this wall to the transmitting antenna. The receiving antenna matching factor, $M_{a\ell}$, was measured as a continuous function of antenna separation distance. In contrast, the transmitting antenna matching factor was found to be insensitive to cart position because of the minimal scattering cross section of the cart and receiving horn.

Path loss measurements were performed with a precision bolometric ratiometer. First, the zero path-loss case was established by removing both antennas from their respective mounts. The transmitting and receiving waveguides were bolted together, and both the mismatch and the received to transmitted power ratio were measured. Path loss between antenna pairs was plotted as a function of distance using an accurate cart position encoder. Chamber multipath reflections were minimal (less than 0.1 dB) because of the careful selection of the proper directivity of antennas and good chamber design. Antenna sidelobe radiation effects and leakage from transmission line connectors were checked and eliminated by various experimental techniques. Both antennas were carefully aligned so that their mechanical boresight axis coincided with the chamber's central axis. Alignments were performed with a laser, rigidly mounted outside the chamber. Its beam was transmitted through the rear wall, parallel to both the chamber's center axis and the rails on which the dielectric cart rode. Special waveguide inserts containing a first surface mirror were placed in each antenna to enable their alignment with the chamber's center axis.

HAZARD PROBE CALIBRATION

Multipath effects due to chamber wall reflections can cause significant

calibration errors when low gain antennas, such as those used in a microwave hazard probe,are exposed at large distances from the transmitting antenna. These reflections may be accounted for, and their effects eliminated as follows: The probe in question is placed on a movable dielectric cart and its received power density indication is plotted as a continuous function of distance to the transmitter. Periodic oscillations appearing on the plot represent multipath effects. Since cart position can be repeated precisely, any probe with nominally identical antenna characteristics may be calibrated and multipath errors corrected for as a function of distance to the transmitting antenna based on the knowledge of the magnitude of the oscillation. Reflections from the cart and dielectric support structures which hold the probe produce additional errors that cannot be detected by moving the cart and probe with respect to the transmitting antenna. A technique was devised to minimize these reflections. Cart reflections may be quantified by varying the cart position, while observing the net field strength standing waves with a stationary isotropic probe of the type to be calibrated. The probe in this case is not on the cart, but is mounted in the center of the chamber between the transmitting antenna and the cart, intercepting the chamber's center axis. Absorbing material is added to the cart until the reflections, as seen by the probe, are minimized. This technique has been utilized not only to quantify cart reflections, but also to facilitate the measurement of reflections from various dielectric objects[9].

Although cart reflections may be reduced through the use of absorber material, second-order errors of several percent remain when a probe is placed on the cart at a great distance from the transmitting antenna. Since the position of standing waves in the observed field strength is known for a stationary probe placed ahead of the cart, "multi-position averaging" over a number of cycles of the standing waves may be used to greatly reduce residual errors due to cart and probe support reflections. The distance D_2 is varied in half-cycle increments of the standing wave (Fig. 7) while distance D_1 is reset to the same value for all measurements. The distance corresponding to one

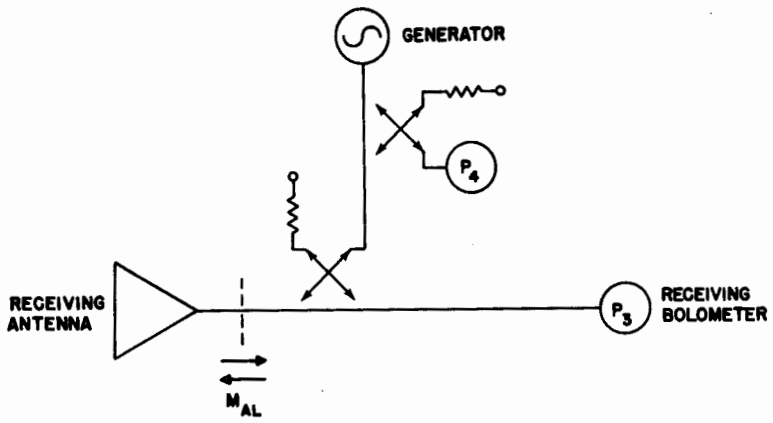


Figure 6. Receiving Antenna Measurement System.

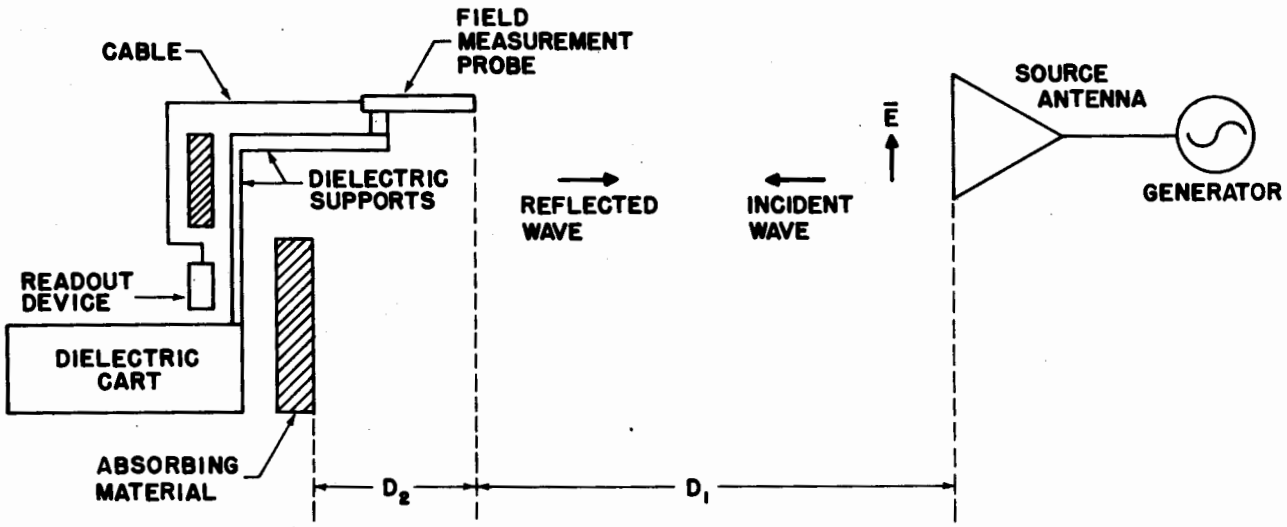


Figure 7. Multi-Position Averaging Technique.

cycle of the standing waves was found to be exactly one-half wavelength, because of the straight-line reflection path from the cart to the probe. Numerical averaging of the indicated power density of the probe was performed for four or more values of D_2 (each one-quarter wavelength greater than the previous value). This resulted in enhanced accuracy, and excellent repeatability of calibration (better than 3%).

The assumption was previously made that the separation between the transmitting antenna (truncated pyramidal horn) and receiving antenna (either an identical horn or small probe) was sufficient to ensure negligible amplitude and phase curvature of the received field. If this were not the actual case, spatial averaging over the large aperture of the receiving horn would occur during gain measurement. This would introduce an error in the calibration of a small probe when the latter was positioned on the boresight of the transmitting antenna, because of the small "effective aperture" of the probe. The worst case occurs in the lower frequency range (915 MHz) where a separation of only ($6.5\ a^2/\lambda$) exists in the center of the chamber. To estimate field curvature, experimental scanning over a plane normal to the axis of propagation was performed with an electrically small probe. Numerical integration of data yielded a spatially-averaged power density value over an area defined by the physical dimensions of the receiving horn. (The receiving antenna was removed from the chamber during the scanning process). A comparison of this spatially-averaged value with the single "spatial maximum" value obtained at the geometric center of the plane was made. The ratio of spatial "maximum" to "average" power density was 0.95 at the above separation. Since the horn antenna's "effective aperture" is considerably smaller than its physical aperture, an error of less than 0.05 db is estimated due to finite antenna separation after an approximate correction factor is assigned to subsequent calibrations.

ERROR ANALYSIS

The uncertainties involved in the power density calibration system may be divided into three main categories: (1) uncertainties associated with the horn gain measurements, (2) uncertainties associated with the calibration of the

forward power monitor, and (3) multipath effects for an isotropic probe calibration. The gain measurements involve uncertainties in antenna mismatches, separation distances, and path loss measurements (including multipath effects).

The error analysis (Table 1) presents the worst-case uncertainty levels that occur in an optimum system. The values are conservative, and because of the random nature of many measurement errors, an actual absolute power density calibration performed with the optimum system is probably more accurate than presented.

TABLE I

PLANE WAVE POWER DENSITY CALIBRATION SYSTEM UNCERTAINTIES

Measurement	Worst Case Uncertainty (Optimum System) 915 MHz	2450 MHz
Antenna Path Loss	(db)	(db)
Distance measurement*	.01	.01
Ratiometer Nonlinearity	.05	.05
Mismatch Measurements	.05	.05
Multipath Effects and Scattering	.15	.05
Antenna alignment	.02	.05
Error Summation - Antenna Pair	.28	.21
Net Gain Uncertainty - Single Antenna	.42 = ε_A	.32 = ε_A
Absolute Transmitted Power		
Coupler/Bolometer Calibration*	.09	.09
Transfer Error	.05	.05
Mismatch Measurements	.05	.05
Total Transmitted Power Uncertainty	.19 = ε_p	.19 = ε_p
Isotropic Probe Calibration		
Residual Chamber Multipath	.05	.02
Residual Cart Reflections	.05	.02
Field Curvature (non-infinite separation)	.05	.01
Total Probe Calibration Uncertainty	.15 = ε_I	.05 = ε_I
Total Calibration System Uncertainty $\varepsilon_A+\varepsilon_p+\varepsilon_I$	.76	.56

*Using NBS-calibrated transfer standards

FUTURE IMPROVEMENTS IN MICROWAVE POWER DENSITY CALIBRATION TECHNIQUES

An improvement of the overall accuracy of plane-wave power density calibration techniques appears possible through the use of near-zone antenna gain calibrations obtained by applying an extrapolation technique developed by Newell[10] and others at NBS. This technique involves the measurement of the power transfer between horns (or other types of antennas) at distances substantially less than the presently used far-field separations. This method eliminates multipath reflection artifacts from anechoic chamber walls, *etc.*, but introduces a large mutual-antenna interaction artifact. While chamber multipath reflections are transcendental in nature and cannot be predicted or described without a very complex analysis of the chamber environment, the mutual interactions between antennas can be analytically described in terms of an exponentially decaying sinusoid vs increased separation distance and are totally independent of the chamber environment. Therefore, the mutual interaction between antennas can be analytically removed, and a power transfer *vs* distance expression can be constructed in the form of an infinite series which is mathematically fit to the experimental near zone data. Thus, power transfer can be analytically predicted at some arbitrary far field separation distance, without the intrinsic chamber multipath errors associated with conventional far-field techniques.

This technique can be adapted to hazard probe calibration applications if one measures the near-zone power transfer between two identical horn antennas, as well as the power transfer between one of the horn antennas and a probe (or a representative probe from the group of nominally identical probes to be calibrated). This will allow one to account for the relatively large non-uniformity of the fields existing in the near-zone of the transmitting antenna. The "spatially averaged" power density measured by a receiving horn (with a relatively large aperture) will differ significantly from the spatial maximum of power density observed by a probe on the boresight of the transmitting horn in the near zone. This difference can be measured, and the power density calibration in the near-zone can be analytically corrected to eliminate this source of near-zone probe calibration error.

GUIDED WAVE CALIBRATION SYSTEMS

Below 500 MHz, serious problems occur when one attempts to calibrate probes via the free space, power density methods involving horn antennas and an anechoic chamber. This is due to the physically-large wavelength and the subsequent requirement for a large and costly anechoic chamber if one wishes to place a probe out of the nonreactive (or near field) zone of the horn antenna. An accurate and convenient guided wave system has been developed by Crawford[11] at NBS. This system utilizes a rectangular TEM transmission-line "cell." The TEM cell consists of a rectangular metallic outer enclosure, a flat, wide center conducting strip, and tapered input and output feed sections which maintain a 50 ohm characteristic impedance throughout the transmission line (Fig. 8). This "rectangular coaxial" line has been thoroughly analyzed, both theoretically and experimentally, and has been developed into a commercially available product by Instruments for Industry , Toledo St., Farmingdale, N. Y. Advantages of the TEM cell are that it can be used to generate E and H fields with an absolute uncertainty of approximately ± 1 db below 500 MHz and that it does not require either high power generators (greater than 100 watts) nor a large amount of physical space. The chief limitation of this family of cells is that the uniform field zone is limited in size as indicated in Table II.

TABLE II

Upper Useful Frequency (MHz)	Plate Separation,b, (cm)	Cell Width,w (cm)
100	90	108
300	30	36
500	18	21

The plate separation, b, represents the separation of the outer conductor walls which are parallel to the center conducting plane. Higher-order modes exist in this type of cell above the upper frequency value, presented above. In addition, only limited volumes located in the central portion of each half of the cell (above or below the center conductor) possess highly uniform fields

(±10%). This uniform volume is bounded by a dimension of approximately b/10 and w/10. Thus, at 500 MHz one may only calibrate a small probe or sensor in a uniform cube-shaped field volume, several centimeters on a side. At lower frequencies, larger cells can be utilized.

A practical problem often occurs due to total reliance on TEM cells for calibration and evaluation of field strength probes. Due to the enclosed nature of this family of cells and the small uniform-field zone, only the probe tip is exposed to RF fields. RF interference (RFI) in the probe handle, readout cable, and readout electronic package is minimized. However, in practical use (such as field-mapping in animal exposure cavities, or hazard surveys of RF emitters such as broadcast transmitters, *etc.*,) the entire measurement system is exposed to high level RF electric and magnetic fields. RF interference does occur in the various system components, resulting in erroneous data obtained with a precisely-calibrated probe. To recognize this problem, one must immerse the entire probe system under evaluation in a uniform field, either in a very large TEM cell, or in a plane wave field in an outdoor test range or large anechoic chamber.

INSTRUMENT EVALUATION

In addition to calibrating an instrument in a known field, the response of that instrument to various field parameters must be known. These parameters are often encountered during the operational measurements of complex fields generated by a near-field source, or existing in a non-ideal, far-field situation. The ambient temperature, the polarization of the electric field and its amplitude modulation, as well as other parameters must be considered and the instrument's response noted. The test apparatus shown in Fig. 9 has been developed by BRH to provide a means for some of this evaluation at microwave frequencies. A probe, supported by a dielectric holder, is positioned in front of a slot source. The holder is mounted on rails as shown. The variation of probe response, as a function of distance from the slot source, can be observed and standing waves occurring in the system may be minimized by adding microwave absorber. Then near *vs* far field responses of various probes may be compared by moving them toward the slot source from a distance. A probe can be

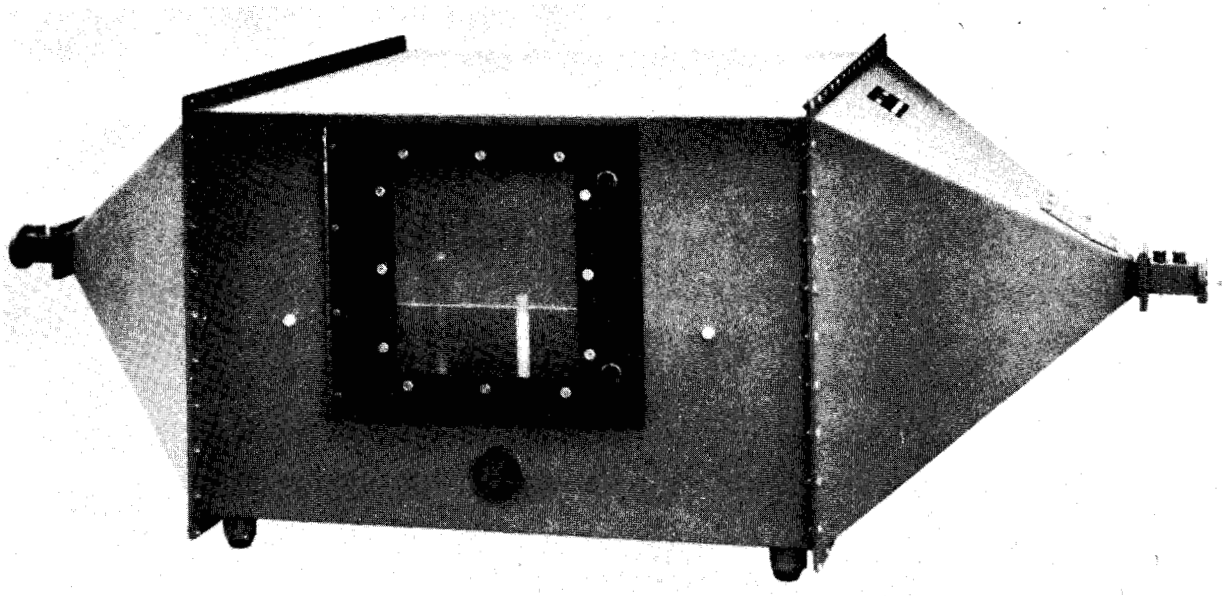


Figure 8. TEM Cell.

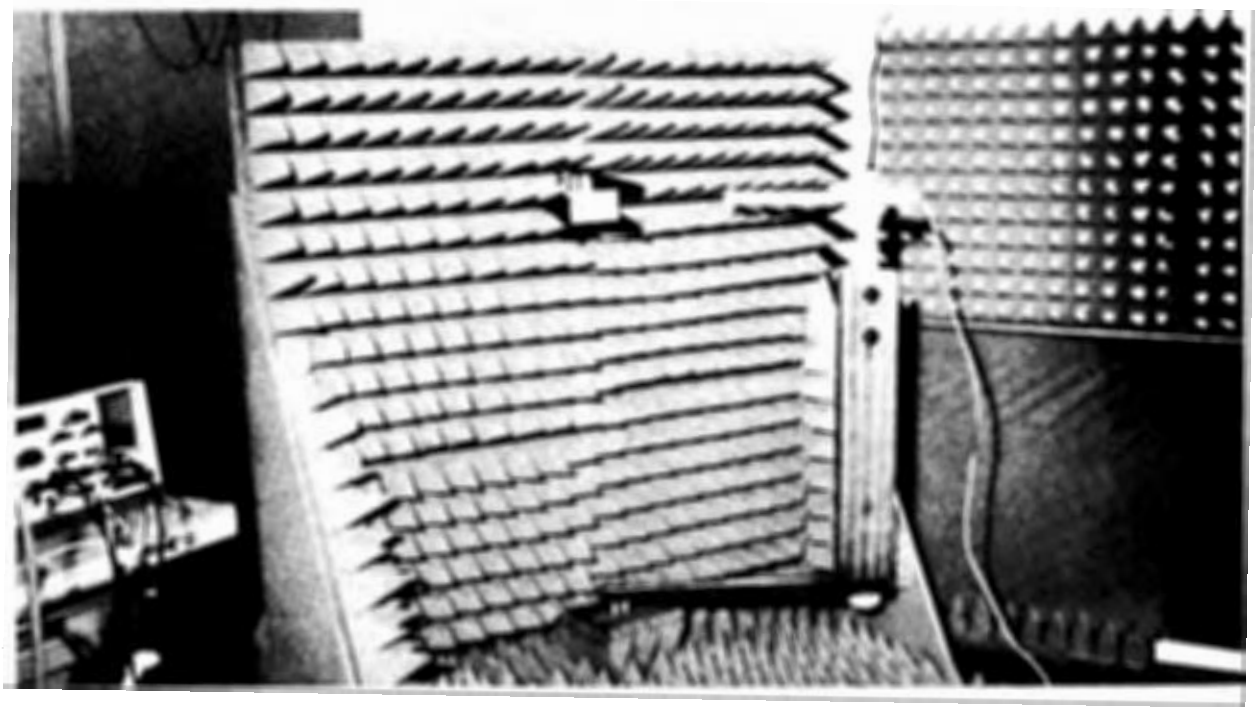


Figure 9. Probe Pattern Evaluation System.

rotated to obtain its angular response (antenna pattern). During this rotation, the center of the receiving sensors of the probe is placed on the probe-holding fixture's axis of rotation. A stable microwave source is used to provide field strengths of appropriate magnitude. In another test, average power to the system is maintained at a constant value while a modulator, driven by a pulse generator, allows complete control of the amplitude modulation impressed upon the radiated fields. This allows the evaluation of instrument response to pulse-modulated fields as well as continuous wave fields of various levels. At RF frequencies, a TEM cell is utilized to perform pulse response and linearity tests.

Another system is used for determining the polarization response of a microwave probe, *i.e.*, the response to a linearly polarized E field as the probe is rotated about its handle axis (Fig. 10). Power is delivered to an absorber-lined box from an open-ended waveguide, while the probe body is supported by a plastic holder. The sensor is maintained at a constant distance from the waveguide. Rotation of the probe about its handle allows one to observe the polarization response or "polarization ellipticity" of the instrument. Similar tests can be performed in TEM cells at RF frequencies.

A specially-designed temperature response evaluation system has been developed. It consists of an absorber-lined environmental chamber (60 cm cubicle) capable of temperature variations from -20° C to $+50^{\circ}$ C using liquid nitrogen cooling and electrical heating. The instrument under test is placed in a plastic holder at a fixed distance from a waveguide slot source (Fig. 11). The fields near the slot have been separately tested for temperature independence. The variation of relative probe response may be observed while constant net power is fed to the slot source at different ambient temperatures. Microwave power is turned off, and the instrument is re-zeroed before readings are taken at each temperature. The entire instrument, including readout, can be placed in the chamber, with the instrument readout viewed through a small plastic window in the side of the chamber.

A final evaluation procedure must be performed to determine the radio-frequency interference susceptibility of the probe body, the cable, and readout meter to strong fields at the specific frequency at which the microwave oven, or other source to be surveyed, operates. The sensor tip of the

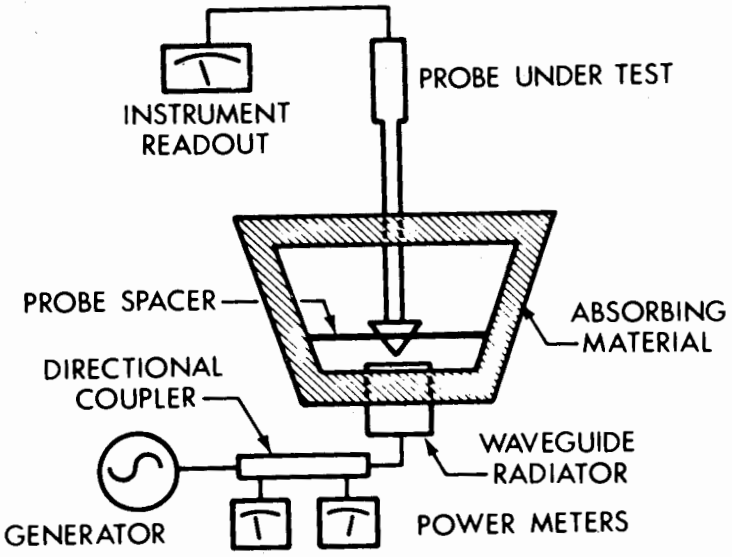


Figure 10. BRH System for Polarization Evaluation.

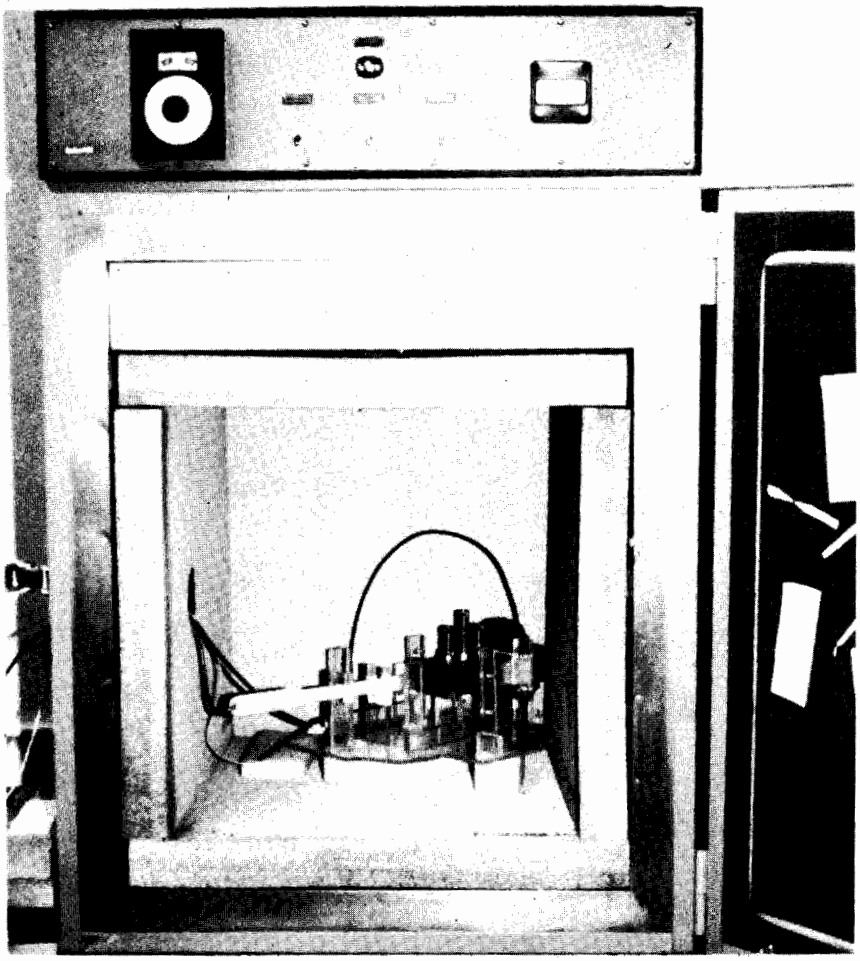


Figure 11. Probe Temperature Response Evaluation System.

probe is totally enclosed in metal foil. The probe body, the cable (which is aligned with the electric field) and the readout meter, are irradiated in a uniform field exposure situation. The response of the readout meter is noted and compared to the reading obtained with the sensor unshielded. Many instruments have failed this test, due to faulty RFI gaskets in readout units, or insufficient filtering in the readout or probe body.

ACKNOWLEDGEMENTS

Dr. Glenn Engen of the National Bureau of Standards, Boulder, Colorado, has provided considerable guidance in the practical application of the power equation techniques to power density calibration. The following members of the Bureau of Radiological Health staff participated in the development of a microwave power density calibration methodology: Mr. W. Herman, Mr. M. Swicord (Chief, Electromagnetics Branch), Mr. S. Neuder and Mr. D. Witters. Mr. P. Ruggera of the Bureau of Radiological Health provided guidance and advice on RF calibration techniques in TEM cells.

REFERENCES

1. T. Chu and R. Semplak, Bell Syst. Tech. J., 527 (1965).
2. W. T. Slayton, *Design and Calibration of Microwave Antenna Gain Standards*, NRL Report 4433 (1954).
3. G. F. Engen, *An Introduction to the Description and Evaluation of Microwave Systems Using Terminal Invariant Parameters*, NBS Monograph 112 (1969).
4. G. F. Engen, *Theory of UHF and Microwave Measurements Using the Power Equation Concept*, NBS Tech. Note 637 (1973).
5. G. F. Engen, IEEE Trans. IM-20, 50 (1971).
6. J. D. Kraus, *Antennas*, New York, McGraw-Hill, (1950).
7. R. Bowman Proc. IEEE 55, 980 (1967).
8. K. Bramall, J. Res. NBS 75C No. 3-4 (1971).
9. J. C. Lin and H. Bassen, IEEE Trans. BM-24, 80 (1977).
10. A. Newell, R. Baird and P. Wacker, IEEE AP-21, 418 (1973).
11. M. Crawford, IEEE Trans. EMC-16, 189 (1974).

* *

DISCUSSION

Where can one buy this instrument? [Priou].

Bassen: It is available from Instruments for Industry, Hicksville, New York. I believe they cost anywhere from $500 to $2000.

What was the comparative temperature response of other instruments? [Priou].

Bassen: We have only tested a Narda probe, and it is somewhat better, but only in the fact that it can be zeroed. I think that most instruments have something like a half-percent per degree C calibration factor response. Although we have not tried many other probes, I think that is typical.

WORKSHOP SUMMARY

S. F. Cleary
Department of Biophysics, Virginia Commonwealth University
Richmond, Virginia 23298

In summarizing the workshop papers I would like to first refer to those papers which related to the development of dosimetry and calibration methods and techniques for quantitating electromagnetic fields. It is apparent that there have been very important advances in this field due to the current awareness of the necessity for accurately measuring field intensities, electric field strengths, and temperatures in tissues. The papers by Gandhi, Cetas, Myers, and Cain all indicated a very keen awareness of the necessity of quantitating the fields in tissue. Hopefully, the outcome will be the development of instrumentation to facilitate the quantitation of parameters such as the E and H fields, the absorbed power, and the tissue temperatures. The papers presented at this workshop strongly suggest that in the near future dosimetric methods and techniques will be improved to the point where the biologist who seeks to relate cause to effect will at least have the physical parameters well defined.

The report by Gandhi indicates that other aspects of electromagnetic interactions are being considered which will aid in the interpretation of biological effects. He has drawn attention to the relationship of energy absorption, radiation frequency, and polarization to the geometrical characteristics of biological absorbers, thus providing additional means for improving upon the interpretation of the results of studies of microwave biological effects. For example, the work by Gandhi relative to electromagnetic field reflections may explain some of the confusion in the past literature on bioeffects of microwaves. It is quite probable that in some instances the exposure conditions were such that there were multiple reflections and standing waves which could have marked effects upon the power densities absorbed by the test specimen to the extent of introducing errors

of at least one order of magnitude. Now that we are aware of the possibilities on intensity amplification due to multiple reflections, we can appreciate the fact that some of the reports in the literature which indicated effects at extremely low levels might, in fact, be explainable in terms of such factors. The awareness of such sources of error will obviously lead to the design of better experiments in the future.

In general, we may conclude that with respect to external and internal field characterization of microwave and radiofrequency radiation, the advances have been rapid in recent years as evidenced by the papers presented at this workshop. Such methods provide the necessary basic information for the determination of physical interaction mechanisms in biological systems.

The next question to be asked is what are the effects of low intensity electromagnetic fields on living systems? In this workshop, interest has been primarily restricted to the microwave, radiofrequency and low frequency regions of the electromagnetic spectrum. Some of the information presented at this workshop relative to the existence of low-intensity field effects is summarized in Table I, along with the estimated field strengths. It should be noted that in addition to these effects there are a number of other reported effects in humans and experimental animals that have been discussed at this workshop and elsewhere.

Probably the most impressive class of low intensity effects of electromagnetic fields involve alterations in the central nervous system. The data presented at this workshop by Dr. Adey concerning the alteration in calcium binding in cerebral tissue is of particular interest in that it not only indicates that changes and direct cortical stimulation are induced at field strengths of 10^{-7} V/cm by exposure to modulated ELF, UHF, and VHF fields but also that in some cases such effects exhibit frequency as well as amplitude windows. Dr. Adey also drew attention to the very interesting finding that sharks and rays apparently can sense electric field strengths of this same order of magnitude, 10^{-8} - 10^{-8} V/cm, indicating the great sensitivity of living systems to certain types of electrical or magnetic stimuli. Another example discussed by Dr. Adey is the possibility that birds utilize induced fields

generated by their flying through the Earth's magnetic field for navigational purposes. Such induced fields are estimated to be on the order of 10^{-8} V/cm.

Dr. Schwan referred to the sensitivity of membranes to low intensity fields of this same order of magnitude, thus drawing attention to biomembranes as the level of organization that may provide a useful model for the transduction of weak electrical or magnetic fields in biological systems. A theoretical membrane-field interaction model, developed by Dr. Grodsky, was presented at this workshop as well as in previous communications.

The effects of low intensity electromagnetic fields are indicated in the abstract by Grundler, Keilmann and Frohlich, who reported frequency-dependent enhancement or retardation of the growth rate of yeast cultures at specific frequencies near 42 GHz, at intensities of a few mW/cm^2 which did not involve discernible temperature increases. Frequency structure on the order of 100 MHz was encountered in this investigation.

The evidence presented at this workshop thus suggests that biological systems are capable of sensing and, in some cases, being altered by exposure to low intensity electric and/or magnetic fields. This then brings us to the purpose of this workshop which was to consider the physical interaction mechanisms that can serve as a basis for the reported low intensity field effects. There is sufficient evidence for the existence of the effects, but the causes must be revealed.

It is obvious that at this point in time theoretical models of the physical mechanisms responsible for such effects are at best in the germinative stage. The suggested mechanisms are in general hypothetical and untested and it is not in general possible to predict their physiological significance. The possibility that more than one interaction mechanism may be required to explain the biological effects discussed in this workshop is suggested by the variety of effects which range from ELF-induced alterations in Ca^{2+} efflux in neurons to growth rate alterations in yeast at frequencies of 40 GHz.

Dr. Illinger provided what may well be a first step toward an understanding of the possible mechanism for high frequency effects. He referred to the possibility of field-induced quasi-resonant transitions which would theoretically be anticipated to occur in the frequency region greater than 10 GHz;

these are primarily due to the probability that coherent vibrational modes could be excited at such frequencies by electromagnetic radiation. In this context it should be noted that molecular vibrational relaxation times for biological systems are significantly longer than the rotational relaxation times induced by lower frequency fields. Quasi-resonant phenomena would thus be much more likely to occur at high frequencies and since such states would have longer lifetimes they could potentially be of greater biological significance.

The question of the effects of field-induced rotation of polar molecules in living systems by radiofrequency and microwave fields remains unanswered. Does dielectric relaxation produce functional alterations *in vivo* other than indirect effects attributable to thermal mechanisms? At present there are no definite indications that field-induced dipole reorientation is associated with any well defined biological effects. In addition to the dielectric relaxation of proteins, nucleic acids, and free and bound water, we must also consider the possible consequences of the field-induced relaxation of cells and cell organelles. Dr. Straub mentioned the rotation of mitochondria or ribosomes and suggested that perhaps the field-induced rotation of such bodies, which have relatively large dipole moments, may be of biological significance. At this point, however, nothing definite can be concluded.

Returning again to the phenomenon of quasi-resonance transitions at high frequencies, Dr. Illinger drew attention to the unique properties of membranes, such as the high intrinsic transmembrane electric field strengths, on the order of 10^5 V/cm, indicating that all biomembranes are in a state of very high potential energy. Dr. Illinger suggested the possibility that membrane fields may interact with weak external fields, providing the nucleus for the development of a theoretical model of the manner in which microwaves and radiofrequency fields could affect biological membranes.

The induction of molecular vibrational modes by electromagnetic fields was discussed by Dr. Prohofsky, who indicated that there are low-lying longitudinal vibrational modes of DNA molecules which could be induced or enhanced by electromagnetic fields at microwave frequencies. Dr. Prohofsky stated that there was no question of the existence of these vibrational modes, but there

is at present some degree of uncertainty regarding the modal frequencies. He indicated that vibrational modes could occur in the microwave frequency region at frequencies of 3 GHz or greater. Such induced modes could theoretically produce conformational changes in the DNA molecule which could result in biologically significant functional alterations. Future developments in this area should provide insight into possible mechanisms of interaction of radio-frequency and microwave fields with biomolecules.

It is interesting to note that the first four effects listed in Table I all involve low frequency fields with modulation frequencies of less than 100 Hz. The frequencies of maximum effect generally coincide with brain wave frequencies. Another intriguing aspect of the studies of Ca^{2+} efflux stimulated by weak electrical fields, which must be taken into account in the development of physical interaction mechanisms, is the existence of frequency and amplitude windows. An intensity window was also reported by Tinney and coworkers with respect to alterations in the heart rate of turtles. The existence of unique low intensity effects that are not encountered at higher intensities must thus be taken into consideration. Adey and Grodsky suggested that such alterations by low-frequency, low-intensity fields may involve field interactions with coherent membrane surface charge sites. Such coherent sites on the surface of cell membranes could be altered by weak fields, although the details of the interaction are unknown at present. Dr. Adey drew on molecular interaction models developed in endocrine studies as well as immunological and neurobiological studies to provide models for the interaction of electric fields with biological systems. For example, it was noted that antigen-antibody interactions appear to involve cooperative intermolecular bonding which confer unique characteristics such as reversibility and low activation energies. In dealing with an ensemble of molecules, such as in a biomembrane, cooperative weak bonding is encountered which may form the basis for the noted sensitivity of such structures to weak fields. The possibility of an ensemble of molecules being triggered by an external field to undergo conformational transitions resulting in functional alterations provides the rudiments of an interaction model, but at this point essential features such as dependency upon the frequency of the impressed field are lacking. The development of an

interaction mechanism that incorporates frequency dependence could, in addition to explaining frequency-dependent field interactions, serve as a basis for an understanding of basic neurophysiological phenomena such as the generation of EEG frequencies in the brain. The focus on biomembranes as the potential site of electromagnetic field interactions was further sharpened by Dr. Adey, who drew attention to those characteristics of membranes such as extremely high resistivity and very narrow bandpasses. Using the known parameters of biomembranes, calculated values of the amplitude of low frequency electrical impulses generated by thermal noise in a living system are on the order of 10^{-8} V/cm, thus suggesting a possible mechanism for the generation of EEG voltages due to synchronous depolarization of neurons.

The comments of Dr. Schwan drew attention to other factors that must be taken into account in developing interaction mechanisms. He noted that the thresholds for a number of well-studied biological effects, such as the disruption of cell membranes by electric fields, are inversely proportional to the volume of the cell, due to the fact that the amplitude of the induced field is dependent upon the shape and size of the system. Such findings provide a possible basis for the apparent variation in the sensitivities of different cell types to electromagnetic fields which obviously could be extended to provide a basis for differences in tissue or organ sensitivities. Studies of the effects of pulsed dc electrical fields on membrane permeability suggest that in addition to a volume effect, field-induced permeability changes are also dependent upon membrane composition.

The studies reported at this workshop by Dr. Sheridan again drew attention to the possibility that the membrane may prove to be the most logical model system to explain the sensitivity of biologic systems to electromagnetic fields. Using the technique of Raman spectroscopy, Dr. Sheridan has demonstrated phase transitions in bilayer lipid sphingomyelin membranes which occurred over a significantly narrower temperature range during low intensity microwave irradiation than in its absence. This effect, which was attributed to differential thermal gradients induced by the microwave field, suggests that the unique physical characteristics of membranes must be taken into account in developing interaction mechanisms. In contrast to the effects

at low field strength and low frequency reported by Adey, which do not apparently involve thermal gradients, Sheridan's findings emphasize the fact that significantly different interaction mechanisms may occur at different field frequencies, although the interactions may in any case occur most prominently at the membrane level of organization. The question of whether or not the effects of electromagnetic radiation are directly related to the electric field strength or are due to indirect effects of thermal absorption will perhaps be dependent upon the radiation frequency.

In spite of the attractiveness of the possibility of interaction mechanisms involving the cell membrane, there is obviously much useful information to be derived from studies of molecular interactions such as those reported by Professor Grant regarding the dielectric properties of bound water. There is a strong possibility that bound water is in much greater preponderance in biological systems than has formerly been recognized and may play a much larger role in the functioning of biological systems than was formerly recognized. Thus our attention is directed to its dielectric behavior as a possible means of furthering our understanding of microwave or radiofrequency interactions in biological systems. One very interesting aspect of Dr. Grant's investigation was the determination that in the frequency range between 1 to 3 GHz, bound water absorbs electromagnetic radiation more efficiently than free water. Thus, for example, alterations in membrane bound water would have to be considered in the development of interaction mechanisms in this frequency range. Additional research is obviously necessary to determine the nature and significance of field-induced alterations in bound water in biological systems.

This Workshop, which to the best of my knowledge represents the first concerted effort to consider the physical interaction mechanisms of electromagnetic fields with biological systems, has afforded an opportunity to discuss a number of potential mechanisms. Unfortunately, none are sufficiently well developed yet to provide a clear indication of how biological systems are altered by low intensity fields. Nevertheless, although we do not yet know the details of how systems are affected, the mechanisms discussed at this workshop should provide the stimulus and direction for the research

needed to further our knowldege in this area. The question of the sites of field interactions has also not been answered but the discussions at this workshop have directed attention to the cell membrane as a likely site for low intensity field-induced alterations. It is to be hoped that this workshop will provide the necessary stimulus for further advances in our understanding of the biological effects of electromagnetic radiation.

TABLE I

BIOLOGICAL EFFECTS OF LOW INTENSITY
ELECTROMAGNETIC FIELDS

EFFECT	FIELD STRENGTH OR INTENSITY
Alteration in Ca^{2+} in cerebral tissue (modulated ELF, VHF, UHF fields)	10^{-7} V/cm
Sensitivity of sharks and ray to weak fields	10^{-8} V/cm
Navigation of birds by the use of fields induced by flying through the Earth's magnetic field	10^{-8} V/cm
Extraordinary sensitivity of membranes to weak electrical fields	10^{-7} - 10^{-8} V/cm
Frequency specific alteration in growth rate of yeast cultures in the region of 42 GHz; 100 MHz spectral fine structure (no detectable temperature effect)	~ 1 mW/cm^2

* *

DISCUSSION

My understanding of Dr. Sheridan's result about the width of the transitions is apparently different from yours. Although he said they were about one or two degrees in width as measured by Raman spectroscopy, he also indicated he had a problem in measuring the line width without knowing where the line is exactly. He also said that measured by calorimetry the width is only a tenth of a degree centigrade. So I do not think you can come directly to these conclusions. [Mangum].

Cleary: Dr. Sheridan is here and can comment.

Professor Cleary interpreted exactly what I attempted to convey. The comments about where the transition is were in reference to a single component, highly pure system. In mixed systems you can measure the width which is a function of the mixture. [Sheridan].

You talk about that as an absolute, not as a width? [Mangum].

In comparison to what Raman spectroscopy can do, yes, calorimetry is much, much better. But what I said was that I could determine the width of the transition of a single component system to within a degree by careful measurements, taking data state-wise at half the interval. One can determine the mid-point of the transition to some degree. As to the width in the mixture, each of those states in the naturally occurring system are several degrees wide and they can be relatively accurately pinpointed by Raman. [Sheridan].

Cleary: I think that the phase transition in the biomembrane is very well established by a number of different investigators. Hopefully, we will soon know more about the extent to which microwave or radiofrequency fields can enhance these phase transitions. It seems to me that certainly when phase transition occurs there will be an alteration of function such as permeability changes. I do think that such effects could be involved in the sort of results which Dr. Adey reported.

I thought I referred to that, and when he showed the graph illustrating the temperature dependency it looked to me very much like the effect of a lipid phase change rather than some cooperative effect although it could be a combination of both. [Sheridan].

Cleary: In a sense the phase transition is a cooperative effect.

Certainly. However, it is not clear what the size of the cooperative unit is. There is the concept of the two-phase region, which does exist at biological temperatures. It is possible this may give some insight into the actual size. [Sheridan].

Do you envision phase transition primarily as a property of the surface of the membrane, or does it have to do very much with what is inside the membrane? [Illinger].

I have been looking inside the membrane; the vibrational band from which I am deriving information relates uniquely to the interior of the biolayer. However, that is not to say that one or other of the transitions that one sees naturally occurring in mixtures is not an indirect function of a surface expansion or rearrangement. [Sheridan].

Cleary: I think that most of the evidence seems to suggest that it is the lipid that is changing.

I wanted to make the point that there is an expansion and a thinning of the membrane when it goes through these phase transitions, thus it must be a combination of effects. But there are obviously two forces and some kind of equilibrium, until the forces get too large and create a new configuration. [Sheridan].

Cleary: Also, referring to a mechanism that Dr. Schwan mentioned, there is the occurrence of dielectric breakdown and the alteration of permeability. The physical model for these alterations involves the electrocompression of the membrane by the field. Thus, it is not unrealistic to suppose that if you expose such a membrane to an alternating field the resulting mechanical oscillations could well involve cooperative quasiresonant effects in the membrane. I believe there is evidence at this point that suggests that membranes are the bodies to study.

Is there evidence concerning the effects of the repetition rate of these high field pulses on membranes. If there is a mechanical effect, it would presumably have some characteristic frequencies. Have measurements been done over a wide range? [Rabinowitz].

Cleary: Most of the studies of which I am aware have been done with just a single pulse. We have not actually looked at pulse repetition effects. However, we found for example, that if we continually pulsed the cell membrane one can induce permeability change at field strengths not sufficient to cause dielectric breakdown or destruction of the membrane. It would be very interesting to look at pulse repetition rate effects.

I would like to suggest that the proteins involved in the membrane transport probably are also affected by conformational changes of some type. Next,

it is impossible at this point to envision theoretically calculating the vibrational motion of such a complex molecule, although there certainly exist such vibrational modes, and they certainly must be involved in conformation changes. [Illinger].

Cleary: I also think that there is some quantitative evidence that would indicate about 0.2 ev as the activation energy for opening and closing ports in tissue membrane. This is a little hard to put into proper context, but I think it at least implies that it is not a high energy transition.

It is not a one-to-one correspondence, whatever the dynamics involved. [Prohofsky].

Cleary: Again, I think advances in membrane biochemistry will be needed.

We tend to look at the isolated protein if possible to try to understand how it responds to microwave interaction, without denaturing. [Prohofsky].

It appears that certaine types of spectroscopic measurement, Raman, optical or infrared, could very well be an avenue toward seeing whether the energy is absorbed in a frequency-selective fashion. For whatever the mechanism, whether it is in the bound water or some vibration of the biopolymer, such measurements are more definitive than chromatic measurements which simply average over the entire input. In these experiments one can look at particular frequencies which correlate strongly to the conformation of the biopolymer. That certainly must be part of the story, for what happens occurs at the organizational level of the biopolymer in the membrane. Beyond saying that it has very unusual dielectric properties, as Fröhlich stresses, we also want to be able to say something about the conversion of the input electromagnetic energy, into the energy of the structural water and then on to free water or vice-versa. We require an experimental method, for there now seems to be no direct way of resolving the problem because the systems are strongly coupled. That does not mean that their properties are irrespective of their overall structure, but there may be no resonant frequency to observe. [Illinger].

I was very much intrigued by Dr. Prohofsky's allusion to the role water molecules are probably playing in the phase changes of the DNA molecule. I wonder if everything that has been said about water in these last days has given him any further ideas. [Snyder].

In the particular model we investigated, certainly, the water was involved, experimentally. When that conformation change occurred much of the normal water of hydration was removed. It is being dried up, but there is still strongly bound water. However, it is being taken out at the groove at which

that conformation change occurs. Normally the groove probably has another sheath or two of water around it. Thus, the particular case we looked at is an unusual situation, in terms of water hydration around the DNA double helix. But certainly it is normal in these forms, and it is in these forms primarily because of the reduced water sheath which is reduced by electrostatic reactions in the interior. [Prohofsky].

Cleary: Are there any additional comments?

I am most curious about what was learned by the three American researchers who were invited to visit the Soviet Union. And I was wondering if Dr. Swicord would tell us what, if anything, he learned there. [Hill].

We were invited to participate in a workshop in a particular institute which has not been involved in microwave research very long. Their principal initial interest is directed towards nervous system effects, and they are starting to repeat some of the work on auditory response in a very interesting way, using themselves for experimental purposes and not paying too much attention to their own radiation safety standards. They are trying to dispel some of the recent theories, particularly the one proposed by Lin which explains this phenomenon on a microthermal basis. Their supposition was that one could change the boundary conditions by immersion in water and, if it is a thermal effect, shift the observed response. However, they have observed no shift. Our question was, was the boundary condition really changed by body immersion in water? Of course, the subject of the workshop was to delve into the basis for exposure standards; we found that their concern was much the same as ours, although from an opposite viewpoint. While we wonder why our standard is so much greater than theirs, they question why their standard is so much less than ours. There is, probably, no more real basis for their exposure standards than for ours. I think there are pressures from their production organizations to relax the standards as well as pressures from the safety organizations to maintain standards. They have built a prototype microwave oven and tested it and it failed their own standard. Now, they do have a different approach to measuring microwave oven leakage. I was unable to obtain specifics. However, Professor Guy said that the last time he visited they were making measurements 50 centimeters away from the front of the oven and averaging; some of the better American ovens could pass this test at their safety standard level. We did not learn anything more specific or see any vital new data. The group at this institute is very strong in biophysics, engineering, and biology and is a well-formed team. They were very critical about some of their own published work and raised some of the same questions that we have raised. [Swicord].

Cleary: The impression that I have gotten from the Russian and European literature is that they seem to stay away very much from any questions about interaction mechanisms.

I felt that this group was very interested in mechanisms. In fact, the deputy director of the institute mentioned that he was planning to have a workshop on mechanisms next spring. Their traditional attitude has been to look more at process, but this group was formed for this specific reason. [Swicord].

Cleary: Can you make any comments regarding what they are doing in the area of dosimetry or field characterization.

My impression is that they are behind us at this point. They do not have the instrumentation that we do for measurements. In fact, I was asked to send them literature on our commercially available instrumentation. [Swicord].

Did they allow you to take any photographs of their laboratory equipment? [Rozzell].

Yes. I have slides which I will be glad to show you. [Swicord].

Were any of the Soviets interested in mixed frequency effects? [Libber].

Are they interested in higher frequencies, beyond radio frequencies or S-band microwaves? [Rozzell].

There is some lower frequency work, but I did not see any evidence of higher frequency work during my visit. Of course, the literature indicates a great deal of such research. [Swicord].

As a comment, I believe that the important thing that has come out of here is the whole idea of a thermal decoupling between parts of biological systems. I think the Soviet literature on this goes back fifteen years or more. [Rabinowitz].

Cleary: Any other comments?

There seemed to be some surprise that there could be an intensity window for some biological effects. However, a number of such windows are very well known in other contexts, including the "killing voltage" which is an obvious intensity window. [Taylor].

Cleary: I think that my remark was to the fact that in this area it had not been encountered previously. I am sure that there are potential explanations for these phenomena.

WORKSHOP ATTENDEES

Eleanor R. Adair
John B. Pierce Foundation
Laboratory
New Haven, Connecticut 06510

W. Ross Adey, Director
Department of Anatomy
University of California
School of Medicine
Los Angeles, California 90024

E. Ronald Atkinson
National Cancer Institute
Bldg. 37, Room 6A01
Bethesda, Maryland 20014

Howard I. Bassen
Bureau of Radiological Health
FDA
12721 Twinbrook Parkway
Rockville, Maryland 20852

Charles A. Cain
Department of Electrical
Engineering
Urbana-Champaign
Urbana, Illinois 61801

Norman Caplan
Devices and Waves Program
Electrical Sciences and
Analysis Section
National Science Foundation
Washington, D. C. 20550

T. C. Cetas
Division of Radiation Oncology
University of Arizona
College of Medicine
Tucson, Arizona 85724

Augustine Y. Cheung
Institute for Physical Science
and Technology
University of Maryland
College Park, Maryland 20742

Chung-Kwang Chou
School of Medicine
Bioelectromagnetics Research
Laboratory
Department of Rehabilitation
Medicine, RJ-30
University of Washington
Seattle, Washington 98195

S. F. Cleary
Virginia Commonwealth University
Medical College of Virginia
Richmond, Virginia 23298

James S. Clegg
Department of Biology
University of Miami
Coral Gables, Florida 33124

Nicholas Dagalakis
Department of Mechanical
University of Maryland
College Park, Maryland 20742

C. Davis
Department of Electrical
University of Maryland
College Park, Maryland 20742

W. Drost-Hansen
Department of Chemistry
University of Miami
Coral Gables, Florida 33124

E. Edelsack
Department of the Navy
Office of Naval Research
Room 322
Arlington, Virginia 22217

Leopold Felsen
Polytechnic Institute of New York
Graduate Center
Farmingdale, New York 11735

K. R. Foster
Department of Bioengineering
University of Pennsylvania
Philadelphia,

WORKSHOP ATTENDEES

A. Friend
Engineering
Support Department
Naval Medical Research
Institute
Bethesda, Maryland 20014

Robert Gammon
Institute for Physical Science
and Technology
University of Maryland
College Park, Maryland 20742

Om P. Gandhi
Department of Electrical Eng.
University of Utah
Salt Lake City, Utah 84112

E. H. Grant
Department of Experimental Physics
University of London
Campden Hill Road
United Kingdom

Irvin T. Grodsky
Physics Department
UCLA
Los Angeles, California 90024

R. Hannemann
Dept. of Mechanical Engineering
University of Maryland
College Park, Maryland 20742

G. Harrison
Division of Radiation Therapy
University of Maryland
Baltimore, Maryland 21201

D. Hazzard
Bureau of Radiological Health
12721 Twinbrook Parkway
Rockville, Maryland 20852

W. Herman
Division of Electronic Products
Bureau of Radiological Health
12721 Twinbrook Parkway
Rockville, Maryland 20852

D. A. Hill
Radiation Biology Section
Defense Research Establishment
Ottawa, Ontario, Canada
K1A 024

Henry Ho
BRH/FDA
5600 Fishers Lane
Rockville, Maryland 20852

C. Illinger
Department of Chemistry
Tufts University
Medford, Massachusetts 02155

G. Kantor
Division of Electronic Products
Bureau of Radiological Health
Rockville, Maryalnd 20852

Ronald P. King
Gordon McKay Laboratory
Harvard University
Cambridge, Massachusetts 02138

David Koopman
Institute for Physical Science
and Technology
University of Maryland
College Park, Maryland 20742

Herbert Lashinsky
Institute for Physical Science
and Technology
University of Maryland
College Park, Maryland

William Leach
Bureau of Radiological Health
Rockville, Maryalnd 20852

Robert M. Lebovitz
Department of Physiology
Southwestern Medical School
Dallas, Texas 75235

Gloria Li
Stanford University School of
Medicine
Department of Radiology
Stanford, California 94305

WORKSHOP ATTENDEES

L. Libber
Physiology Program
Office of Naval Research
Arlington, Virginia 22217

James C. Lin
Department of Electrical Engineering
Wayne State University
Detroit Michigan 48202

Li-Ming Liu
University of Virginia
Charlottesville, Virginia

Donald I. McRee
NIEHS
Post Office Box 12233
Research Triangle Park
North Carolina 27709

D. McCulloch
University of Maryland Hospital
22 Greene Street
Baltimore, Maryland

Richard Magin
National Institute of Health
HCI-DCT, Bldg. 37, Room 5-A13
Bethesda, Maryland 20014

B. W. Mangum
National Bureau of Standards
Physics B122
Washington D. C. 20234

Robert Neil
Bureau of Radiological Health
Rockville, Maryland 20852

S. Neuder
Division of Electronic Products
Bureau of Radiological Health
Rockville, Md. 20852

R. G. Olsen
Biomedical Research Division
Naval Aerospace Medical Research Laboratory
Pensacola, Florida 32508

E. W. Prohofsky
Department of Physics
Purdue University
West Lafayette, Indiana 47907

Elliot Postow
Naval Medical Research and Development Command
Bldg. 142-NNMC
Bethesda, Maryland 20014

Alain Priou
Onera-CERT
Dermo Laboratories
2, Avenue Edouard-Belin BP4025
31055 Toulouse, France CDEX

James Rabinowitz
New York University Medical Center
Institute of Environmental Medicine
550 First Avenue
Mew York, New York 10016

Joseph Richman
Temperature Section
National Bureau of Standards
Gaithersburg, Maryland 20760

Thomas C. Rozzell
Office of Naval Research
Physiology Program/Code 441
800 Quincy Street
Arlington, Virginia 22217

Eugene Robinson
Division of Radiation Therapy
University of Maryland
Baltimore, Maryland 21201

G. M. Samaras
Division of Radiation Therapy
University of Maryland
Baltimore, Maryland 21201

O. Schmitt
Biophysics Group
200 T N C E
University of Minnesota
Department of Electrical Eng.
Minneapolis, Minnesota 55455

WORKSHOP ATTENDEES

Roger H. Schneider
HFX-200
Division of Electronic Products
BRH, FDA, HEW
Rockville, Maryland 20852

H. P. Schwan
Moore School of Engineering
University of Pennsylvania 19104

James Sheridan
Naval Research Laboratory
Washington, D. C.

Morris Shore
Bureau of Radiological Health
Rockville, Maryland 20852

Joseph Silverman
Institute for Physical Science
and Technology
University of Maryland
College Park, Maryland 20742

Glenn S. Smith
Department of Electrical Engineering
Georgia Institute of Technology
Atlanta, Georgia 30332

Karl David Straub
Veterans Administration Hospital
300 Roosevelt Road
Little Rock, Arkansas 72206

I. Takashima
Department of Biophysics
University of Pennsylvania
Philadelphia, Pennsylvania 19104

Leonard Taylor
Department of Electrical Engineering
University of Maryland
College Park, Maryland 20742

J. C. Toler
Engineering Experiment Station
Georgia Institute of Technology
Atlanta, Georgia 30332

M. Toman
Walter Reed Army Institute
of Research
Washington, D. C. 20012

Paul Tyler
Naval Medical Research and
Development Command
National Naval Medical Center
Bethesda, Maryland 20014

Lt. Col. Robert Wangeman
Radiation & Environmental
Sciences Division
U. S. Army Environmental
Health Agency
Aberdeen Proving Grounds, Md.